COMPUTATIONAL METHODS FOR PLASTICITY

THEORY AND APPLICATIONS

EA de Souza Neto

D Perić

DRJ Owen

Civil and Computational Engineering Centre, Swansea University

WILEY

A John Wiley and Sons, Ltd, Publication

CONTENTS

Preface xx

Part One Basic concepts 1

1 Introduction 3
- 1.1 Aims and scope . . . 3
  - 1.1.1 Readership . . . 4
- 1.2 Layout . . . 4
  - 1.2.1 The use of boxes . . . 7
- 1.3 General scheme of notation . . . 7
  - 1.3.1 Character fonts. General convention . . . 8
  - 1.3.2 Some important characters . . . 9
  - 1.3.3 Indicial notation, subscripts and superscripts . . . 13
  - 1.3.4 Other important symbols and operations . . . 14

2 Elements of tensor analysis 17
- 2.1 Vectors . . . 17
  - 2.1.1 Inner product, norm and orthogonality . . . 17
  - 2.1.2 Orthogonal bases and Cartesian coordinate frames . . . 18
- 2.2 Second-order tensors . . . 19
  - 2.2.1 The transpose. Symmetric and skew tensors . . . 19
  - 2.2.2 Tensor products . . . 20
  - 2.2.3 Cartesian components and matrix representation . . . 21
  - 2.2.4 Trace, inner product and Euclidean norm . . . 22
  - 2.2.5 Inverse tensor. Determinant . . . 23
  - 2.2.6 Orthogonal tensors. Rotations . . . 23
  - 2.2.7 Cross product . . . 24
  - 2.2.8 Spectral decomposition . . . 25
  - 2.2.9 Polar decomposition . . . 28
- 2.3 Higher-order tensors . . . 28
  - 2.3.1 Fourth-order tensors . . . 29
  - 2.3.2 Generic-order tensors . . . 30
- 2.4 Isotropic tensors . . . 30
  - 2.4.1 Isotropic second-order tensors . . . 30
  - 2.4.2 Isotropic fourth-order tensors . . . 30

2.5 Differentiation . . . 32
2.5.1 The derivative map. Directional derivative . . . 32
2.5.2 Linearisation of a nonlinear function . . . 32
2.5.3 The gradient . . . 32
2.5.4 Derivatives of functions of vector and tensor arguments . . . 33
2.5.5 The chain rule . . . 36
2.5.6 The product rule . . . 37
2.5.7 The divergence . . . 37
2.5.8 Useful relations involving the gradient and the divergence . . . 38
2.6 Linearisation of nonlinear problems . . . 38
2.6.1 The nonlinear problem and its linearised form . . . 38
2.6.2 Linearisation in infinite-dimensional functional spaces . . . 39

3 Elements of continuum mechanics and thermodynamics 41
3.1 Kinematics of deformation . . . 41
3.1.1 Material and spatial fields . . . 44
3.1.2 Material and spatial gradients, divergences and time derivatives . 46
3.1.3 The deformation gradient . . . 46
3.1.4 Volume changes. The determinant of the deformation gradient . . 47
3.1.5 Isochoric/volumetric split of the deformation gradient . . . 49
3.1.6 Polar decomposition. Stretches and rotation . . . 49
3.1.7 Strain measures . . . 52
3.1.8 The velocity gradient. Rate of deformation and spin . . . 55
3.1.9 Rate of volume change . . . 56
3.2 Infinitesimal deformations . . . 57
3.2.1 The infinitesimal strain tensor . . . 57
3.2.2 Infinitesimal rigid deformations . . . 58
3.2.3 Infinitesimal isochoric and volumetric deformations . . . 58
3.3 Forces. Stress Measures . . . 60
3.3.1 Cauchy's axiom. The Cauchy stress vector . . . 61
3.3.2 The axiom of momentum balance . . . 61
3.3.3 The Cauchy stress tensor . . . 62
3.3.4 The First Piola–Kirchhoff stress . . . 64
3.3.5 The Second Piola–Kirchhoff stress . . . 66
3.3.6 The Kirchhoff stress . . . 67
3.4 Fundamental laws of thermodynamics . . . 67
3.4.1 Conservation of mass . . . 67
3.4.2 Momentum balance . . . 67
3.4.3 The first principle . . . 68
3.4.4 The second principle . . . 68
3.4.5 The Clausius–Duhem inequality . . . 69
3.5 Constitutive theory . . . 69
3.5.1 Constitutive axioms . . . 69
3.5.2 Thermodynamics with internal variables . . . 71
3.5.3 Phenomenological and micromechanical approaches . . . 74

3.5.4 The purely mechanical theory . . . 75
3.5.5 The constitutive initial value problem . . . 76
3.6 Weak equilibrium. The principle of virtual work . . . 77
3.6.1 The spatial version . . . 77
3.6.2 The material version . . . 78
3.6.3 The infinitesimal case . . . 78
3.7 The quasi-static initial boundary value problem . . . 79
3.7.1 Finite deformations . . . 79
3.7.2 The infinitesimal problem . . . 81

4 The finite element method in quasi-static nonlinear solid mechanics 83
4.1 Displacement-based finite elements . . . 84
4.1.1 Finite element interpolation . . . 85
4.1.2 The discretised virtual work . . . 86
4.1.3 Some typical isoparametric elements . . . 90
4.1.4 Example. Linear elasticity . . . 93
4.2 Path-dependent materials. The incremental finite element procedure . . . 94
4.2.1 The incremental constitutive function . . . 95
4.2.2 The incremental boundary value problem . . . 95
4.2.3 The nonlinear incremental finite element equation . . . 96
4.2.4 Nonlinear solution. The Newton–Raphson scheme . . . 96
4.2.5 The consistent tangent modulus . . . 98
4.2.6 Alternative nonlinear solution schemes . . . 99
4.2.7 Non-incremental procedures for path-dependent materials . . . 101
4.3 Large strain formulation . . . 102
4.3.1 The incremental constitutive function . . . 102
4.3.2 The incremental boundary value problem . . . 103
4.3.3 The finite element equilibrium equation . . . 103
4.3.4 Linearisation. The consistent spatial tangent modulus . . . 103
4.3.5 Material and geometric stiffnesses . . . 106
4.3.6 Configuration-dependent loads. The load-stiffness matrix . . . 106
4.4 Unstable equilibrium. The arc-length method . . . 107
4.4.1 The arc-length method . . . 107
4.4.2 The combined Newton–Raphson/arc-length procedure . . . 108
4.4.3 The predictor solution . . . 111

5 Overview of the program structure 115
5.1 Introduction . . . 115
5.1.1 Objectives . . . 115
5.1.2 Remarks on program structure . . . 116
5.1.3 Portability . . . 116
5.2 The main program . . . 117
5.3 Data input and initialisation . . . 117
5.3.1 The global database . . . 117
5.3.2 Main problem-defining data. Subroutine `INDATA` . . . 119

5.3.3 External loading. Subroutine INLOAD . . . 119
5.3.4 Initialisation of variable data. Subroutine INITIA . . . 120
5.4 The load incrementation loop. Overview . . . 120
5.4.1 Fixed increments option . . . 120
5.4.2 Arc-length control option . . . 120
5.4.3 Automatic increment cutting . . . 123
5.4.4 The linear solver. Subroutine FRONT . . . 124
5.4.5 Internal force calculation. Subroutine INTFOR . . . 124
5.4.6 Switching data. Subroutine SWITCH . . . 124
5.4.7 Output of converged results. Subroutines OUTPUT and RSTART . . 125
5.5 Material and element modularity . . . 125
5.5.1 Example. Modularisation of internal force computation . . . 125
5.6 Elements. Implementation and management . . . 128
5.6.1 Element properties. Element routines for data input . . . 128
5.6.2 Element interfaces. Internal force and stiffness computation . . . 129
5.6.3 Implementing a new finite element . . . 129
5.7 Material models: implementation and management . . . 131
5.7.1 Material properties. Material-specific data input . . . 131
5.7.2 State variables and other Gauss point quantities. Material-specific state updating routines . . . 132
5.7.3 Material-specific switching/initialising routines . . . 133
5.7.4 Material-specific tangent computation routines . . . 134
5.7.5 Material-specific results output routines . . . 134
5.7.6 Implementing a new material model . . . 135

Part Two Small strains **137**

6 The mathematical theory of plasticity **139**
6.1 Phenomenological aspects . . . 140
6.2 One-dimensional constitutive model . . . 141
6.2.1 Elastoplastic decomposition of the axial strain . . . 142
6.2.2 The elastic uniaxial constitutive law . . . 143
6.2.3 The yield function and the yield criterion . . . 143
6.2.4 The plastic flow rule. Loading/unloading conditions . . . 144
6.2.5 The hardening law . . . 145
6.2.6 Summary of the model . . . 145
6.2.7 Determination of the plastic multiplier . . . 146
6.2.8 The elastoplastic tangent modulus . . . 147
6.3 General elastoplastic constitutive model . . . 148
6.3.1 Additive decomposition of the strain tensor . . . 148
6.3.2 The free energy potential and the elastic law . . . 148
6.3.3 The yield criterion and the yield surface . . . 150
6.3.4 Plastic flow rule and hardening law . . . 150
6.3.5 Flow rules derived from a flow potential . . . 151
6.3.6 The plastic multiplier . . . 152

6.3.7 Relation to the general continuum constitutive theory . . . 153
6.3.8 Rate form and the elastoplastic tangent operator . . . 153
6.3.9 Non-smooth potentials and the subdifferential . . . 153
6.4 Classical yield criteria . . . 157
6.4.1 The Tresca yield criterion . . . 157
6.4.2 The von Mises yield criterion . . . 162
6.4.3 The Mohr–Coulomb yield criterion . . . 163
6.4.4 The Drucker–Prager yield criterion . . . 166
6.5 Plastic flow rules . . . 168
6.5.1 Associative and non-associative plasticity . . . 168
6.5.2 Associative laws and the principle of maximum plastic dissipation 170
6.5.3 Classical flow rules . . . 171
6.6 Hardening laws . . . 177
6.6.1 Perfect plasticity . . . 177
6.6.2 Isotropic hardening . . . 178
6.6.3 Thermodynamical aspects. Associative isotropic hardening . . . 182
6.6.4 Kinematic hardening. The Bauschinger effect . . . 185
6.6.5 Mixed isotropic/kinematic hardening . . . 189

7 Finite elements in small-strain plasticity problems **191**
7.1 Preliminary implementation aspects . . . 192
7.2 General numerical integration algorithm for elastoplastic constitutive equations . . . 193
7.2.1 The elastoplastic constitutive initial value problem . . . 193
7.2.2 Euler discretisation: the incremental constitutive problem . . . 194
7.2.3 The elastic predictor/plastic corrector algorithm . . . 196
7.2.4 Solution of the return-mapping equations . . . 198
7.2.5 Closest point projection interpretation . . . 200
7.2.6 Alternative justification: operator split method . . . 201
7.2.7 Other elastic predictor/return-mapping schemes . . . 201
7.2.8 Plasticity and differential-algebraic equations . . . 209
7.2.9 Alternative mathematical programming-based algorithms . . . 210
7.2.10 Accuracy and stability considerations . . . 210
7.3 Application: integration algorithm for the isotropically hardening von Mises model . . . 215
7.3.1 The implemented model . . . 216
7.3.2 The implicit elastic predictor/return-mapping scheme . . . 217
7.3.3 The incremental constitutive function for the stress . . . 220
7.3.4 Linear isotropic hardening and perfect plasticity: the closed-form return mapping . . . 223
7.3.5 Subroutine SUVM . . . 224
7.4 The consistent tangent modulus . . . 228
7.4.1 Consistent tangent operators in elastoplasticity . . . 229
7.4.2 The elastoplastic consistent tangent for the von Mises model with isotropic hardening . . . 232
7.4.3 Subroutine CTVM . . . 235

7.4.4 The general elastoplastic consistent tangent operator for implicit return mappings . . . 238
7.4.5 Illustration: the von Mises model with isotropic hardening . . . 240
7.4.6 Tangent operator symmetry: incremental potentials . . . 243
7.5 Numerical examples with the von Mises model . . . 244
7.5.1 Internally pressurised cylinder . . . 244
7.5.2 Internally pressurised spherical shell . . . 247
7.5.3 Uniformly loaded circular plate . . . 250
7.5.4 Strip-footing collapse . . . 252
7.5.5 Double-notched tensile specimen . . . 255
7.6 Further application: the von Mises model with nonlinear mixed hardening . 257
7.6.1 The mixed hardening model: summary . . . 257
7.6.2 The implicit return-mapping scheme . . . 258
7.6.3 The incremental constitutive function . . . 260
7.6.4 Linear hardening: closed-form return mapping . . . 261
7.6.5 Computational implementation aspects . . . 261
7.6.6 The elastoplastic consistent tangent . . . 262

8 Computations with other basic plasticity models 265
8.1 The Tresca model . . . 266
8.1.1 The implicit integration algorithm in principal stresses . . . 268
8.1.2 Subroutine SUTR . . . 279
8.1.3 Finite step accuracy: iso-error maps . . . 283
8.1.4 The consistent tangent operator for the Tresca model . . . 286
8.1.5 Subroutine CTTR . . . 291
8.2 The Mohr–Coulomb model . . . 295
8.2.1 Integration algorithm for the Mohr–Coulomb model . . . 297
8.2.2 Subroutine SUMC . . . 310
8.2.3 Accuracy: iso-error maps . . . 315
8.2.4 Consistent tangent operator for the Mohr–Coulomb model . . . 316
8.2.5 Subroutine CTMC . . . 319
8.3 The Drucker–Prager model . . . 324
8.3.1 Integration algorithm for the Drucker–Prager model . . . 325
8.3.2 Subroutine SUDP . . . 334
8.3.3 Iso-error map . . . 337
8.3.4 Consistent tangent operator for the Drucker–Prager model . . . 337
8.3.5 Subroutine CTDP . . . 340
8.4 Examples . . . 343
8.4.1 Bending of a V-notched Tresca bar . . . 343
8.4.2 End-loaded tapered cantilever . . . 344
8.4.3 Strip-footing collapse . . . 346
8.4.4 Circular-footing collapse . . . 350
8.4.5 Slope stability . . . 351

9 Plane stress plasticity 357
9.1 The basic plane stress plasticity problem . . . 357
9.1.1 Plane stress linear elasticity . . . 358
9.1.2 The constrained elastoplastic initial value problem . . . 359
9.1.3 Procedures for plane stress plasticity . . . 360
9.2 Plane stress constraint at the Gauss point level . . . 361
9.2.1 Implementation aspects . . . 362
9.2.2 Plane stress enforcement with nested iterations . . . 362
9.2.3 Plane stress von Mises with nested iterations . . . 364
9.2.4 The consistent tangent for the nested iteration procedure . . . 366
9.2.5 Consistent tangent computation for the von Mises model . . . 366
9.3 Plane stress constraint at the structural level . . . 367
9.3.1 The method . . . 367
9.3.2 The implementation . . . 368
9.4 Plane stress-projected plasticity models . . . 370
9.4.1 The plane stress-projected von Mises model . . . 371
9.4.2 The plane stress-projected integration algorithm . . . 373
9.4.3 Subroutine SUVMPS . . . 378
9.4.4 The elastoplastic consistent tangent operator . . . 382
9.4.5 Subroutine CTVMPS . . . 383
9.5 Numerical examples . . . 386
9.5.1 Collapse of an end-loaded cantilever . . . 387
9.5.2 Infinite plate with a circular hole . . . 387
9.5.3 Stretching of a perforated rectangular plate . . . 390
9.5.4 Uniform loading of a concrete shear wall . . . 391
9.6 Other stress-constrained states . . . 396
9.6.1 A three-dimensional von Mises Timoshenko beam . . . 396
9.6.2 The beam state-projected integration algorithm . . . 400

10 Advanced plasticity models 403
10.1 A modified Cam-Clay model for soils . . . 403
10.1.1 The model . . . 404
10.1.2 Computational implementation . . . 406
10.2 A capped Drucker–Prager model for geomaterials . . . 409
10.2.1 Capped Drucker–Prager model . . . 410
10.2.2 The implicit integration algorithm . . . 412
10.2.3 The elastoplastic consistent tangent operator . . . 413
10.3 Anisotropic plasticity: the Hill, Hoffman and Barlat–Lian models . . . 414
10.3.1 The Hill orthotropic model . . . 414
10.3.2 Tension–compression distinction: the Hoffman model . . . 420
10.3.3 Implementation of the Hoffman model . . . 423
10.3.4 The Barlat–Lian model for sheet metals . . . 427
10.3.5 Implementation of the Barlat–Lian model . . . 431

11 Viscoplasticity **435**
11.1 Viscoplasticity: phenomenological aspects . . . 436
11.2 One-dimensional viscoplasticity model . . . 437
11.2.1 Elastoplastic decomposition of the axial strain . . . 437
11.2.2 The elastic law . . . 438
11.2.3 The yield function and the elastic domain . . . 438
11.2.4 Viscoplastic flow rule . . . 438
11.2.5 Hardening law . . . 439
11.2.6 Summary of the model . . . 439
11.2.7 Some simple analytical solutions . . . 439
11.3 A von Mises-based multidimensional model . . . 445
11.3.1 A von Mises-type viscoplastic model with isotropic strain hardening . . . 445
11.3.2 Alternative plastic strain rate definitions . . . 447
11.3.3 Other isotropic and kinematic hardening laws . . . 448
11.3.4 Viscoplastic models without a yield surface . . . 448
11.4 General viscoplastic constitutive model . . . 450
11.4.1 Relation to the general continuum constitutive theory . . . 450
11.4.2 Potential structure and dissipation inequality . . . 451
11.4.3 Rate-independent plasticity as a limit case . . . 452
11.5 General numerical framework . . . 454
11.5.1 A general implicit integration algorithm . . . 454
11.5.2 Alternative Euler-based algorithms . . . 457
11.5.3 General consistent tangent operator . . . 458
11.6 Application: computational implementation of a von Mises-based model . 460
11.6.1 Integration algorithm . . . 460
11.6.2 Iso-error maps . . . 463
11.6.3 Consistent tangent operator . . . 464
11.6.4 Perzyna-type model implementation . . . 466
11.7 Examples . . . 467
11.7.1 Double-notched tensile specimen . . . 467
11.7.2 Plane stress: stretching of a perforated plate . . . 469

12 Damage mechanics **471**
12.1 Physical aspects of internal damage in solids . . . 472
12.1.1 Metals . . . 472
12.1.2 Rubbery polymers . . . 473
12.2 Continuum damage mechanics . . . 473
12.2.1 Original development: creep-damage . . . 474
12.2.2 Other theories . . . 475
12.2.3 Remarks on the nature of the damage variable . . . 476
12.3 Lemaitre's elastoplastic damage theory . . . 478
12.3.1 The model . . . 478
12.3.2 Integration algorithm . . . 482
12.3.3 The tangent operators . . . 485

12.4 A simplified version of Lemaitre's model . . . 486
12.4.1 The single-equation integration algorithm . . . 486
12.4.2 The tangent operator . . . 490
12.4.3 Example. Fracturing of a cylindrical notched specimen . . . 493
12.5 Gurson's void growth model . . . 496
12.5.1 The model . . . 497
12.5.2 Integration algorithm . . . 501
12.5.3 The tangent operator . . . 502
12.6 Further issues in damage modelling . . . 504
12.6.1 Crack closure effects in damaged elastic materials . . . 504
12.6.2 Crack closure effects in damage evolution . . . 510
12.6.3 Anisotropic ductile damage . . . 512

Part Three Large strains **517**

13 Finite strain hyperelasticity **519**
13.1 Hyperelasticity: basic concepts . . . 520
13.1.1 Material objectivity: reduced form of the free-energy function . . . 520
13.1.2 Isotropic hyperelasticity . . . 521
13.1.3 Incompressible hyperelasticity . . . 524
13.1.4 Compressible regularisation . . . 525
13.2 Some particular models . . . 525
13.2.1 The Mooney–Rivlin and the neo-Hookean models . . . 525
13.2.2 The Ogden material model . . . 527
13.2.3 The Hencky material . . . 528
13.2.4 The Blatz–Ko material . . . 530
13.3 Isotropic finite hyperelasticity in plane stress . . . 530
13.3.1 The plane stress incompressible Ogden model . . . 531
13.3.2 The plane stress Hencky model . . . 532
13.3.3 Plane stress with nested iterations . . . 533
13.4 Tangent moduli: the elasticity tensors . . . 534
13.4.1 Regularised neo-Hookean model . . . 535
13.4.2 Principal stretches representation: Ogden model . . . 535
13.4.3 Hencky model . . . 537
13.4.4 Blatz–Ko material . . . 537
13.5 Application: Ogden material implementation . . . 538
13.5.1 Subroutine `SUOGD` . . . 538
13.5.2 Subroutine `CSTOGD` . . . 542
13.6 Numerical examples . . . 546
13.6.1 Axisymmetric extension of an annular plate . . . 547
13.6.2 Stretching of a square perforated rubber sheet . . . 547
13.6.3 Inflation of a spherical rubber balloon . . . 550
13.6.4 Rugby ball . . . 551
13.6.5 Inflation of initially flat membranes . . . 552

13.6.6 Rubber cylinder pressed between two plates . . . 555
13.6.7 Elastomeric bead compression . . . 556
13.7 Hyperelasticity with damage: the Mullins effect . . . 557
13.7.1 The Gurtin–Francis uniaxial model . . . 560
13.7.2 Three-dimensional modelling. A brief review . . . 562
13.7.3 A simple rate-independent three-dimensional model . . . 562
13.7.4 Example: the model problem . . . 565
13.7.5 Computational implementation . . . 565
13.7.6 Example: inflation/deflation of a damageable rubber balloon . . . 569

14 Finite strain elastoplasticity **573**
14.1 Finite strain elastoplasticity: a brief review . . . 574
14.2 One-dimensional finite plasticity model . . . 575
14.2.1 The multiplicative split of the axial stretch . . . 575
14.2.2 Logarithmic stretches and the Hencky hyperelastic law . . . 576
14.2.3 The yield function . . . 576
14.2.4 The plastic flow rule . . . 576
14.2.5 The hardening law . . . 577
14.2.6 The plastic multiplier . . . 577
14.3 General hyperelastic-based multiplicative plasticity model . . . 578
14.3.1 Multiplicative elastoplasticity kinematics . . . 578
14.3.2 The logarithmic elastic strain measure . . . 582
14.3.3 A general isotropic large-strain plasticity model . . . 583
14.3.4 The dissipation inequality . . . 586
14.3.5 Finite strain extension to infinitesimal theories . . . 588
14.4 The general elastic predictor/return-mapping algorithm . . . 590
14.4.1 The basic constitutive initial value problem . . . 590
14.4.2 Exponential map backward discretisation . . . 591
14.4.3 Computational implementation of the general algorithm . . . 595
14.5 The consistent spatial tangent modulus . . . 597
14.5.1 Derivation of the spatial tangent modulus . . . 598
14.5.2 Computational implementation . . . 599
14.6 Principal stress space-based implementation . . . 599
14.6.1 Stress-updating algorithm . . . 600
14.6.2 Tangent modulus computation . . . 601
14.7 Finite plasticity in plane stress . . . 601
14.7.1 The plane stress-projected finite von Mises model . . . 601
14.7.2 Nested iteration for plane stress enforcement . . . 604
14.8 Finite viscoplasticity . . . 605
14.8.1 Numerical treatment . . . 606
14.9 Examples . . . 606
14.9.1 Finite strain bending of a V-notched Tresca bar . . . 606
14.9.2 Necking of a cylindrical bar . . . 607
14.9.3 Plane strain localisation . . . 611
14.9.4 Stretching of a perforated plate . . . 613
14.9.5 Thin sheet metal-forming application . . . 614

14.10 Rate forms: hypoelastic-based plasticity models . . . 615
14.10.1 Objective stress rates . . . 619
14.10.2 Hypoelastic-based plasticity models . . . 621
14.10.3 The Jaumann rate-based model . . . 622
14.10.4 Hyperelastic-based models and equivalent rate forms . . . 624
14.10.5 Integration algorithms and incremental objectivity . . . 625
14.10.6 Objective algorithm for Jaumann rate-based models . . . 628
14.10.7 Integration of Green–Naghdi rate-based models . . . 632
14.11 Finite plasticity with kinematic hardening . . . 633
14.11.1 A model of finite strain kinematic hardening . . . 633
14.11.2 Integration algorithm . . . 637
14.11.3 Spatial tangent operator . . . 642
14.11.4 Remarks on predictive capability . . . 644
14.11.5 Alternative descriptions . . . 644

15 Finite elements for large-strain incompressibility **647**
15.1 The *F-bar* methodology . . . 648
15.1.1 Stress computation: the *F-bar* deformation gradient . . . 649
15.1.2 The internal force vector . . . 651
15.1.3 Consistent linearisation: the tangent stiffness . . . 652
15.1.4 Plane strain implementation . . . 655
15.1.5 Computational implementation aspects . . . 656
15.1.6 Numerical tests . . . 656
15.1.7 Other centroid sampling-based *F-bar* elements . . . 663
15.1.8 A more general *F-bar* methodology . . . 663
15.1.9 The *F-bar*-Patch Method for simplex elements . . . 665
15.2 Enhanced assumed strain methods . . . 669
15.2.1 Enhanced three-field variational principle . . . 669
15.2.2 EAS finite elements . . . 671
15.2.3 Finite element equations: static condensation . . . 676
15.2.4 Implementation aspects . . . 678
15.2.5 The stability of EAS elements . . . 678
15.3 Mixed *u/p* formulations . . . 683
15.3.1 The two-field variational principle . . . 683
15.3.2 Finite element equations . . . 685
15.3.3 Solution: static condensation . . . 687
15.3.4 Implementation aspects . . . 689

16 Anisotropic finite plasticity: Single crystals **691**
16.1 Physical aspects . . . 692
16.1.1 Plastic deformation by slip: slip-systems . . . 692
16.2 Plastic slip and the Schmid resolved shear stress . . . 693
16.3 Single crystal simulation: a brief review . . . 694
16.4 A general continuum model of single crystals . . . 694
16.4.1 The plastic flow equation . . . 695
16.4.2 The resolved Schmid shear stress . . . 696

16.4.3 Multisurface formulation of the flow rule 696
16.4.4 Isotropic Taylor hardening 698
16.4.5 The hyperelastic law 698
16.5 A general integration algorithm 699
16.5.1 The search for an active set of slip systems 703
16.6 An algorithm for a planar double-slip model 705
16.6.1 A planar double-slip model 705
16.6.2 The integration algorithm 707
16.6.3 Example: the model problem 710
16.7 The consistent spatial tangent modulus 713
16.7.1 The elastic modulus: compressible neo-Hookean model 713
16.7.2 The elastoplastic consistent tangent modulus 714
16.8 Numerical examples 716
16.8.1 Symmetric strain localisation on a rectangular strip 717
16.8.2 Unsymmetric localisation 720
16.9 Viscoplastic single crystals 721
16.9.1 Rate-dependent formulation 723
16.9.2 The exponential map-based integration algorithm 724
16.9.3 The spatial tangent modulus: neo-Hookean-based model 725
16.9.4 Rate-dependent crystal: model problem 726

Appendices **729**

A Isotropic functions of a symmetric tensor **731**
A.1 Isotropic scalar-valued functions 731
A.1.1 Representation 732
A.1.2 The derivative of an isotropic scalar function 732
A.2 Isotropic tensor-valued functions 733
A.2.1 Representation 733
A.2.2 The derivative of an isotropic tensor function 734
A.3 The two-dimensional case 735
A.3.1 Tensor function derivative 736
A.3.2 Plane strain and axisymmetric problems 738
A.4 The three-dimensional case 739
A.4.1 Function computation 739
A.4.2 Computation of the function derivative 740
A.5 A particular class of isotropic tensor functions 740
A.5.1 Two dimensions 742
A.5.2 Three dimensions 743
A.6 Alternative procedures 744

B The tensor exponential **747**
B.1 The tensor exponential function 747
B.1.1 Some properties of the tensor exponential function 748
B.1.2 Computation of the tensor exponential function 749
B.2 The tensor exponential derivative 750
B.2.1 Computer implementation 751
B.3 Exponential map integrators 751
B.3.1 The generalised exponential map midpoint rule 752

C Linearisation of the virtual work **753**
C.1 Infinitesimal deformations 753
C.2 Finite strains and deformations 755
C.2.1 Material description 755
C.2.2 Spatial description 756

D Array notation for computations with tensors **759**
D.1 Second-order tensors 759
D.2 Fourth-order tensors 761
D.2.1 Operations with non-symmetric tensors 763

References **765**

Index **783**

A simple example

Let $\mathscr{X}$ now be a space of sufficiently smooth[¶] functions $x : \mathscr{R}^n \to \mathscr{R}$. We define a *functional* $y : \mathscr{X} \to \mathscr{R}$ as

$$y(x) \equiv \int_\Omega \sin(x(\boldsymbol{p}))\, \mathrm{d}\boldsymbol{p}, \tag{2.153}$$

where $\Omega \subset \mathscr{R}^n$ is a given integration domain. Linearisation of the above functional about a given argument (function) x_0 is the following generalisation of (2.114):

$$l(u) = y(x_0) + \mathrm{D}y(x_0)\,[u] = \int_\Omega \sin(x_0(\boldsymbol{p}))\, \mathrm{d}\boldsymbol{p} + \mathrm{D}y(x_0)\,[u], \tag{2.154}$$

where the directional derivative $\mathrm{D}y(x_0)\,[u]$ is now a linear transformation on the *function* $u \in \mathscr{X}$ and can be determined by direct generalisation of (2.113):

$$\begin{aligned} \mathrm{D}y(x_0)\,[u] &= \frac{\mathrm{d}}{\mathrm{d}\epsilon} y(x_0 + \epsilon u)\bigg|_{\epsilon=0} \\ &= \frac{\mathrm{d}}{\mathrm{d}\epsilon} \int_\Omega \sin(x_0(\boldsymbol{p}) + \epsilon\, u(\boldsymbol{p}))\, \mathrm{d}\boldsymbol{p}\bigg|_{\epsilon=0} \\ &= \int_\Omega \cos(x_0(\boldsymbol{p}))\, u(\boldsymbol{p})\, \mathrm{d}\boldsymbol{p}. \end{aligned} \tag{2.155}$$

From the above, the linearisation of the functional (2.153) at x_0 is then established as

$$l(u) = \int_\Omega \sin(x_0(\boldsymbol{p}))\, \mathrm{d}\boldsymbol{p} + \int_\Omega \cos(x_0(\boldsymbol{p}))\, u(\boldsymbol{p})\, \mathrm{d}\boldsymbol{p}. \tag{2.156}$$

[¶]To avoid a precise statement of regularity properties of functions, we frequently use the term *sufficiently smooth* in the present text, meaning that functions have a sufficient degree of regularity so that all operations in which they are involved are properly defined.

3 ELEMENTS OF CONTINUUM MECHANICS AND THERMODYNAMICS

THIS chapter reviews some basic concepts of mechanics and thermodynamics of continuous media. The definitions and notation introduced will be systematically employed throughout the subsequent chapters of this book. The material presented here is well established in the continuum mechanics literature and an effort has been made to follow the notation and nomenclature in use in standard textbooks (Billington and Tate, 1981; Bonet and Wood, 1997; Ciarlet, 1988; Gurtin, 1981; Lemaitre and Chaboche, 1990; Ogden, 1984; Spencer, 1980; Truesdell and Noll, 1965).

3.1. Kinematics of deformation

Let $\mathscr{B}$ be a *body* which occupies an open region Ω of the three-dimensional Euclidean space $\mathscr{E}$ with a regular boundary $\partial\Omega$ in its *reference* configuration. A *deformation* of $\mathscr{B}$ (Figure 3.1) is defined by a smooth one-to-one function

$$\boldsymbol{\varphi} : \Omega \to \mathscr{E}$$

that maps each material particle[†] $\boldsymbol{p}$ of $\mathscr{B}$ into a point

$$\boldsymbol{x} = \boldsymbol{\varphi}(\boldsymbol{p}) \tag{3.1}$$

where the particle is positioned in the *deformed* configuration of $\mathscr{B}$. The region of $\mathscr{E}$ occupied by $\mathscr{B}$ in its deformed configuration will be denoted

$$\boldsymbol{\varphi}(\Omega).$$

The vector field $\boldsymbol{u}(\boldsymbol{p})$, defined by

$$\boldsymbol{u}(\boldsymbol{p}) = \boldsymbol{\varphi}(\boldsymbol{p}) - \boldsymbol{p}, \tag{3.2}$$

is the *displacement* of $\boldsymbol{p}$. Thus, one may write

$$\boldsymbol{x} = \boldsymbol{p} + \boldsymbol{u}(\boldsymbol{p}). \tag{3.3}$$

[†]For convenience, material particles of $\mathscr{B}$ will be identified with their positions in the reference configuration of $\mathscr{B}$.

Computational Methods for Plasticity: Theory and Applications EA de Souza Neto, D Perić and DRJ Owen

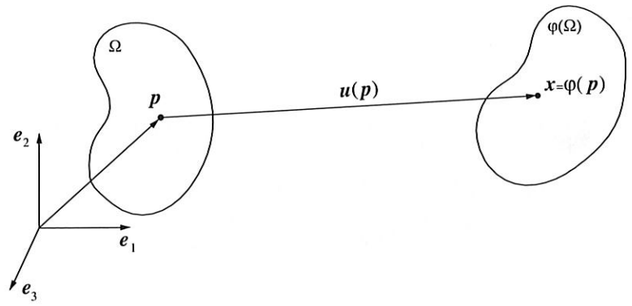

Figure 3.1. Deformation.

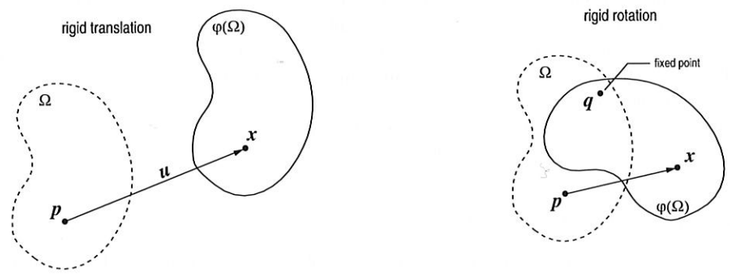

Figure 3.2. Rigid deformations.

A *rigid deformation* of $\mathscr{B}$ is a deformation that preserves the distances between all material particles of $\mathscr{B}$. A rigid deformation (Figure 3.2) can be a translation, a rotation, or a combination of a translation and a rotation. A *rigid translation* is a deformation with constant displacement vector ($\boldsymbol{u}$ independent of $\boldsymbol{p}$):

$$\boldsymbol{\varphi}(\boldsymbol{p}) = \boldsymbol{p} + \boldsymbol{u}. \tag{3.4}$$

A *rigid rotation* is a deformation that can be expressed as

$$\boldsymbol{\varphi}(\boldsymbol{p}) = \boldsymbol{q} + \boldsymbol{R}\,(\boldsymbol{p} - \boldsymbol{q}), \tag{3.5}$$

where $\boldsymbol{R}$ is a proper orthogonal tensor (a rotation) and $\boldsymbol{q}$ is the point about which $\mathscr{B}$ is rotated. A deformation is rigid, including translations and/or rotations, if and only if it can be expressed in the form:

$$\boldsymbol{\varphi}(\boldsymbol{p}) = \boldsymbol{\varphi}(\boldsymbol{q}) + \boldsymbol{R}\,(\boldsymbol{p} - \boldsymbol{q}). \tag{3.6}$$

The deformation map above represents a rigid translation with displacement $\boldsymbol{\varphi}(\boldsymbol{q}) - \boldsymbol{q}$ superimposed on a rigid rotation $\boldsymbol{R}$ about point $\boldsymbol{q}$.

A time-dependent deformation of $\mathscr{B}$ is called a *motion* of $\mathscr{B}$. A motion (Figure 3.3) is defined by a function

$$\boldsymbol{\varphi} : \Omega \times \mathscr{R} \to \mathscr{E},$$

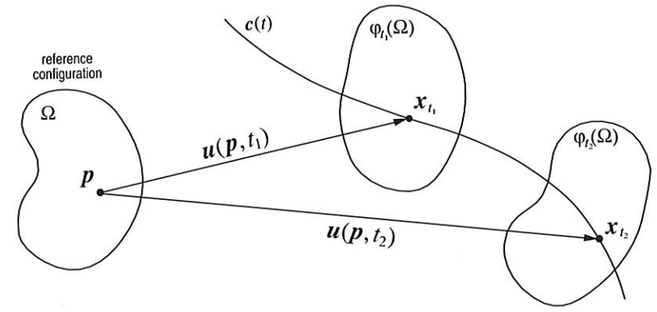

Figure 3.3. Motion.

so that for each time t, the map $\boldsymbol{\varphi}(\cdot, t)$ is a deformation of $\mathscr{B}$. The deformation map at time t will be also denoted $\boldsymbol{\varphi}_t$. During the motion $\boldsymbol{\varphi}$, the position $\boldsymbol{x}$ of a material particle $\boldsymbol{p}$ at time t is given by

$$\boldsymbol{x} = \boldsymbol{\varphi}(\boldsymbol{p}, t). \tag{3.7}$$

Similarly,

$$\boldsymbol{\varphi}(\Omega, t)$$

will denote the region of $\mathscr{E}$ occupied by the body $\mathscr{B}$ at time t. In terms of the displacement field the motion is expressed as

$$\boldsymbol{\varphi}(\boldsymbol{p}, t) = \boldsymbol{p} + \boldsymbol{u}(\boldsymbol{p}, t). \tag{3.8}$$

The parametric curve $\boldsymbol{c}(t)$, defined as

$$\boldsymbol{c}(t) = \boldsymbol{\varphi}(\boldsymbol{p}, t) \tag{3.9}$$

for a *fixed* material point $\boldsymbol{p}$, describes the *trajectory* of $\boldsymbol{p}$ during the motion of $\mathscr{B}$.

During a motion $\boldsymbol{\varphi}$, the *velocity* of a material particle $\boldsymbol{p}$ is defined by

$$\dot{\boldsymbol{x}}(\boldsymbol{p}, t) = \frac{\partial \boldsymbol{\varphi}(\boldsymbol{p}, t)}{\partial t}. \tag{3.10}$$

Since at each time t the map $\boldsymbol{\varphi}(\cdot, t)$ is one-to-one (and hence invertible) by assumption, material points can be expressed in terms of the place they occupy at a time t as

$$\boldsymbol{p} = \boldsymbol{\varphi}^{-1}(\boldsymbol{x}, t) = \boldsymbol{x} - \boldsymbol{u}(\boldsymbol{\varphi}^{-1}(\boldsymbol{x}, t), t). \tag{3.11}$$

The map $\boldsymbol{\varphi}^{-1}$ is called the *reference map*. Using the reference map, one may define the function

$$\boldsymbol{v}(\boldsymbol{x}, t) \equiv \dot{\boldsymbol{x}}(\boldsymbol{\varphi}^{-1}(\boldsymbol{x}, t), t). \tag{3.12}$$

The field $\boldsymbol{v}$ is called the *spatial velocity* and gives the velocity of the material particle positioned at $\boldsymbol{x}$ at time t.

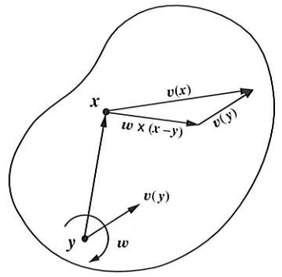

Figure 3.4. Rigid velocity.

A *rigid motion* of $\mathscr{B}$ is a motion for which, at each time t, the map $\varphi(\cdot, t)$ is a rigid deformation. A motion φ is rigid if and only if at each time t, the spatial velocity v admits the representation

$$v(x, t) = v(y, t) + W(t)\,(x - y) \tag{3.13}$$

for all $x, y \in \varphi(\Omega, t)$, with $W(t)$ a *skew* tensor. The velocity at x is given as the sum of a uniform velocity $v(y, t)$ and a superimposed rotation about the line that passes through y and is parallel to the axial vector associated to the skew tensor W. By denoting $w(t)$ the axial vector of $W(t)$, the velocity field above can be re-written as

$$v(x, t) = v(y, t) + w(t) \times (x - y), \tag{3.14}$$

which is the standard formula for the velocity field of classical rigid-body dynamics. The vector $w(t)$ is called the *angular velocity* of the body. The rigid velocity field is schematically illustrated in Figure 3.4.

3.1.1. MATERIAL AND SPATIAL FIELDS

Both fields $\dot{x}$ and v introduced above describe the velocity of material particles. However, $\dot{x}$ and v have different arguments. While $\dot{x}$ has material particle and time as arguments, the arguments of v are spatial position and time. This motivates the following definitions: Let a general time-dependent (scalar, vectorial or tensorial) field α be defined over the body $\mathscr{B}$. If the domain of α is $\Omega \times \mathscr{R}$, i.e. if the value of α is expressed as a function of material particles p (and time) then α is said to be a *material field*. On the other hand, if its domain is $\varphi_t(\Omega) \times \mathscr{R}$, then α is said to be a *spatial field*. Using (3.7), the *material description* of a spatial field $\alpha(x, t)$ is defined by

$$\alpha_m(p, t) = \alpha(\varphi(p, t), t). \tag{3.15}$$

Conversely, the *spatial description* of a material field $\beta(p, t)$ is defined by

$$\beta_s(x, t) = \beta(\varphi^{-1}(x, t), t). \tag{3.16}$$

It should be noted that *any* field associated with a motion of $\mathscr{B}$ can be expressed as a function of time and material particles *or* spatial position. A material (spatial) field does

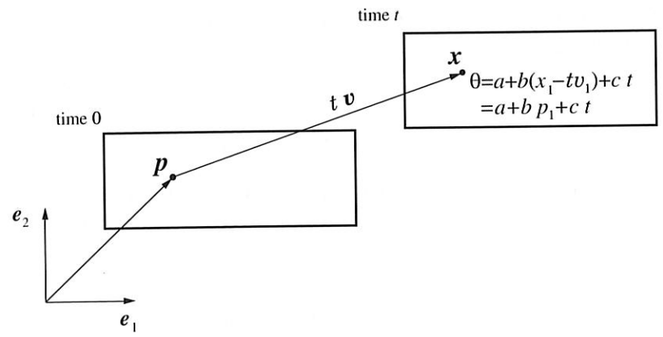

Figure 3.5. Material and spatial descriptions.

not necessarily represent a quantity physically associated with the reference (deformed) configuration of the body.

Example 3.1.1. Consider, for instance, the rectangular body of Figure 3.5 subjected to the *rigid translation*:

$$x = \varphi(p, t) \equiv p + t\,v,$$

with constant velocity v. Assume that, during the motion φ, the temperature field of the body in question is linearly distributed along its longitudinal axis and varies uniformly throughout the body at a constant rate. Taking the initial configuration (at $t = 0$) as the reference configuration (and, therefore, labelling material particles of the body with their position p at time 0), the material description of this temperature field reads

$$\theta_m(p, t) = a + b\,p_1 + c\,t,$$

where a, b and c are constants. In view of the assumed motion φ, the spatial description of the same field is given by

$$\theta_s(x, t) = \theta_m(p(x, t), t) = a + b(x_1 - t\,v_1) + c\,t.$$

Note that, in spite of having p as one of its arguments, θ_m (as θ_s) expresses a physical quantity associated with the configuration of time t. The spatial description θ_s gives the temperature, at time t, of the material particle whose position at time t is x. In experimental terms, it would be the temperature read from a thermometer held fixed in space at x. The function θ_m gives the temperature, at time t, of the material particle whose position at time 0 is p. It would be the temperature indicated by a thermometer attached to this material particle.

To avoid notational complexity, the subscripts m and s employed above to denote the material and spatial descriptions of general fields will not be used throughout this book unless absolutely necessary. In general, the description employed will be evident either from the context or from the argument used (p or x).

3.1.2. MATERIAL AND SPATIAL GRADIENTS, DIVERGENCES AND TIME DERIVATIVES

The *material* and *spatial gradients* of a general field α, denoted respectively $\nabla_p \alpha$ and $\nabla_x \alpha$, are defined as

$$\nabla_p \alpha = \frac{\partial}{\partial \boldsymbol{p}} \alpha_m(\boldsymbol{p}, t), \quad \nabla_x \alpha = \frac{\partial}{\partial \boldsymbol{x}} \alpha_s(\boldsymbol{x}, t), \tag{3.17}$$

i.e. they are, respectively, the derivatives of α with respect to $\boldsymbol{p}$ and $\boldsymbol{x}$ holding t fixed.

Similarly, the *material* and *spatial time derivatives* of α, denoted respectively $\dot{\alpha}$ and α', are defined by

$$\dot{\alpha} = \frac{\partial}{\partial t} \alpha_m(\boldsymbol{p}, t), \quad \alpha' = \frac{\partial}{\partial t} \alpha_s(\boldsymbol{x}, t). \tag{3.18}$$

The material time derivative $\dot{\alpha}$ measures the rate of change of α at a *fixed material particle* $\boldsymbol{p}$. The spatial time derivative, on the other hand, measures the rate of change of α observed at a *fixed spatial position* $\boldsymbol{x}$. In the example of Figure 3.5, the material and spatial time derivatives of the temperature field θ are given by

$$\dot{\theta} = c, \quad \theta' = -b\, v_1 + c.$$

The material time derivative in this case corresponds to the temperature rate computed from a thermometer attached to a material particle $\boldsymbol{p}$ whilst θ' is the temperature rate observed in a thermometer held fixed in space at $\boldsymbol{x}$. Note that the extra term $-b\, v_1$ added to θ' is a contribution to the rate of change of temperature at $\boldsymbol{x}$ due to the motion of the body combined with its non-uniform distribution of temperature. This contribution vanishes if the body moves parallel to $\boldsymbol{e}_2$ ($v_1 = 0$), i.e. the direction of temperature isolines. It would also vanish if the temperature were uniform throughout the body ($b = 0$).

Analogously to (2.145) (page 37), we define the *spatial* and *material divergence* of a vector field $\boldsymbol{v}$, respectively, as

$$\mathrm{div}_p\, \boldsymbol{v} = \mathrm{tr}(\nabla_p \boldsymbol{v}), \quad \mathrm{div}_x\, \boldsymbol{v} = \mathrm{tr}(\nabla_x \boldsymbol{v}). \tag{3.19}$$

In addition (refer to (2.147)), for a tensor field $\boldsymbol{T}$, the spatial and material divergence are given, in Cartesian components, by

$$(\mathrm{div}_x\, \boldsymbol{T})_i = \frac{\partial T_{ij}}{\partial x_j}, \quad (\mathrm{div}_p\, \boldsymbol{T})_i = \frac{\partial T_{ij}}{\partial p_j}. \tag{3.20}$$

The compact definition (2.146) is also applicable to the material and spatial divergence of a tensor.

3.1.3. THE DEFORMATION GRADIENT

The *deformation gradient* of the motion $\boldsymbol{\varphi}$ is the second-order tensor $\boldsymbol{F}$ defined by

$$\boldsymbol{F}\,(\boldsymbol{p}, t) = \nabla_p \boldsymbol{\varphi}(\boldsymbol{p}, t) = \frac{\partial \boldsymbol{x}_t}{\partial \boldsymbol{p}}. \tag{3.21}$$

In view of (3.8) it can be written as

$$\boldsymbol{F} = \boldsymbol{I} + \nabla_p \boldsymbol{u}. \tag{3.22}$$

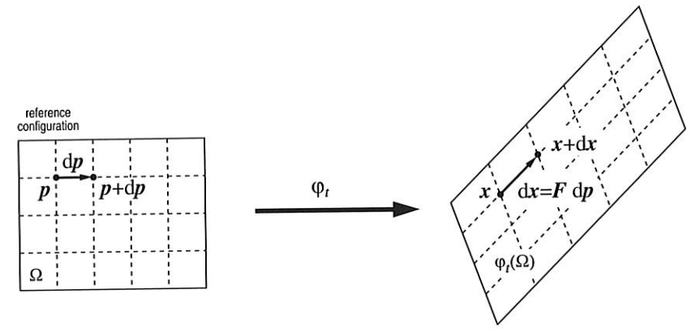

Figure 3.6. The deformation gradient.

The Cartesian components of $\boldsymbol{F}$ are given by

$$\begin{aligned} F_{ij} &= \frac{\partial x_i}{\partial p_j} \\ &= \delta_{ij} + \frac{\partial u_i}{\partial p_j}, \end{aligned} \tag{3.23}$$

where x_i denote the components of $\boldsymbol{x}_t$. In terms of the reference map (3.11), the deformation gradient may be equivalently expressed as

$$\boldsymbol{F}\,(\boldsymbol{x}, t) = [\nabla_x \boldsymbol{\varphi}^{-1}(\boldsymbol{x}, t)]^{-1} = [\boldsymbol{I} - \nabla_x \boldsymbol{u}]^{-1}. \tag{3.24}$$

Consider the infinitesimal material fibre $\mathrm{d}\boldsymbol{p}$ that connects two neighbouring material particles $\boldsymbol{p}$ and $\boldsymbol{p} + \mathrm{d}\boldsymbol{p}$ of a deforming body (Figure 3.6). Under the deformation $\boldsymbol{\varphi}_t$, these particles are mapped, respectively, into $\boldsymbol{x}$ and $\boldsymbol{x} + \mathrm{d}\boldsymbol{x}$. The deformation gradient is the linear operator that relates infinitesimal material fibres $\mathrm{d}\boldsymbol{p}$ with their deformed counterparts $\mathrm{d}\boldsymbol{x}$:

$$\mathrm{d}\boldsymbol{x} = \boldsymbol{F}\ \mathrm{d}\boldsymbol{p}. \tag{3.25}$$

A deformation of $\mathscr{B}$ with uniform deformation gradient ($\boldsymbol{F}$ independent of $\boldsymbol{p}$) is called a *homogeneous deformation*. A deformation is homogeneous if and only if it admits the representation

$$\boldsymbol{\varphi}(\boldsymbol{p}) = \boldsymbol{\varphi}(\boldsymbol{q}) + \boldsymbol{F}\,(\boldsymbol{p} - \boldsymbol{q}) \tag{3.26}$$

for all points $\boldsymbol{p}$, $\boldsymbol{q} \in \mathscr{B}$, with $\boldsymbol{F}$ a positive definite tensor. Clearly, rigid translations and rotations are homogeneous deformations.

3.1.4. VOLUME CHANGES. THE DETERMINANT OF THE DEFORMATION GRADIENT

Consider now the infinitesimal volume $\mathrm{d}v_0$ defined by the infinitesimal vectors $\mathrm{d}\boldsymbol{a}$, $\mathrm{d}\boldsymbol{b}$ and $\mathrm{d}\boldsymbol{c}$ emanating from the material particle $\boldsymbol{p}$ in the reference configuration (Figure 3.7). Trivially,

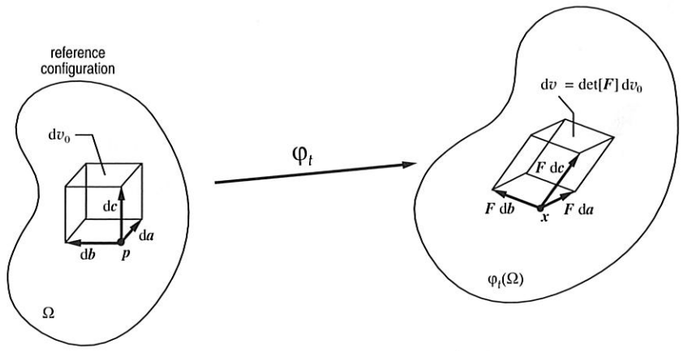

Figure 3.7. The determinant of the deformation gradient.

one has

$$\mathrm{d}v_0 = (\mathrm{d}\boldsymbol{a} \times \mathrm{d}\boldsymbol{b}) \cdot \mathrm{d}\boldsymbol{c}. \tag{3.27}$$

The deformation φ_t maps the infinitesimal vectors, respectively, into $\boldsymbol{F}\,\mathrm{d}\boldsymbol{a}$, $\boldsymbol{F}\,\mathrm{d}\boldsymbol{b}$ and $\boldsymbol{F}\,\mathrm{d}\boldsymbol{c}$, so that the deformed infinitesimal volume is given by

$$\mathrm{d}v = (\boldsymbol{F}\,\mathrm{d}\boldsymbol{a} \times \boldsymbol{F}\,\mathrm{d}\boldsymbol{b}) \cdot \boldsymbol{F}\,\mathrm{d}\boldsymbol{c}. \tag{3.28}$$

By making use of identity (2.54), it follows that

$$\det \boldsymbol{F} = \frac{\mathrm{d}v}{\mathrm{d}v_0}, \tag{3.29}$$

i.e. the determinant of the deformation gradient represents, locally, the volume after deformation per unit reference volume (or *volume change ratio*). Throughout this book, we will adopt the following notation

$$J \equiv \det \boldsymbol{F}. \tag{3.30}$$

From (3.29) it follows that if $\det \boldsymbol{F} = 0$, then the infinitesimal volume has collapsed into a material particle. Since the body is not allowed to penetrate itself (this restriction is embodied in the assumption that the deformation map is one-to-one), this represents a physically unacceptable situation. Also note that, at the reference configuration, $\boldsymbol{F} = \boldsymbol{I}$ and, consequently, $J = 1$. Thus, a configuration with $J < 0$ cannot be reached from the reference configuration without having, at some stage, $J = 0$. Therefore, in any deformed configuration of a body, J satisfies

$$J > 0. \tag{3.31}$$

Isochoric deformations

Isochoric (or *volume-preserving*) deformations are deformations that do not produce changes in volume. A locally isochoric deformation is characterised by

$$J = 1. \tag{3.32}$$

Volumetric deformations

Volumetric deformations (i.e. *pure contractions/dilations*) are deformations consisting purely of a uniform contraction/dilation in all directions. The deformation gradient of any volumetric deformation is a spherical tensor:

$$\boldsymbol{F} = \alpha\, \boldsymbol{I}, \tag{3.33}$$

where the *scalar* α is the corresponding contraction/dilation ratio. With l_0 and l denoting, respectively, the undeformed and deformed lengths of a material fibre, for a locally volumetric deformation we have:

$$\frac{l}{l_0} = \alpha \tag{3.34}$$

in *all directions*.

3.1.5. ISOCHORIC/VOLUMETRIC SPLIT OF THE DEFORMATION GRADIENT

Any deformation can be locally decomposed as a purely volumetric deformation followed by an isochoric deformation or as an isochoric deformation followed by a pure volumetric deformation. To see this, note that the deformation gradient can always be multiplicatively split as

$$\boldsymbol{F} = \boldsymbol{F}_{\mathrm{iso}}\, \boldsymbol{F}_{\mathrm{v}} = \boldsymbol{F}_{\mathrm{v}}\, \boldsymbol{F}_{\mathrm{iso}}, \tag{3.35}$$

where

$$\boldsymbol{F}_{\mathrm{v}} \equiv (\det \boldsymbol{F})^{\frac{1}{3}}\, \boldsymbol{I} \tag{3.36}$$

is the *volumetric* component of $\boldsymbol{F}$ and

$$\boldsymbol{F}_{\mathrm{iso}} \equiv (\det \boldsymbol{F})^{-\frac{1}{3}}\, \boldsymbol{F} \tag{3.37}$$

is the *isochoric* (*volume-preserving* or *unimodular*) component. Note that, by construction, $\boldsymbol{F}_{\mathrm{v}}$ corresponds indeed to a purely volumetric deformation (it has the representation (3.33)) and, since

$$\det \boldsymbol{F}_{\mathrm{v}} = [(\det \boldsymbol{F})^{\frac{1}{3}}]^3 \det \boldsymbol{I} = \det \boldsymbol{F}, \tag{3.38}$$

$\boldsymbol{F}_{\mathrm{v}}$ produces the same volume change as $\boldsymbol{F}$. The isochoric component in turn represents a volume preserving deformation, that is,

$$\det \boldsymbol{F}_{\mathrm{iso}} = [(\det \boldsymbol{F})^{-\frac{1}{3}}]^3 \det \boldsymbol{F} = 1. \tag{3.39}$$

3.1.6. POLAR DECOMPOSITION. STRETCHES AND ROTATION

By applying the *polar decomposition* to the deformation gradient, one obtains:

$$\boldsymbol{F} = \boldsymbol{R}\boldsymbol{U} = \boldsymbol{V}\boldsymbol{R}, \tag{3.40}$$

where the proper orthogonal tensor $\boldsymbol{R}$ is the local *rotation tensor* and the symmetric positive definite tensors $\boldsymbol{U}$ and $\boldsymbol{V}$ are, respectively, the *right* and *left stretch tensors*. The right and left stretch tensors are related by the rotation

$$\boldsymbol{V} = \boldsymbol{R}\boldsymbol{U}\boldsymbol{R}^T. \tag{3.41}$$

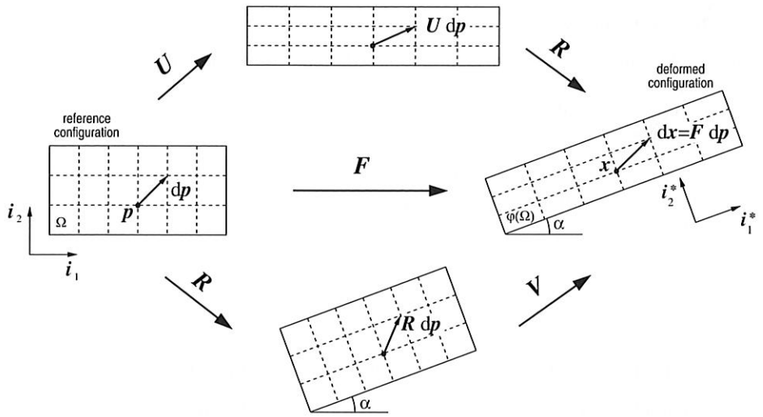

Figure 3.8. Polar decomposition of the deformation gradient. Stretches and rotation.

The stretch tensors $\boldsymbol{U}$ and $\boldsymbol{V}$ can be expressed as

$$\boldsymbol{U} = \sqrt{\boldsymbol{C}}, \quad \boldsymbol{V} = \sqrt{\boldsymbol{B}}, \tag{3.42}$$

where $\boldsymbol{C}$ and $\boldsymbol{B}$ – named, respectively, the *right* and *left Cauchy–Green strain tensors* – are defined by

$$\boldsymbol{C} = \boldsymbol{U}^2 = \boldsymbol{F}^T\boldsymbol{F}, \quad \boldsymbol{B} = \boldsymbol{V}^2 = \boldsymbol{F}\,\boldsymbol{F}^T. \tag{3.43}$$

Example 3.1.2 (A simple plane deformation). To illustrate the meaning of the polar decomposition of $\boldsymbol{F}$, a simple example consisting of a body subjected to a homogeneous deformation, i.e. with $\boldsymbol{F}$ independent of $\boldsymbol{p}$, is given in what follows. Consider the rectangular body of Figure 3.8 subjected to homogeneous stretching/compression in the directions of its longitudinal and transversal axes (respectively, the directions of $\boldsymbol{i}_1$ and $\boldsymbol{i}_2$ in the reference configuration) with a superimposed rigid rotation of angle α. With p_i and x_i denoting coordinates of $\boldsymbol{p}$ and $\boldsymbol{x}$ in the Cartesian system associated with the orthonormal basis $\{\boldsymbol{i}_1, \boldsymbol{i}_2\}$, the deformation map is defined as

$$\varphi : \begin{cases} x_1 = p_1\,\lambda_1\,\cos\alpha - p_2\,\lambda_2\,\sin\alpha \\ x_2 = p_1\,\lambda_1\,\sin\alpha + p_2\,\lambda_2\,\cos\alpha, \end{cases} \tag{3.44}$$

where the factors λ_1 and λ_2 determine how much stretching/compression occurs, respectively, along the longitudinal and transversal axes. In the basis $\{\boldsymbol{i}_1, \boldsymbol{i}_2\}$, the matrix representation of the corresponding deformation gradient is given by

$$\boldsymbol{F} = \begin{bmatrix} \lambda_1\,\cos\alpha & -\lambda_2\,\sin\alpha \\ \lambda_1\,\sin\alpha & \lambda_2\,\cos\alpha \end{bmatrix}. \tag{3.45}$$

The rotation tensor, obtained from the polar decomposition of $\boldsymbol{F}$, is represented by

$$\boldsymbol{R} = \begin{bmatrix} \cos\alpha & -\sin\alpha \\ \sin\alpha & \cos\alpha \end{bmatrix} \tag{3.46}$$

and the right and left stretch tensors by

$$\boldsymbol{U} = \begin{bmatrix} \lambda_1 & 0 \\ 0 & \lambda_2 \end{bmatrix} \tag{3.47}$$

and

$$\boldsymbol{V} = \begin{bmatrix} \lambda_1\,\cos^2\alpha + \lambda_2\,\sin^2\alpha & (\lambda_1 - \lambda_2)\,\sin\alpha\,\cos\alpha \\ (\lambda_1 - \lambda_2)\,\sin\alpha\,\cos\alpha & \lambda_1\,\sin^2\alpha + \lambda_2\,\cos^2\alpha \end{bmatrix}. \tag{3.48}$$

Insight into the meaning of the polar decomposition of the deformation gradient can be gained by focusing now on the generic infinitesimal fibre represented by $\mathrm{d}\boldsymbol{p}$ in Figure 3.8. Under deformation, $\mathrm{d}\boldsymbol{p}$ is mapped into $\mathrm{d}\boldsymbol{x} = \boldsymbol{F}\,\mathrm{d}\boldsymbol{p}$. With use of the polar decomposition of $\boldsymbol{F}$, this mapping can be split into two sequential steps. If the *right* polar decomposition $\boldsymbol{F} = \boldsymbol{R}\,\boldsymbol{U}$ is used, the two steps are:

1. $\mathrm{d}\boldsymbol{p} \longrightarrow \boldsymbol{U}\,\mathrm{d}\boldsymbol{p}$,
2. $\boldsymbol{U}\,\mathrm{d}\boldsymbol{p} \longrightarrow \boldsymbol{R}\,(\boldsymbol{U}\,\mathrm{d}\boldsymbol{p}) = \boldsymbol{F}\,\mathrm{d}\boldsymbol{p}$.

In the first operation, $\mathrm{d}\boldsymbol{p}$ deforms as if the body were being purely stretched (or compressed) along the directions of its longitudinal and transversal axes (which at this stage coincide with $\boldsymbol{i}_1$ and $\boldsymbol{i}_2$ respectively). The second mapping is a pure rotation (of angle α) of the deformed fibre $\boldsymbol{U}\,\mathrm{d}\boldsymbol{p}$ and corresponds to a rigid rotation of the body. If the *left* polar decomposition $\boldsymbol{F} = \boldsymbol{V}\boldsymbol{R}$ is employed instead, the sequence is reversed:

1. $\mathrm{d}\boldsymbol{p} \longrightarrow \boldsymbol{R}\,\mathrm{d}\boldsymbol{p}$,
2. $\boldsymbol{R}\,\mathrm{d}\boldsymbol{p} \longrightarrow \boldsymbol{V}(\boldsymbol{R}\,\mathrm{d}\boldsymbol{p}) = \boldsymbol{F}\,\mathrm{d}\boldsymbol{p}$.

In this case, the fibre is first rigidly rotated by an angle α. The second operation corresponds to the deformation of the fibre under pure stretching/compression of the body along its axial and transversal directions. However, due to the previous rotation, these directions coincide now with $\boldsymbol{i}_1^* = \boldsymbol{R}\,\boldsymbol{i}_1$ and $\boldsymbol{i}_2^* = \boldsymbol{R}\,\boldsymbol{i}_2$, respectively. Note that if the basis $\{\boldsymbol{i}_1^*, \boldsymbol{i}_2^*\}$ is used, the matrix representation of $\boldsymbol{V}$ reads

$$\boldsymbol{V} = \begin{bmatrix} \lambda_1 & 0 \\ 0 & \lambda_2 \end{bmatrix}, \tag{3.49}$$

so that the transformation $(\cdot) \to \boldsymbol{V}(\cdot)$ indeed corresponds to stretchings along the directions of $\boldsymbol{i}_1^*$ and $\boldsymbol{i}_2^*$.

The above example has illustrated the significance of the polar decomposition of $\boldsymbol{F}$. The discussion has been restricted to a homogeneous deformation only to ease visualisation of the stretches and rotation involved in the decomposition of the deformation gradient. It should be

remarked that for a generic deformation of a body, in which $\boldsymbol{F}$ is a function of $\boldsymbol{p}$, intermediate configurations of the body corresponding to pure stretching or pure rigid rotation (such as those illustrated in Figure 3.8) do not exist in general. Nevertheless, the interpretation of $\boldsymbol{U}$ and $\boldsymbol{V}$ as pure stretchings and of $\boldsymbol{R}$ as a rigid rotation remain valid in a *local* sense. Note that for *any* deformation φ, one may write:

$$\boldsymbol{x} + \mathrm{d}\boldsymbol{x} = \varphi(\boldsymbol{p} + \mathrm{d}\boldsymbol{p}) = \boldsymbol{p} + \boldsymbol{F}(\boldsymbol{p})\,\mathrm{d}\boldsymbol{p}, \tag{3.50}$$

that is, within an infinitesimal neighbourhood of a material point $\boldsymbol{p}$, the deformation behaves like a homogeneous deformation with gradient $\boldsymbol{F}(\boldsymbol{p})$. Thus, within this infinitesimal neighbourhood of $\boldsymbol{p}$, $\boldsymbol{U}(\boldsymbol{p})$ and $\boldsymbol{V}(\boldsymbol{p})$ measure stretches from $\boldsymbol{p}$ and $\boldsymbol{R}(\boldsymbol{p})$ measures the local rigid rotation.

Spectral decomposition of the stretch tensors

Since $\boldsymbol{U}$ and $\boldsymbol{V}$ are symmetric, it follows from the *spectral theorem* that they admit the spectral decomposition

$$\boldsymbol{U} = \sum_{i=1}^{3} \lambda_i\, \boldsymbol{l}_i \otimes \boldsymbol{l}_i, \quad \boldsymbol{V} = \sum_{i=1}^{3} \lambda_i\, \boldsymbol{e}_i \otimes \boldsymbol{e}_i, \tag{3.51}$$

where the $\{\lambda_1, \lambda_2, \lambda_3\}$ are the eigenvalues of $\boldsymbol{U}$ (and $\boldsymbol{V}$) named the *principal stretches*. The vectors $\boldsymbol{l}_i$ and $\boldsymbol{e}_i$ are unit eigenvectors of $\boldsymbol{U}$ and $\boldsymbol{V}$ respectively. The triads $\{\boldsymbol{l}_1, \boldsymbol{l}_2, \boldsymbol{l}_3\}$ and $\{\boldsymbol{e}_1, \boldsymbol{e}_2, \boldsymbol{e}_3\}$ form orthonormal bases for the space $\mathscr{V}$ of vectors in $\mathscr{E}$. They are called, respectively, the *Lagrangian* and *Eulerian triads* and define the *Lagrangian* and *Eulerian principal directions*.

Substitution of (3.41) into (3.51) gives the following relationship between the eigenvectors of $\boldsymbol{V}$ and $\boldsymbol{U}$:

$$\boldsymbol{l}_i = \boldsymbol{R}\,\boldsymbol{e}_i, \tag{3.52}$$

that is, each vector $\boldsymbol{e}_i$ differs from the corresponding $\boldsymbol{l}_i$ by a rotation $\boldsymbol{R}$.

The spectral decomposition of the right and left stretch tensors implies that in *any* deformation, the local stretching from a material particle can always be expressed as a superposition of stretches along three mutually orthogonal directions. In the example discussed above, illustrated by Figure 3.8, $\{\lambda_1, \lambda_2\}$ are the principal stretches and the Lagrangian and Eulerian bases are, respectively, $\{\boldsymbol{i}_1, \boldsymbol{i}_2\}$ and $\{\boldsymbol{i}_1^*, \boldsymbol{i}_2^*\}$.

3.1.7. STRAIN MEASURES

In the above section, we have seen that in a local sense, i.e. within an infinitesimal neighbourhood of a generic material particle $\boldsymbol{p}$, pure rotations can be distinguished from pure stretching by means of the polar decomposition of the deformation gradient. Under the action of pure rotations, the distances between particles within this neighbourhood remain fixed. When the distances between material particles are identical to their values in the reference configuration, we say that the region surrounding $\boldsymbol{p}$ is *unstrained*. In this case, the difference between the deformed neighbourhood of $\boldsymbol{p}$ and its reference configuration is a rigid deformation. Pure stretching, on the other hand, characterised by $\boldsymbol{U}$ or $\boldsymbol{V}$, changes the

distance between material particles. Under stretching, we say that the region surrounding $\boldsymbol{p}$ is *strained*. To quantify straining, i.e. to evaluate how much $\boldsymbol{U}$ (or $\boldsymbol{V}$) departs from $\boldsymbol{I}$ (a rigid deformation), some kind of *strain measure* needs to be defined.

Let us consider, again, the generic material fibre represented by the infinitesimal vector $\mathrm{d}\boldsymbol{p}$ that emanates from $\boldsymbol{p}$ (Figure 3.8 serves as an illustration). The deformation maps $\mathrm{d}\boldsymbol{p}$ into $\mathrm{d}\boldsymbol{x} = \boldsymbol{F}\,\mathrm{d}\boldsymbol{p}$. Thus, the square of the deformed length of the material fibre in question reads

$$\|\mathrm{d}\boldsymbol{x}\|^2 = \boldsymbol{F}\,\mathrm{d}\boldsymbol{p} \cdot \boldsymbol{F}\,\mathrm{d}\boldsymbol{p} = \boldsymbol{C}\,\mathrm{d}\boldsymbol{p} \cdot \mathrm{d}\boldsymbol{p} = (\boldsymbol{I} + 2\,\boldsymbol{E}^{(2)})\,\mathrm{d}\boldsymbol{p} \cdot \mathrm{d}\boldsymbol{p}, \tag{3.53}$$

where $\boldsymbol{C} = \boldsymbol{F}^T\,\boldsymbol{F} = \boldsymbol{U}^2$ is the right Cauchy–Green tensor and the *strain measure* $\boldsymbol{E}^{(2)}$ (the meaning of the superscript will be made clear below) is the so-called *Green–Lagrange* strain tensor *defined* as

$$\begin{aligned} \boldsymbol{E}^{(2)} &= \tfrac{1}{2}(\boldsymbol{C} - \boldsymbol{I}) \\ &= \tfrac{1}{2}[\nabla_p \boldsymbol{u} + (\nabla_p \boldsymbol{u})^T + (\nabla_p \boldsymbol{u})^T \nabla_p \boldsymbol{u}]. \end{aligned} \tag{3.54}$$

No straining occurs, that is, the size of any infinitesimal material fibre emanating from $\boldsymbol{p}$ remains constant ($\|\mathrm{d}\boldsymbol{x}\| = \|\mathrm{d}\boldsymbol{p}\|, \ \forall\ \mathrm{d}\boldsymbol{p}$), if and only if $\boldsymbol{E}^{(2)} = \boldsymbol{0}$. This condition is equivalent to $\boldsymbol{C} = \boldsymbol{U} = \boldsymbol{I}$, implying that $\boldsymbol{F}$ is an orthogonal tensor and the deformation is rigid (pure translation and/or rotation) in the neighbourhood of $\boldsymbol{p}$. From the definition of $\boldsymbol{E}^{(2)}$, its eigenvectors coincide with the Lagrangian triad so that it can be expressed as

$$\boldsymbol{E}^{(2)} = \sum_{i=1}^{3} \tfrac{1}{2}(\lambda_i^2 - 1)\,\boldsymbol{l}_i \otimes \boldsymbol{l}_i, \tag{3.55}$$

and, since it measures strains along the principal *Lagrangian* directions, it is called a *Lagrangian strain measure*.

It must be emphasised that the Green–Lagrange strain measure is *defined* by expression (3.54). It is by no means the unique way of quantifying straining. In fact, the definition of a strain measure is somewhat arbitrary and a specific choice is usually dictated by mathematical and physical convenience. An important family of *Lagrangian strain tensors*, i.e. strain measures based on the Lagrangian triad, is defined by Seth (1964), Hill (1978) and Ogden (1984)

$$\boldsymbol{E}^{(m)} = \begin{cases} \dfrac{1}{m}(\boldsymbol{U}^m - \boldsymbol{I}) & m \neq 0 \\ \ln[\boldsymbol{U}] & m = 0 \end{cases} \tag{3.56}$$

where m is a real number and $\ln[\,\cdot\,]$ denotes the *tensor logarithm* of $[\,\cdot\,]$. Equivalently, in terms of its spectral decomposition, (3.56) may be rephrased as

$$\boldsymbol{E}^{(m)} = \sum_{i=1}^{3} f(\lambda_i)\,\boldsymbol{l}_i \otimes \boldsymbol{l}_i, \tag{3.57}$$

where

$$f(\lambda_i) = \begin{cases} \dfrac{1}{m}(\lambda_i^m - 1) & m \neq 0 \\ \ln \lambda_i & m = 0. \end{cases} \tag{3.58}$$

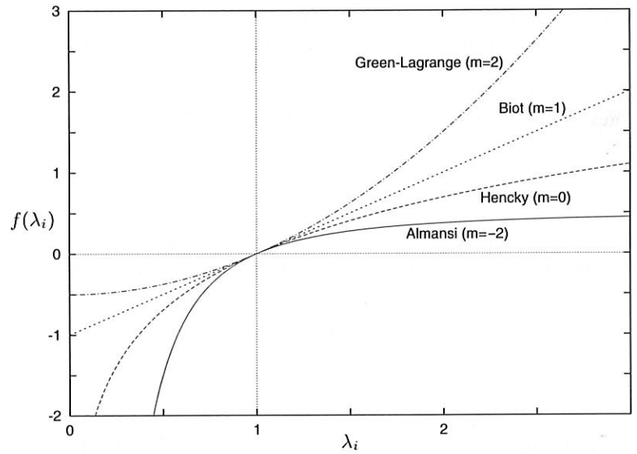

Figure 3.9. Strain measures. Principal strain as a function of the principal stretch for various strain measures.

The Green–Lagrange strain tensor, $\boldsymbol{E}^{(2)}$, is a particular member of this family (with $m = 2$). Other commonly used members of this family are the Biot ($m = 1$), Hencky ($m = 0$) and Almansi ($m = -2$) strain tensors. Note that for any m, the associated strain tensor vanishes if and only if the deformation gradient represents, locally, a rigid deformation, i.e.

$$\boldsymbol{E}^{(m)} = \boldsymbol{0} \iff \boldsymbol{U} = \boldsymbol{I} \iff \boldsymbol{F} = \boldsymbol{R}. \tag{3.59}$$

To illustrate the relationship between the stretch and strain tensors, the principal strain for various strain measures is plotted in Figure 3.9 as a function of the corresponding principal stretch.

Analogously to the strain measures discussed above, it is also possible to define tensors that measure strain along the principal *Eulerian* directions or, simply, *Eulerian strain tensors*. Based on the *left* stretch tensor, the Eulerian counterpart of the Lagrangian family of strain measures above is defined by

$$\boldsymbol{\varepsilon}^{(m)} = \begin{cases} \dfrac{1}{m}(\boldsymbol{V}^m - \boldsymbol{I}) & m \neq 0 \\ \ln[\boldsymbol{V}] & m = 0, \end{cases} \tag{3.60}$$

or, using the Eulerian triad,

$$\boldsymbol{\varepsilon}^{(m)} = \sum_{i=1}^{3} f(\lambda_i)\, \boldsymbol{e}_i \otimes \boldsymbol{e}_i. \tag{3.61}$$

Lagrangian and Eulerian strain tensors are related by

$$\boldsymbol{\varepsilon}^{(m)} = \boldsymbol{R}\, \boldsymbol{E}^{(m)} \boldsymbol{R}^T, \tag{3.62}$$

that is, they differ by the local rotation $\boldsymbol{R}$.

3.1.8. THE VELOCITY GRADIENT. RATE OF DEFORMATION AND SPIN

The spatial field $\boldsymbol{L}$, defined as

$$\boldsymbol{L} = \nabla_x \boldsymbol{v}, \tag{3.63}$$

is named the *velocity gradient*. Equivalently, with application of the chain rule one has

$$\boldsymbol{L} = \frac{\partial}{\partial t}\left(\frac{\partial \boldsymbol{\varphi}}{\partial \boldsymbol{p}}\right)\frac{\partial \boldsymbol{p}}{\partial \boldsymbol{x}} = \dot{\boldsymbol{F}}\, \boldsymbol{F}^{-1}. \tag{3.64}$$

Two important tensors are obtained by splitting $\boldsymbol{L}$ into its symmetric and skew parts. Namely, the *rate of deformation* tensor (also referred to as the *stretching* tensor), $\boldsymbol{D}$, and the *spin* tensor, $\boldsymbol{W}$, are defined by

$$\boldsymbol{D} = \mathrm{sym}(\boldsymbol{L}), \quad \boldsymbol{W} = \mathrm{skew}(\boldsymbol{L}). \tag{3.65}$$

To gain insight into the physical meaning of the tensors $\boldsymbol{D}$ and $\boldsymbol{W}$, it is convenient to consider a body undergoing a motion with uniform (independent of $\boldsymbol{x}$) velocity gradient. For such a motion the velocity field reads

$$\boldsymbol{v}(\boldsymbol{x}, t) = \boldsymbol{v}(\boldsymbol{y}, t) + \boldsymbol{L}(t)\,(\boldsymbol{x} - \boldsymbol{y}). \tag{3.66}$$

If the decomposition of $\boldsymbol{L}$ into its symmetric and skew parts is introduced, the velocity field can be split as

$$\boldsymbol{v}(\boldsymbol{x}, t) = \boldsymbol{v}^R(\boldsymbol{x}, t) + \boldsymbol{v}^S(\boldsymbol{x}, t), \tag{3.67}$$

where the following definitions have been used:

$$\begin{aligned} \boldsymbol{v}^R(\boldsymbol{x}, t) &= \boldsymbol{v}(\boldsymbol{y}, t) + \boldsymbol{W}(t)\,(\boldsymbol{x} - \boldsymbol{y}), \\ \boldsymbol{v}^S(\boldsymbol{x}, t) &= \boldsymbol{D}(t)\,(\boldsymbol{x} - \boldsymbol{y}). \end{aligned} \tag{3.68}$$

By recalling expression (3.13), the velocity $\boldsymbol{v}^R$, associated with the spin tensor $\boldsymbol{W}$, can be immediately identified as a *rigid* velocity. The only contribution to straining is then provided by the term $\boldsymbol{v}^S$, associated with the rate of deformation tensor. Note that, due to its symmetry, $\boldsymbol{D}$ admits the representation

$$\boldsymbol{D} = \sum_{i=1}^{3} d_i\, \boldsymbol{e}_i \otimes \boldsymbol{e}_i, \tag{3.69}$$

with d_i and $\{\boldsymbol{e}_i\}$, respectively, the eigenvalues and an orthonormal basis of eigenvectors of $\boldsymbol{D}$. With the spectral representation above, the velocity field $\boldsymbol{v}^S$ can be decomposed as a sum of three linearly independent velocities of the form:

$$d_i\,(\boldsymbol{e}_i \otimes \boldsymbol{e}_i)\,(\boldsymbol{x} - \boldsymbol{y}),$$

with no summation implied on i, so that the components of $\boldsymbol{v}^S$ relative to the basis $\{\boldsymbol{e}_1, \boldsymbol{e}_2, \boldsymbol{e}_3\}$ are given by

$$v_i^S = d_i\,(x_i - y_i), \tag{3.70}$$

again with no summation implied, where x_i and y_i denote the coordinates of points $\boldsymbol{x}$ and $\boldsymbol{y}$ in a Cartesian system associated to $\{\boldsymbol{e}_1, \boldsymbol{e}_2, \boldsymbol{e}_3\}$. As schematically illustrated in Figure 3.10,

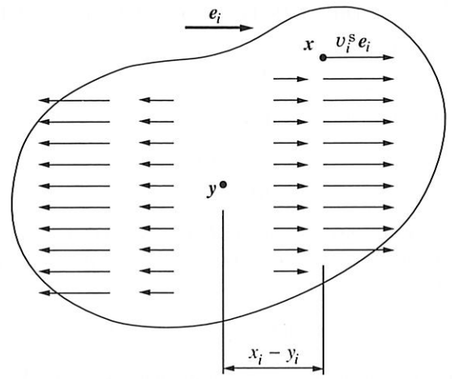

Figure 3.10. Straining velocity field.

each v_i^S corresponds to a velocity field that purely stretches the body in the direction of $\boldsymbol{e}_i$, with the plane perpendicular to $\boldsymbol{e}_i$ that passes through $\boldsymbol{y}$ fixed. Thus, the rate of deformation tensor corresponds indeed to a pure stretching of the body.

If a general motion (in which $\boldsymbol{L}$ is not necessarily uniform) is considered, the above decomposition of the velocity field into the sum of a rigid velocity and a straining velocity remains valid in the *local* sense. In this case, consider a point $\boldsymbol{x}$ and a point $\boldsymbol{x} + \mathrm{d}\boldsymbol{x}$ lying within an infinitesimal neighbourhood of $\boldsymbol{x}$. The velocity field within this infinitesimal neighbourhood of $\boldsymbol{x}$ is given by

$$\boldsymbol{v}(\boldsymbol{x} + \mathrm{d}\boldsymbol{x}, t) = \boldsymbol{v}(\boldsymbol{x}, t) + \boldsymbol{L}(\boldsymbol{x}, t)\, \mathrm{d}\boldsymbol{x}, \tag{3.71}$$

so that, in any motion, the velocity field can be *locally* decomposed as a sum of a rigid velocity

$$\boldsymbol{v}(\boldsymbol{x}, t) + \boldsymbol{W}(\boldsymbol{x}, t)\, \mathrm{d}\boldsymbol{x},$$

associated with the spin tensor $\boldsymbol{W}$, and a straining velocity

$$\boldsymbol{D}(\boldsymbol{x}, t)\, \mathrm{d}\boldsymbol{x},$$

associated exclusively to the rate of deformation tensor $\boldsymbol{D}$.

3.1.9. RATE OF VOLUME CHANGE

The *rate of volume change*, $\dot{J}$, is related to the rate of deformation tensor through the expression

$$\dot{J} = J \operatorname{tr} \boldsymbol{D}. \tag{3.72}$$

To derive this expression, we first apply the chain rule to obtain

$$\dot{J} \equiv (\det \boldsymbol{F})^{\cdot} = \frac{\partial(\det \boldsymbol{F})}{\partial \boldsymbol{F}} : \dot{\boldsymbol{F}} = J\, \boldsymbol{F}^{-T} : \dot{\boldsymbol{F}}, \tag{3.73}$$

where we have made use of relation (2.140) (page 36) for the derivative of the determinant. This, together with definition (2.36) (page 22) of the trace of a tensor and the fact that the skew symmetry of $\boldsymbol{W}$ implies

$$\operatorname{tr} \boldsymbol{L} = \operatorname{tr} \boldsymbol{D}, \tag{3.74}$$

leading to (3.72).

Also note that from the definition (2.145) of the divergence of a vector field we have

$$\operatorname{tr} \boldsymbol{D} = \operatorname{div}_x \boldsymbol{v}, \tag{3.75}$$

so that the rate of volume change can be equivalently expressed as

$$\dot{J} = J \operatorname{div}_x \boldsymbol{v}. \tag{3.76}$$

3.2. Infinitesimal deformations

Small or infinitesimal deformations are deformations with sufficiently small displacement gradient, $\nabla_p \boldsymbol{u}$. For such deformations, the description of kinematics can be substantially simplified.

3.2.1. THE INFINITESIMAL STRAIN TENSOR

Recall definition (3.43) of the Cauchy–Green tensors. In terms of the displacement gradient, one has

$$\begin{aligned} \boldsymbol{C} &= \boldsymbol{I} + \nabla_p \boldsymbol{u} + (\nabla_p \boldsymbol{u})^T + (\nabla_p \boldsymbol{u})^T\, \nabla_p \boldsymbol{u}, \\ \boldsymbol{B} &= \boldsymbol{I} + \nabla_p \boldsymbol{u} + (\nabla_p \boldsymbol{u})^T + \nabla_p \boldsymbol{u}\, (\nabla_p \boldsymbol{u})^T. \end{aligned} \tag{3.77}$$

If the displacement gradient is sufficiently small, the second-order terms in $\nabla_p \boldsymbol{u}$ of the expressions above can be neglected so that, under small deformations, the following approximation can be made

$$\boldsymbol{C} \approx \boldsymbol{B} \approx \boldsymbol{I} + \nabla_p \boldsymbol{u} + (\nabla_p \boldsymbol{u})^T. \tag{3.78}$$

From the above expression and the definitions of the Green–Lagrange strain tensor $\boldsymbol{E}^{(2)}$ and its Eulerian counterpart $\boldsymbol{\varepsilon}^{(2)}$, it follows that, to the same order of approximation,

$$\boldsymbol{E}^{(2)} \approx \boldsymbol{\varepsilon}^{(2)} \approx \tfrac{1}{2}[\nabla_p \boldsymbol{u} + (\nabla_p \boldsymbol{u})^T]. \tag{3.79}$$

This motivates the definition of the *infinitesimal strain tensor* to measure strains under small deformations

$$\boldsymbol{\varepsilon} \equiv \nabla_p^s \boldsymbol{u}, \tag{3.80}$$

where we have introduced the notation

$$\nabla^s(\cdot) = \operatorname{sym}[\nabla(\cdot)] = \tfrac{1}{2}[\nabla(\cdot) + \nabla(\cdot)^T], \tag{3.81}$$

for the *symmetric gradient* of a vector field. It is worth pointing out here that $\boldsymbol{\varepsilon}$ is a *linear* functional of $\boldsymbol{u}$. This fact greatly simplifies the description of small deformations.

In fact, it can be easily shown that not only $\boldsymbol{E}^{(2)}$ and $\boldsymbol{\varepsilon}^{(2)}$ but *all* Lagrangian and Eulerian strain measures defined by expressions (3.56) and (3.60) have the same small deformation limit, i.e. for any m and to within an error of second order in $\nabla_p \boldsymbol{u}$, one has

$$\boldsymbol{\varepsilon}^{(m)} \approx \boldsymbol{E}^{(m)} \approx \boldsymbol{\varepsilon}. \tag{3.82}$$

3.2.2. INFINITESIMAL RIGID DEFORMATIONS

In terms of the infinitesimal strain tensor, the square of the deformed length of a generic material fibre $\mathrm{d}\boldsymbol{p}$ (recall the text preceding expression (3.53)) reads

$$\|\mathrm{d}\boldsymbol{x}\|^2 = (\boldsymbol{I} + 2\,\boldsymbol{\varepsilon})\,\mathrm{d}\boldsymbol{p}\cdot\mathrm{d}\boldsymbol{p} + o(\nabla_p \boldsymbol{u}) \tag{3.83}$$

with $o(\nabla_p \boldsymbol{u})$ a term of second order in $\nabla_p \boldsymbol{u}$. It is clear from this expression that, to within an error of $o(\nabla_p \boldsymbol{u})$, only the symmetric part $\boldsymbol{\varepsilon}$ of $\nabla_p \boldsymbol{u}$ is associated with local straining. The skew part of $\nabla_p \boldsymbol{u}$ produces no straining and is associated exclusively with local infinitesimal rigid rotations. For a pure local infinitesimal rigid rotation ($\|\mathrm{d}\boldsymbol{x}\| = \|\mathrm{d}\boldsymbol{p}\|, \ \forall\ \|\mathrm{d}\boldsymbol{p}\|$) the tensor $\boldsymbol{\varepsilon}$ vanishes or, equivalently, $\nabla_p \boldsymbol{u}$ is skew.

For a body under an arbitrary homogeneous deformation ($\nabla_p \boldsymbol{u}$ independent of $\boldsymbol{p}$), the displacement field can be written as

$$\boldsymbol{u}(\boldsymbol{p}) = \boldsymbol{u}(\boldsymbol{q}) + \nabla_p \boldsymbol{u}\,(\boldsymbol{p} - \boldsymbol{q}), \tag{3.84}$$

for all points $\boldsymbol{p}$ and $\boldsymbol{q}$. For infinitesimal rigid deformations and within an approximation of second order in the displacement gradient, $\nabla_p \boldsymbol{u}$ is skew and the field $\boldsymbol{u}$ can be written as

$$\boldsymbol{u}(\boldsymbol{p}) = \boldsymbol{u}(\boldsymbol{q}) + \boldsymbol{A}\,(\boldsymbol{p} - \boldsymbol{q}), \tag{3.85}$$

for all points $\boldsymbol{p}$ and $\boldsymbol{q}$ with $\boldsymbol{A} \equiv \nabla_p \boldsymbol{u}$ a skew tensor. Alternatively, with $\boldsymbol{a}$ denoting the axial vector of $\boldsymbol{A}$, $\boldsymbol{u}$ can be expressed as

$$\boldsymbol{u}(\boldsymbol{p}) = \boldsymbol{u}(\boldsymbol{q}) + \boldsymbol{a} \times (\boldsymbol{p} - \boldsymbol{q}). \tag{3.86}$$

Any displacement that admits the representation (3.85)–(3.86) is called an *infinitesimal rigid displacement* field. Note that infinitesimal rigid displacements have the same representation as rigid velocity fields (see expressions (3.13) and (3.14)).

3.2.3. INFINITESIMAL ISOCHORIC AND VOLUMETRIC DEFORMATIONS

Analogously to the isochoric/volumetric split of the deformation gradient in the finite strain context (refer to Section 3.1.5), the infinitesimal strain tensor $\boldsymbol{\varepsilon}$ can also be split into a purely volumetric and a volume-preserving contribution. The isochoric/volumetric split of the infinitesimal strain tensor is *additive* (in contrast to the *multiplicative* split of the deformation gradient in the finite strain theory) and reads

$$\boldsymbol{\varepsilon} = \boldsymbol{\varepsilon}_{\mathrm{d}} + \boldsymbol{\varepsilon}_{\mathrm{v}}, \tag{3.87}$$

where

$$\boldsymbol{\varepsilon}_{\mathrm{d}} \equiv \boldsymbol{\varepsilon} - \boldsymbol{\varepsilon}_{\mathrm{v}} \tag{3.88}$$

is the isochoric component, known as the *strain deviator* or *deviatoric strain*, which measures pure infinitesimal distortions. The tensor

$$\boldsymbol{\varepsilon}_{\mathrm{v}} \equiv \tfrac{1}{3}\,\varepsilon_{\mathrm{v}}\,\boldsymbol{I} \tag{3.89}$$

is the infinitesimal *volumetric strain tensor*. The scalar invariant of $\boldsymbol{\varepsilon}$, defined as

$$\varepsilon_{\mathrm{v}} \equiv I_1(\boldsymbol{\varepsilon}) = \mathrm{tr}\,\boldsymbol{\varepsilon} = \mathrm{tr}\,\nabla^s \boldsymbol{u} = \mathrm{tr}\,\nabla \boldsymbol{u} \tag{3.90}$$

is named the infinitesimal *volumetric strain*. An infinitesimal deformation is volume-preserving if and only if

$$\varepsilon_{\mathrm{v}} = 0. \tag{3.91}$$

The tensors $\boldsymbol{\varepsilon}_{\mathrm{d}}$ and $\boldsymbol{\varepsilon}_{\mathrm{v}}$ can be equivalently written in terms of linear operations on $\boldsymbol{\varepsilon}$ as

$$\boldsymbol{\varepsilon}_{\mathrm{d}} = [\mathsf{I}_S - \tfrac{1}{3}\,\boldsymbol{I}\otimes\boldsymbol{I}] : \boldsymbol{\varepsilon}, \quad \boldsymbol{\varepsilon}_{\mathrm{v}} = \tfrac{1}{3}\,(\boldsymbol{I}\otimes\boldsymbol{I}) : \boldsymbol{\varepsilon}. \tag{3.92}$$

It should be noted that the strain deviator is a *traceless* tensor, i.e.

$$\mathrm{tr}\,\boldsymbol{\varepsilon}_{\mathrm{d}} = 0. \tag{3.93}$$

The fourth-order tensor defined as

$$\mathsf{I}_{\mathrm{d}} \equiv \mathsf{I}_S - \tfrac{1}{3}\,\boldsymbol{I}\otimes\boldsymbol{I}, \tag{3.94}$$

is referred to as the *deviatoric projection tensor*. It projects second-order symmetric tensors into the *deviatoric subspace*, i.e. into the space of traceless tensors. Throughout this book we shall often use the alternative notation

$$\mathrm{dev}(\boldsymbol{S})$$

to represent the deviator of a symmetric tensor $\boldsymbol{S}$, i.e.

$$\mathrm{dev}(\boldsymbol{S}) \equiv \mathsf{I}_{\mathrm{d}} : \boldsymbol{S}. \tag{3.95}$$

From finite to infinitesimal isochoric and volumetric strains

Analogously to Section 3.2.1, where the infinitesimal strain tensor is derived from the finite strain theory, the above isochoric/volumetric split can also be obtained from its finite deformation counterpart by neglecting higher order terms in $\nabla_p \boldsymbol{u}$.

To show this, let us consider the Green–Lagrange strain tensor, $\boldsymbol{E}^{(2)}$. Following the isochoric/volumetric split of the deformation gradient given by (3.35), we define the corresponding isochoric and volumetric Green–Lagrange strains

$$\boldsymbol{E}^{(2)}_{\mathrm{iso}} \equiv \tfrac{1}{2}(\boldsymbol{C}_{\mathrm{iso}} - \boldsymbol{I}); \quad \boldsymbol{E}^{(2)}_{\mathrm{v}} \equiv \tfrac{1}{2}(\boldsymbol{C}_{\mathrm{v}} - \boldsymbol{I}), \tag{3.96}$$

where

$$\boldsymbol{C}_{\mathrm{iso}} \equiv \boldsymbol{F}^T_{\mathrm{iso}}\,\boldsymbol{F}_{\mathrm{iso}} = (\det\,\boldsymbol{F})^{-\frac{2}{3}}\,\boldsymbol{F}^T\,\boldsymbol{F} = (\det\,\boldsymbol{F})^{-\frac{2}{3}}\,\boldsymbol{C} \tag{3.97}$$

and

$$\boldsymbol{C}_{\mathrm{v}} \equiv \boldsymbol{F}^T_{\mathrm{v}}\,\boldsymbol{F}_{\mathrm{v}} = (\det\,\boldsymbol{F})^{\frac{2}{3}}\,\boldsymbol{I}. \tag{3.98}$$

Now we proceed to show that, under small strain conditions (small $\nabla_p \boldsymbol{u}$), the volumetric Green–Lagrange strain defined above leads to definition (3.90). From $(3.96)_2$ and (3.98), we have

$$\boldsymbol{E}^{(2)}_{\mathrm{v}} = \tfrac{1}{2}\,[(\det\,\boldsymbol{F})^{\frac{2}{3}} - 1]\,\boldsymbol{I}. \tag{3.99}$$

From the standard concepts of differentiation discussed in Section 2.5 together with the definition $\boldsymbol{F} = \boldsymbol{I} + \nabla_p \boldsymbol{u}$ and the expression given in (iii) of page 36 for the derivative of the determinant, we find that

$$\begin{aligned} \det \boldsymbol{F} &= \det(\boldsymbol{I} + \nabla_p \boldsymbol{u}) \\ &= \det \boldsymbol{I} + (\det \boldsymbol{I})\, \boldsymbol{I} : \nabla_p \boldsymbol{u} + o(\nabla_p \boldsymbol{u}) \\ &= 1 + \operatorname{tr} \nabla_p \boldsymbol{u} + o(\nabla_p \boldsymbol{u}) \end{aligned} \tag{3.100}$$

and

$$(\det \boldsymbol{F})^{\frac{2}{3}} = 1 + \tfrac{2}{3} \operatorname{tr} \nabla_p \boldsymbol{u} + o(\nabla_p \boldsymbol{u}). \tag{3.101}$$

With the substitution of the above expression into (3.99), we then obtain

$$\boldsymbol{E}_{\mathrm{v}}^{(2)} = \boldsymbol{\varepsilon}_{\mathrm{v}} + \boldsymbol{o}(\nabla_p \boldsymbol{u}). \tag{3.102}$$

Thus, if higher-order terms are neglected, we have the following approximation

$$\boldsymbol{E}_{\mathrm{v}}^{(2)} \approx \boldsymbol{\varepsilon}_{\mathrm{v}}. \tag{3.103}$$

Following a completely analogous procedure with the isochoric Green–Lagrange strain, we obtain

$$\begin{aligned} \boldsymbol{E}_{\mathrm{iso}}^{(2)} &= \tfrac{1}{2}[(\det \boldsymbol{F})^{-\frac{2}{3}} (\boldsymbol{I} + \nabla_p^T \boldsymbol{u} + \nabla_p \boldsymbol{u} + \nabla_p^T \boldsymbol{u}\, \nabla_p \boldsymbol{u}) - \boldsymbol{I}] \\ &= \tfrac{1}{2}\{[1 - \tfrac{2}{3} \operatorname{tr} \nabla_p \boldsymbol{u} + o(\nabla_p \boldsymbol{u})][\boldsymbol{I} + \nabla_p^T \boldsymbol{u} + \nabla_p \boldsymbol{u} + o(\nabla_p \boldsymbol{u})] - \boldsymbol{I}\} \\ &= \boldsymbol{\varepsilon} - \tfrac{1}{3}(\operatorname{tr} \nabla_p \boldsymbol{u})\boldsymbol{I} + o(\nabla_p \boldsymbol{u}) \\ &= \boldsymbol{\varepsilon}_{\mathrm{d}} + \boldsymbol{o}(\nabla_p \boldsymbol{u}). \end{aligned} \tag{3.104}$$

Thus, to within second-order terms in $\nabla_p \boldsymbol{u}$, we have

$$\boldsymbol{E}_{\mathrm{iso}}^{(2)} \approx \boldsymbol{\varepsilon}_{\mathrm{d}}. \tag{3.105}$$

The infinitesimal limits above are valid for all Lagrangian and Eulerian finite strain measures defined by expressions (3.56) and (3.60).

3.3. Forces. Stress Measures

The previous sections of this chapter have been limited to the mathematical description of the kinematics of deformation. In particular, concepts such as the deformation gradient, rotations and the different strain measures used to quantify internal straining are of utmost importance in the formulation of the mechanical and thermodynamical theory of continua. It should be noted that, thus far, no reference has been made to *forces* and how they are transferred within continuum bodies.

The forces associated with the mechanical description of a body can be classed into three categories:[‡]

[‡] Stress *couples* could also be considered but these are outside the scope of this book and fall within the realm of the so-called *polar* continuum theories (Cosserrat and Cosserrat, 1909; Toupin, 1962; Truesdell and Noll, 1965).

1. *Boundary forces*. Forces applied to the boundary of the body such as those resulting from contact with another body. The dimension of boundary forces is force per unit area.
2. *Body forces*. Forces exerted on the interior of the body. Gravitational and magnetic forces are typical examples of such forces. The dimension of body forces is force per unit mass (or volume).
3. *Internal interactions between adjacent parts of a body*. The dimension of such interactions is force per unit area.

Internal interaction forces arise from the action of one part of the body upon an adjacent part and are transmitted across the surface that separate them. Boundary forces represent interactions between the exterior and the interior of a body and, as internal interactions, are transmitted across a surface (the boundary of the body in this case). Thus, boundary forces and interactions between distinct parts of a body are forces of essentially the same type and will be collectively called *surface forces*. To describe surface forces mathematically, the concept of *stress* as well as the different ways of quantifying it are introduced in this section.

3.3.1. CAUCHY'S AXIOM. THE CAUCHY STRESS VECTOR

Crucial to the description of surface forces is *Cauchy's axiom* stated in what follows. Consider a body $\mathscr{B}$ in an arbitrarily deformed configuration (Figure 3.11). Let $\mathscr{S}$ be an oriented surface of $\mathscr{B}$ with unit normal vector $\boldsymbol{n}$ at a point $\boldsymbol{x}$. Cauchy's axiom states that 'At $\boldsymbol{x}$, the surface force, i.e. the force per unit area, exerted across $\mathscr{S}$ by the material on the side of $\mathscr{S}$ into which $\boldsymbol{n}$ is pointing upon the material on the other side of $\mathscr{S}$ depends on $\mathscr{S}$ only through its normal $\boldsymbol{n}$'. This means that identical forces are transmitted across *any* surfaces with normal $\boldsymbol{n}$ at $\boldsymbol{x}$ (such as surfaces $\mathscr{S}$ and $\mathscr{T}$ in Figure 3.11). This force (per unit area) is called the *Cauchy stress vector* and will be denoted

$$\boldsymbol{t}(\boldsymbol{n}),$$

with dependence on $\boldsymbol{x}$ and time omitted for notational convenience. If $\mathscr{S}$ belongs to the boundary of $\mathscr{B}$, then the Cauchy stress vector represents the contact force exerted by the surrounding environment on $\mathscr{B}$.

3.3.2. THE AXIOM OF MOMENTUM BALANCE

Let $\mathscr{B}$ now be subjected to a system of surface forces, $\boldsymbol{t}(\boldsymbol{x}, \boldsymbol{n})$, and body forces, $\boldsymbol{b}(\boldsymbol{x})$. The spatial field $\boldsymbol{b}(\boldsymbol{x})$ represents force per unit mass acting on the interior of $\mathscr{B}$. The *axiom of momentum balance* asserts that 'For any part $\mathscr{P}$ of the deformed configuration of $\mathscr{B}$, with boundary $\mathscr{S}$, the *balance of linear momentum*,

$$\int_{\mathscr{S}} \boldsymbol{t}(\boldsymbol{n})\, \mathrm{d}a + \int_{\mathscr{P}} \rho\, \boldsymbol{b}\, \mathrm{d}v = \int_{\mathscr{P}} \rho\, \dot{\boldsymbol{v}}\, \mathrm{d}v \tag{3.106}$$

and the *balance of angular momentum*,

$$\int_{\mathscr{S}} \boldsymbol{x} \times \boldsymbol{t}(\boldsymbol{n})\, \mathrm{d}a + \int_{\mathscr{P}} \boldsymbol{x} \times \rho\, \boldsymbol{b}\, \mathrm{d}v = \int_{\mathscr{P}} \boldsymbol{x} \times \rho\, \dot{\boldsymbol{v}}\, \mathrm{d}v \tag{3.107}$$

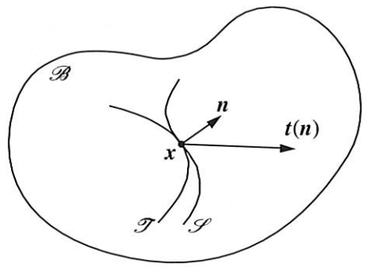

Figure 3.11. Surface forces.

are satisfied, with $\rho = \rho(\boldsymbol{x})$ denoting the *mass density* field, i.e. the mass per unit volume in the deformed configuration of $\mathscr{B}$'. The right-hand sides of (3.106) and (3.107) contain the *inertia* terms, with $\dot{\boldsymbol{v}} = \ddot{\boldsymbol{u}}$ denoting the acceleration field of $\mathscr{B}$.

3.3.3. THE CAUCHY STRESS TENSOR

One of the most fundamental results in continuum mechanics is *Cauchy's theorem* which establishes that, as a consequence of the axiom of momentum balance, the dependence of the surface force $\boldsymbol{t}$ upon the normal $\boldsymbol{n}$ is *linear*, i.e. there exists (recall Section 2.2, starting page 19) a *second-order tensor* field $\boldsymbol{\sigma}(\boldsymbol{x})$ such that the Cauchy stress vector (see Figure 3.12) is given by

$$\boldsymbol{t}(\boldsymbol{x}, \boldsymbol{n}) = \boldsymbol{\sigma}(\boldsymbol{x})\, \boldsymbol{n}. \tag{3.108}$$

Further, $\boldsymbol{\sigma}$ is *symmetric*,[§]

$$\boldsymbol{\sigma} = \boldsymbol{\sigma}^T. \tag{3.109}$$

The tensor $\boldsymbol{\sigma}$ is called the *Cauchy stress tensor* and is often referred to as the *true stress tensor* or, simply, *stress tensor*. Formal proofs to Cauchy's theorem can be found, among others, in Wang and Truesdell (1973), Gurtin (1972, 1981), Gurtin and Martins (1976), Marsden and Hughes (1983) and Ciarlet (1988).

At this point, it should be emphasised that, in real life bodies, forces are actually transferred by atomic interactions which are clearly *discrete* quantities. The continuum mathematical representation of such interactions by means of a stress tensor is meaningful only in an average sense and is valid only for a sufficiently large volume of material. This observation applies equally to quantities such as strain measures or any other continuum fields associated with the body. The smallest volume of material for which the continuum representation makes sense is called the *representative volume element*.

Cauchy stress components

Using an orthonormal basis $\{\boldsymbol{e}_1, \boldsymbol{e}_2, \boldsymbol{e}_3\}$, the Cauchy stress tensor is represented as

$$\boldsymbol{\sigma} = \sigma_{ij}\, \boldsymbol{e}_i \otimes \boldsymbol{e}_j, \tag{3.110}$$

[§]The symmetry of $\boldsymbol{\sigma}$ is a result of the balance of angular momentum.

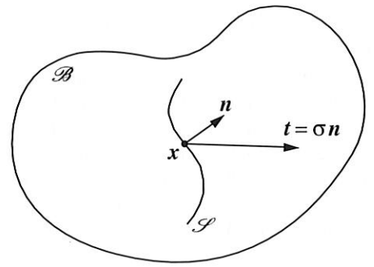

Figure 3.12. The Cauchy stress.

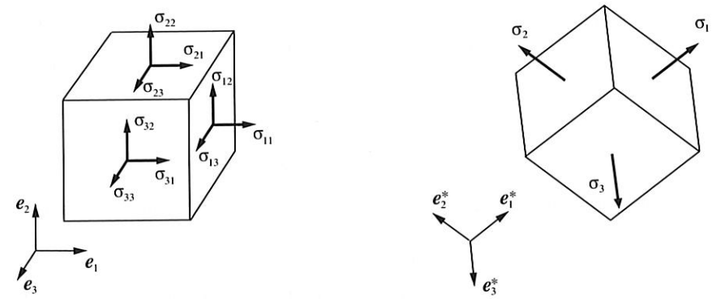

Figure 3.13. Cauchy stress tensor components and principal Cauchy stresses.

with summation on repeated indices implied and the components σ_{ij} given by

$$\sigma_{ij} = (\boldsymbol{\sigma}\, \boldsymbol{e}_i) \cdot \boldsymbol{e}_j. \tag{3.111}$$

From (3.108), it follows that the vector $\boldsymbol{\sigma}\, \boldsymbol{e}_i$ is the force per unit area exerted across a surface whose unit normal vector is $\boldsymbol{e}_i$ at the point of interest. The component σ_{ij} of the Cauchy stress tensor is the magnitude of the projection of $\boldsymbol{\sigma}\, \boldsymbol{e}_i$ in the direction of $\boldsymbol{e}_j$. The schematic representation of such projections is illustrated in Figure 3.13 where an infinitesimal cube with faces normal to the base vectors $\boldsymbol{e}_1$, $\boldsymbol{e}_2$ and $\boldsymbol{e}_3$ is considered. The components σ_{11}, σ_{22} and σ_{33} represent the tractions *normal* to the faces of the infinitesimal cube whereas the remaining components, σ_{12}, σ_{13}, σ_{21}, σ_{23}, σ_{31} and σ_{32} are the *shear* tractions acting parallel to the faces.

Principal Cauchy stresses

Due to its symmetry, the Cauchy stress tensor admits the spectral representation

$$\boldsymbol{\sigma} = \sum_{i=1}^{3} \sigma_i\, \boldsymbol{e}_i^* \otimes \boldsymbol{e}_i^*, \tag{3.112}$$

that is, there exists an orthonormal basis $\{e_1^*, e_2^*, e_3^*\}$, for which all shear components of the Cauchy stress tensor vanish and only the normal components may be non-zero. The normal components, σ_i, are the eigenvalues of $\boldsymbol{\sigma}$ and are called the *principal Cauchy stresses*. The directions defined by the basis $\{e_1^*, e_2^*, e_3^*\}$ are named the *principal stress directions*. The schematic representation of the forces acting on the faces of the infinitesimal cube oriented according to the principal stress directions is shown in Figure 3.13. The forces are exclusively normal to the faces of this cube. Note that, analogously to the representation of the stress tensor in terms of principal stresses, the spectral decomposition has been used in Section 3.1 to represent the stretch tensors $\boldsymbol{U}$ and $\boldsymbol{V}$ in terms of principal stretches (see expression (3.51)).

Deviatoric and hydrostatic stresses

It is often convenient, particularly for the purpose of constitutive modelling, to split the stress tensor $\boldsymbol{\sigma}$ into the sum of a *spherical* and a *traceless* component

$$\boldsymbol{\sigma} = \boldsymbol{s} + p\,\boldsymbol{I}, \tag{3.113}$$

where the invariant

$$p \equiv \tfrac{1}{3}\, I_1(\boldsymbol{\sigma}) = \tfrac{1}{3}\,\mathrm{tr}\,\boldsymbol{\sigma} \tag{3.114}$$

is the *hydrostatic pressure* (also referred to as *hydrostatic stress*, *mean stress* or *mean normal pressure*), and

$$\boldsymbol{s} \equiv \boldsymbol{\sigma} - p\,\boldsymbol{I} = \mathsf{I}_{\mathrm{d}} : \boldsymbol{\sigma}, \tag{3.115}$$

with I_d defined by (3.94), is a traceless tensor named the *deviatoric stress* or *stress deviator*. The tensor

$$p\,\boldsymbol{I} = \tfrac{1}{3}(\boldsymbol{I} \otimes \boldsymbol{I}) : \boldsymbol{\sigma} \tag{3.116}$$

is called the *spherical stress tensor*. The above decomposition is analogous to the isochoric/volumetric split of the infinitesimal strain tensor discussed in Section 3.2.3.

3.3.4. THE FIRST PIOLA–KIRCHHOFF STRESS

The traction vector $\boldsymbol{t}$ of expression (3.108) measures the force exerted across a material surface per unit *deformed* area. Crucial to the definition of the first Piola–Kirchhoff stress is the counterpart $\bar{\boldsymbol{t}}$ of $\boldsymbol{t}$ that measures, at the point of interest, the force that acts across any surface whose normal is $\boldsymbol{n}$ in the deformed configuration per unit *reference* area. With $\mathrm{d}a$ denoting an infinitesimal element of area of a surface normal to $\boldsymbol{n}$ in the deformed configuration and with $\mathrm{d}a_0$ being its undeformed counterpart, $\bar{\boldsymbol{t}}$ is expressed as (Figure 3.14)

$$\bar{\boldsymbol{t}} = \frac{\mathrm{d}a}{\mathrm{d}a_0}\,\boldsymbol{t} = \frac{\mathrm{d}a}{\mathrm{d}a_0}\,\boldsymbol{\sigma}\,\boldsymbol{n}. \tag{3.117}$$

Consider the surface $\mathscr{S}$ in the *reference* configuration of $\mathscr{B}$ (Figure 3.14). Let $\mathrm{d}\boldsymbol{p}_1$ and $\mathrm{d}\boldsymbol{p}_2$ be infinitesimal (linearly independent) vectors tangent to $\mathscr{S}$ at the material point $\boldsymbol{p}$ and let $\mathrm{d}a_0$ be the area element generated by $\mathrm{d}\boldsymbol{p}_1$ and $\mathrm{d}\boldsymbol{p}_2$. With $\boldsymbol{m}$ denoting the unit normal to $\mathscr{S}$ at $\boldsymbol{p}$, one has

$$\boldsymbol{m}\,\mathrm{d}a_0 = \mathrm{d}\boldsymbol{p}_1 \times \mathrm{d}\boldsymbol{p}_2. \tag{3.118}$$

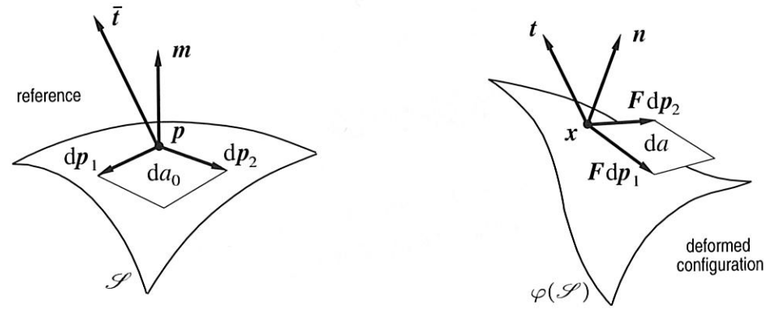

Figure 3.14. The first Piola–Kirchhoff stress tensor.

Under deformation, the tangent vectors $\mathrm{d}\boldsymbol{p}_1$ and $\mathrm{d}\boldsymbol{p}_2$ are mapped, respectively, into $\boldsymbol{F}\,\mathrm{d}\boldsymbol{p}_1$ and $\boldsymbol{F}\,\mathrm{d}\boldsymbol{p}_2$ so that the unit normal to the deformed configuration of $\mathscr{S}$ reads

$$\boldsymbol{n}\,\mathrm{d}a = \boldsymbol{F}\,\mathrm{d}\boldsymbol{p}_1 \times \boldsymbol{F}\,\mathrm{d}\boldsymbol{p}_2, \tag{3.119}$$

where $\mathrm{d}a$ is the corresponding deformed area element. Pre-multiplication of both sides of the expression above by $\boldsymbol{F}^T$ together with use of the identity

$$\boldsymbol{S}\boldsymbol{u} \times \boldsymbol{S}\boldsymbol{v} = (\det \boldsymbol{S})\,\boldsymbol{S}^{-T}\,(\boldsymbol{u} \times \boldsymbol{v}), \tag{3.120}$$

valid for any invertible tensor $\boldsymbol{S}$ and vectors $\boldsymbol{u}$ and $\boldsymbol{v}$, leads to

$$\boldsymbol{F}^T\boldsymbol{n}\,\mathrm{d}a = J\,\mathrm{d}\boldsymbol{p}_1 \times \mathrm{d}\boldsymbol{p}_2 = J\,\boldsymbol{m}\,\mathrm{d}a_0, \tag{3.121}$$

where $J \equiv \det \boldsymbol{F}$. This is equivalent to

$$\frac{\mathrm{d}a}{\mathrm{d}a_0}\,\boldsymbol{n} = J\,\boldsymbol{F}^{-T}\boldsymbol{m}. \tag{3.122}$$

Finally, with substitution of the expression above into (3.117), $\bar{\boldsymbol{t}}$ may be written in terms of the reference unit normal $\boldsymbol{m}$ as

$$\bar{\boldsymbol{t}} = J\,\boldsymbol{\sigma}\,\boldsymbol{F}^{-T}\,\boldsymbol{m}. \tag{3.123}$$

This last expression motivates the following definition

$$\boldsymbol{P} \equiv J\,\boldsymbol{\sigma}\,\boldsymbol{F}^{-T}, \tag{3.124}$$

so that the force transmitted across $\mathscr{S}$ measured per unit *reference* area reads

$$\bar{\boldsymbol{t}} = \boldsymbol{P}\,\boldsymbol{m}. \tag{3.125}$$

The tensor $\boldsymbol{P}$ is called the *first Piola–Kirchhoff stress* and is often referred to as the *Piola–Kirchhoff stress* or *nominal stress*.¶ The vector $\bar{\boldsymbol{t}}$ is obtained by applying the first Piola–Kirchhoff stress to the unit vector $\boldsymbol{m}$, normal to the *reference* configuration of $\mathscr{S}$ at the point of interest. Note that in contrast to the Cauchy stress, $\boldsymbol{P}$ is generally *unsymmetric*.

¶Some authors (Billington and Tate, 1981; Nemat-Nasser, 1999) define the nominal stress as the transpose of the first Piola–Kirchhoff stress tensor.

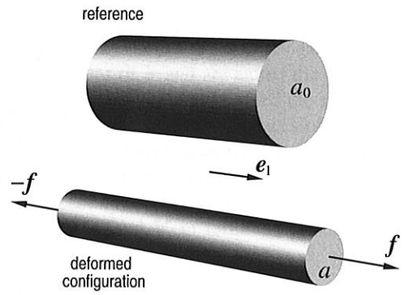

Figure 3.15. The first Piola–Kirchhoff stress. Example.

Example 3.3.1 (The Piola–Kirchhoff stress). Consider a cylindrical bar (Figure 3.15) with cross-sectional area a_0 in its initial configuration (taken as reference). During a uniaxial experiment this bar is stretched along its longitudinal axis (direction of $\boldsymbol{e}_1$) with a simultaneous reduction of its cross section. Assume that the final deformed configuration of the bar corresponds to a state of homogeneous deformation with cross-sectional area a. Furthermore, assume that the bar is subjected to a state of *uniaxial* stress, with constant $\boldsymbol{\sigma}$ given by

$$\boldsymbol{\sigma} = \sigma_{11}\, \boldsymbol{e}_1 \otimes \boldsymbol{e}_1.$$

Let $\boldsymbol{f} = f\, \boldsymbol{e}_1$ be the total force applied to the deformed configuration of the bar (by the experimental equipment). Under the assumption of uniform stress distribution in the cross-section of the bar, force balance requires that the Cauchy stress component σ_{11} be given by

$$\sigma_{11} = \frac{f}{a}.$$

In practice, the force $\boldsymbol{f}$ (and not the stress component) is what can actually be measured in an experiment. Thus, after $\boldsymbol{f}$ is measured, the Cauchy stress σ_{11} is determined according to the expression above. If instead of a, the *reference* cross-sectional area a_0 is used, then the *first Piola–Kirchhoff* or *nominal* stress component is determined

$$P_{11} = \frac{f}{a_0}.$$

It is obvious that, in this case, the corresponding tractions $\boldsymbol{t}$ and $\bar{\boldsymbol{t}}$, respectively per unit deformed and reference area, are simply

$$\boldsymbol{t} = \sigma_{11}\, \boldsymbol{e}_1 = \frac{1}{a}\, \boldsymbol{f}, \quad \bar{\boldsymbol{t}} = P_{11}\, \boldsymbol{e}_1 = \frac{1}{a_0}\, \boldsymbol{f}.$$

3.3.5. THE SECOND PIOLA–KIRCHHOFF STRESS

The *Second Piola–Kirchhoff* stress tensor, denoted $\boldsymbol{S}$, is the tensor defined as

$$\boldsymbol{S} \equiv J \boldsymbol{F}^{-1} \boldsymbol{\sigma} \boldsymbol{F}^{-T}. \tag{3.126}$$

Note that from this definition, we have

$$\boldsymbol{S}^T = J \boldsymbol{F}^{-1} \boldsymbol{\sigma}^T \boldsymbol{F}^{-T}, \tag{3.127}$$

so that the symmetry of $\boldsymbol{\sigma}$ implies that $\boldsymbol{S}$ is symmetric.

3.3.6. THE KIRCHHOFF STRESS

Another important measure of stress is the *Kirchhoff stress tensor*, $\boldsymbol{\tau}$, defined by

$$\boldsymbol{\tau} \equiv J\, \boldsymbol{\sigma}. \tag{3.128}$$

Due to the symmetry of $\boldsymbol{\sigma}$, the Kirchhoff stress is symmetric. Its spectral representation reads

$$\boldsymbol{\tau} = \sum_{i=1}^{3} \tau_i\, \boldsymbol{e}_i^* \otimes \boldsymbol{e}_i^*, \tag{3.129}$$

where the *principal Kirchhoff stresses*, τ_i, are related to the principal Cauchy stresses, σ_i, by

$$\tau_i = J\, \sigma_i. \tag{3.130}$$

Later in this book, frequent reference to the principal Kirchhoff stresses will be made in the formulation of various constitutive models.

3.4. Fundamental laws of thermodynamics

In order to state the fundamental laws of thermodynamics, it is necessary to introduce the scalar fields θ, e, s and r defined over $\mathscr{B}$ which represent, respectively, the *temperature*, *specific internal energy*, *specific entropy* and the *density of heat production*. In addition, $\boldsymbol{b}$ and $\boldsymbol{q}$ will denote the vector fields corresponding, respectively, to the *body force* (force per unit volume in the deformed configuration) and *heat flux*.

3.4.1. CONSERVATION OF MASS

The postulate of conservation of mass requires that

$$\dot{\rho} + \rho\, \mathrm{div}_x\, \dot{\boldsymbol{u}} = 0. \tag{3.131}$$

3.4.2. MOMENTUM BALANCE

In terms of the Cauchy stress tensor, whose existence has been established in Section 3.3.3, the balance of momentum for $\mathscr{B}$ can be expressed by the following partial differential equation with boundary condition:‖

$$\begin{aligned} \mathrm{div}_x\, \boldsymbol{\sigma} + \boldsymbol{b} &= \rho\, \ddot{\boldsymbol{u}} \quad \text{in } \varphi(\Omega) \\ \boldsymbol{t} &= \boldsymbol{\sigma}\, \boldsymbol{n} \quad \text{in } \varphi(\partial\Omega), \end{aligned} \tag{3.132}$$

‖ Equations (3.132) are also a result of Cauchy's theorem, alluded to in page 62.

where $\boldsymbol{n}$ is the outward unit vector normal to the deformed boundary $\boldsymbol{\varphi}(\partial\Omega)$ of $\mathscr{B}$ and $\boldsymbol{t}$ is the applied boundary traction vector field on $\boldsymbol{\varphi}(\partial\Omega)$. Equations (3.132) are often referred to as the *strong*, *local* or *point-wise* form of equilibrium. Equation $(3.132)_1$ is known as *Cauchy's equation of motion*.

The above momentum balance equations are formulated in the *spatial* (deformed) configuration. Equivalently, they may be expressed in the *reference* (or material) configuration of $\mathscr{B}$ in terms of the first Piola–Kirchhoff stress tensor as

$$\begin{aligned} \operatorname{div}_p \boldsymbol{P} + \bar{\boldsymbol{b}} &= \bar{\rho}\,\ddot{\boldsymbol{u}} \quad \text{in } \Omega \\ \bar{\boldsymbol{t}} &= \boldsymbol{P}\,\boldsymbol{m} \qquad \text{in } \partial\Omega, \end{aligned} \tag{3.133}$$

where

$$\bar{\boldsymbol{b}} = J\,\boldsymbol{b} \tag{3.134}$$

is the *reference body force*, i.e. the body force measured per unit volume in the reference configuration,

$$\bar{\rho} = J\,\rho, \tag{3.135}$$

is the *reference density* (mass per unit volume in the reference configuration), $\bar{\boldsymbol{t}}$ is the *reference boundary traction* (boundary force per unit reference area) and $\boldsymbol{m}$ is the outward normal to the boundary of $\mathscr{B}$ in its reference configuration.

3.4.3. THE FIRST PRINCIPLE

The first principle of thermodynamics postulates the *conservation of energy*. Before stating this principle, it is convenient to introduce the product

$$\boldsymbol{\sigma} : \boldsymbol{D},$$

which represents the *stress power* per unit volume in the deformed configuration of a body. The first principle of thermodynamics is mathematically expressed by the equation

$$\rho\,\dot{e} = \boldsymbol{\sigma} : \boldsymbol{D} + \rho\,r - \operatorname{div}_x \boldsymbol{q}. \tag{3.136}$$

In words, the rate of internal energy per unit deformed volume must equal the sum of the stress power and heat production per unit deformed volume minus the spatial divergence of the heat flux.

3.4.4. THE SECOND PRINCIPLE

The second principle of thermodynamics postulates the *irreversibility of entropy production*. It is expressed by means of the inequality

$$\rho\,\dot{s} + \operatorname{div}_x\left[\frac{\boldsymbol{q}}{\theta}\right] - \frac{\rho\,r}{\theta} \geq 0. \tag{3.137}$$

3.4.5. THE CLAUSIUS–DUHEM INEQUALITY

By combination of the first and second principles stated above, one easily obtains the fundamental inequality

$$\rho\,\dot{s} + \operatorname{div}_x\left[\frac{\boldsymbol{q}}{\theta}\right] - \frac{1}{\theta}(\rho\,\dot{e} - \boldsymbol{\sigma} : \boldsymbol{D} + \operatorname{div}_x \boldsymbol{q}) \geq 0. \tag{3.138}$$

The introduction of the *specific free energy* ψ (also known as the *Helmholtz free energy per unit mass*), defined by

$$\psi = e - \theta\,s, \tag{3.139}$$

along with the identity

$$\operatorname{div}_x\left[\frac{\boldsymbol{q}}{\theta}\right] = \frac{1}{\theta}\operatorname{div}_x \boldsymbol{q} - \frac{1}{\theta^2}\,\boldsymbol{q}\cdot\nabla_x\theta, \tag{3.140}$$

into the above fundamental inequality results in the *Clausius–Duhem inequality*

$$\boldsymbol{\sigma} : \boldsymbol{D} - \rho(\dot{\psi} + s\,\dot{\theta}) - \frac{1}{\theta}\,\boldsymbol{q}\cdot\boldsymbol{g} \geq 0, \tag{3.141}$$

where we have defined $\boldsymbol{g} = \nabla_x\theta$. The left-hand side of (3.141) represents the dissipation per unit *deformed* volume. Equivalently, by making use of (3.135), the Clausius–Duhem inequality can be expressed in terms of dissipation per unit *reference* volume as

$$\boldsymbol{\tau} : \boldsymbol{D} - \bar{\rho}(\dot{\psi} + s\,\dot{\theta}) - \frac{J}{\theta}\,\boldsymbol{q}\cdot\boldsymbol{g} \geq 0. \tag{3.142}$$

3.5. Constitutive theory

The balance principles presented so far are valid for any continuum body, regardless of the material of which the body is made. In order to distinguish between different types of material, a *constitutive model* must be introduced. In this section, we review the principles that form the basis of the constitutive theories discussed in later chapters of this book. We start by stating, in Section 3.5.1, three fundamental axioms that define a rather general class of constitutive models of continua. The use of internal variables to formulate constitutive models of dissipative materials is then addressed in Section 3.5.2. We remark that all dissipative constitutive models discussed in Parts Two and Three of this book are based on the internal variable approach. Section 3.5.4 summarises a generic *purely mechanical* internal variable model. The discussion on constitutive theory ends in Section 3.5.5 where the fundamental constitutive initial value problems are stated.

3.5.1. CONSTITUTIVE AXIOMS

In the present context, the axioms stated in this section must be satisfied for any constitutive model. Before going further, it is convenient to introduce the definitions of *thermokinetic* and *calorodynamic* processes (Truesdell, 1969). A *thermokinetic process* of $\mathscr{B}$ is a pair of fields

$$\boldsymbol{\varphi}(\boldsymbol{p}, t) \quad \text{and} \quad \theta(\boldsymbol{p}, t).$$

A set

$$\{\boldsymbol{\sigma}(\boldsymbol{p}, t),\ e(\boldsymbol{p}, t),\ s(\boldsymbol{p}, t),\ r(\boldsymbol{p}, t),\ \boldsymbol{b}(\boldsymbol{p}, t),\ \boldsymbol{q}(\boldsymbol{p}, t)\}$$

of fields satisfying the balance of momentum, the first and the second principles of thermodynamics is called a *calorodynamic process* of $\mathscr{B}$.

Thermodynamic determinism

The basic axiom underlying the constitutive theory discussed here is the *principle of thermodynamically compatible determinism* (Truesdell, 1969). It postulates that 'the history of the thermokinetic process to which a neighbourhood of a point $\boldsymbol{p}$ of $\mathscr{B}$ has been subjected determines a calorodynamic process for $\mathscr{B}$ at $\boldsymbol{p}$'. In particular, we shall be concerned with so-called *simple materials*, for which the *local* history (history at point $\boldsymbol{p}$ only) of $\boldsymbol{F}$, θ and $\boldsymbol{g}$ suffices to determine the history of the thermokinetic process for constitutive purposes. In this case, regarding the body force $\boldsymbol{b}$ and heat supply r as delivered, respectively, by the linear momentum balance $(3.132)_1$ and conservation of energy (3.136) and introducing the specific free energy (3.139), the principle of thermodynamic determinism implies the existence of constitutive functionals $\mathfrak{F}$, $\mathfrak{G}$, $\mathfrak{H}$ and $\mathfrak{I}$ of the histories of $\boldsymbol{F}$, θ and $\boldsymbol{g}$ such that, for a point $\boldsymbol{p}$,

$$\begin{aligned} \boldsymbol{\sigma}(t) &= \mathfrak{F}\,(\boldsymbol{F}^{\,t}, \theta^t, \boldsymbol{g}^t) \\ \psi(t) &= \mathfrak{G}(\boldsymbol{F}^{\,t}, \theta^t, \boldsymbol{g}^t) \\ s(t) &= \mathfrak{H}(\boldsymbol{F}^{\,t}, \theta^t, \boldsymbol{g}^t) \\ \boldsymbol{q}(t) &= \mathfrak{I}\,(\boldsymbol{F}^{\,t}, \theta^t, \boldsymbol{g}^t) \end{aligned} \tag{3.143}$$

and the Clausius–Duhem inequality (3.141) holds for every thermokinetic process of $\mathscr{B}$. The dependence on $\boldsymbol{p}$ is understood on both sides of (3.143) and $(\cdot)^t$ on the right-hand sides denotes the *history* of $(\cdot)$ at $\boldsymbol{p}$ up to time t.

Material objectivity

Another fundamental axiom of the constitutive theory is the *principle of material objectivity* (or *frame invariance*). It states that 'the material response is independent of the observer'. The motion $\boldsymbol{\varphi}^*$ is related to the motion $\boldsymbol{\varphi}$ by a change in observer if it can be expressed as

$$\boldsymbol{\varphi}^*(\boldsymbol{p}, t) = \boldsymbol{y}(t) + \boldsymbol{Q}(t)\,[\boldsymbol{\varphi}(\boldsymbol{p}, t) - \boldsymbol{x}_0], \tag{3.144}$$

where $\boldsymbol{y}(t)$ is a point in space, $\boldsymbol{Q}(t)$ is a rotation and $\boldsymbol{\varphi}(\boldsymbol{p}, t) - \boldsymbol{x}_0$ is the position vector of $\boldsymbol{\varphi}(\boldsymbol{p}, t)$ relative to an arbitrary origin $\boldsymbol{x}_0$. This relation corresponds to a rigid relative movement between the different observers and the deformation gradient corresponding to $\boldsymbol{\varphi}^*$ is given by

$$\boldsymbol{F}^{\,*} = \boldsymbol{Q}\,\boldsymbol{F}. \tag{3.145}$$

Scalar fields (such as θ, ψ and s) are unaffected by a change in observer but the Cauchy stress $\boldsymbol{\sigma}(t)$, heat flux $\boldsymbol{q}(t)$ and the temperature gradient $\boldsymbol{g}(t)$ transform according to the rules

$$\begin{aligned} \boldsymbol{\sigma} &\longrightarrow \boldsymbol{\sigma}^* = \boldsymbol{Q}\,\boldsymbol{\sigma}\,\boldsymbol{Q}^T \\ \boldsymbol{q} &\longrightarrow \boldsymbol{q}^* = \boldsymbol{Q}\,\boldsymbol{q} \\ \boldsymbol{g} &\longrightarrow \boldsymbol{g}^* = \boldsymbol{Q}\,\boldsymbol{g}. \end{aligned} \tag{3.146}$$

The principle of material objectivity places restrictions on the constitutive functionals (3.143). Formally, it requires that $\mathfrak{F}$, $\mathfrak{G}$, $\mathfrak{H}$ and $\mathfrak{I}$ satisfy

$$\begin{aligned} \boldsymbol{\sigma}^*(t) &= \mathfrak{F}\,(\boldsymbol{F}^{\,t*}, \theta^t, \boldsymbol{g}^{t*}) \\ \psi(t) &= \mathfrak{G}(\boldsymbol{F}^{\,t*}, \theta^t, \boldsymbol{g}^{t*}) \\ s(t) &= \mathfrak{H}(\boldsymbol{F}^{\,t*}, \theta^t, \boldsymbol{g}^{t*}) \\ \boldsymbol{q}^*(t) &= \mathfrak{I}\,(\boldsymbol{F}^{\,t*}, \theta^t, \boldsymbol{g}^{t*}) \end{aligned} \tag{3.147}$$

for any transformation of the form (3.145, 3.146).

Material symmetry

The *symmetry group* of a material is the set of density preserving changes of reference configuration under which the material response functionals $\mathfrak{F}$, $\mathfrak{G}$, $\mathfrak{H}$ and $\mathfrak{I}$ are not affected. The symmetry group of a *solid* material is a subset of the proper orthogonal group $\mathscr{O}^+$, that is, a set of *rotations*. Thus, the symmetry group of a solid material is the set of rotations of the reference configuration under which the response functionals remain unchanged. This concept is expressed mathematically as follows. A subgroup $\mathscr{S}$ of $\mathscr{O}^+$ is said to be the symmetry group of the material defined by the constitutive functionals $\mathfrak{F}$, $\mathfrak{G}$, $\mathfrak{H}$ and $\mathfrak{I}$ if the relations

$$\begin{aligned} \mathfrak{F}\,(\boldsymbol{F}^{\,t}, \theta^t, \boldsymbol{g}^t) &= \mathfrak{F}\,([\boldsymbol{F}\,\boldsymbol{Q}]^t, \theta^t, \boldsymbol{g}^t) \\ \mathfrak{G}\,(\boldsymbol{F}^{\,t}, \theta^t, \boldsymbol{g}^t) &= \mathfrak{G}([\boldsymbol{F}\,\boldsymbol{Q}]^t, \theta^t, \boldsymbol{g}^t) \\ \mathfrak{H}\,(\boldsymbol{F}^{\,t}, \theta^t, \boldsymbol{g}^t) &= \mathfrak{H}([\boldsymbol{F}\,\boldsymbol{Q}]^t, \theta^t, \boldsymbol{g}^t) \\ \mathfrak{I}\,(\boldsymbol{F}^{\,t}, \theta^t, \boldsymbol{g}^t) &= \mathfrak{I}\,([\boldsymbol{F}\,\boldsymbol{Q}]^t, \theta^t, \boldsymbol{g}^t) \end{aligned} \tag{3.148}$$

hold for any time-*independent* rotation $\boldsymbol{Q} \in \mathscr{S}$. A solid is said to be *isotropic*** if its symmetry group is the entire proper orthogonal group. In the development of any constitutive model, the constitutive functionals must comply with the restrictions imposed by the symmetries of the material in question.

3.5.2. THERMODYNAMICS WITH INTERNAL VARIABLES

The constitutive equations (3.143) written in terms of functionals of the history of $\boldsymbol{F}$, θ and $\boldsymbol{g}$, in that format, are far too general to have practical utility in modelling real materials undergoing real thermodynamical process. This is especially true if one has in mind the experimental identification of the constitutive functionals and the solution of the boundary value problems of practical interest. Therefore, it is imperative that simplifying assumptions are added to the general forms of the constitutive relations stated above.

An effective alternative to the general description based on history functionals is the adoption of the so-called *thermodynamics with internal variables*. The starting point of the thermodynamics with internal variables is the hypothesis that at any instant of a thermodynamical process the thermodynamic state (defined by $\boldsymbol{\sigma}$, ψ, s and $\boldsymbol{q}$) at a given

**We remark that most constitutive models discussed in this book are isotropic.

point $\boldsymbol{p}$ can be completely determined by the knowledge of a finite number of *state variables*. The thermodynamic state depends only on the *instantaneous* value of the state variables and not on their past history.

Mathematically, state variable models can be seen as particular instances of the general history functional-based constitutive theory. The relationship between the two approaches is discussed in detail by Kestin and Bataille (1977) and Bataille and Kestin (1979). In general terms, state variable models can be obtained from the general history functional-based description by re-defining the history of the thermokinetic process in terms of a finite number of parameters (the state variables).

The state variables

For the applications with which we are mostly concerned, it will be convenient to assume that at any time t, the thermodynamic state at a point is determined by the following set of *state variables*:

$$\{\boldsymbol{F},\ \theta,\ \boldsymbol{g},\ \boldsymbol{\alpha}\},$$

where $\boldsymbol{F}$, θ and $\boldsymbol{g}$ are the *instantaneous* values of deformation gradient, temperature and the temperature gradient and

$$\boldsymbol{\alpha} = \{\alpha_k\} \tag{3.149}$$

is a set of *internal variables* containing, in general, entities of scalar, vectorial and tensorial nature associated with dissipative mechanisms.

Thermodynamic potential. Stress constitutive equation

Following the above hypothesis, the specific free energy is assumed to have the form[††]

$$\psi = \psi(\boldsymbol{F},\ \theta,\ \boldsymbol{\alpha}), \tag{3.150}$$

so that its rate of change is given by

$$\dot{\psi} = \frac{\partial \psi}{\partial \boldsymbol{F}} : \dot{\boldsymbol{F}} + \frac{\partial \psi}{\partial \theta}\,\dot{\theta} + \frac{\partial \psi}{\partial \alpha_k}\,\dot{\alpha}_k, \tag{3.151}$$

where summation over k is implied. In this case, using the connection

$$\boldsymbol{\sigma} : \boldsymbol{D} = \boldsymbol{\sigma}\,\boldsymbol{F}^{-T} : \dot{\boldsymbol{F}}\,, \tag{3.152}$$

for the stress power, one obtains for the Clausius–Duhem inequality

$$\left(\boldsymbol{\sigma}\,\boldsymbol{F}^{-T} - \rho\,\frac{\partial \psi}{\partial \boldsymbol{F}}\right) : \dot{\boldsymbol{F}} - \rho\left(s + \frac{\partial \psi}{\partial \theta}\right)\dot{\theta} - \rho\,\frac{\partial \psi}{\partial \alpha_k}\,\dot{\alpha}_k - \frac{1}{\theta}\,\boldsymbol{q}\cdot\boldsymbol{g} \geq 0. \tag{3.153}$$

Equivalently, in terms of power per unit *reference* volume, we have

$$\left(\boldsymbol{P} - \bar{\rho}\,\frac{\partial \psi}{\partial \boldsymbol{F}}\right) : \dot{\boldsymbol{F}} - \bar{\rho}\left(s + \frac{\partial \psi}{\partial \theta}\right)\dot{\theta} - \bar{\rho}\,\frac{\partial \psi}{\partial \alpha_k}\,\dot{\alpha}_k - \frac{J}{\theta}\,\boldsymbol{q}\cdot\boldsymbol{g} \geq 0. \tag{3.154}$$

[††]The dependence of ψ on the temperature gradient is disregarded as it contradicts the second principle of thermodynamics (Coleman and Gurtin, 1967).

Expression (3.154) is obtained from (3.153), by simply using relation (3.135).

The principle of thermodynamic determinism requires that the constitutive equations must be such that the above inequality holds for any thermokinetic process. Thus, (3.154) must remain valid for any pair of functions $\{\dot{\boldsymbol{F}}(t), \dot{\theta}(t)\}$. This implies the constitutive equations

$$\boldsymbol{P} = \bar{\rho}\,\frac{\partial \psi}{\partial \boldsymbol{F}}, \quad s = -\frac{\partial \psi}{\partial \theta}, \tag{3.155}$$

for the first Piola–Kirchhoff stress and entropy. Equation $(3.155)_1$ is equivalent to the following constitutive relations for the Cauchy and Kirchoff stress tensors:

$$\boldsymbol{\sigma} = \frac{1}{J}\,\bar{\rho}\,\frac{\partial \psi}{\partial \boldsymbol{F}}\,\boldsymbol{F}^{T}, \quad \boldsymbol{\tau} = \bar{\rho}\,\frac{\partial \psi}{\partial \boldsymbol{F}}\,\boldsymbol{F}^{T}. \tag{3.156}$$

Thermodynamical forces

For each internal variable α_k of the set $\boldsymbol{\alpha}$, we define the *conjugate thermodynamical force*

$$A_k \equiv \bar{\rho}\,\frac{\partial \psi}{\partial \alpha_k}. \tag{3.157}$$

With this definition and the identities (3.155), the Clausius–Duhem inequality can be rewritten as

$$-A_k * \dot{\alpha}_k - \frac{J}{\theta}\,\boldsymbol{q}\cdot\boldsymbol{g} \geq 0, \tag{3.158}$$

where we recall that the symbol '$*$' denotes the appropriate product operation between A_k and $\dot{\alpha}_k$. In what follows, we will adopt for convenience the notation

$$\boldsymbol{A} \equiv \{A_k\} \tag{3.159}$$

for the set of thermodynamical forces, so that (3.158) can be expressed in a more compact form as

$$-\boldsymbol{A} * \dot{\boldsymbol{\alpha}} - \frac{J}{\theta}\,\boldsymbol{q}\cdot\boldsymbol{g} \geq 0. \tag{3.160}$$

Dissipation. Evolution of the internal variables

In order to completely characterise a constitutive model, complementary laws associated with the dissipative mechanisms are required. Namely, constitutive equations for the flux variables $\frac{1}{\theta}\boldsymbol{q}$ and $\dot{\boldsymbol{\alpha}}$ must be postulated. In the general case, we assume that the flux variables are given functions of the state variables. The following constitutive equations are then postulated

$$\begin{aligned} \dot{\boldsymbol{\alpha}} &= f(\boldsymbol{F}, \theta, \boldsymbol{g}, \boldsymbol{\alpha}) \\ \frac{1}{\theta}\boldsymbol{q} &= h(\boldsymbol{F}, \theta, \boldsymbol{g}, \boldsymbol{\alpha}). \end{aligned} \tag{3.161}$$

Recalling the principle of thermodynamic determinism, the Clausius–Duhem inequality, now expressed by (3.158), must hold for any process. This requirement places restrictions on the possible forms of the general constitutive functions f and h in (3.161) (the reader is referred to Coleman and Gurtin, 1967; Truesdell, 1969, for further details on this issue). It is also

important to mention that when internal variables of vectorial or tensorial nature are present, it is frequently convenient to re-formulate $(3.161)_1$ in terms of so-called *objective rates* rather than the standard material time derivative of $\boldsymbol{\alpha}$. Objective rates are insensitive to rigid-body motions and may be essential in the definition of a *frame invariant* evolution law for variables representing physical states associated with material directions. Objective rates are discussed in Section 14.10 (starting page 615) in the context of the hypoelastic-based formulation of plasticity models.

Dissipation potential. Normal dissipativity

An effective way of ensuring that (3.158) is satisfied consists in postulating the existence of a scalar-valued *dissipation potential* of the form

$$\Xi = \Xi(\boldsymbol{A}, \boldsymbol{g}; \boldsymbol{F}, \theta, \boldsymbol{\alpha}), \tag{3.162}$$

where the state variables $\boldsymbol{F}$, θ and $\boldsymbol{\alpha}$ appear as parameters. The potential Ξ is assumed convex with respect to each A_k and $\boldsymbol{g}$, non-negative and zero valued at the origin, $\{\boldsymbol{A}, \boldsymbol{g}\} = \{\boldsymbol{0}, \boldsymbol{0}\}$. In addition, the hypothesis of *normal dissipativity* is introduced, i.e. the flux variables are assumed to be determined by the laws

$$\dot{\alpha}_k = -\frac{\partial \Xi}{\partial A_k}, \quad \frac{1}{\theta}\boldsymbol{q} = -\frac{\partial \Xi}{\partial \boldsymbol{g}}. \tag{3.163}$$

A constitutive model defined by (3.150), (3.155) and (3.163) satisfies *a priori* the dissipation inequality. It should be noted, however, that the constitutive description by means of convex potentials as described above is *not* a consequence of thermodynamics but, rather, a convenient tool for formulating constitutive equations without violating thermodynamics. Examples of constitutive models supported by experimental evidence which do not admit representation by means of dissipation potentials are discussed by Onat and Leckie (1988).

3.5.3. PHENOMENOLOGICAL AND MICROMECHANICAL APPROACHES

The success of a constitutive model intended to describe the behaviour of a particular material depends critically on the choice of an appropriate set of internal variables. Since no plausible model will be general enough to describe the response of a material under all processes, we should have in mind that the choice of internal variables must be guided not only by the specific material in question but, equally importantly, by the processes (i.e. the range of thermokinetic processes defined by strain and temperature histories as well as the time span) under which the model is meant to describe the behaviour of the material. The importance of considering the possible thermokinetic processes when devising a constitutive model can be clearly illustrated, for instance, by considering a simple steel bar. When subjected to a sufficiently small axial strain at room temperature, the bar exhibits a behaviour that can be accurately modelled by linear elasticity theory (generalised Hooke's law). If strains become larger, however, linear elasticity may no longer capture the observed response satisfactorily. In this case, a plasticity theory may be more appropriate. With further increase in complexity of the strain history (by introducing, say, cyclic extension), other phenomena such as internal damaging and possibly fracturing may take place and more

refined constitutive models, incorporating a larger number of state variables, will be required. Due account of the possible temperature histories and time span to be considered is also fundamental. At higher temperatures, the long-term behaviour of the steel bar subjected to even a very small strain, may no longer be accurately modelled by the linear elasticity theory. In this case the introduction of time-dependent effects (creep/relaxation) may be essential to produce an acceptable model. In an extreme situation, if the temperature rises above melting point, the bar will cease to be a solid. Under such circumstances, a fluid mechanics theory will be needed to describe the behaviour of the material.

In general, due to the difficulty involved in the identification of the underlying dissipative mechanisms, the choice of the appropriate set of internal variables is somewhat subtle and tends to be biased by the preferences and background of the investigator. In simplistic terms, we may say that constitutive modelling by means of internal variables relies either on a micromechanical or on a phenomenological approach. The micromechanical approach involves the determination of mechanisms and related variables at the atomic, molecular or crystalline levels. In general, these variables are discrete quantities and their continuum (macroscopic) counterparts can be defined by means of homogenisation techniques. The phenomenological approach, on the other hand, is based on the study of the response of the *representative volume element*, i.e. the element of matter large enough to be regarded as a homogeneous continuum. The internal variables in this case will be directly associated with the dissipative behaviour observed at the *macroscopic* level in terms of continuum quantities (such as strain, temperature, etc.). Despite the macroscopic nature of theories derived on the basis of the phenomenological methodology, it should be expected that 'good' phenomenological internal variables will be somehow related to the underlying microscopic dissipation mechanisms.

The phenomenological approach to irreversible thermodynamics has been particularly successful in the field of solid mechanics. Numerous well-established models of solids, such as classical isotropic elastoplasticity and viscoplasticity, discussed in Parts Two and Three of this book, have been developed on a purely phenomenological basis providing evidence of how powerful such an approach to irreversible thermodynamics can be when the major concern is the description of the essentially macroscopic behaviour. In some instances, however, the inclusion of microscopic information becomes essential and a purely phenomenological methodology is unlikely to describe the behaviour of the material with sufficient accuracy. One such case is illustrated in Chapter 16, where a microscopically-based continuum model of ductile metallic crystals is described.

3.5.4. THE PURELY MECHANICAL THEORY

Thermal effects are ignored in the constitutive theories addressed in Parts Two and Three of this book. It is, therefore, convenient at this point to summarise the general internal variable-based constitutive equations in the purely mechanical case. By removing the thermally-related terms of the above theory, we end up with the following set of mechanical constitutive equations:

$$\begin{cases} \psi = \psi(\boldsymbol{F}, \boldsymbol{\alpha}) \\ \boldsymbol{P} = \bar{\rho}\,\dfrac{\partial \psi}{\partial \boldsymbol{F}} \\ \dot{\boldsymbol{\alpha}} = f(\boldsymbol{F}, \boldsymbol{\alpha}). \end{cases} \tag{3.164}$$

The infinitesimal strain case

In *the infinitesimal strain case*, the infinitesimal strain tensor, $\boldsymbol{\varepsilon}$, replaces the deformation gradient and the stress tensor $\boldsymbol{\sigma}$ of the infinitesimal theory replaces the first Piola–Kirchhoff stress. We then have the general constitutive law

$$\begin{cases} \psi = \psi(\boldsymbol{\varepsilon}, \boldsymbol{\alpha}) \\ \boldsymbol{\sigma} = \bar{\rho}\, \dfrac{\partial \psi}{\partial \boldsymbol{\varepsilon}} \\ \dot{\boldsymbol{\alpha}} = f(\boldsymbol{\varepsilon}, \boldsymbol{\alpha}). \end{cases} \tag{3.165}$$

3.5.5. THE CONSTITUTIVE INITIAL VALUE PROBLEM

Our basic constitutive problem is defined as follows: '*Given the history of the deformation gradient (and the history of temperature and temperature gradient, if thermal effects are considered), find the free-energy and stress (plus entropy and heat flux, in the thermomechanical case) according to the constitutive law conceptually expressed by (3.143)*'. If the internal variable approach is adopted in the formulation of the constitutive equations, the generic constitutive problem reduces to the following fundamental mechanical *initial value problem*.

Problem 3.1 (The mechanical constitutive initial value problem). *Given the initial values of the internal variables $\boldsymbol{\alpha}(t_0)$ and the history of the deformation gradient,*

$$\boldsymbol{F}(t), \quad t \in [t_0, T],$$

find the functions $\boldsymbol{P}(t)$ and $\boldsymbol{\alpha}(t)$, for the first Piola–Kirchhoff stress and the set of internal variables, such that the constitutive equations

$$\begin{cases} \boldsymbol{P}(t) = \bar{\rho}\, \dfrac{\partial \psi}{\partial \boldsymbol{F}}\bigg|_t \\ \dot{\boldsymbol{\alpha}}(t) = f(\boldsymbol{F}(t), \boldsymbol{\alpha}(t)) \end{cases} \tag{3.166}$$

are satisfied for every $t \in [t_0, T]$.

In the infinitesimal case, $\boldsymbol{P}$ and $\boldsymbol{F}$ are replaced with $\boldsymbol{\sigma}$ and $\boldsymbol{\varepsilon}$, respectively, in the above initial value problem. For completeness, the infinitesimal constitutive initial value problem is stated in the following.

Problem 3.2 (The infinitesimal constitutive initial value problem). *Given the initial values of the internal variables $\boldsymbol{\alpha}(t_0)$ and the history of the infinitesimal strain tensor,*

$$\boldsymbol{\varepsilon}(t), \quad t \in [t_0, T],$$

find the functions $\boldsymbol{\sigma}(t)$ and $\boldsymbol{\alpha}(t)$, for the stress tensor and the set of internal variables, such that the constitutive equations

$$\begin{cases} \boldsymbol{\sigma}(t) = \bar{\rho}\, \dfrac{\partial \psi}{\partial \boldsymbol{\varepsilon}}\bigg|_t \\ \dot{\boldsymbol{\alpha}}(t) = f(\boldsymbol{\varepsilon}(t), \boldsymbol{\alpha}(t)) \end{cases} \tag{3.167}$$

are satisfied for every $t \in [t_0, T]$.

3.6. Weak equilibrium. The principle of virtual work

The *strong* (point-wise, local or differential) forms of the momentum balance have been stated in Section 3.4 by expressions (3.132) and (3.133). In this section, we state the momentum balance equations in their corresponding *weak* (global or integral) forms. The weak equilibrium statement – the *Principle of Virtual Work* – is fundamental to the definition of the basic initial boundary value problem stated in Section 3.7 and, as we shall see in Chapter 4, is the starting point of displacement-based finite element procedures for the analysis of solids.

Again, let us consider the body $\mathscr{B}$ which occupies the region $\Omega \subset \mathscr{E}$ with boundary $\partial\Omega$ in its reference configuration subjected to body forces in its interior and surface tractions on its boundary. In its deformed configuration, $\mathscr{B}$ occupies the region $\boldsymbol{\varphi}(\Omega)$ with boundary $\boldsymbol{\varphi}(\partial\Omega)$ defined through the deformation map $\boldsymbol{\varphi}$.

3.6.1. THE SPATIAL VERSION

The *spatial* version of the principle of virtual work states that the body $\mathscr{B}$ is in *equilibrium* if, and only if, its Cauchy stress field, $\boldsymbol{\sigma}$, satisfies the equation

$$\int_{\varphi(\Omega)} [\boldsymbol{\sigma} : \nabla_x \boldsymbol{\eta} - (\boldsymbol{b} - \rho\, \ddot{\boldsymbol{u}}) \cdot \boldsymbol{\eta}]\, \mathrm{d}v - \int_{\varphi(\partial\Omega)} \boldsymbol{t} \cdot \boldsymbol{\eta}\, \mathrm{d}a = 0, \quad \forall\, \boldsymbol{\eta} \in \mathscr{V}, \tag{3.168}$$

where $\boldsymbol{b}$ and $\boldsymbol{t}$ are the body force per unit deformed volume and boundary traction per unit deformed area and $\mathscr{V}$ is the *space of virtual displacements* of $\mathscr{B}$, i.e. the space of sufficiently regular arbitrary displacements

$$\boldsymbol{\eta} : \boldsymbol{\varphi}(\Omega) \to \mathscr{U}.$$

Equivalence between strong and weak equilibrium statements

When the stress field $\boldsymbol{\sigma}$ is sufficiently smooth, the virtual work equation is equivalent to the strong momentum balance equations (3.132). To show this, let us start by assuming that the field $\boldsymbol{\sigma}$ is sufficiently regular so that we can use the identity (v) of Section 2.5.8 (page 38) to obtain

$$\boldsymbol{\sigma} : \nabla_x \boldsymbol{\eta} = \mathrm{div}_x(\boldsymbol{\sigma}\, \boldsymbol{\eta}) - (\mathrm{div}_x \boldsymbol{\sigma}) \cdot \boldsymbol{\eta}. \tag{3.169}$$

In obtaining the above identity we have used the fact that $\boldsymbol{\sigma}$ is symmetric. Next, by substituting the above expression into (3.168), it follows that

$$\int_{\varphi(\Omega)} [\mathrm{div}_x(\boldsymbol{\sigma}\, \boldsymbol{\eta}) - (\mathrm{div}_x\, \boldsymbol{\sigma} + \boldsymbol{b} - \rho \ddot{\boldsymbol{u}}) \cdot \boldsymbol{\eta}]\, \mathrm{d}v - \int_{\varphi(\partial\Omega)} \boldsymbol{t} \cdot \boldsymbol{\eta}\, \mathrm{d}a = 0, \quad \forall\, \boldsymbol{\eta} \in \mathscr{V}. \tag{3.170}$$

We now concentrate on the first term within the square brackets of the above equation. The divergence theorem (expression $(2.148)_2$, page 37) implies the following identity

$$\int_{\varphi(\Omega)} \mathrm{div}_x(\boldsymbol{\sigma}\, \boldsymbol{\eta})\, \mathrm{d}v = \int_{\varphi(\partial\Omega)} \boldsymbol{\sigma}\, \boldsymbol{\eta} \cdot \boldsymbol{n}\, \mathrm{d}a. \tag{3.171}$$

By taking into account the symmetry of $\boldsymbol{\sigma}$, which implies $\boldsymbol{\sigma}\boldsymbol{\eta} \cdot \boldsymbol{n} = \boldsymbol{\sigma}\boldsymbol{n} \cdot \boldsymbol{\eta}$, together with the above identity, equation (3.170) can be rewritten in the equivalent form

$$\int_{\varphi(\Omega)} (\mathrm{div}_x\, \boldsymbol{\sigma} + \boldsymbol{b} - \rho \ddot{\boldsymbol{u}}) \cdot \boldsymbol{\eta}\, \mathrm{d}v + \int_{\varphi(\partial\Omega)} (\boldsymbol{t} - \boldsymbol{\sigma}\, \boldsymbol{n}) \cdot \boldsymbol{\eta}\, \mathrm{d}a = 0, \quad \forall\, \boldsymbol{\eta} \in \mathscr{V}. \tag{3.172}$$

Finally, since this equation holds for all virtual displacement fields $\boldsymbol{\eta}$, then it follows from the fundamental theorem of variational calculus (refer, for instance, to Gurtin 1972; Oden 1979 or Reddy 1998) that each bracketed term of the above equation must vanish pointwise within their respective domains, i.e. we recover the strong equilibrium equations (3.132).

Conversely, the strong form yields the weak form of equilibrium. This can be shown in a relatively straightforward manner by applying a weighted residual method to the strong form together with use of the divergence theorem.

3.6.2. THE MATERIAL VERSION

The virtual work equation can be equivalently expressed in the *reference* configuration of $\mathscr{B}$. The corresponding *material* (or *reference*) version of the Principle of Virtual Work states that $\mathscr{B}$ is in equilibrium if and only if its first Piola–Kirchhoff stress field, $\boldsymbol{P}$, satisfies

$$\int_{\Omega} [\boldsymbol{P} : \nabla_p \boldsymbol{\eta} - (\bar{\boldsymbol{b}} - \bar{\rho}\ddot{\boldsymbol{u}}) \cdot \boldsymbol{\eta}] \, \mathrm{d}v - \int_{\partial\Omega} \bar{\boldsymbol{t}} \cdot \boldsymbol{\eta} \, \mathrm{d}a = 0, \quad \forall \, \boldsymbol{\eta} \in \mathscr{V}, \tag{3.173}$$

where $\bar{\boldsymbol{b}}$ and $\bar{\boldsymbol{t}}$ are, respectively, the body force per unit reference volume and the surface traction per unit reference area and $\bar{\rho}$ is the mass density in the reference configuration. The space of virtual displacements, $\mathscr{V}$, is accordingly defined as the space of sufficiently regular arbitrary displacement fields

$$\boldsymbol{\eta} : \Omega \to \mathscr{U}.$$

The material version of the virtual work equation is obtained by introducing, in its spatial counterpart, the identities

$$\boldsymbol{\sigma} = \frac{1}{J} \boldsymbol{P} \, \boldsymbol{F}^T; \quad \nabla_x \boldsymbol{a} = \nabla_p \boldsymbol{a} \, \boldsymbol{F}^{-1}, \tag{3.174}$$

where the second expression holds for a generic vector field $\boldsymbol{a}$, and making use of the standard relation (Gurtin, 1981)

$$\int_{\varphi(\Omega)} a(\boldsymbol{x}) \, \mathrm{d}v = \int_{\Omega} J(\boldsymbol{p}) \, a(\boldsymbol{\varphi}(\boldsymbol{p})) \, \mathrm{d}v, \tag{3.175}$$

valid for any scalar field a.

The proof of equivalence between (3.173) and the strong form (3.133) under conditions of sufficient regularity is then analogous to that given for the spatial version discussed in Section 3.6.1 above.

3.6.3. THE INFINITESIMAL CASE

Under infinitesimal deformations, reference and deformed configurations coincide and the virtual work equation reads simply

$$\int_{\Omega} [\boldsymbol{\sigma} : \nabla \boldsymbol{\eta} - (\boldsymbol{b} - \rho \ddot{\boldsymbol{u}}) \cdot \boldsymbol{\eta}] \, dv - \int_{\partial\Omega} \boldsymbol{t} \cdot \boldsymbol{\eta} \, \mathrm{d}a = 0, \quad \forall \, \boldsymbol{\eta} \in \mathscr{V}. \tag{3.176}$$

3.7. The quasi-static initial boundary value problem

Having defined the generic constitutive initial value problems in Section 3.5 and the weak equilibrium statements in Section 3.6, we are now in a position to state the weak form of fundamental initial boundary value problems, whose numerical solution by the finite element method is the main subject of the subsequent chapters of this book. The problems formulated here are restricted to *quasi-static* conditions, where inertia effects are ignored. This is the case on which the numerical methods discussed in this book are focused.

3.7.1. FINITE DEFORMATIONS

Let the body $\mathscr{B}$ (Figure 3.16) be subjected to a prescribed history of body forces

$$\boldsymbol{b}(t), \quad t \in [t_0, T]$$

in its interior. In the above, dependence of $\boldsymbol{b}$ on $\boldsymbol{x}$ is implicitly assumed. In addition, the following boundary conditions are imposed.

(i) *The natural boundary condition*. The history of the surface traction

$$\boldsymbol{t}(t), \quad t \in [t_0, T],$$

with dependence on $\boldsymbol{x}$ implied, is prescribed over the portion of the boundary of $\mathscr{B}$ that occupies the region $\partial\Omega_t$ in its reference configuration.

(ii) *The essential boundary condition*. The *motion* is a prescribed function on the part of the boundary of $\mathscr{B}$ that occupies the region $\partial\Omega_u$ in the reference configuration

$$\bar{\boldsymbol{\varphi}}(\boldsymbol{p}, t) = \boldsymbol{p} + \bar{\boldsymbol{u}}(\boldsymbol{p}, t) \quad t \in [t_0, T], \; \boldsymbol{p} \in \partial\Omega_u,$$

where $\bar{\boldsymbol{u}}$ is the corresponding prescribed boundary displacement field. For simplicity, it is assumed here that $\partial\Omega_u \bigcap \partial\Omega_t = \emptyset$. We define the set of *kinematically admissible displacements* of $\mathscr{B}$ as the set of all sufficiently regular displacement functions that satisfy the kinematic constraint (the essential boundary condition)

$$\mathscr{K} = \{\boldsymbol{u} : \Omega \times \mathscr{R} \to \mathscr{U} | \; \boldsymbol{u}(\boldsymbol{p}, t) = \bar{\boldsymbol{u}}(\boldsymbol{p}, t), \; t \in [t_0, T], \; \boldsymbol{p} \in \partial\Omega_u\}. \tag{3.177}$$

The body $\mathscr{B}$ is assumed to be made from a generic material modelled by the internal variable-based constitutive equations associated with Problem 3.1 (page 76) and the internal variable field, $\boldsymbol{\alpha}$, is known at the initial time t_0, i.e.

$$\boldsymbol{\alpha}(\boldsymbol{p}, t_0) = \boldsymbol{\alpha}_0(\boldsymbol{p}). \tag{3.178}$$

The fundamental quasi-static initial boundary value problem is stated in its spatial version in the following.

Problem 3.3 (The spatial quasi-static initial boundary value problem). *Find a kinematically admissible displacement function, $\boldsymbol{u} \in \mathscr{K}$, such that, for all $t \in [t_0, T]$, the virtual work*

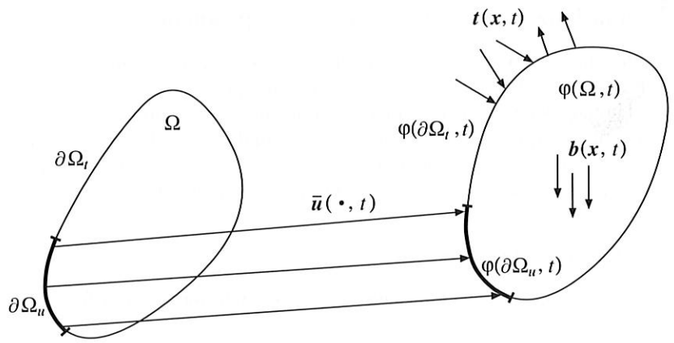

Figure 3.16. The initial boundary value problem. Schematic illustration.

equation is satisfied

$$\int_{\varphi(\Omega,t)} [\boldsymbol{\sigma}(t) : \nabla_x \boldsymbol{\eta} - \boldsymbol{b}(t) \cdot \boldsymbol{\eta}] \, \mathrm{d}v - \int_{\varphi(\partial\Omega_t,t)} \boldsymbol{t}(t) \cdot \boldsymbol{\eta} \, \mathrm{d}a = 0, \quad \forall\, \boldsymbol{\eta} \in \mathscr{V}_t. \tag{3.179}$$

The space of virtual displacements at time t is defined by

$$\mathscr{V}_t = \{\boldsymbol{\eta} : \boldsymbol{\varphi}(\Omega, t) \to \mathscr{U} \mid \boldsymbol{\eta} = \mathbf{0} \text{ on } \boldsymbol{\varphi}(\partial\Omega_u, t)\} \tag{3.180}$$

and, at each point of $\mathscr{B}$, the Cauchy stress is given by

$$\boldsymbol{\sigma}(t) = \boldsymbol{P}(t)\boldsymbol{F}(t)^T / J(t), \tag{3.181}$$

where $\boldsymbol{P}(t)$ is the solution of constitutive initial value Problem 3.1 (page 76) with prescribed deformation gradient

$$\boldsymbol{F}(t) = \nabla_p \boldsymbol{\varphi}(\boldsymbol{p}, t) = \boldsymbol{I} + \nabla_p \boldsymbol{u}(\boldsymbol{p}, t). \tag{3.182}$$

The problem can be equivalently formulated in the reference configuration of $\mathscr{B}$ in terms of the material version of the principle of virtual work (3.173). For completeness, we state the material version of the fundamental initial boundary value problem in the following.

Problem 3.4 (The material quasi-static initial boundary value problem). *Find a kinematically admissible displacement function, $\boldsymbol{u} \in \mathscr{K}$, such that, for all $t \in [t_0, T]$,*

$$\int_\Omega [\boldsymbol{P}(t) : \nabla_p \boldsymbol{\eta} - \bar{\boldsymbol{b}}(t) \cdot \boldsymbol{\eta}] \, \mathrm{d}v - \int_{\partial\Omega_t} \bar{\boldsymbol{t}}(t) \cdot \boldsymbol{\eta} \, \mathrm{d}a = 0, \quad \forall\, \boldsymbol{\eta} \in \mathscr{V}, \tag{3.183}$$

where

$$\mathscr{V} = \{\boldsymbol{\eta} : \Omega \to \mathscr{U} \mid \boldsymbol{\eta} = \mathbf{0} \text{ on } \partial\Omega_u\} \tag{3.184}$$

and the Piola–Kirchhoff stress, $\boldsymbol{P}(t)$, is the solution of initial value Problem 3.1 with prescribed deformation gradient (3.182).

3.7.2. THE INFINITESIMAL PROBLEM

Under infinitesimal deformations, the quasi-static initial boundary value problem is based on the weak form (3.176). It is stated in the following.

Problem 3.5 (The infinitesimal quasi-static initial boundary value problem). *Find a kinematically admissible displacement, $\boldsymbol{u} \in \mathscr{K}$, such that, for $t \in [t_0, T]$,*

$$\int_\Omega [\boldsymbol{\sigma}(t) : \nabla \boldsymbol{\eta} - \boldsymbol{b}(t) \cdot \boldsymbol{\eta}] \, \mathrm{d}v - \int_{\partial\Omega_t} \boldsymbol{t}(t) \cdot \boldsymbol{\eta} \, \mathrm{d}a = 0, \quad \forall\, \boldsymbol{\eta} \in \mathscr{V}, \tag{3.185}$$

where

$$\mathscr{V} = \{\boldsymbol{\eta} : \Omega \to \mathscr{U} \mid \boldsymbol{\eta} = \mathbf{0} \text{ on } \partial\Omega_u\} \tag{3.186}$$

and, at each point $\boldsymbol{p}$, $\boldsymbol{\sigma}(t)$ is the solution of the constitutive initial value Problem 3.2 (page 76) with prescribed strain

$$\boldsymbol{\varepsilon}(t) = \nabla^s \boldsymbol{u}(\boldsymbol{p}, t). \tag{3.187}$$

6 THE MATHEMATICAL THEORY OF PLASTICITY

THE mathematical theory of plasticity provides a general framework for the continuum constitutive description of the behaviour of an important class of materials. Basically, the theory of plasticity is concerned with solids that, after being subjected to a loading programme, may sustain permanent (or *plastic*) deformations when completely unloaded. In particular, this theory is restricted to the description of materials (and conditions) for which the permanent deformations do *not* depend on the rate of application of loads and is often referred to as *rate-independent* plasticity. Materials whose behaviour can be adequately described by the theory of plasticity are called *plastic* (or *rate-independent plastic*) materials. A large number of engineering materials, such as metals, concrete, rocks, clays and soils in general, may be modelled as plastic under a wide range of circumstances of practical interest. The origins of the theory of plasticity can be traced back to the middle of the nineteenth century and, following the substantial development that took place, particularly in the first half of the twentieth century, this theory is today established on sound mathematical foundations and is regarded as one of the most successful phenomenological constitutive models of solid materials.

The present chapter reviews the mathematical theory of plasticity. The theory presented here is restricted to infinitesimal deformations and provides the basis for the numerical simulation of the behaviour of elastoplastic solids to be discussed in Chapter 7. We remark that only the most important concepts and mathematical expressions are reviewed. Attention is focused on the description of mathematical models of elastoplastic materials and, in particular, issues such as limit analysis and slip-line field theory are not addressed. For a more comprehensive treatment of the theory of plasticity, the reader is referred to Hill (1950), Prager (1959), Lubliner (1990) and Jirásek and Bažant (2002). A more mathematically oriented approach to the subject is presented by Halphen and Nguyen (1975), Duvaut and Lions (1976), Matthies (1979), Suquet (1981) and Han and Reddy (1999).

This chapter is organised as follows. In Section 6.1, aspects of the phenomenological behaviour of materials classed as plastic are discussed and the main properties are pointed out in the analysis of a simple uniaxial tension experiment. The discussion is followed, in Section 6.2, by the formulation of a mathematical model of the uniaxial experiment. The uniaxial model, though simple, embodies all the essential concepts of the mathematical theory of plasticity and provides the foundation for the general multidimensional model established in Section 6.3. The remainder of the chapter focuses on the detailed description of the plasticity models most commonly used in engineering analysis: the models of Tresca, von Mises, Mohr–Coulomb and Drucker–Prager. The corresponding yield criteria are

Computational Methods for Plasticity: Theory and Applications EA de Souza Neto, D Perić and DRJ Owen

described in Section 6.4. Plastic flow rules and hardening laws are addressed, respectively, in Sections 6.5 and 6.6.

6.1. Phenomenological aspects

In spite of their qualitatively distinct mechanical responses, materials as contrasting as metals and soils share some important features of their phenomenological behaviour that make them amenable to modelling by means of the theory of plasticity. To illustrate such common features, a uniaxial tension experiment with a metallic bar is discussed in what follows.

Typically, uniaxial tension tests with ductile metals produce stress–strain curves of the type shown in Figure 6.1. In the schematic diagram of Figure 6.1, where the axial stress, σ, is plotted against the axial strain, ε, a load programme has been considered in which the bar is initially subjected to a monotonic increase in axial stress from zero to a prescribed value, σ_0. The bar is then unloaded back to an unstressed state and subsequently reloaded to a higher stress level σ_1. The stress–strain curve follows the path $O_0Y_0Z_0O_1Y_1Z_1$ shown. In this path, the initial line segment O_0Y_0 is virtually straight and, if the bar is unloaded from point Y_0 (or before it is reached), it returns to the original unstressed state O_0. Thus, in segment O_0Y_0 the behaviour of the material is regarded as *linear elastic*. Beyond Y_0, the slope of the stress–strain curve changes dramatically and if the stress (or strain) loading is reversed at, say, point Z_0, the bar returns to an unstressed state via path Z_0O_1. The new unstressed state, O_1, differs from the initial unstressed state, O_0, in that a permanent change in the shape of the bar is observed. This shape change is represented in the graph by the permanent (or *plastic*) axial strain ε^p. Monotonic reloading of the bar to a stress level σ_1 will follow the path $O_1Y_1Z_1$. Similarly to the initial *elastic* segment O_0Y_0, the portion O_1Y_1 is also virtually straight and unloading from Y_1 (or before Y_1 is reached) will bring the stress–strain state back to the unstressed configuration O_1, with no further plastic straining of the bar. Therefore, the behaviour of the material in the segment O_1Y_1 may also be regarded as linear elastic. Here, it is important to emphasise that, even though some discrepancy between unloading and reloading curves (such as lines Z_0O_1 and O_1Y_1) is observed in typical experiments, the actual difference between them is in fact much smaller than that shown in the diagram of Figure 6.1. Again, loading beyond an *elastic limit* (point Y_1 in this case) will cause further increase in plastic deformation.

Some important phenomenological properties can be identified in the above described uniaxial test. They are enumerated below:

1. The existence of an *elastic domain*, i.e. a range of stresses within which the behaviour of the material can be considered as purely elastic, without evolution of permanent (plastic) strains. The elastic domain is delimited by the so-called *yield stress*. In Figure 6.1, segments O_0Y_0 and O_1Y_1 define the elastic domain at two different states. The associated yield stresses correspond to points Y_0 and Y_1.

2. If the material is further loaded at the yield stress, then *plastic yielding* (or *plastic flow*), i.e. evolution of plastic strains, takes place.

3. Accompanying the evolution of the plastic strain, an *evolution of the yield stress* itself is also observed (note that the yield stresses corresponding to points Y_0 and Y_1 are different). This phenomenon is known as *hardening*.

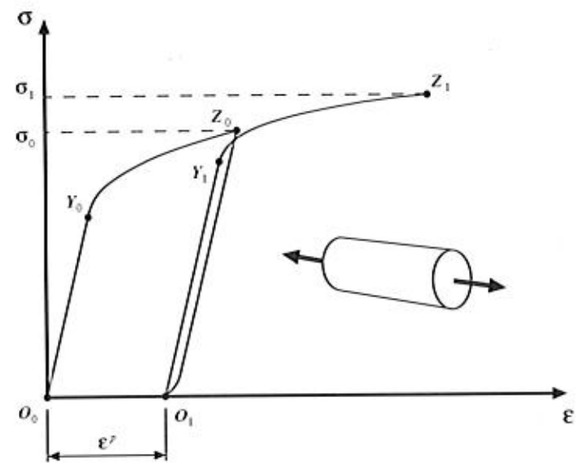

Figure 6.1. Uniaxial tension experiment with ductile metals.

It is emphasised that the above properties can be observed not only in metals but also in a wide variety of materials such as concrete, rocks, soils and many others. Obviously, the microscopic mechanisms that give rise to these common phenomenological characteristics can be completely distinct for different types of material. It is also important to note that, according to the type of material, different experimental procedures may be required for the verification of such properties. For instance, in materials such as soils, which typically cannot resist tensile stresses, uniaxial tension tests do not make physical sense. In this case, experiments such as *triaxial shear tests*, in which the sides of the specimen are subjected to a confining hydrostatic pressure prior to the application of longitudinal compression, are more appropriate.

The object of the mathematical theory of plasticity is to provide continuum constitutive models capable of describing (qualitatively and quantitavely) with sufficient accuracy the phenomenological behaviour of materials that possess the characteristics discussed in the above.

6.2. One-dimensional constitutive model

A simple mathematical model of the uniaxial experiment discussed in the previous section is formulated in what follows. In spite of its simplicity the one-dimensional constitutive model contains all the essential features that form the basis of the mathematical theory of plasticity.

At the outset, the original stress–strain curve of Figure 6.1, that resulted from the loading programme described in the previous section, is approximated by the idealised version shown in Figure 6.2. The assumptions involved in the approximation are summarised in the following. Firstly, the difference between unloading and reloading curves (segments Z_0O_1 and O_1Y_1 of Figure 6.1) is ignored and points Z_0 and Y_1, that correspond respectively to

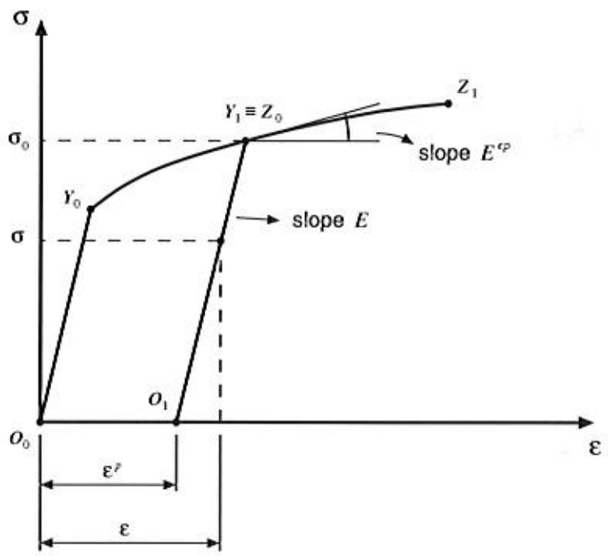

Figure 6.2. Uniaxial tension experiment. Mathematical model.

the beginning of unloading and the onset of plastic yielding upon subsequent reloading, are assumed to coincide. The transition between the elastic region and the elastoplastic regime is now clearly marked by a non-smooth change of slope (points Y_0 and Y_1). During plastic yielding, the stress–strain curve always follows the path defined by $O_0Y_0Y_1Z_1$. This path is normally referred to as the *virgin curve* and is obtained by a continuous monotonic loading from the initial unstressed state O_0.

Under the above assumptions, after being monotonically loaded from the initial unstressed state to the stress level σ_0, the behaviour of the bar between states O_1 and Y_1 is considered to be linear elastic, with constant plastic strain, ε^p, and yield limit, σ_0. Thus, within the segment O_1Y_1, the uniaxial stress corresponding to a configuration with *total* strain ε is given by

$$\sigma = E\,(\varepsilon - \varepsilon^p), \tag{6.1}$$

where E denotes the Young's modulus of the material of the bar. Note that the difference between the total strain and the current plastic strain, $\varepsilon - \varepsilon^p$, is *fully reversible*; that is, upon complete unloading of the bar, $\varepsilon - \varepsilon^p$ is fully recovered without further evolution of plastic strains. This motivates the additive decomposition of the axial strain described in the following section.

6.2.1. ELASTOPLASTIC DECOMPOSITION OF THE AXIAL STRAIN

One of the chief hypotheses underlying the small strain theory of plasticity is the decomposition of the *total strain*, ε, into the sum of an *elastic* (or reversible) component, ε^e, and a

plastic (or permanent) component, ε^p,

$$\varepsilon = \varepsilon^e + \varepsilon^p, \tag{6.2}$$

where the *elastic strain* has been defined as

$$\varepsilon^e = \varepsilon - \varepsilon^p. \tag{6.3}$$

6.2.2. THE ELASTIC UNIAXIAL CONSTITUTIVE LAW

Following the above definition of the elastic axial strain, the constitutive law for the axial stress can be expressed as

$$\sigma = E\,\varepsilon^e. \tag{6.4}$$

The next step in the definition of the uniaxial constitutive model is to derive formulae that express mathematically the fundamental phenomenological properties enumerated in Section 6.1. The items 1 and 2 of Section 6.1 are associated with the formulation of a *yield criterion* and a *plastic flow rule*, whereas item 3 requires the formulation of a *hardening law*. These are described in the following.

6.2.3. THE YIELD FUNCTION AND THE YIELD CRITERION

The existence of an elastic domain delimited by a yield stress has been pointed out in item 1 of Section 6.1. With the introduction of a *yield function*, Φ, of the form

$$\Phi(\sigma, \sigma_y) = |\sigma| - \sigma_y, \tag{6.5}$$

the *elastic domain* at a state with uniaxial yield stress σ_y can be defined in the one-dimensional plasticity model as the set

$$\mathcal{E} = \{\sigma \mid \Phi(\sigma, \sigma_y) < 0\}, \tag{6.6}$$

or, equivalently, the elastic domain is the set of stresses σ that satisfy

$$|\sigma| < \sigma_y. \tag{6.7}$$

Generalising the results of the uniaxial *tension* test discussed, it has been assumed in the above that the yield stress in compression is identical to that in tension. The corresponding idealised elastic domain is illustrated in Figure 6.3.

It should be noted that, at any stage, no stress level is allowed above the current yield stress, i.e. *plastically admissible stresses* lie either in the elastic domain or on its boundary (the yield limit). Thus, any admissible stress must satisfy the restriction

$$\Phi(\sigma, \sigma_y) \leq 0. \tag{6.8}$$

For stress levels within the elastic domain, only elastic straining may occur, whereas on its boundary (at the yield stress), either elastic unloading or plastic yielding (or plastic loading) takes place. This *yield criterion* can be expressed by

$$\begin{aligned} &\text{If } \Phi(\sigma, \sigma_y) < 0 \Longrightarrow \dot{\varepsilon}^p = 0, \\ &\text{If } \Phi(\sigma, \sigma_y) = 0 \Longrightarrow \begin{cases} \dot{\varepsilon}^p = 0 & \text{for elastic unloading,} \\ \dot{\varepsilon}^p \neq 0 & \text{for plastic loading.} \end{cases} \end{aligned} \tag{6.9}$$

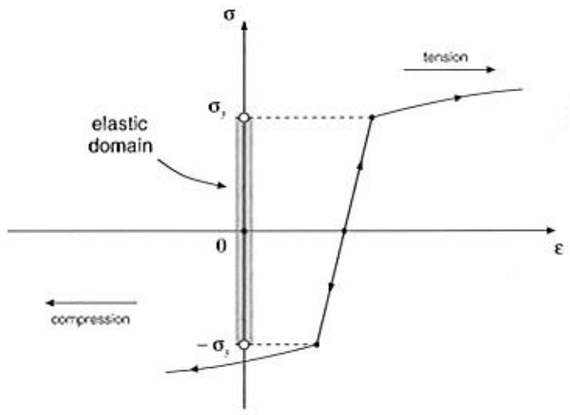

Figure 6.3. Uniaxial model. Elastic domain.

6.2.4. THE PLASTIC FLOW RULE. LOADING/UNLOADING CONDITIONS

Expressions (6.9) above have defined a criterion for plastic yielding, i.e. they have set the conditions under which plastic straining may occur. By noting in Figure 6.3 that, upon plastic loading, the plastic strain rate $\dot{\varepsilon}^p$ is positive (stretching) under tension (positive σ) and negative (compressive) under compression (negative σ), the *plastic flow rule* for the uniaxial model can be formally established as

$$\dot{\varepsilon}^p = \dot{\gamma}\,\mathrm{sign}(\sigma), \tag{6.10}$$

where sign is the *signum* function defined as

$$\mathrm{sign}(a) = \begin{cases} +1 & \text{if } a \geq 0 \\ -1 & \text{if } a < 0 \end{cases} \tag{6.11}$$

for any scalar a and the scalar $\dot{\gamma}$ is termed the *plastic multiplier*. The plastic multiplier is *non-negative*,

$$\dot{\gamma} \geq 0, \tag{6.12}$$

and satisfies the *complementarity condition*

$$\Phi\,\dot{\gamma} = 0. \tag{6.13}$$

The constitutive equations (6.10) to (6.13) imply that, as stated in the yield criterion (6.9), the plastic strain rate vanishes within the elastic domain, i.e.

$$\Phi < 0 \implies \dot{\gamma} = 0 \implies \dot{\varepsilon}^p = 0, \tag{6.14}$$

and plastic flow ($\dot{\varepsilon}^p \neq 0$) may occur only when the stress level σ coincides with the current yield stress

$$|\sigma| = \sigma_y \implies \Phi = 0 \implies \dot{\gamma} \geq 0. \tag{6.15}$$

Expressions (6.8), (6.12) and (6.13) define the so-called *loading/unloading conditions* of the elasticplastic model; that is, the constraints

$$\Phi \leq 0, \quad \dot{\gamma} \geq 0, \quad \dot{\gamma}\Phi = 0, \tag{6.16}$$

establish when plastic flow may occur.

6.2.5. THE HARDENING LAW

Finally, the complete characterisation of the uniaxial model is achieved with the introduction of the *hardening law*. As remarked in item 3 of Section 6.1, an evolution of the yield stress accompanies the evolution of the plastic strain. This phenomenon, known as *hardening*, can be incorporated into the uniaxial model simply by assuming that, in the definition (6.5) of Φ, the yield stress σ_y is a given function

$$\sigma_y = \sigma_y(\bar{\varepsilon}^p) \tag{6.17}$$

of the *accumulated* axial plastic strain, $\bar{\varepsilon}^p$. The accumulated axial plastic strain is defined as

$$\bar{\varepsilon}^p \equiv \int_0^t |\dot{\varepsilon}^p|\,\mathrm{d}t, \tag{6.18}$$

thus ensuring that both tensile and compressive plastic straining contribute to $\bar{\varepsilon}^p$. Clearly, in a monotonic tensile test we have

$$\bar{\varepsilon}^p = \varepsilon^p, \tag{6.19}$$

whereas in a monotonic compressive uniaxial test,

$$\bar{\varepsilon}^p = -\varepsilon^p. \tag{6.20}$$

The curve defined by the hardening function $\sigma_y(\bar{\varepsilon}^p)$ is usually referred to as the *hardening curve* (Figure 6.4).

From the definition of $\bar{\varepsilon}^p$, it follows that its evolution law is given by

$$\dot{\bar{\varepsilon}}^p = |\dot{\varepsilon}^p|, \tag{6.21}$$

which, in view of the plastic flow rule, is equivalent to

$$\dot{\bar{\varepsilon}}^p = \dot{\gamma}. \tag{6.22}$$

6.2.6. SUMMARY OF THE MODEL

The overall one-dimensional plasticity model is defined by the constitutive equations (6.2), (6.4), (6.5), (6.10), (6.16), (6.17), and (6.22). The model is summarised in Box 6.1.

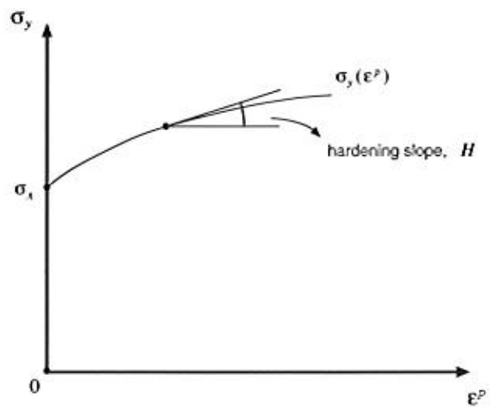

Figure 6.4. One-dimensional model. Hardening curve.

Box 6.1. One-dimensional elastoplastic constitutive model.

1. Elastoplastic split of the axial strain

$$\varepsilon = \varepsilon^e + \varepsilon^p$$

2. Uniaxial elastic law

$$\sigma = E\,\varepsilon^e$$

3. Yield function

$$\Phi(\sigma, \sigma_y) = |\sigma| - \sigma_y$$

4. Plastic flow rule

$$\dot{\varepsilon}^p = \dot{\gamma}\,\mathrm{sign}(\sigma)$$

5. Hardening law

$$\sigma_y = \sigma_y(\bar{\varepsilon}^p)$$

$$\dot{\bar{\varepsilon}}^p = \dot{\gamma}$$

6. Loading/unloading criterion

$$\Phi \le 0, \quad \dot{\gamma} \ge 0, \quad \dot{\gamma}\Phi = 0$$

6.2.7. DETERMINATION OF THE PLASTIC MULTIPLIER

So far, in the uniaxial plasticity model introduced above, the *plastic multiplier*, $\dot{\gamma}$, was left indeterminate during plastic yielding. Indeed, expressions (6.12) and (6.13) just tell us that $\dot{\gamma}$ vanishes during elastic straining but may assume *any* non-negative value during plastic flow. In order to eliminate this indetermination, it should be noted firstly that, *during plastic flow*,

the value of the yield function remains constant

$$\Phi = 0, \tag{6.23}$$

as the absolute value of the current stress always coincides with the current yield stress. Therefore, the following additional complementarity condition may be established:

$$\dot{\Phi}\,\dot{\gamma} = 0 \tag{6.24}$$

which implies that the rate of Φ vanishes whenever plastic yielding occurs ($\dot{\gamma} \neq 0$),

$$\dot{\Phi} = 0, \tag{6.25}$$

and, during elastic straining, ($\dot{\gamma} = 0$), $\dot{\Phi}$ may assume any value. Equation (6.25) is called the *consistency condition*. By taking the time derivative of the yield function (6.5), one obtains

$$\dot{\Phi} = \mathrm{sign}(\sigma)\,\dot{\sigma} - H\,\dot{\bar{\varepsilon}}^p, \tag{6.26}$$

where H is called the *hardening modulus*, or *hardening slope*, and is defined as (refer to Figure 6.4)

$$H = H(\bar{\varepsilon}^p) = \frac{\mathrm{d}\sigma_y}{\mathrm{d}\bar{\varepsilon}^p}. \tag{6.27}$$

Under plastic yielding, equation (6.25) holds so that one has the following expression for the stress rate

$$\mathrm{sign}(\sigma)\,\dot{\sigma} = H\,\dot{\bar{\varepsilon}}^p. \tag{6.28}$$

From the elastic law, it follows that

$$\dot{\sigma} = E(\dot{\varepsilon} - \dot{\varepsilon}^p). \tag{6.29}$$

Finally, by combining the above expression with (6.22), (6.28) and (6.10), the plastic multiplier, $\dot{\gamma}$, is *uniquely* determined during plastic yielding as

$$\dot{\gamma} = \frac{E}{H+E}\,\mathrm{sign}(\sigma)\,\dot{\varepsilon} = \frac{E}{H+E}\,|\dot{\varepsilon}|. \tag{6.30}$$

6.2.8. THE ELASTOPLASTIC TANGENT MODULUS

Let us now return to the stress–strain curve of Figure 6.2. Plastic flow at a generic yield limit produces the following tangent relation between strain and stress

$$\dot{\sigma} = E^{ep}\,\dot{\varepsilon}, \tag{6.31}$$

where E^{ep} is called the *elastoplastic tangent modulus*. By combining expressions (6.31), (6.29), the flow rule (6.10) and (6.30) the following expression is obtained for the elastoplastic tangent modulus

$$E^{ep} = \frac{E\,H}{E+H}. \tag{6.32}$$

Equivalently, the hardening modulus, H, can be expressed in terms of the elastic modulus and the elastoplastic modulus as

$$H = \frac{E^{ep}}{1 - E^{ep}/E}. \tag{6.33}$$

6.3. General elastoplastic constitutive model

A mathematical model of a uniaxial tension experiment with a ductile metal has been described in the previous section. As already mentioned, the one-dimensional equations contain all basic components of a general elastoplastic constitutive model:

- the elastoplastic strain decomposition;
- an elastic law;
- a yield criterion, stated with the use of a yield function;
- a plastic flow rule defining the evolution of the plastic strain; and
- a hardening law, characterising the evolution of the yield limit.

The generalisation of these concepts for application in two- and three-dimensional situations is described in this section.

6.3.1. ADDITIVE DECOMPOSITION OF THE STRAIN TENSOR

Following the decomposition of the uniaxial strain given in the previous section, the corresponding generalisation is obtained by splitting the strain *tensor*, $\boldsymbol{\varepsilon}$, into the sum of an elastic component, $\boldsymbol{\varepsilon}^e$, and a plastic component, $\boldsymbol{\varepsilon}^p$; that is,

$$\boldsymbol{\varepsilon} = \boldsymbol{\varepsilon}^e + \boldsymbol{\varepsilon}^p. \tag{6.34}$$

The tensors $\boldsymbol{\varepsilon}^e$ and $\boldsymbol{\varepsilon}^p$ are known, respectively, as the *elastic strain tensor* and the *plastic strain tensor*. The corresponding rate form of the additive split reads

$$\dot{\boldsymbol{\varepsilon}} = \dot{\boldsymbol{\varepsilon}}^e + \dot{\boldsymbol{\varepsilon}}^p. \tag{6.35}$$

Note that (6.35) together with the given initial condition

$$\boldsymbol{\varepsilon}(t_0) = \boldsymbol{\varepsilon}^e(t_0) + \boldsymbol{\varepsilon}^p(t_0) \tag{6.36}$$

at a (pseudo-)time t_0 is equivalent to (6.34).

6.3.2. THE FREE ENERGY POTENTIAL AND THE ELASTIC LAW

The formulation of general dissipative models of solids within the framework of thermodynamics with an internal variable has been addressed in Section 3.5 of Chapter 3. Recall that the free energy potential plays a crucial role in the derivation of the model and provides the constitutive law for stress. The starting point of the theories of plasticity treated in this book is the assumption that the free energy, ψ, is a function

$$\psi(\boldsymbol{\varepsilon}, \boldsymbol{\varepsilon}^p, \boldsymbol{\alpha}),$$

of the total strain, the plastic strain (taken as an internal variable) and a set $\boldsymbol{\alpha}$ of internal variables associated with the phenomenon of hardening. It is usual to assume that the free

energy can be split as

$$\begin{aligned}\psi(\boldsymbol{\varepsilon}, \boldsymbol{\varepsilon}^p, \boldsymbol{\alpha}) &= \psi^e(\boldsymbol{\varepsilon} - \boldsymbol{\varepsilon}^p) + \psi^p(\boldsymbol{\alpha}) \\ &= \psi^e(\boldsymbol{\varepsilon}^e) + \psi^p(\boldsymbol{\alpha})\end{aligned} \tag{6.37}$$

into a sum of an elastic contribution, ψ^e, whose dependence upon strains and internal variables appears only through the elastic strain, and a contribution due to hardening, ψ^p.

Following the above expression for the free energy, the Clausius–Duhem inequality reads

$$\left(\boldsymbol{\sigma} - \bar{\rho}\,\frac{\partial \psi^e}{\partial \boldsymbol{\varepsilon}^e}\right) : \dot{\boldsymbol{\varepsilon}}^e + \boldsymbol{\sigma} : \dot{\boldsymbol{\varepsilon}}^p - \boldsymbol{A} * \dot{\boldsymbol{\alpha}} \geq 0, \tag{6.38}$$

where

$$\boldsymbol{A} \equiv \bar{\rho}\,\partial \psi^p / \partial \boldsymbol{\alpha} \tag{6.39}$$

is the *hardening thermodynamical force* and we note that $-\boldsymbol{\sigma}$ is the thermodynamical force associated with the plastic strain while the symbol * indicates the appropriate product between $\boldsymbol{A}$ and $\dot{\boldsymbol{\alpha}}$. The above inequality implies a general elastic law of the form

$$\boldsymbol{\sigma} = \bar{\rho}\,\frac{\partial \psi^e}{\partial \boldsymbol{\varepsilon}^e}, \tag{6.40}$$

so that the requirement of non-negative dissipation can be reduced to

$$\Upsilon^p(\boldsymbol{\sigma}, \boldsymbol{A}; \dot{\boldsymbol{\varepsilon}}^p, \dot{\boldsymbol{\alpha}}) \geq 0, \tag{6.41}$$

where the function Υ^p, defined by

$$\Upsilon^p(\boldsymbol{\sigma}, \boldsymbol{A}; \dot{\boldsymbol{\varepsilon}}^p, \dot{\boldsymbol{\alpha}}) \equiv \boldsymbol{\sigma} : \dot{\boldsymbol{\varepsilon}}^p - \boldsymbol{A} * \dot{\boldsymbol{\alpha}}, \tag{6.42}$$

is called the *plastic dissipation function*.

This chapter is focused on materials whose elastic behaviour is *linear* (as in the uniaxial model of the previous section) and isotropic. In this case, the elastic contribution to the free energy is given by

$$\begin{aligned}\bar{\rho}\,\psi^e(\boldsymbol{\varepsilon}^e) &= \tfrac{1}{2}\,\boldsymbol{\varepsilon}^e : \mathbf{D}^e : \boldsymbol{\varepsilon}^e \\ &= G\,\boldsymbol{\varepsilon}^e_d : \boldsymbol{\varepsilon}^e_d + \tfrac{1}{2}\,K\,(\varepsilon^e_v)^2\end{aligned} \tag{6.43}$$

where $\mathbf{D}^e$ is the standard isotropic elasticity tensor and G and K are, respectively the shear and bulk moduli. The tensor $\boldsymbol{\varepsilon}^e_d$ is the deviatoric component of the elastic strain and $\varepsilon^e_v \equiv \mathrm{tr}[\boldsymbol{\varepsilon}^e]$ is the volumetric elastic strain. Thus, the general counterpart of uniaxial elastic law (6.4) is given by

$$\begin{aligned}\boldsymbol{\sigma} &= \mathbf{D}^e : \boldsymbol{\varepsilon}^e \\ &= 2G\,\boldsymbol{\varepsilon}^e_d + K\,\varepsilon^e_v\,\boldsymbol{I}.\end{aligned} \tag{6.44}$$

6.3.3. THE YIELD CRITERION AND THE YIELD SURFACE

Recall that in the uniaxial yield criterion it was established that plastic flow may occur when the uniaxial stress attains a critical value. This principle could be expressed by means of a yield function which is negative when only elastic deformations are possible and reaches zero when plastic flow is imminent. Extension of this concept to the three-dimensional case is obtained by stating that plastic flow may occur only when

$$\Phi(\boldsymbol{\sigma}, \boldsymbol{A}) = 0, \tag{6.45}$$

where the scalar yield function, Φ, is now a function of the stress *tensor* and a set $\boldsymbol{A}$ of hardening thermodynamical forces. Analogously to the uniaxial case, a yield function defines the *elastic domain* as the set

$$\mathscr{E} = \{\boldsymbol{\sigma} \mid \Phi(\boldsymbol{\sigma}, \boldsymbol{A}) < 0\} \tag{6.46}$$

of stresses for which plastic yielding is not possible. Any stress lying in the elastic domain or on its boundary is said to be *plastically admissible*. We then define the *set of plastically admissible stresses* (or *plastically admissible domain*) as

$$\bar{\mathscr{E}} = \{\boldsymbol{\sigma} \mid \Phi(\boldsymbol{\sigma}, \boldsymbol{A}) \leq 0\}. \tag{6.47}$$

The yield locus, i.e. the set of stresses for which plastic yielding may occur, is the boundary of the elastic domain, where $\Phi(\boldsymbol{\sigma}, \boldsymbol{A}) = 0$. The yield locus in this case is represented by a hypersurface in the space of stresses. This hypersurface is termed the *yield surface* and is defined as

$$\mathscr{Y} = \{\boldsymbol{\sigma} \mid \Phi(\boldsymbol{\sigma}, \boldsymbol{A}) = 0\}. \tag{6.48}$$

6.3.4. PLASTIC FLOW RULE AND HARDENING LAW

The complete characterisation of the general plasticity model requires the definition of the evolution laws for the internal variables, i.e. the variables associated with the dissipative phenomena. In the present case, the internal variables are the plastic strain tensor and the set $\boldsymbol{\alpha}$ of hardening variables. The following plastic flow rule and hardening law are then postulated

$$\dot{\boldsymbol{\varepsilon}}^p = \dot{\gamma}\, \boldsymbol{N} \tag{6.49}$$

$$\dot{\boldsymbol{\alpha}} = \dot{\gamma}\, \boldsymbol{H}, \tag{6.50}$$

where the tensor

$$\boldsymbol{N} = \boldsymbol{N}(\boldsymbol{\sigma}, \boldsymbol{A}) \tag{6.51}$$

is termed the *flow vector* and the function

$$\boldsymbol{H} = \boldsymbol{H}(\boldsymbol{\sigma}, \boldsymbol{A}) \tag{6.52}$$

is the *generalised hardening modulus* which defines the evolution of the hardening variables. The evolution equations (6.49) and (6.50) are complemented by the loading/unloading conditions

$$\Phi \leq 0, \quad \dot{\gamma} \geq 0, \quad \Phi\dot{\gamma} = 0, \tag{6.53}$$

that define when evolution of plastic strains and internal variables ($\dot{\gamma} \neq 0$) may occur.

For convenience, the general plasticity model resulting from the above equations is listed in Box 6.2.

Box 6.2. A general elastoplastic constitutive model.

1. Additive decomposition of the strain tensor

$$\boldsymbol{\varepsilon} = \boldsymbol{\varepsilon}^e + \boldsymbol{\varepsilon}^p$$

or

$$\dot{\boldsymbol{\varepsilon}} = \dot{\boldsymbol{\varepsilon}}^e + \dot{\boldsymbol{\varepsilon}}^p, \quad \boldsymbol{\varepsilon}(t_0) = \boldsymbol{\varepsilon}^e(t_0) + \boldsymbol{\varepsilon}^p(t_0)$$

2. Free-energy function

$$\psi = \psi(\boldsymbol{\varepsilon}^e, \boldsymbol{\alpha})$$

where $\boldsymbol{\alpha}$ is a set of hardening internal variables

3. Constitutive equation for $\boldsymbol{\sigma}$ and hardening thermodynamic forces $\boldsymbol{A}$

$$\boldsymbol{\sigma} = \bar{\rho}\, \frac{\partial \psi}{\partial \boldsymbol{\varepsilon}^e}, \quad \boldsymbol{A} = \bar{\rho}\, \frac{\partial \psi}{\partial \boldsymbol{\alpha}}$$

4. Yield function

$$\Phi = \Phi(\boldsymbol{\sigma}, \boldsymbol{A})$$

5. Plastic flow rule and hardening law

$$\dot{\boldsymbol{\varepsilon}}^p = \dot{\gamma}\, \boldsymbol{N}(\boldsymbol{\sigma}, \boldsymbol{A})$$

$$\dot{\boldsymbol{\alpha}} = \dot{\gamma}\, \boldsymbol{H}(\boldsymbol{\sigma}, \boldsymbol{A})$$

6. Loading/unloading criterion

$$\Phi \leq 0, \quad \dot{\gamma} \geq 0, \quad \dot{\gamma}\Phi = 0$$

6.3.5. FLOW RULES DERIVED FROM A FLOW POTENTIAL

In the formulation of multidimensional plasticity models, it is often convenient to define the flow rule (and possibly the hardening law) in terms of a *flow* (or *plastic*) *potential*. The starting point of such an approach is to postulate the existence of a flow potential with general form

$$\Psi = \Psi(\boldsymbol{\sigma}, \boldsymbol{A}) \tag{6.54}$$

from which the flow vector, $\boldsymbol{N}$, is obtained as

$$\boldsymbol{N} \equiv \frac{\partial \Psi}{\partial \boldsymbol{\sigma}}. \tag{6.55}$$

If the hardening law is assumed to be derived from the same potential, then we have in addition

$$\boldsymbol{H} \equiv -\frac{\partial \Psi}{\partial \boldsymbol{A}}. \tag{6.56}$$

When such an approach is adopted, the plastic potential, Ψ, is required to be a non-negative convex function of both $\boldsymbol{\sigma}$ and $\boldsymbol{A}$ and zero-valued at the origin,

$$\Psi(\boldsymbol{0}, \boldsymbol{0}) = 0. \tag{6.57}$$

These restrictions ensure that the dissipation inequality (6.41) is satisfied *a priori* by the evolution equations (6.49) and (6.50).

Associative flow rule

As we shall see later, many plasticity models, particularly for ductile metals, have their yield function, Φ, as a flow potential, i.e.

$$\Psi \equiv \Phi. \tag{6.58}$$

Such models are called *associative* (or *associated*) plasticity models. The issue of associativity will be further discussed in Section 6.5.1.

6.3.6. THE PLASTIC MULTIPLIER

Here we extend to the multidimensional case the procedure for the determination of the plastic multiplier, $\dot{\gamma}$, described in Section 6.2.7 for the one-dimensional plasticity model. Following the same arguments employed in Section 6.2.7, the starting point in the determination of $\dot{\gamma}$ is the consideration of the additional complementarity equation

$$\dot{\Phi}\,\dot{\gamma} = 0, \tag{6.59}$$

which implies the *consistency condition*

$$\dot{\Phi} = 0 \tag{6.60}$$

under plastic yielding (when $\dot{\gamma} \neq 0$). By differentiating the yield function with respect to time, we obtain

$$\dot{\Phi} = \frac{\partial \Phi}{\partial \boldsymbol{\sigma}} : \dot{\boldsymbol{\sigma}} + \frac{\partial \Phi}{\partial A} * \dot{A}. \tag{6.61}$$

By taking into account the additive split of the strain tensor, the elastic law and the plastic flow rule (6.49), we promptly find the obvious rate form

$$\dot{\boldsymbol{\sigma}} = \mathbf{D}^e : (\dot{\boldsymbol{\varepsilon}} - \dot{\boldsymbol{\varepsilon}}^p) = \mathbf{D}^e : (\dot{\boldsymbol{\varepsilon}} - \dot{\gamma}\, \boldsymbol{N}). \tag{6.62}$$

This, together with the definition of A in terms of the free-energy potential (refer to expression (6.39)) and the evolution law (6.50), allow us to write (6.61) equivalently as

$$\begin{aligned} \dot{\Phi} &= \frac{\partial \Phi}{\partial \boldsymbol{\sigma}} : \mathbf{D}^e : (\dot{\boldsymbol{\varepsilon}} - \dot{\boldsymbol{\varepsilon}}^p) + \frac{\partial \Phi}{\partial A} * \bar{\rho} \frac{\partial^2 \psi^p}{\partial \boldsymbol{\alpha}^2} * \dot{\boldsymbol{\alpha}}. \\ &= \frac{\partial \Phi}{\partial \boldsymbol{\sigma}} : \mathbf{D}^e : (\dot{\boldsymbol{\varepsilon}} - \dot{\gamma}\, \boldsymbol{N}) + \dot{\gamma}\, \frac{\partial \Phi}{\partial A} * \bar{\rho} \frac{\partial^2 \psi^p}{\partial \boldsymbol{\alpha}^2} * \boldsymbol{H}. \end{aligned} \tag{6.63}$$

Finally, the above expression and the consistency condition (6.60) lead to the following closed formula for the plastic multiplier

$$\dot{\gamma} = \frac{\partial \Phi / \partial \boldsymbol{\sigma} : \mathbf{D}^e : \dot{\boldsymbol{\varepsilon}}}{\partial \Phi / \partial \boldsymbol{\sigma} : \mathbf{D}^e : \boldsymbol{N} - \partial \Phi / \partial A * \bar{\rho} \partial^2 \psi^p / \partial \boldsymbol{\alpha}^2 * \boldsymbol{H}}. \tag{6.64}$$

6.3.7. RELATION TO THE GENERAL CONTINUUM CONSTITUTIVE THEORY

At this point, we should emphasise that the general rate-independent plasticity model described above can under some conditions be shown to be a particular instance of the general constitutive theory postulated in Section 3.5.2, starting page 71. The link between the two theories can be clearly demonstrated when rate-independent plasticity is obtained as a limit case of rate-dependent plasticity (or viscoplasticity).

However, since the theory of elasto-viscoplasticity is introduced only in Chapter 11, we find it convenient to carry on focusing on rate-independent plasticity and postpone the demonstration until that chapter. Those wishing to see now the link between rate-independent plasticity and the general constitutive theory are referred to Section 11.4.3, starting on page 452. We remark, though, that the concept of subdifferential, introduced below in Section 6.3.9, is fundamental to the demonstration. Readers not yet familiar with this concept are advised to read through Section 6.3.9 before moving to Section 11.4.3.

6.3.8. RATE FORM AND THE ELASTOPLASTIC TANGENT OPERATOR

In the elastic regime, the rate constitutive equation for stress reads simply

$$\dot{\boldsymbol{\sigma}} = \mathbf{D}^e : \dot{\boldsymbol{\varepsilon}}. \tag{6.65}$$

Under plastic flow, the corresponding rate relation can be obtained by introducing expression (6.64) into (6.62). The rate equation reads

$$\dot{\boldsymbol{\sigma}} = \mathbf{D}^{ep} : \dot{\boldsymbol{\varepsilon}}, \tag{6.66}$$

where $\mathbf{D}^{ep}$ is the *elastoplastic tangent modulus* given by

$$\mathbf{D}^{ep} = \mathbf{D}^e - \frac{(\mathbf{D}^e : \boldsymbol{N}) \otimes (\mathbf{D}^e : \partial \Phi / \partial \boldsymbol{\sigma})}{\partial \Phi / \partial \boldsymbol{\sigma} : \mathbf{D}^e : \boldsymbol{N} - \partial \Phi / \partial A * \bar{\rho} \partial^2 \psi^p / \partial \boldsymbol{\alpha}^2 * \boldsymbol{H}}. \tag{6.67}$$

In obtaining the above expression, we have made use of the fact that the symmetry (refer to equation (2.87), page 29) of the elasticity tensor implies

$$\partial \Phi / \partial \boldsymbol{\sigma} : \mathbf{D}^e : \dot{\boldsymbol{\varepsilon}} = \mathbf{D}^e : \partial \Phi / \partial \boldsymbol{\sigma} : \dot{\boldsymbol{\varepsilon}}. \tag{6.68}$$

The fourth-order tensor $\mathbf{D}^{ep}$ is the multidimensional generalisation of the scalar modulus E^{ep} associated with the slope of the uniaxial stress–strain curve under plastic flow. In the computational plasticity literature, $\mathbf{D}^{ep}$ is frequently referred to as the *continuum* elastoplastic tangent operator.

Remark 6.1 (The symmetry of $\mathbf{D}^{ep}$). Note that if the plastic flow rule is *associative*, i.e. if $\boldsymbol{N} \equiv \partial \Phi / \partial \boldsymbol{\sigma}$, then the continuum elastoplastic tangent operator is *symmetric*. For models with non-associative plastic flow, $\mathbf{D}^{ep}$ is generally unsymmetric.

6.3.9. NON-SMOOTH POTENTIALS AND THE SUBDIFFERENTIAL

It should be noted that expressions (6.55) and (6.56) only make sense if the potential Ψ is differentiable. When that happens, the flow vector, $\boldsymbol{N}$, can be interpreted as a vector

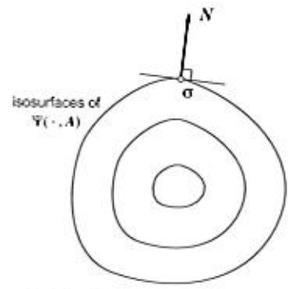

Figure 6.5. The flow vector. Smooth potential.

normal to the iso-surfaces of function Ψ in the space of stresses (with fixed $\boldsymbol{A}$). A schematic representation of $\boldsymbol{N}$ in this case is shown in Figure 6.5. The generalised modulus, H, can be interpreted in a completely analogous way.

The requirement of differentiability of the flow potential is, however, too restrictive and many practical plasticity models are based on the use of a non-differentiable Ψ. Specific examples are given later in this chapter. For a more comprehensive account of such theories the reader is referred to Duvaut and Lions (1976), Eve *et al.* (1990) and Han and Reddy (1999). In such cases, the function Ψ is called a *pseudo-potential* or *generalised potential* and the formulation of the evolution laws for the internal variables can be dealt with by introducing the concept of *subdifferential sets*, which generalises the classical definition of derivative.[†]

Subgradients and the subdifferential

Let us consider a *scalar* function $y : \mathscr{R}^n \to \mathscr{R}$. The *subdifferential* of y at a point $\bar{\boldsymbol{x}}$ is the set

$$\partial y(\bar{\boldsymbol{x}}) = \{s \in \mathscr{R}^n \mid y(\boldsymbol{x}) - y(\bar{\boldsymbol{x}}) \geq \boldsymbol{s} \cdot (\boldsymbol{x} - \bar{\boldsymbol{x}}),\ \forall\, \boldsymbol{x} \in \mathscr{R}^n\}. \tag{6.69}$$

If the set ∂y is not empty at $\bar{\boldsymbol{x}}$, the function y is said to be *subdifferentiable* at $\bar{\boldsymbol{x}}$. The elements of ∂y are called *subgradients* of y. If the function y is *differentiable*, then the subdifferential contains a *unique* subgradient which coincides with the derivative of y,

$$\partial y = \left\{\frac{\mathrm{d}y}{\mathrm{d}\boldsymbol{x}}\right\}. \tag{6.70}$$

A schematic illustration of the concept of subdifferential is shown in Figure 6.6 for $n = 1$. In this case, when y is subdifferentiable (but not necessarily differentiable) at a point $\bar{x}$, the subdifferential at that point is composed of all slopes s lying between the slopes on the right and left of $\bar{x}$ (the two one-sided derivatives of y at $\bar{x}$).

[†]The concept of subdifferential sets is exploited extensively in convex analysis. The reader is referred to Rockafellar (1970), Part V, for a detailed account of the theory of subdifferentiable functions.

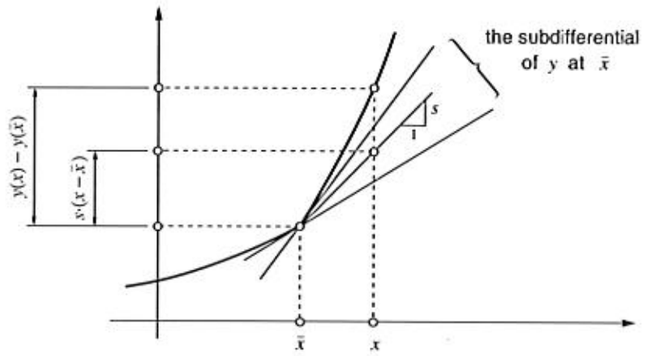

Figure 6.6. The subdifferential of a convex function.

Plastic flow with subdifferentiable flow potentials

Assume now that the (pseudo-) potential Ψ is a subdifferentiable function of $\boldsymbol{\sigma}$ and $\boldsymbol{A}$. At points where Ψ is non-differentiable in $\boldsymbol{\sigma}$, the isosurfaces of Ψ in the space of stresses contain a singularity (corner) where the normal direction is not uniquely defined. A typical situation is schematically illustrated in Figure 6.7 where two distinct normals, $\boldsymbol{N}_1$ and $\boldsymbol{N}_2$, are assumed to exist. In this case, the subdifferential of Ψ with respect to $\boldsymbol{\sigma}$, denoted $\partial_{\boldsymbol{\sigma}}\Psi$, is the set of vectors contained in the cone defined by all linear combinations (with positive coefficients) of $\boldsymbol{N}_1$ and $\boldsymbol{N}_2$. The generalisation of the plastic flow rule (6.49) is obtained by replacing expression (6.55) for the flow vector with

$$\boldsymbol{N} \in \partial_{\boldsymbol{\sigma}}\Psi, \tag{6.71}$$

i.e. the flow vector $\boldsymbol{N}$ is now assumed to be a *subgradient* of Ψ. Analogously, the evolution law (6.50) for $\boldsymbol{\alpha}$ can be generalised with the replacement of the definition (6.56) by

$$\boldsymbol{H} \in -\partial_{\boldsymbol{A}}\Psi. \tag{6.72}$$

At this point, it should be remarked that differentiability of Ψ with respect to the stress tensor is violated for some very basic plasticity models, such as the Tresca, Mohr–Coulomb and Drucker–Prager theories to be seen later. Therefore, the concepts of subgradient and subdifferential sets introduced above are important in the formulation of evolution laws for $\boldsymbol{\varepsilon}^p$.

An alternative definition of the plastic flow rule with non-smooth potentials, which incorporates a wide class of models, is obtained as follows. Firstly assume that a *finite* number, n, of distinct normals $(\boldsymbol{N}_1, \boldsymbol{N}_2, \ldots, \boldsymbol{N}_n)$ is defined at a generic singular point of an isosurface of Ψ. In this case, any subgradient of Ψ can be written as a linear combination

$$c_1\boldsymbol{N}_1 + c_2\boldsymbol{N}_2 + \cdots + c_n\boldsymbol{N}_n,$$

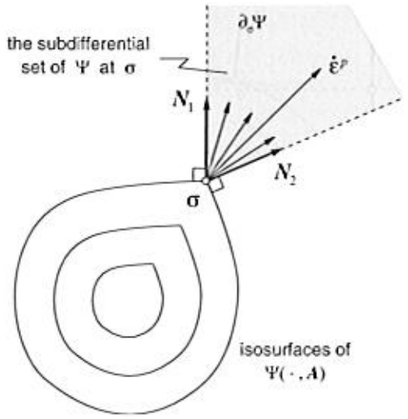

Figure 6.7. The flow vector. Non-smooth potential.

with *non-negative* coefficients $c_1, c_2, \ldots, c_n$.[‡] Based on this observation, the flow rule (6.49) can be generalised as

$$\dot{\varepsilon}^p = \sum_{i=1}^{n} \dot{\gamma}_i N_i, \tag{6.73}$$

with all n plastic multipliers required to be non-negative

$$\dot{\gamma}_i \geq 0, \quad i = 1, \ldots, n. \tag{6.74}$$

The generalisation of the plastic flow law, in this format, was originally proposed by Koiter (1953).

Multisurface models

The above concepts are particularly useful in defining evolution laws for *multisurface* plasticity models. In a generic multisurface model, the elastic domain is bound by a *set* of n surfaces in the space of stresses which intersect in a non-smooth fashion. In this case, n yield functions (Φ_i, $i = 1, \ldots, n$) are defined so that each bounding surface is given by an equation

$$\Phi_i(\boldsymbol{\sigma}, \boldsymbol{A}) = 0. \tag{6.75}$$

The elastic domain in this case reads

$$\mathscr{E} = \{\boldsymbol{\sigma} \mid \Phi_i(\boldsymbol{\sigma}, \boldsymbol{A}) < 0, \ i = 1, \ldots, n\}, \tag{6.76}$$

and the yield surface, i.e. the boundary of $\mathscr{E}$, is the set of all stresses such that $\Phi_i(\boldsymbol{\sigma}, \boldsymbol{A}) = 0$ for at least one i and $\Phi_j(\boldsymbol{\sigma}, \boldsymbol{A}) \leq 0$ for all other indices $j \neq i$.

[‡] It should be emphasised that this representation is not valid for certain types of singularity where the corresponding subdifferential set cannot be generated by a finite number of vectors.

Assuming associativity ($\Psi \equiv \Phi$), the situation discussed previously, where the subgradient of the flow potential is a linear combination of a finite number of normals, is recovered. Thus, the plastic flow rule can be written in the general form (6.73) with the normals being defined here as

$$N_i = \frac{\partial \Phi_i}{\partial \boldsymbol{\sigma}}. \tag{6.77}$$

In the present case, the standard loading/unloading criterion (6.53) is replaced by the generalisation

$$\Phi_i \leq 0, \quad \dot{\gamma}_i \geq 0, \quad \Phi_i \dot{\gamma}_i = 0, \tag{6.78}$$

which must hold for each $i = 1, \ldots, n$. Note that summation on repeated indices is not implied in the above law.

6.4. Classical yield criteria

The general constitutive model for elastoplastic materials has been established in the previous section. There, the yield criterion has been stated in its general form, without reference to any particular criteria. In this section, some of the most common yield criteria used in engineering practice are described in detail; namely, the criteria of *Tresca*, *von Mises*, *Mohr–Coulomb* and *Drucker–Prager*.

6.4.1. THE TRESCA YIELD CRITERION

This criterion was proposed by Tresca (1868) to describe plastic yielding in metals. The Tresca yield criterion assumes that *plastic yielding begins when the maximum shear stress reaches a critical value*.

Recall the spectral representation of the stress tensor,

$$\boldsymbol{\sigma} = \sum_{i=1}^{3} \sigma_i \, \boldsymbol{e}_i \otimes \boldsymbol{e}_i, \tag{6.79}$$

where σ_i are the *principal stresses* and $\boldsymbol{e}_i$ the associated unit eigenvectors, and let $\sigma_{\max}$ and $\sigma_{\min}$ be, respectively, the maximum and minimum principal stresses

$$\begin{aligned} \sigma_{\max} &= \max(\sigma_1, \sigma_2, \sigma_3); \\ \sigma_{\min} &= \min(\sigma_1, \sigma_2, \sigma_3). \end{aligned} \tag{6.80}$$

The *maximum shear stress*, $\tau_{\max}$, is given by

$$\tau_{\max} = \tfrac{1}{2}(\sigma_{\max} - \sigma_{\min}). \tag{6.81}$$

According to the Tresca criterion, the onset of plastic yielding is defined by the condition

$$\tfrac{1}{2}(\sigma_{\max} - \sigma_{\min}) = \tau_y(\alpha), \tag{6.82}$$

where τ_y is the *shear yield stress*, here assumed to be a function of a *hardening internal variable*, α, to be defined later. The shear yield stress is the yield limit under a state of pure shear.

In view of (6.82), the yield function associated with the Tresca yield criterion can be represented as

$$\Phi(\boldsymbol{\sigma}) = \tfrac{1}{2}(\sigma_{\max} - \sigma_{\min}) - \tau_y(\alpha), \tag{6.83}$$

with the onset of yielding characterised by $\Phi = 0$. Alternatively, the Tresca yield function may be defined as

$$\Phi(\boldsymbol{\sigma}) = (\sigma_{\max} - \sigma_{\min}) - \sigma_y(\alpha), \tag{6.84}$$

where σ_y is the *uniaxial* yield stress

$$\sigma_y = 2\,\tau_y, \tag{6.85}$$

that is, it is the stress level at which plastic yielding begins under *uniaxial* stress conditions. That σ_y is indeed the uniaxial yield stress for the Tresca theory can be established by noting that, when plastic yielding begins under uniaxial stress conditions, we have

$$\sigma_{\max} = \sigma_y, \quad \sigma_{\min} = 0. \tag{6.86}$$

The substitution of the above into (6.82) gives (6.85). The elastic domain for the Tresca criterion can be defined as

$$\mathcal{E} = \{\boldsymbol{\sigma} \mid \Phi(\boldsymbol{\sigma}, \sigma_y) < 0\}. \tag{6.87}$$

Pressure-insensitivity

Due to its definition exclusively in terms of *shear* stress, the Tresca criterion is *pressure insensitive*, that is, the hydrostatic pressure component,

$$p \equiv \tfrac{1}{3}\,\mathrm{tr}[\boldsymbol{\sigma}] = \tfrac{1}{3}\,(\sigma_1 + \sigma_2 + \sigma_3), \tag{6.88}$$

of the stress tensor does *not* affect yielding. Indeed, note that the superposition of an arbitrary pressure, p^*, on the stress tensor does not affect the value of the Tresca yield function

$$\Phi(\boldsymbol{\sigma} + p^*\boldsymbol{I}) = \Phi(\boldsymbol{\sigma}). \tag{6.89}$$

We remark that the von Mises criterion described in Section 6.4.2 below is also pressure-insensitive. This property is particularly relevant in the modelling of metals as, for these materials, the influence of the hydrostatic stress on yielding is usually negligible in practice.

Isotropy

One very important aspect of the Tresca criterion is its *isotropy* (a property shared by the von Mises, Mohr–Coulomb and Drucker–Prager criteria described in the following sections).

Note that, since Φ in (6.83) or (6.84) is defined as a function of the principal stresses, the Tresca yield function is an *isotropic* function of the stress tensor (refer to Section A.1, page 731, for the definition of isotropic scalar functions of a symmetric tensor), i.e. it satisfies

$$\Phi(\boldsymbol{\sigma}) = \Phi(\boldsymbol{Q}\boldsymbol{\sigma}\boldsymbol{Q}^T) \tag{6.90}$$

for all rotations $\boldsymbol{Q}$; that is, rotations of the state of stress do not affect the value of the yield function.

At this point, it is convenient to introduce the following definition: *A plastic yield criterion is said to be isotropic if it is defined in terms of an isotropic yield function of the stress tensor.*

Graphical representation

Since any isotropic scalar function of a symmetric tensor can be described as a function of the principal values of its argument, it follows that any iso-surface (i.e. any subset of the function domain with fixed function value) of such functions can be graphically represented as a surface in the space of principal values of the argument. This allows, in particular, the yield surface (refer to expression (6.48), page 150) of any isotropic yield criterion to be represented in a particularly simple and useful format as a three-dimensional surface in the space of principal stresses.

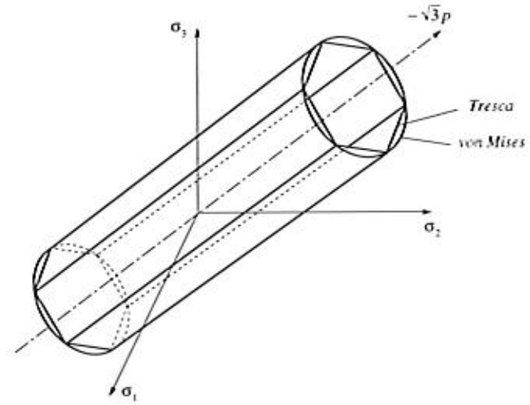

Figure 6.8. The Tresca and von Mises yield surfaces in principal stress space.

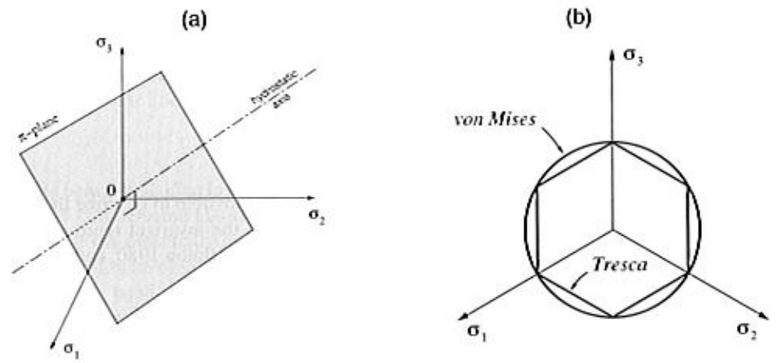

Figure 6.9. (a) The π-plane in principal stress space and, (b) the π-plane representation of the Tresca and von Mises yield surfaces.

In principal stress space, the Tresca yield surface, i.e. the set of stresses for which $\Phi = 0$, is graphically represented by the surface of an infinite hexagonal prism with axis coinciding with the hydrostatic line (also known as the space diagonal), defined by $\sigma_1 = \sigma_2 = \sigma_3$. This is illustrated in Figure 6.8. The elastic domain (for which $\Phi < 0$) corresponds to the interior of the prism. Due to the assumed insensitivity to pressure, a further simplification in the representation of the yield surface is possible in this case. The Tresca yield surface may be represented, without loss of generality, by its projection on the subspace of stresses with zero hydrostatic pressure component ($\sigma_1 + \sigma_2 + \sigma_3 = 0$). This subspace is called the *deviatoric plane*, also referred to as the π-*plane*. It is graphically illustrated in Figure 6.9(a). Figure 6.9(b) shows the π-plane projection of the Tresca yield surface.

Multisurface representation

Equivalently to the above representation, the Tresca yield criterion can be expressed by means of the following six yield functions

$$\begin{aligned}
\Phi_1(\boldsymbol{\sigma}, \sigma_y) &= \sigma_1 - \sigma_3 - \sigma_y \\
\Phi_2(\boldsymbol{\sigma}, \sigma_y) &= \sigma_2 - \sigma_3 - \sigma_y \\
\Phi_3(\boldsymbol{\sigma}, \sigma_y) &= \sigma_2 - \sigma_1 - \sigma_y \\
\Phi_4(\boldsymbol{\sigma}, \sigma_y) &= \sigma_3 - \sigma_1 - \sigma_y \\
\Phi_5(\boldsymbol{\sigma}, \sigma_y) &= \sigma_3 - \sigma_2 - \sigma_y \\
\Phi_6(\boldsymbol{\sigma}, \sigma_y) &= \sigma_1 - \sigma_2 - \sigma_y,
\end{aligned} \tag{6.91}$$

so that, for fixed σ_y, the equation

$$\Phi_i(\boldsymbol{\sigma}, \sigma_y) = 0 \tag{6.92}$$

corresponds to a *plane* in the space of principal stresses for each $i = 1, \ldots, 6$ (Figure 6.10).

In the multisurface representation, the elastic domain for a given σ_y can be defined as

$$\mathcal{E} = \{\boldsymbol{\sigma} \mid \Phi_i(\boldsymbol{\sigma}, \sigma_y) < 0,\ i = 1, \ldots, 6\}. \tag{6.93}$$

Definitions (6.87) and (6.93) are completely equivalent. The yield surface – the boundary of $\mathcal{E}$ – is defined in this case as the set of stresses for which $\Phi_i(\boldsymbol{\sigma}, \sigma_y) = 0$ for at least one i with $\Phi_j(\boldsymbol{\sigma}, \sigma_y) \leq 0$ for $j \neq i$.

Invariant representation

Alternatively to the representations discussed above, it is also possible to describe the yield locus of the Tresca criterion in terms of *stress invariants*. In the invariant representation, proposed by Nayak and Zienkiewicz (1972) (see also Owen and Hinton 1980, and Crisfield 1997), the yield function assumes the format

$$\Phi = 2\sqrt{J_2}\cos\theta - \sigma_y, \tag{6.94}$$

where $J_2 = J_2(\boldsymbol{s})$ is the invariant of the stress deviator, $\boldsymbol{s}$, defined by

$$J_2 \equiv -I_2(\boldsymbol{s}) = \tfrac{1}{2}\,\mathrm{tr}[\boldsymbol{s}^2] = \tfrac{1}{2}\,\boldsymbol{s} : \boldsymbol{s} = \tfrac{1}{2}\,\|\boldsymbol{s}\|^2. \tag{6.95}$$

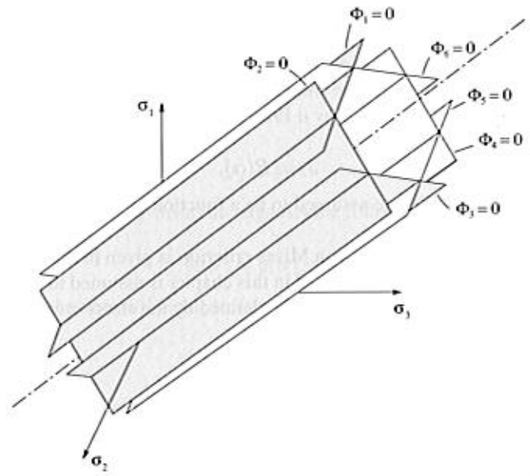

Figure 6.10. The Tresca criterion. Multisurface representation in principal stress space.

Recall that the stress deviator is given by

$$\boldsymbol{s} \equiv \boldsymbol{\sigma} - \tfrac{1}{3}(\mathrm{tr}\boldsymbol{\sigma})\boldsymbol{I}. \tag{6.96}$$

The *Lode angle*, θ, is a function of the deviatoric stress defined as

$$\theta \equiv \tfrac{1}{3}\sin^{-1}\left(\frac{-3\sqrt{3}\,J_3}{2J_2^{\frac{3}{2}}}\right), \tag{6.97}$$

where J_3 is the third principal invariant of stress deviator[5]

$$J_3 \equiv I_3(\boldsymbol{s}) \equiv \det \boldsymbol{s} = \tfrac{1}{3}\,\mathrm{tr}(\boldsymbol{s})^3. \tag{6.98}$$

The Lode angle is the angle, on the deviatoric plane, between $\boldsymbol{s}$ and the nearest pure shear line (a pure shear line is graphically represented in Figure 6.11). It satisfies

$$-\frac{\pi}{6} \leq \theta \leq \frac{\pi}{6}. \tag{6.99}$$

Despite being used often in computational plasticity, the above invariant representation results in rather cumbersome algorithms for integration of the evolution equations of the Tresca model. This is essentially due to the high degree of nonlinearity introduced by the trigonometric function involved in the definition of the Lode angle. The multisurface representation, on the other hand, is found by the authors to provide an optimal parametrisation of the Tresca surface which results in a simpler numerical algorithm and will be adopted in the computational implementation of the model addressed in Chapter 8.

[5] The equivalence between the two rightmost terms in (6.98) is established by summing the characteristic equation (2.73) (page 27) for $i = 1, 2, 3$ and taking into account the fact that $I_1(\boldsymbol{s}) = 0$ ($\boldsymbol{s}$ is a traceless tensor) and that $\mathrm{tr}(\boldsymbol{S})^3 = \sum_i s_i^3$ for any symmetric tensor $\boldsymbol{S}$.

6.4.2. THE VON MISES YIELD CRITERION

Also appropriate to describe plastic yielding in metals, this criterion was proposed by von Mises (1913). According to the von Mises criterion, *plastic yielding begins when the J_2 stress deviator invariant reaches a critical value*. This condition is mathematically represented by the equation

$$J_2 = R(\alpha), \tag{6.100}$$

where R is the critical value, here assumed to be a function of a hardening internal variable, α, to be defined later.

The physical interpretation of the von Mises criterion is given in the following. Since the elastic behaviour of the materials described in this chapter is assumed to be linear elastic, the stored elastic strain-energy at the generic state defined by the stress σ can be decomposed as the sum

$$\psi^e = \psi^e_d + \psi^e_v, \tag{6.101}$$

of a *distortional* contribution,

$$\bar{\rho}\,\psi^e_d = \frac{1}{2\,G}\,\boldsymbol{s} : \boldsymbol{s} = \frac{1}{G}\,J_2, \tag{6.102}$$

and a *volumetric* contribution,

$$\bar{\rho}\,\psi^e_v = \frac{1}{K}\,p^2, \tag{6.103}$$

where G and K are, respectively, the shear and bulk modulus. In view of (6.102), the von Mises criterion is equivalent to stating that *plastic yielding begins when the distortional elastic strain-energy reaches a critical value*. The corresponding critical value of the distortional energy is

$$\frac{1}{G}\,R.$$

It should be noted that, as in the Tresca criterion, the pressure component of the stress tensor does not take part in the definition of the von Mises criterion and only the deviatoric stress can influence plastic yielding. Thus, the von Mises criterion is also *pressure-insensitive*.

In a state of *pure shear*, i.e. a state with stress tensor

$$[\boldsymbol{\sigma}] = \begin{bmatrix} 0 & \tau & 0 \\ \tau & 0 & 0 \\ 0 & 0 & 0 \end{bmatrix}, \tag{6.104}$$

we have, $\boldsymbol{s} = \boldsymbol{\sigma}$ and

$$J_2 = \tau^2. \tag{6.105}$$

Thus, a yield function for the von Mises criterion can be defined as

$$\Phi(\boldsymbol{\sigma}) = \sqrt{J_2(\boldsymbol{s}(\boldsymbol{\sigma}))} - \tau_y, \tag{6.106}$$

where $\tau_y \equiv \sqrt{R}$ is the *shear* yield stress. Let us now consider a state of *uniaxial stress*:

$$[\boldsymbol{\sigma}] = \begin{bmatrix} \sigma & 0 & 0 \\ 0 & 0 & 0 \\ 0 & 0 & 0 \end{bmatrix}. \tag{6.107}$$

In this case, we have

$$[\boldsymbol{s}] = \begin{bmatrix} \frac{2}{3}\sigma & 0 & 0 \\ 0 & -\frac{1}{3}\sigma & 0 \\ 0 & 0 & -\frac{1}{3}\sigma \end{bmatrix} \tag{6.108}$$

and

$$J_2 = \tfrac{1}{3}\sigma^2. \tag{6.109}$$

The above expression for the J_2-invariant suggests the following alternative definition of the von Mises yield function:

$$\Phi(\boldsymbol{\sigma}) = q(\boldsymbol{\sigma}) - \sigma_y, \tag{6.110}$$

where $\sigma_y \equiv \sqrt{3R}$ is the *uniaxial* yield stress and

$$q(\boldsymbol{\sigma}) \equiv \sqrt{3\,J_2(\boldsymbol{s}(\boldsymbol{\sigma}))} \tag{6.111}$$

is termed the *von Mises effective* or *equivalent stress*. The uniaxial and shear yield stresses for the von Mises criterion are related by

$$\sigma_y = \sqrt{3}\,\tau_y. \tag{6.112}$$

Note that this relation differs from that of the Tresca criterion given by (6.85). Obviously, due to its definition in terms of an invariant of the stress tensor, the von Mises yield function is an isotropic function of $\boldsymbol{\sigma}$.

The von Mises and Tresca criteria may be set to agree with one another in either uniaxial stress or pure shear states. If they are set by using the yield functions (6.84) and (6.110) so that both predict the same uniaxial yield stress σ_y, then, under pure shear, the von Mises criterion will predict a yield stress $2/\sqrt{3}$ (≈ 1.155) times that given by the Tresca criterion. On the other hand, if both criteria are made to coincide under pure shear (expressions (6.83) and (6.106) with the same τ_y), then, in uniaxial stress states, the von Mises criterion will predict yielding at a stress level $\sqrt{3}/2$ (≈ 0.866) times the level predicted by Tresca's law.

The yield surface ($\Phi = 0$) associated with the von Mises criterion is represented, in the space of principal stresses, by the surface of an infinite circular cylinder, the axis of which coincides with the hydrostatic axis. The von Mises surface is illustrated in Figure 6.8 where it has been set to match the Tresca surface (shown in the same figure) under uniaxial stress. The corresponding π-plane representation is shown in Figure 6.9(b). The von Mises circle intersects the vertices of the Tresca hexagon. The yield surfaces for the von Mises and Tresca criteria set to coincide in shear is shown in Figure 6.11. In this case, the von Mises circle is tangent to the sides of the Tresca hexagon. It is remarked that, for many metals, experimentally determined yield surfaces fall between the von Mises and Tresca surfaces. A more general model, which includes both the Tresca and the von Mises yield surfaces as particular cases (and, in addition, allows for anisotropy of the yield surface), is described in Section 10.3.4 (starting page 427).

6.4.3. THE MOHR–COULOMB YIELD CRITERION

The criteria presented so far are pressure-insensitive and adequate to describe metals. For materials such as soils, rocks and concrete, whose behaviour is generally characterised by

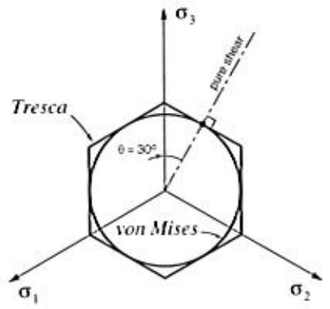

Figure 6.11. Yield surfaces for the Tresca and von Mises criteria coinciding in pure shear.

a strong dependence of the yield limit on the hydrostatic pressure, appropriate description of plastic yielding requires the introduction of *pressure-sensitivity*. A classical example of a pressure-sensitive law is given by the Mohr–Coulomb yield criterion described in the following.

The Mohr–Coulomb criterion is based on the assumption that the phenomenon of macroscopic plastic yielding is, essentially, the result of frictional sliding between material particles. Generalising Coulomb's friction law, this criterion states that *plastic yielding begins when, on a plane in the body, the shearing stress, τ, and the normal stress, σ_n, reach the critical combination*

$$\tau = c - \sigma_n \tan\phi, \tag{6.113}$$

where c is the cohesion and ϕ is the angle of internal friction or frictional angle. In the above, the normal stress, σ_n, was assumed tensile positive.

The yield locus of the Mohr–Coulomb criterion is the set of all stress states such that there exists a plane in which (6.113) holds. The Mohr–Coulomb yield locus can be easily visualised in the Mohr plane representation shown in Figure 6.12. It is the set of all stresses whose largest Mohr circle, i.e. the circle associated with the maximum and minimum principal stresses ($\sigma_{\max}$ and $\sigma_{\min}$, respectively), is tangent to the critical line defined by $\tau = c - \sigma_n \tan\phi$. The elastic domain for the Mohr–Coulomb law is the set of stresses whose all three Mohr circles are below the critical line. From Figure 6.12, the yield condition (6.113) is found to be equivalent to the following form in terms of principal stresses

$$\frac{\sigma_{\max} - \sigma_{\min}}{2}\cos\phi = c - \left(\frac{\sigma_{\max} + \sigma_{\min}}{2} + \frac{\sigma_{\max} - \sigma_{\min}}{2}\sin\phi\right)\tan\phi, \tag{6.114}$$

which, rearranged, gives

$$(\sigma_{\max} - \sigma_{\min}) + (\sigma_{\max} + \sigma_{\min})\sin\phi = 2\,c\,\cos\phi. \tag{6.115}$$

In view of (6.115), a yield function expressed in terms of the principal stresses can be immediately defined for the Mohr–Coulomb criterion as

$$\Phi(\boldsymbol{\sigma}, c) = (\sigma_{\max} - \sigma_{\min}) + (\sigma_{\max} + \sigma_{\min})\,\sin\phi - 2\,c\,\cos\phi. \tag{6.116}$$

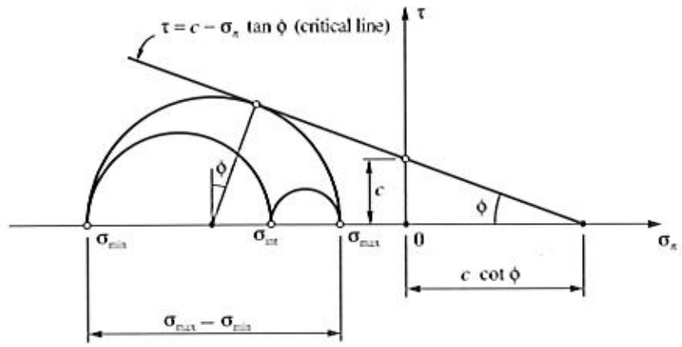

Figure 6.12. The Mohr–Coulomb criterion. Mohr plane representation.

Due to its definition in terms of principal stresses, this yield function is an isotropic function of $\boldsymbol{\sigma}$. The corresponding yield surface ($\Phi = 0$) is a hexagonal pyramid aligned with the hydrostatic axis and whose apex is located at

$$p = c\,\cot\phi \tag{6.117}$$

on the tensile side of the hydrostatic axis. The Mohr–Coulomb surface is illustrated in Figure 6.13. Its pyramidal shape, as opposed to the prismatic shape of the Tresca surface, is a consequence of the *pressure-sensitivity* of the Mohr–Coulomb criterion. It should be noted, however, that both criteria coincide in the absence of internal friction, i.e. when $\phi = 0$. As no stress state is allowed on the outside of the yield surface, the apex of the pyramid (point A in the figure) defines the limit of resistance of the material to tensile pressures. Limited strength under tensile pressure is a typical characteristic of materials such as concrete, rock and soils, to which the Mohr–Coulomb criterion is most applicable.

Multisurface representation

Analogously to the multisurface representation of the Tresca criterion, the Mohr–Coulomb criterion can also be expressed by means of six functions:

$$\begin{aligned}
\Phi_1(\boldsymbol{\sigma}, c) &= \sigma_1 - \sigma_3 + (\sigma_1 + \sigma_3)\sin\phi - 2\,c\,\cos\phi \\
\Phi_2(\boldsymbol{\sigma}, c) &= \sigma_2 - \sigma_3 + (\sigma_2 + \sigma_3)\sin\phi - 2\,c\,\cos\phi \\
\Phi_3(\boldsymbol{\sigma}, c) &= \sigma_2 - \sigma_1 + (\sigma_2 + \sigma_1)\sin\phi - 2\,c\,\cos\phi \\
\Phi_4(\boldsymbol{\sigma}, c) &= \sigma_3 - \sigma_1 + (\sigma_3 + \sigma_1)\sin\phi - 2\,c\,\cos\phi \\
\Phi_5(\boldsymbol{\sigma}, c) &= \sigma_3 - \sigma_2 + (\sigma_3 + \sigma_2)\sin\phi - 2\,c\,\cos\phi \\
\Phi_6(\boldsymbol{\sigma}, c) &= \sigma_1 - \sigma_2 + (\sigma_1 + \sigma_2)\sin\phi - 2\,c\,\cos\phi.
\end{aligned} \tag{6.118}$$

whose roots, $\Phi_i(\boldsymbol{\sigma}, c) = 0$ (for fixed c), define six planes in the principal stress space. Each plane contains one face of the Mohr–Coulomb pyramid represented in Figure 6.13.

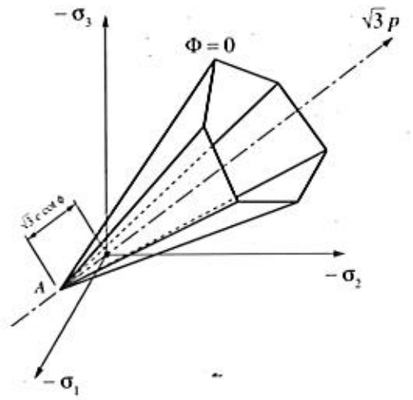

Figure 6.13. The Mohr–Coulomb yield surface in principal stress space.

The definition of the elastic domain and the yield surface in the multisurface representation is completely analogous to that of the Tresca criterion.

Invariant representation

Analogously to the invariant representation (6.94) of the Tresca criterion, the Mohr–Coulomb yield function can be expressed as (Owen and Hinton 1980, and Crisfield 1997):

$$\Phi = \left(\cos\theta - \frac{1}{\sqrt{3}}\sin\theta\,\sin\phi\right)\sqrt{J_2(\boldsymbol{s})} + p(\boldsymbol{\sigma})\,\sin\phi - c\,\cos\phi, \tag{6.119}$$

where the Lode angle, θ, is defined in (6.97). As for the Tresca model, in spite of its frequent use in computational plasticity, the invariant representation of the Mohr–Coulomb surface renders more complex numerical algorithms so that the multisurface representation is preferred in the computational implementation of the model described in Chapter 8.

6.4.4. THE DRUCKER–PRAGER YIELD CRITERION

This criterion has been proposed by Drucker and Prager (1952) as a smooth approximation to the Mohr–Coulomb law. It consists of a modification of the von Mises criterion in which an extra term is included to introduce pressure-sensitivity. The Drucker–Prager criterion states that *plastic yielding begins when the J_2 invariant of the deviatoric stress and the hydrostatic stress, p, reach a critical combination*. The onset of plastic yielding occurs when the equation

$$\sqrt{J_2(\boldsymbol{s})} + \eta\, p = \bar{c}, \tag{6.120}$$

is satisfied, where η and $\bar{c}$ are material parameters. Represented in the principal stress space, the yield locus of this criterion is a circular cone whose axis is the hydrostatic line. For $\eta = 0$, the von Mises cylinder is recovered. The Drucker–Prager cone is illustrated in Figure 6.14.

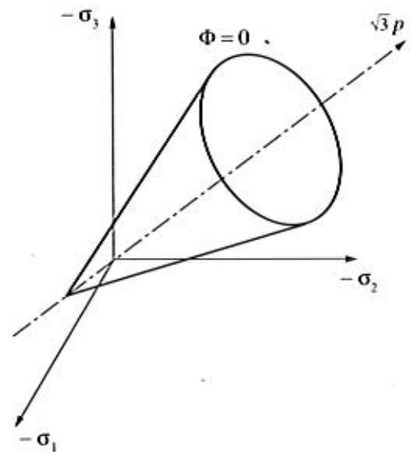

Figure 6.14. The Drucker–Prager yield surface in principal stress space.

In order to approximate the Mohr–Coulomb yield surface, it is convenient to define the Drucker–Prager yield function as

$$\Phi(\boldsymbol{\sigma}, c) = \sqrt{J_2(\boldsymbol{s}(\boldsymbol{\sigma}))} + \eta\, p(\boldsymbol{\sigma}) - \xi\, c, \tag{6.121}$$

where c is the *cohesion* and the parameters η and ξ are chosen according to the required approximation to the Mohr–Coulomb criterion. Note that the isotropy of the Mohr–Coulomb yield function follows from the fact that it is defined in terms of invariants of the stress tensor ($J_2(\boldsymbol{s})$ and p). Two of the most common approximations used are obtained by making the yield surfaces of the Drucker–Prager and Mohr–Coulomb criteria coincident either at the outer or inner edges of the Mohr–Coulomb surface. Coincidence at the *outer* edges is obtained when

$$\eta = \frac{6\,\sin\phi}{\sqrt{3}\,(3 - \sin\phi)}, \quad \xi = \frac{6\,\cos\phi}{\sqrt{3}\,(3 - \sin\phi)}, \tag{6.122}$$

whereas, coincidence at the *inner* edges is given by the choice

$$\eta = \frac{6\,\sin\phi}{\sqrt{3}\,(3 + \sin\phi)}, \quad \xi = \frac{6\,\cos\phi}{\sqrt{3}\,(3 + \sin\phi)}. \tag{6.123}$$

The outer and inner cones are known, respectively, as the *compression cone* and the *extension cone*. The inner cone matches the Mohr–Coulomb criterion in uniaxial tension and biaxial compression. The outer edge approximation matches the Mohr–Coulomb surface in uniaxial compression and biaxial tension. The π-plane section of both surfaces is shown in Figure 6.15. Another popular Drucker–Prager approximation to the Mohr–Coulomb criterion is obtained by forcing both criteria to predict identical collapse loads under *plane strain* conditions. In this case (the reader is referred to Section 4.7 of Chen and Mizuno (1990) for

derivation) the constants η and ξ read

$$\eta = \frac{3\ \tan\phi}{\sqrt{9 + 12\ \tan^2\phi}}, \quad \xi = \frac{3}{\sqrt{9 + 12\ \tan^2\phi}}. \tag{6.124}$$

For all three sets of parameters above, the apex of the approximating Drucker–Prager cone coincides with the apex of the corresponding Mohr–Coulomb yield surface. It should be emphasised here that any of the above approximations to the Mohr–Coulomb criterion can give a poor description of the material behaviour for certain states of stress. Thus, according to the dominant stress state in a particular problem to be analysed, other approximations may be more appropriate. For instance, under plane stress, which can be assumed in the analysis of structures such as concrete walls, it may be convenient to use an approximation such that both criteria match under, say, uniaxial tensile and uniaxial compressive stress states. For the Mohr–Coulomb criterion to fit a given uniaxial tensile strength, f'_t, and a given uniaxial compressive strength, f'_c, the parameters ϕ and c have to be chosen as

$$\phi = \sin^{-1}\left(\frac{f'_c - f'_t}{f'_c + f'_t}\right), \quad c = \frac{f'_c f'_t}{f'_c - f'_t}\tan\phi. \tag{6.125}$$

The corresponding Drucker–Prager cone (Figure 6.16) that predicts the same uniaxial failure loads is obtained by setting

$$\eta = \frac{3\ \sin\phi}{\sqrt{3}}, \quad \xi = \frac{2\cos\phi}{\sqrt{3}}. \tag{6.126}$$

Its apex no longer coincides with the apex of the original Mohr–Coulomb pyramid. For problems where the failure mechanism is indeed dominated by uniaxial tension/compression, the above approximation should produce reasonable results. However, if for a particular problem, failure occurs under biaxial *compression* instead (with stresses near point f'_{bc} of Figure 6.16), then the above approximation will largely overestimate the limit load, particularly for high ratios f'_c/f'_t which are typical for concrete. Under such a condition, a different approximation (such as the inner cone that matches point f'_{bc}) needs to be adopted to produce sensible predictions. Another useful approximation for plane stress, where the Drucker–Prager cone coincides with the Mohr–Coulomb surface in biaxial tension (point f'_{bt}) and biaxial compression (point f'_{bc}), is obtained by setting

$$\eta = \frac{3\ \sin\phi}{2\sqrt{3}}, \quad \xi = \frac{2\cos\phi}{\sqrt{3}}. \tag{6.127}$$

Drucker–Prager approximations to the Mohr–Coulomb criterion are thoroughly discussed by Chen (1982), Chen and Mizuno (1990) and Zienkiewicz *et al.* (1978).

6.5. Plastic flow rules

6.5.1. ASSOCIATIVE AND NON-ASSOCIATIVE PLASTICITY

It has already been said that a plasticity model is classed as *associative* if the yield function, Φ, is taken as the flow potential, i.e.

$$\Psi = \Phi. \tag{6.128}$$

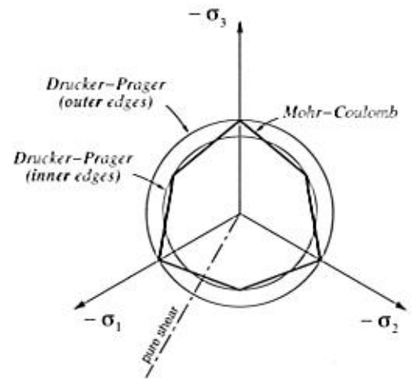

Figure 6.15. The π-plane section of the Mohr–Coulomb surface and the Drucker–Prager approximations.

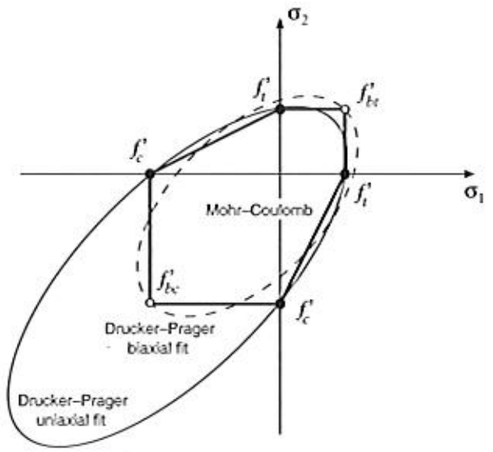

Figure 6.16. Plane stress. Drucker–Prager approximation matching the Mohr–Coulomb surface in uniaxial tension and uniaxial compression.

Any other choice of flow potential characterises a *non-associative* (or *non-associated*) plasticity model.

In associative models, the evolution equations for the plastic strain and hardening variables are given by

$$\dot{\boldsymbol{\varepsilon}}^p = \dot{\gamma}\,\frac{\partial \Phi}{\partial \boldsymbol{\sigma}}, \tag{6.129}$$

and

$$\dot{\boldsymbol{\alpha}} = -\dot{\gamma}\,\frac{\partial \Phi}{\partial \boldsymbol{A}}. \tag{6.130}$$

Associativity implies that the plastic strain rate is a tensor *normal to the yield surface* in the space of stresses. In the generalised case of non-smooth yield surfaces, the flow vector is a subgradient of the yield function, i.e. we have

$$\dot{\boldsymbol{\varepsilon}}^p = \dot{\gamma}\boldsymbol{N}; \quad \boldsymbol{N} \in \partial_{\sigma}\Phi. \tag{6.131}$$

In non-associative models, the plastic strain rate is not normal to the yield surface in general.

6.5.2. ASSOCIATIVE LAWS AND THE PRINCIPLE OF MAXIMUM PLASTIC DISSIPATION

It can be shown that the associative laws are a consequence of the *principle of maximum plastic dissipation*. Before stating the principle of maximum plastic dissipation, recall that for a state defined by a hardening force $\boldsymbol{A}$, the admissible stress states are those that satisfy $\Phi(\boldsymbol{\sigma}, \boldsymbol{A}) \leq 0$. Thus, it makes sense to define

$$\mathscr{A} = \{(\boldsymbol{\sigma}, \boldsymbol{A}) \mid \Phi(\boldsymbol{\sigma}, \boldsymbol{A}) \leq 0\} \tag{6.132}$$

as the set of all admissible pairs (combinations) of stress and hardening force. The principle of maximum dissipation postulates that *among all admissible pairs* $(\boldsymbol{\sigma}^*, \boldsymbol{A}^*) \in \mathscr{A}$, *the actual state* $(\boldsymbol{\sigma}, \boldsymbol{A})$ *maximises the dissipation function* (6.42) *for a given plastic strain rate,* $\dot{\boldsymbol{\varepsilon}}^p$, *and rate* $\dot{\boldsymbol{\alpha}}$ *of hardening internal variables*. The principle of maximum plastic dissipation requires that, for given $(\dot{\boldsymbol{\varepsilon}}^p, \dot{\boldsymbol{\alpha}})$,

$$\Upsilon^p(\boldsymbol{\sigma}, \boldsymbol{A}; \dot{\boldsymbol{\varepsilon}}^p, \dot{\boldsymbol{\alpha}}) \geq \Upsilon^p(\boldsymbol{\sigma}^*, \boldsymbol{A}^*; \dot{\boldsymbol{\varepsilon}}^p, \dot{\boldsymbol{\alpha}}), \ \forall\, (\boldsymbol{\sigma}^*, \boldsymbol{A}^*) \in \mathscr{A}. \tag{6.133}$$

In other words, the actual state $(\boldsymbol{\sigma}, \boldsymbol{A})$ of stress and hardening force is a solution to the following constrained optimisation problem:

$$\begin{aligned} &\text{maximise } \Upsilon^p(\boldsymbol{\sigma}^*, \boldsymbol{A}^*, \dot{\boldsymbol{\varepsilon}}^p, \dot{\boldsymbol{\alpha}}) \\ &\text{subject to } \Phi(\boldsymbol{\sigma}^*, \boldsymbol{A}^*) \leq 0. \end{aligned} \tag{6.134}$$

The *Kuhn–Tucker optimality conditions* (Luenberger, 1973, Chapter 10) for this optimisation problem are precisely the associative plastic flow rule (6.129), the associative hardening rule (6.130) and the loading/unloading conditions

$$\Phi(\boldsymbol{\sigma}, \boldsymbol{A}) \leq 0, \quad \dot{\gamma} \geq 0, \quad \Phi(\boldsymbol{\sigma}, \boldsymbol{A})\dot{\gamma} = 0. \tag{6.135}$$

Remark 6.2. The postulate of maximum plastic dissipation, and the corresponding associative laws, are *not* universal. Based on physical considerations, maximum dissipation has been shown to hold in crystal plasticity and is particularly successful when applied to the description of metals. Nevertheless, for many materials, particularly soils and granular materials in general, associative laws frequently do not correspond to experimental evidence. In such cases, the maximum dissipation postulate is clearly not applicable and the use of non-associative laws is essential.

6.5.3. CLASSICAL FLOW RULES

The Prandtl–Reuss equations

The Prandtl–Reuss plasticity law is the flow rule obtained by taking the von Mises yield function (6.110) as the flow potential. The corresponding flow vector is given by

$$\boldsymbol{N} \equiv \frac{\partial \Phi}{\partial \boldsymbol{\sigma}} = \frac{\partial}{\partial \boldsymbol{\sigma}}[\sqrt{3\,J_2(\boldsymbol{s})}] = \sqrt{\tfrac{3}{2}}\,\frac{\boldsymbol{s}}{||\boldsymbol{s}||}, \tag{6.136}$$

and the flow rule results in

$$\dot{\boldsymbol{\varepsilon}}^p = \dot{\gamma}\,\sqrt{\tfrac{3}{2}}\,\frac{\boldsymbol{s}}{||\boldsymbol{s}||}. \tag{6.137}$$

Here, it should be noted that the Prandtl–Reuss flow vector is the derivative of an isotropic scalar function of a symmetric tensor – the von Mises yield function. Thus (refer to Section A.1.2, page 732, where the derivative of isotropic functions of this type is discussed), $\boldsymbol{N}$ and $\boldsymbol{\sigma}$ are coaxial, i.e. the principal directions of $\boldsymbol{N}$ coincide with those of $\boldsymbol{\sigma}$. Due to the pressure-insensitivity of the von Mises yield function, the plastic flow vector is *deviatoric*. The Prandtl–Reuss flow vector is a tensor parallel to the deviatoric projection $\boldsymbol{s}$ of the stress tensor. Its principal stress representation is depicted in Figure 6.17. The Prandtl–Reuss rule is usually employed in conjunction with the von Mises criterion and the resulting plasticity model is referred to as the von Mises associative model or, simply, the von Mises model.

Associative Tresca

The associative Tresca flow rule utilises the yield function (6.84) as the flow potential. Since Φ here is also an isotropic function of $\boldsymbol{\sigma}$, the rate of plastic strain has the same principal directions as $\boldsymbol{\sigma}$. The Tresca yield function is differentiable when the three principal stresses are distinct ($\sigma_1 \neq \sigma_2 \neq \sigma_3$) and non-differentiable when two principal stresses coincide (at the edges of the Tresca hexagonal prism). Hence, the Tresca associative plastic flow rule is generally expressed as

$$\dot{\boldsymbol{\varepsilon}}^p = \dot{\gamma}\boldsymbol{N}, \tag{6.138}$$

where $\boldsymbol{N}$ is a subgradient of the Tresca function

$$\boldsymbol{N} \in \partial_{\sigma}\Phi. \tag{6.139}$$

Its multisurface-based representation reads

$$\dot{\boldsymbol{\varepsilon}}^p = \sum_{i=1}^{6} \dot{\gamma}^i \boldsymbol{N}^i = \sum_{i=1}^{6} \dot{\gamma}^i \frac{\partial \Phi_i}{\partial \boldsymbol{\sigma}}, \tag{6.140}$$

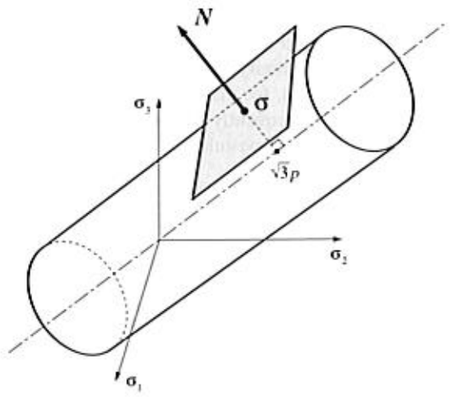

Figure 6.17. The Prandtl–Reuss flow vector.

with the yield functions Φ_i defined by (6.91). Each vector N^i is normal to the plane defined by $\Phi_i = 0$.

The above flow rule can be alternatively expressed as follows. Firstly assume, without loss of generality, that the principal stresses are ordered as $\sigma_1 \geq \sigma_2 \geq \sigma_3$, so that the discussion can be concentrated on the sextant of the π-plane illustrated in Figure 6.18. Three different possibilities have to be considered in this sextant:

(a) yielding at a stress state on the *side* (main plane) of the Tresca hexagon ($\Phi_1 = 0, \Phi_2 < 0$ and $\Phi_6 < 0$);

(b) yielding from the *right corner*, R ($\Phi_1 = 0, \Phi_6 = 0$ and $\Phi_2 < 0$); and

(c) Yielding from the *left corner*, L ($\Phi_1 = 0, \Phi_2 = 0$ and $\Phi_6 < 0$).

When the stress is on the side of the hexagon, only one multiplier may be non-zero and the plastic flow rule reads

$$\dot{\varepsilon}^p = \dot{\gamma}\, N^a, \tag{6.141}$$

where the flow vector is the normal to the plane $\Phi_1 = 0$, given by

$$\begin{aligned} N^a \equiv N^1 &= \frac{\partial \Phi_1}{\partial \boldsymbol{\sigma}} = \frac{\partial}{\partial \boldsymbol{\sigma}}(\sigma_1 - \sigma_3) \\ &= \boldsymbol{e}_1 \otimes \boldsymbol{e}_1 - \boldsymbol{e}_3 \otimes \boldsymbol{e}_3, \end{aligned} \tag{6.142}$$

with $\boldsymbol{e}_i$ denoting the eigenvector of $\boldsymbol{\sigma}$ associated with the principal stress σ_i. In deriving the last right-hand side of (6.142), use has been made of the expression (A.27) of page 736 for the derivative of an eigenvalue of a symmetric tensor.

At the right and left corners of the hexagon, where two planes intersect, two multipliers may be non-zero. Thus, the plastic flow equation is

$$\dot{\varepsilon}^p = \dot{\gamma}^a\, N^a + \dot{\gamma}^b\, N^b. \tag{6.143}$$

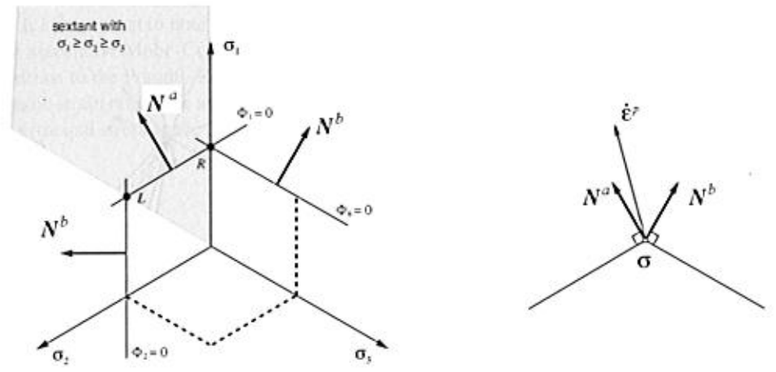

Figure 6.18. The associative Tresca flow rule.

The vector N^a is the normal to the plane $\Phi_1 = 0$, already defined. In the *right corner* (repeated minimum principal stress), the second vector, N^b, is normal to the plane $\Phi_6 = 0$ and is obtained analogously to (6.142) as

$$N^b \equiv N^6 = \boldsymbol{e}_1 \otimes \boldsymbol{e}_1 - \boldsymbol{e}_2 \otimes \boldsymbol{e}_2. \tag{6.144}$$

In the *left corner* (repeated maximum principal stress), N^b, is normal to the plane $\Phi_2 = 0$,

$$N^b \equiv N^2 = \boldsymbol{e}_2 \otimes \boldsymbol{e}_2 - \boldsymbol{e}_3 \otimes \boldsymbol{e}_3. \tag{6.145}$$

It should be noted that, as for the Prandtl–Reuss rule, the plastic flow predicted by the associative Tresca law is *volume-preserving*. Indeed, note that, in the above, we have trivially

$$\operatorname{tr} N^a = \operatorname{tr} N^b = 0. \tag{6.146}$$

This is due to the pressure-insensitivity of the Tresca yield function.

Associative and non-associative Mohr–Coulomb

In the associative Mohr–Coulomb law, the Mohr–Coulomb yield function (6.116) is adopted as the flow potential. Its multisurface representation is based on the yield functions (6.118). The flow rule, which requires consideration of the intersections between the yield surfaces, is derived in a manner analogous to the Tresca law described above. However, it should be noted that in addition to the edge singularities, the present surface has an extra singularity in its apex (Figure 6.13). Plastic yielding may then take place from a face, from an edge or from the apex of the Mohr–Coulomb pyramid.

Again, in the derivation of the flow rules at faces and edges, it is convenient to assume that the principal stresses are ordered as $\sigma_1 \geq \sigma_2 \geq \sigma_3$ so that, without loss of generality, the analysis can be reduced to a single sextant of a cross-section of the Mohr–Coulomb pyramid as illustrated in Figure 6.19. The situation is identical to Tresca's (Figure 6.18) except that

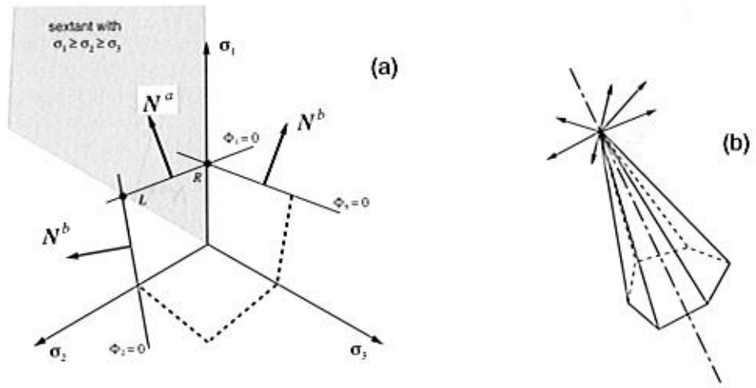

Figure 6.19. The Mohr–Coulomb flow rule; (a) faces and edges, and (b) apex.

the normal vectors N^a and N^b are no longer deviatoric, i.e. they have a non-zero component along the hydrostatic axis (the vectors shown in Figure 6.19 are deviatoric projections of the actual normals). For plastic yielding from the face, the flow rule is given by

$$\dot{\varepsilon}^p = \dot{\gamma}\, N^a, \tag{6.147}$$

where N^a is normal to the plane $\Phi_1 = 0$,

$$\begin{aligned} N^a = \frac{\partial \Phi_1}{\partial \boldsymbol{\sigma}} &= \frac{\partial}{\partial \boldsymbol{\sigma}} \left[\sigma_1 - \sigma_3 + (\sigma_1 + \sigma_3) \sin\phi\right] \\ &= (1 + \sin\phi)\boldsymbol{e}_1 \otimes \boldsymbol{e}_1 - (1 - \sin\phi)\boldsymbol{e}_3 \otimes \boldsymbol{e}_3. \end{aligned} \tag{6.148}$$

At the corners, the above flow rule is replaced by

$$\dot{\varepsilon}^p = \dot{\gamma}^a\, N^a + \dot{\gamma}^b\, N^b. \tag{6.149}$$

At the *right* (extension) corner, R, the second vector, N^b, is normal to the plane $\Phi_6 = 0$ and is given by

$$N^b = (1 + \sin\phi)\, \boldsymbol{e}_1 \otimes \boldsymbol{e}_1 - (1 - \sin\phi)\, \boldsymbol{e}_2 \otimes \boldsymbol{e}_2, \tag{6.150}$$

whereas, at the *left* (compression) corner, L, the tensor N^b is normal to the plane $\Phi_2 = 0$,

$$N^b = (1 + \sin\phi)\, \boldsymbol{e}_2 \otimes \boldsymbol{e}_2 - (1 - \sin\phi)\, \boldsymbol{e}_3 \otimes \boldsymbol{e}_3. \tag{6.151}$$

At the apex of the Mohr–Coulomb surface, all six planes intersect and, therefore, six normals are defined and up to six plastic multipliers may be non-zero. This situation is schematically illustrated in Figure 6.19(b). The plastic strain rate tensor lies within the pyramid defined by the six normals:

$$\dot{\varepsilon}^p = \sum_{i=1}^{6} \dot{\gamma}^i\, N^i. \tag{6.152}$$

It is important to note that, due to the pressure sensitivity of the Mohr–Coulomb criterion, the associative Mohr–Coulomb rule predicts a non-zero *volumetric* plastic straining. This is in contrast to the Prandtl–Reuss and associative Tresca laws. The volumetric component of the plastic strain rate in the associative Mohr–Coulomb law can be obtained by expanding (6.152) in principal stress space taking into account the definitions of N^i. This gives

$$\begin{bmatrix} \dot{\varepsilon}_1^p \\ \dot{\varepsilon}_2^p \\ \dot{\varepsilon}_3^p \end{bmatrix} = \begin{bmatrix} \alpha & 0 & \beta & \beta & 0 & \alpha \\ 0 & \alpha & \alpha & 0 & \beta & \beta \\ \beta & \beta & 0 & \alpha & \alpha & 0 \end{bmatrix} \begin{bmatrix} \dot{\gamma}^1 \\ \dot{\gamma}^2 \\ \dot{\gamma}^3 \\ \dot{\gamma}^4 \\ \dot{\gamma}^5 \\ \dot{\gamma}^6 \end{bmatrix}, \tag{6.153}$$

where

$$\alpha \equiv 1 + \sin\phi, \quad \beta \equiv -1 + \sin\phi. \tag{6.154}$$

The above trivially yields

$$\dot{\varepsilon}_v^p \equiv \dot{\varepsilon}_1^p + \dot{\varepsilon}_2^p + \dot{\varepsilon}_3^p = 2\, \sin\phi \sum_{i=1}^{6} \dot{\gamma}^i. \tag{6.155}$$

As all $\dot{\gamma}^i$'s are non-negative, the volumetric plastic strain rate is positive and, therefore, *dilatant*. The phenomenon of dilatancy during plastic flow is observed for many materials, particularly geomaterials. However, the dilatancy predicted by the associative Mohr–Coulomb law is often excessive. To overcome this problem, it is necessary to use a *non-associated* flow rule in conjunction with the Mohr–Coulomb criterion. The non-associated Mohr–Coulomb law adopts, as flow potential, a Mohr–Coulomb yield function with the frictional angle ϕ replaced by a different (smaller) angle ψ. The angle ψ is called the *dilatancy angle* and the amount of dilation predicted is proportional to its sine. Note that for $\psi = 0$, the plastic flow becomes purely deviatoric and the flow rule reduces to the associative Tresca law.

Associative and non-associative Drucker–Prager

The associative Drucker–Prager model employs as flow potential the yield function defined by (6.121). To derive the corresponding flow rule, one should note first that the Drucker–Prager function is singular at the apex of the yield surface and is smooth anywhere else. Thus, two situations need to be considered:

(a) plastic yielding at (smooth portion of) the cone surface; and

(b) plastic yielding at the apex.

At the cone surface, where the Drucker–Prager yield function is differentiable, the flow vector is obtained by simply differentiating (6.121) which gives (Figure 6.20(a))

$$N = \frac{1}{2\sqrt{J_2(s)}}\, s + \frac{\eta}{3}\, I, \tag{6.156}$$

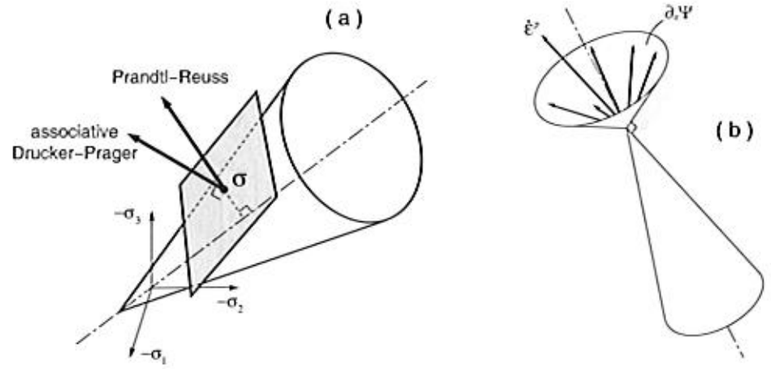

Figure 6.20. The Drucker–Prager flow vector; (a) cone surface, and (b) apex.

where η is given by $(6.122)_1$, $(6.123)_1$ or $(6.124)_1$, according to the chosen approximation to the Mohr–Coulomb surface. The flow rule is then

$$\dot{\varepsilon}^p = \dot{\gamma}\, N. \tag{6.157}$$

The deviatoric/volumetric decomposition of the Drucker–Prager flow vector gives

$$N_d = \frac{1}{2\sqrt{J_2(s)}}\, s, \quad N_v = \eta. \tag{6.158}$$

At the apex singularity, the flow vector is an element of the subdifferential of the yield function (6.121):

$$N \in \partial_\sigma \Phi. \tag{6.159}$$

It lies within the complementary cone to the Drucker–Prager yield surface, i.e. the cone whose wall is normal to the Drucker–Prager cone illustrated in Figure 6.20(b). From standard properties of subdifferentials (Rockafellar, 1970; Rockafellar and Wets, 1998) it can be established that the deviatoric/volumetric split of N in this case is given by

$$N_d \in \partial_\sigma \Phi_d, \quad N_v = \eta, \tag{6.160}$$

where $\Phi_d \equiv \sqrt{J_2(s)}$. Expressions (6.157), (6.158) and (6.160) result in the following rate of (dilatant) volumetric plastic strain for the associative Drucker–Prager flow rule:

$$\dot{\varepsilon}_v^p = \dot{\gamma}\, \eta. \tag{6.161}$$

This expression is analogous to (6.155).

Similarly to the associative Mohr–Coulomb flow rule, the often excessive dilatancy predicted by the associated rule in the present case is avoided by using a non-associated law. The non-associative Drucker–Prager law is obtained by adopting, as the flow potential, a Drucker–Prager yield function with the frictional angle ϕ replaced by a dilatancy angle

$\psi < \phi$; that is, we define

$$\Psi(\boldsymbol{\sigma}, c) = \sqrt{J_2(\boldsymbol{s}(\boldsymbol{\sigma}))} + \bar{\eta}\, p, \tag{6.162}$$

where $\bar{\eta}$ is obtained by replacing ϕ with ψ in the definition of η given by $(6.122)_1$, $(6.123)_1$ or $(6.124)_1$. In other words,

$$\bar{\eta} = \frac{6\,\sin\psi}{\sqrt{3}\,(3-\sin\psi)}, \tag{6.163}$$

when the outer cone approximation to the Mohr–Coulomb criterion is employed. When the inner cone approximation is used,

$$\bar{\eta} = \frac{6\,\sin\psi}{\sqrt{3}\,(3+\sin\psi)}, \tag{6.164}$$

whereas, for the plane strain match,

$$\bar{\eta} = \frac{3\,\tan\psi}{\sqrt{9+12\,\tan^2\psi}}. \tag{6.165}$$

The non-associated Drucker–Prager flow vector differs from its associated counterpart only in the volumetric component which, for the non-associated case, reads

$$N_v = \bar{\eta}. \tag{6.166}$$

If the dilatancy angle of the non-associative potential is chosen as $\psi = 0$, then the volumetric component, N_v, vanishes and the flow rule reduces to the Prandtl–Reuss law that predicts volume-preserving plastic flow (refer to Figure 6.20(a)).

6.6. Hardening laws

The phenomenon of hardening has been identified in the uniaxial experiment described in Section 6.1. Essentially, hardening is characterised by a dependence of yield stress level upon the history of plastic straining to which the body has been subjected. In the uniaxial model, formulated in Section 6.2, this phenomenon has been incorporated by allowing the uniaxial yield stress to vary (as a function of the axial accumulated plastic strain) during plastic flow. In the two- and three-dimensional situations, hardening is represented by changes in the hardening thermodynamical force, A, during plastic yielding. These changes may, in general, affect the size, shape and orientation of the yield surface, defined by $\Phi(\boldsymbol{\sigma}, \boldsymbol{A}) = 0$.

6.6.1. PERFECT PLASTICITY

A material model is said to be *perfectly plastic* if *no hardening* is allowed, that is, the yield stress level does *not* depend in any way on the degree of plastification. In this case, the yield surface remains fixed regardless of any deformation process the material may experience and, in a uniaxial test, the elastoplastic modulus, E^{ep}, vanishes. In the von Mises, Tresca, Drucker–Prager and Mohr–Coulomb models described above, perfect plasticity corresponds to a *constant* uniaxial yield stress, σ_y (or constant cohesion, c). Figure 6.21 shows the stress–strain curve of a typical uniaxial cyclic (tension–compression) test with a perfectly plastic

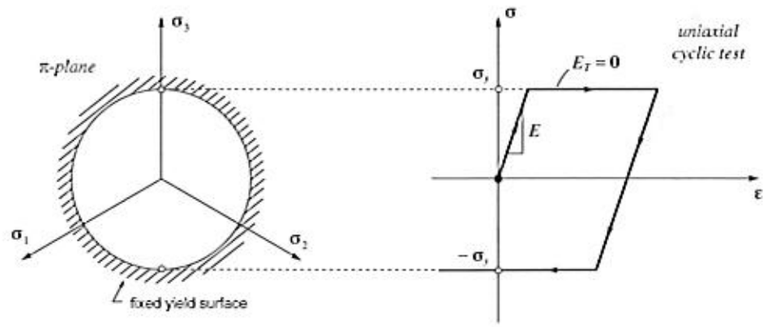

Figure 6.21. Perfect plasticity. Uniaxial test and π-plane representation.

von Mises model along with the corresponding π-plane representation of the yield surface. Perfectly plastic models are particularly suitable for the analysis of the stability of structures and soils and are widely employed in engineering practice for the determination of limit loads and safety factors.

6.6.2. ISOTROPIC HARDENING

A plasticity model is said to be *isotropic hardening* if the evolution of the yield surface is such that, at any state of hardening, it corresponds to a uniform (isotropic) expansion of the initial yield surface, without translation. The uniaxial model described in Section 6.2 is a typical example of an isotropic hardening model. For that model, the elastic domain expands equally in tension and compression during plastic flow. For a multiaxial plasticity model with a von Mises yield surface, isotropic hardening corresponds to the increase in radius of the von Mises cylinder in principal stress space. This, together with a typical stress–strain curve for a uniaxial cyclic test for an isotropic hardening von Mises model is illustrated in Figure 6.22.

The choice of a suitable set (denoted $\boldsymbol{\alpha}$ in Section 6.3) of hardening internal variables must be obviously dependent on the specific characteristics of the material considered. In metal plasticity, for instance, the hardening internal variable is intrinsically connected with the density of dislocations in the crystallographic microstructure that causes an isotropic increase in resistance to plastic flow. In the constitutive description of isotropic hardening, the set $\boldsymbol{\alpha}$ normally contains a single *scalar* variable, which determines the size of the yield surface. Two approaches, *strain hardening* and *work hardening*, are particularly popular in the treatment of isotropic hardening and are suitable for modelling the behaviour of a wide range of materials. These are described below.

Strain hardening

In this case the hardening internal state variable is some suitably chosen scalar measure of *strain*. A typical example is the von Mises *effective plastic strain*, also referred to as the

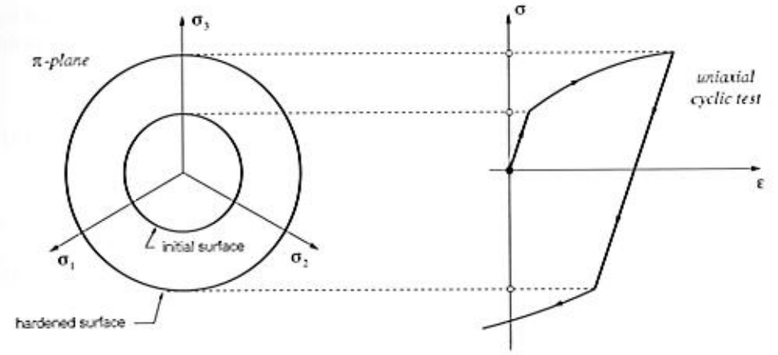

Figure 6.22. Isotropic hardening. Uniaxial test and π-plane representation.

von Mises *equivalent* or *accumulated plastic strain*, defined as

$$\bar{\varepsilon}^p \equiv \int_0^t \sqrt{\tfrac{2}{3}\,\dot{\boldsymbol{\varepsilon}}^p : \dot{\boldsymbol{\varepsilon}}^p}\,\mathrm{d}t = \int_0^t \sqrt{\tfrac{2}{3}}\,\|\dot{\boldsymbol{\varepsilon}}^p\|\,\mathrm{d}t. \tag{6.167}$$

The above definition generalises the accumulated axial plastic strain (6.18) (page 145) of the one-dimensional model to the multiaxially strained case. Its rate evolution equation reads

$$\dot{\bar{\varepsilon}}^p = \sqrt{\tfrac{2}{3}\,\dot{\boldsymbol{\varepsilon}}^p : \dot{\boldsymbol{\varepsilon}}^p} = \sqrt{\tfrac{2}{3}}\,\|\dot{\boldsymbol{\varepsilon}}^p\|, \tag{6.168}$$

or, equivalently, in view of the Prandtl–Reuss flow equation (6.137),

$$\dot{\bar{\varepsilon}}^p = \dot{\gamma}. \tag{6.169}$$

Accordingly, a von Mises isotropic *strain-hardening* model is obtained by letting the uniaxial yield stress be a function of the accumulated plastic strain:

$$\sigma_y = \sigma_y(\bar{\varepsilon}^p). \tag{6.170}$$

This function defines the *strain-hardening curve* (or *strain-hardening function*) that can be obtained, for instance, from a uniaxial tensile test.

Behaviour under uniaxial stress conditions

Under uniaxial stress conditions the von Mises model with isotropic strain hardening reproduces the behaviour of the one-dimensional plasticity model discussed in Section 6.2 and summarised in Box 6.1 (page 146). This is demonstrated in the following. Let us assume that both models share the same Young's modulus, E, and hardening function $\sigma_y = \sigma_y(\bar{\varepsilon}^p)$. Clearly, the two models have identical uniaxial elastic behaviour and initial yield stress. Hence, we only need to show next that their behaviour under plastic yielding is also identical.

Under a uniaxial stress state with axial stress σ and axial stress rate $\dot{\sigma}$ in the direction of the base vector $\boldsymbol{e}_1$, the matrix representations of the stress tensor and the stress rate tensor in the three-dimensional model are given by

$$[\boldsymbol{\sigma}] = \sigma \begin{bmatrix} 1 & 0 & 0 \\ 0 & 0 & 0 \\ 0 & 0 & 0 \end{bmatrix}, \quad [\dot{\boldsymbol{\sigma}}] = \dot{\sigma} \begin{bmatrix} 1 & 0 & 0 \\ 0 & 0 & 0 \\ 0 & 0 & 0 \end{bmatrix}. \tag{6.171}$$

The corresponding stress deviator reads

$$[\boldsymbol{s}] = \tfrac{2}{3}\sigma \begin{bmatrix} 1 & 0 & 0 \\ 0 & -\frac{1}{2} & 0 \\ 0 & 0 & -\frac{1}{2} \end{bmatrix}. \tag{6.172}$$

In this case, the Prandtl–Reuss flow equation (6.137) gives

$$[\dot{\boldsymbol{\varepsilon}}^p] = \dot{\varepsilon}^p \begin{bmatrix} 1 & 0 & 0 \\ 0 & -\frac{1}{2} & 0 \\ 0 & 0 & -\frac{1}{2} \end{bmatrix}, \tag{6.173}$$

where

$$\dot{\varepsilon}^p = \dot{\gamma}\ \mathrm{sign}(\sigma) \tag{6.174}$$

is the axial plastic strain rate. Note that the above expression coincides with the one-dimensional plastic flow rule (6.10). Now, we recall the consistency condition (6.60), which must be satisfied under plastic flow. In the present case, by taking the derivatives of the von Mises yield function (6.110), with σ_y defined by (6.170), we obtain

$$\dot{\Phi} = \boldsymbol{N} : \dot{\boldsymbol{\sigma}} - H\,\dot{\bar{\varepsilon}}^p = 0, \tag{6.175}$$

where $\boldsymbol{N} \equiv \partial\Phi/\partial\boldsymbol{\sigma}$ is the Prandtl–Reuss flow vector (6.136) and $H = H(\bar{\varepsilon}^p)$ is the hardening modulus defined in (6.27). To conclude the demonstration, we combine (6.175) with (6.136), $(6.171)_2$ and (6.172) to recover (6.28) and, then, following the same arguments as in the one-dimensional case we find that, under uniaxial stress conditions, the isotropic strain hardening von Mises model predicts the tangential axial stress–strain relation

$$\dot{\sigma} = \frac{EH}{E+H}\,\dot{\varepsilon}, \tag{6.176}$$

which is identical to equation (6.31) of the one-dimensional model.

Work hardening

In work-hardening models, the variable defining the state of hardening is the dissipated *plastic work*,[¶] w^p, defined by

$$w^p \equiv \int_0^t \boldsymbol{\sigma} : \dot{\boldsymbol{\varepsilon}}^p\, \mathrm{d}t. \tag{6.177}$$

[¶]The term *work hardening* is adopted by many authors as a synonym for the phenomenon of hardening in general. Materials that harden, i.e. materials whose yield stress level depends on the history of strains, are frequently referred to as *work-hardening materials*. In this text, however, the term *work hardening* is reserved for plasticity models in which the dissipated plastic work is taken as the state variable associated with hardening.

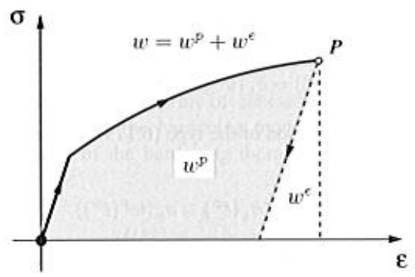

Figure 6.23. The plastic work.

In a uniaxial test, for instance (Figure 6.23), the total work w necessary to deform the material up to point P is given by the total area under the corresponding stress–strain curve. Part of this work, w^e, is stored in the form of elastic energy and is fully recovered upon elastic unloading. The remaining (shaded) area, w^p, is the *plastic work*. It corresponds to the energy dissipated by the plastic mechanisms and cannot be recovered. From the definition of w^p, its evolution equation is given by

$$\dot{w}^p = \boldsymbol{\sigma} : \dot{\boldsymbol{\varepsilon}}^p. \tag{6.178}$$

An isotropic *work-hardening* von Mises model is obtained by postulating

$$\sigma_y = \sigma_y(w^p). \tag{6.179}$$

This defines the *work-hardening curve* (or *work-hardening function*).

Equivalence between strain and work hardening

Under some circumstances, the strain-hardening and work-hardening descriptions are equivalent. This is shown in the following for the von Mises model with associative flow rule (6.137).

The substitution of (6.137) into (6.178), together with the identity $\sqrt{3/2}\|\boldsymbol{s}\| = \sigma_y$ valid for the von Mises model under plastic flow, gives

$$\dot{w}^p = \sigma_y\,\dot{\bar{\varepsilon}}^p, \tag{6.180}$$

or, equivalently,

$$\frac{\mathrm{d}w^p}{\mathrm{d}\bar{\varepsilon}^p} = \sigma_y. \tag{6.181}$$

As σ_y is strictly positive ($\sigma_y > 0$), the above differential relation implies that the mapping between w^p and $\bar{\varepsilon}^p$ is one-to-one and, therefore, invertible so that

$$w^p = w^p(\bar{\varepsilon}^p) \tag{6.182}$$

and

$$\bar{\varepsilon}^p = \bar{\varepsilon}^p(w^p). \tag{6.183}$$

This allows any given strain-hardening function of the type (6.170) to be expressed as an equivalent work-hardening function,

$$\sigma_y(\bar{\varepsilon}^p) = \tilde{\sigma}_y(w^p) \equiv \sigma_y(\bar{\varepsilon}^p(w^p)), \tag{6.184}$$

and any given work-hardening function of the type (6.179) to be expressed as an equivalent strain-hardening function,

$$\sigma_y(w^p) = \hat{\sigma}_y(\bar{\varepsilon}^p) \equiv \sigma_y(w^p(\bar{\varepsilon}^p)). \tag{6.185}$$

Expressions (6.184) and (6.185) establish the equivalence between the strain and work-hardening descriptions for the von Mises model with associative flow rule.

Linear and nonlinear hardening

A model is said to be *linear hardening* if the strain-hardening function (6.170) is linear, i.e. if it can be expressed as

$$\sigma_y(\bar{\varepsilon}^p) = \sigma_{y0} + H\bar{\varepsilon}^p, \tag{6.186}$$

with *constant* σ_{y0} and H. The constant σ_{y0} is the *initial yield stress*, i.e. the uniaxial yield stress at the initial (*virgin*) state of the material, and H is called the *linear isotropic hardening modulus*. Any other hardening model is said to be *nonlinear hardening*. Note that perfect plasticity (defined in Section 6.6.1) is obtained if we set $H = 0$ in (6.186).

It should also be noted that a linear *work*-hardening function corresponds in general to an equivalent *nonlinear* strain-hardening function (i.e. a nonlinear hardening model). This can be easily established by observing that (6.181) defines a nonlinear relation between w^p and $\bar{\varepsilon}^p$ if σ_y is not a constant.

6.6.3. THERMODYNAMICAL ASPECTS. ASSOCIATIVE ISOTROPIC HARDENING

Within the formalism of thermodynamics with internal variables, the above isotropic strain-hardening law corresponds to the assumption that the plastic contribution, ψ^p, to the free energy (recall expression (6.37), page 149) is a function of a single scalar argument – the accumulated plastic strain. That is, the set $\boldsymbol{\alpha}$ of hardening variables is defined as

$$\boldsymbol{\alpha} \equiv \{\bar{\varepsilon}^p\} \tag{6.187}$$

and

$$\psi^p = \psi^p(\bar{\varepsilon}^p). \tag{6.188}$$

The set of hardening thermodynamic forces in this case specialises as

$$\boldsymbol{A} \equiv \{\kappa\}, \tag{6.189}$$

where the scalar thermodynamic force, κ, associated to isotropic hardening is defined by

$$\kappa \equiv \bar{\rho}\frac{\partial \psi^p}{\partial \bar{\varepsilon}^p} = \kappa(\bar{\varepsilon}^p). \tag{6.190}$$

The hardening curve is postulated in terms of κ as

$$\sigma_y(\bar{\varepsilon}^p) \equiv \sigma_{y0} + \kappa(\bar{\varepsilon}^p). \tag{6.191}$$

If the state of hardening is defined in terms of cohesion (or shear yield stress), c (or τ_y) replaces σ_y in (6.191). Note that the hardening modulus H, initially defined in (6.27), represents the rate of change of the hardening thermodynamic force with respect to the hardening internal variable, i.e.

$$H(\bar{\varepsilon}^p) \equiv \frac{\partial \sigma_y}{\partial \bar{\varepsilon}^p} = \frac{\partial \kappa}{\partial \bar{\varepsilon}^p}. \tag{6.192}$$

For the strain-hardening von Mises model the evolution law (6.168) and (6.169) for the internal variable, $\bar{\varepsilon}^p$, follows from the hypothesis of *associativity*, that relies on the choice of the yield function as the plastic potential. The associative evolution equation for $\bar{\varepsilon}^p$ in this case is a specialisation of (6.130); that is, we have

$$\dot{\bar{\varepsilon}}^p = \dot{\gamma}\boldsymbol{H} = \dot{\gamma}. \tag{6.193}$$

The associative generalised modulus $\boldsymbol{H}$ is given by

$$\boldsymbol{H} = -\frac{\partial \Phi}{\partial \boldsymbol{A}} \equiv -\frac{\partial \Phi}{\partial \kappa} = 1, \tag{6.194}$$

where Φ is the von Mises yield function (6.110). A hardening law defined by means of the associativity hypothesis is called an *associative hardening* law. Any other hardening rule is said to be *non-associative*.

Multisurface models with associative hardening

Analogously to the associative plastic flow rule definition (6.73), (6.77) and (6.78), associative hardening for multisurface plasticity models can be defined by postulating the following generic evolution equation for the accumulated plastic strain:

$$\dot{\bar{\varepsilon}}^p = -\sum_{i=1}^{n} \dot{\gamma}^i \frac{\partial \Phi_i}{\partial \kappa}. \tag{6.195}$$

Note that, here, the accumulated plastic strain, $\bar{\varepsilon}^p$, is being *defined* by evolution equation (6.195). Its actual physical meaning depends on the specific format of the functions Φ_i and is generally different from that of (6.167) adopted for the von Mises model.

A simple example of associative isotropic hardening law of the type (6.195) is obtained for the Tresca model. Here, we refer to the plastic flow equations (6.141) and (6.143), defined respectively on the side (smooth portion) and corner of the Tresca yield surface. The corresponding associative evolution equations that define the accumulated plastic strain $\bar{\varepsilon}^p$ are

$$\dot{\bar{\varepsilon}}^p = -\dot{\gamma}\frac{\partial \Phi_1}{\partial \kappa} = \dot{\gamma} \tag{6.196}$$

and

$$\dot{\bar{\varepsilon}}^p = -\dot{\gamma}^a \frac{\partial \Phi_1}{\partial \kappa} - \dot{\gamma}^b \frac{\partial \Phi_6}{\partial \kappa} = \dot{\gamma}^a + \dot{\gamma}^b, \tag{6.197}$$

respectively, where functions Φ_1 and Φ_6 are defined by (6.91) with σ_y related to κ through (6.191).

For Mohr–Coulomb plasticity, one of the possibilities in defining a hardening law is to assume the *cohesion*, c, that takes part of the yield function (6.116) or (6.121) to be a function of the hardening internal variable:

$$c = c(\bar{\varepsilon}^p). \tag{6.198}$$

This type of hardening description is often used in practice in the modelling of soils – for which cohesion is a fundamental strength parameter. This assumption will be adopted in the computer implementation of Mohr–Coulomb and Drucker–Prager models described in Chapter 8. If hardening associativity is also assumed, then similarly to (6.191) we define

$$c(\bar{\varepsilon}^p) = c_0 + \kappa(\bar{\varepsilon}^p), \tag{6.199}$$

and the internal variable $\bar{\varepsilon}^p$ – the accumulated plastic strain for associative Mohr–Coulomb hardening – is defined by the corresponding particularisation of general evolution law (6.195). This gives the general expression

$$\dot{\bar{\varepsilon}}^p = 2\cos\phi \sum_{i=1}^{6} \dot{\gamma}^i. \tag{6.200}$$

When flow takes place at the smooth portion of a Mohr–Coulomb pyramid face, this is reduced to

$$\dot{\bar{\varepsilon}}^p = 2\cos\phi\,\dot{\gamma}. \tag{6.201}$$

At the corners (refer to the plastic flow equation (6.149)), we have

$$\dot{\bar{\varepsilon}}^p = 2\cos\phi\,(\dot{\gamma}^a + \dot{\gamma}^b). \tag{6.202}$$

Note that if it is insisted to adopt the von Mises accumulated plastic strain rate definition (6.167) in conjunction, say, with the Tresca model with associative plastic flow, (6.141) to (6.143), the evolution equation for $\bar{\varepsilon}^p$ will result in

$$\dot{\bar{\varepsilon}}^p = \sqrt{\tfrac{2}{3}\,\dot{\boldsymbol{\varepsilon}}^p : \dot{\boldsymbol{\varepsilon}}^p} = \tfrac{2}{\sqrt{3}}\,\dot{\gamma} \tag{6.203}$$

for flow from the smooth portions of the Tresca surface, and

$$\dot{\bar{\varepsilon}}^p = \sqrt{\tfrac{2}{3}\,\dot{\boldsymbol{\varepsilon}}^p : \dot{\boldsymbol{\varepsilon}}^p} = \tfrac{2}{\sqrt{3}}\,\sqrt{(\dot{\gamma}^a)^2 + \dot{\gamma}^a\dot{\gamma}^b + (\dot{\gamma}^b)^2}, \tag{6.204}$$

for flow from a corner. In this case, the isotropic hardening law is *non-associative* in spite of the associativity of the plastic flow rule.

Drucker–Prager associative hardening

Associative hardening for Drucker–Prager plasticity is obtained by combining assumption (6.199) and the yield function definition (6.121) with the general associative evolution law (6.130) for the hardening internal variable. The accumulated plastic strain in this case is then defined by the evolution equation

$$\dot{\bar{\varepsilon}}^p = -\dot{\gamma}\,\frac{\partial \Phi}{\partial \kappa} = \dot{\gamma}\,\xi. \tag{6.205}$$

Other hardening models

Further refinements to capture hardening behaviour more accurately can be incorporated in Mohr–Coulomb based plasticity models by assuming, in addition, the frictional angle to be a function, for example, of the accumulated plastic strain:

$$\phi = \phi(\bar{\varepsilon}^p). \tag{6.206}$$

For Drucker–Prager-based models, the above would correspond to having

$$\eta = \eta(\bar{\varepsilon}^p), \quad \xi = \xi(\bar{\varepsilon}^p). \tag{6.207}$$

The direction of plastic flow is generally affected by the history of plastic straining in materials such as soils and rocks. This phenomenon can be accounted for in non-associative flow Mohr–Coulomb type models by letting the dilatancy angle, ψ, be a function of the hardening internal variable. For Drucker–Prager-based models, this can be obtained by having the parameter $\bar{\eta}$ as a function of the hardening variable.

6.6.4. KINEMATIC HARDENING. THE BAUSCHINGER EFFECT

When the yield surfaces preserve their shape and size but *translate* in the stress space as a rigid body, *kinematic hardening* is said to take place. It is frequently observed in experiments that, after being loaded (and hardened) in one direction, many materials show a decreased resistance to plastic yielding in the opposite direction (Lemaitre and Chaboche, 1990). This phenomenon is known as the *Bauschinger effect* and can be modelled with the introduction of kinematic hardening. A number of constitutive models have been proposed to describe elastoplastic behaviour under cyclic loading conditions (Lemaitre and Chaboche, 1990; Mróz, 1967; Skrzypek, 1993). The typical result of a uniaxial cyclic test showing the Bauschinger effect is illustrated in Figure 6.24. The evolution of a kinematically hardening von Mises-type yield surface (in the deviatoric plane) used to model the phenomenon is shown alongside. The yield function for the kinematically hardening model is given by

$$\Phi(\boldsymbol{\sigma}, \boldsymbol{\beta}) = \sqrt{3\,J_2(\boldsymbol{\eta}(\boldsymbol{\sigma}, \boldsymbol{\beta}))} - \sigma_y, \tag{6.208}$$

where

$$\boldsymbol{\eta}(\boldsymbol{\sigma}, \boldsymbol{\beta}) \equiv \boldsymbol{s}(\boldsymbol{\sigma}) - \boldsymbol{\beta} \tag{6.209}$$

is the *relative stress* tensor, defined as the difference between the stress deviator and the symmetric deviatoric (stress-like) tensor, $\boldsymbol{\beta}$, known as the *back-stress* tensor. Note that, by definition, the relative stress is *deviatoric*. The back-stress tensor is the thermodynamical force associated with kinematic hardening and represents the translation (Figure 6.24) of the yield surface in the space of stresses. The *constant* σ_y in (6.208) defines the radius of the yield surface. When $\boldsymbol{\beta} = \mathbf{0}$, we have $\boldsymbol{\eta} = \boldsymbol{s}$ and the yield surface defined by $\Phi = 0$ is the isotropic von Mises yield surface with uniaxial yield stress σ_y.

It is important to observe that, unlike the isotropically hardening von Mises model, the yield function Φ defined by (6.208) is *not* an isotropic function of the stress tensor for kinematically hardened states ($\boldsymbol{\beta} \neq \mathbf{0}$). The function (6.208) is an isotropic function of the *relative stress*, $\boldsymbol{\eta}$. Analogously to expression (6.208), it is possible to introduce kinematic hardening in other plasticity models simply by replacing $\boldsymbol{\sigma}$ with a relative stress measure, defined as the difference $\boldsymbol{\sigma} - \boldsymbol{\beta}$, in the definition of the corresponding yield function.

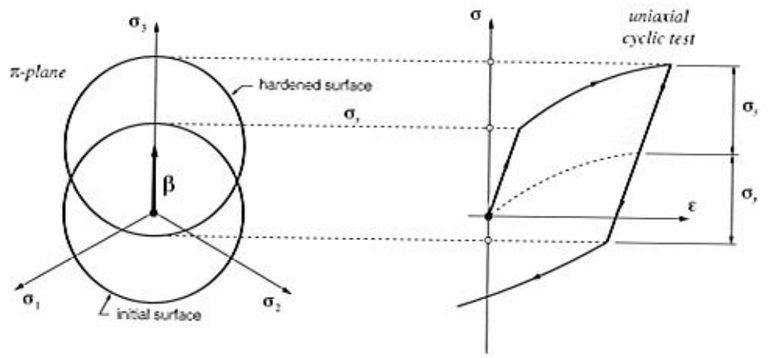

Figure 6.24. Kinematic hardening and the *Bauschinger effect*. Uniaxial test and π-plane representation. Loading in one direction results in decreased resistance to plastic yielding in the opposite direction.

Plastic flow rule with kinematic hardening

The von Mises model with kinematic hardening is used in conjunction with an *associative* flow rule. The flow vector in this case reads

$$N \equiv \frac{\partial \Phi}{\partial \boldsymbol{\sigma}} = \sqrt{\tfrac{3}{2}} \frac{\boldsymbol{\eta}}{\|\boldsymbol{\eta}\|} \tag{6.210}$$

and we have the following plastic strain rate equation:

$$\dot{\boldsymbol{\varepsilon}}^P = \dot{\gamma}\, N = \dot{\gamma} \sqrt{\tfrac{3}{2}} \frac{\boldsymbol{\eta}}{\|\boldsymbol{\eta}\|}. \tag{6.211}$$

This rule extends the Prandtl–Reuss equation to account for kinematic hardening. Note that the plastic flow is in the direction of the (deviatoric) relative stress, $\boldsymbol{\eta}$, and coincides with the Prandtl–Reuss equation if $\boldsymbol{\beta} = \mathbf{0}$.

Prager's linear kinematic hardening

To complete the definition of the kinematic hardening plasticity model, evolution equations for $\boldsymbol{\beta}$ are required. One of the most commonly used laws is *Prager's linear kinematic hardening rule*, where the rate evolution equation for $\boldsymbol{\beta}$ is given by

$$\dot{\boldsymbol{\beta}} = \tfrac{2}{3} H\, \dot{\boldsymbol{\varepsilon}}^P = \dot{\gamma} \sqrt{\tfrac{2}{3}}\, H \frac{\boldsymbol{\eta}}{\|\boldsymbol{\eta}\|}. \tag{6.212}$$

The material constant H is the *linear kinematic hardening modulus*.

Behaviour under monotonic uniaxial stress loading

For monotonic loading under uniaxial stress conditions, the stress–strain behaviour of the model defined by equations (6.208), with constant $\sigma_y = \sigma_{y0}$, (6.211) and (6.212) and initial

state of hardening defined by $\boldsymbol{\beta} = \mathbf{0}$ is identical to the behaviour of the purely isotropic hardening von Mises model with linear hardening curve (6.186) and initial state of hardening $\bar{\varepsilon}^P = 0$. It is assumed in this statement that both models share the same Young's modulus, E. Under the above conditions, it is clear that both models have the same elastic behaviour and uniaxial yield stress, σ_{y0}. To show that their plastic behaviour also coincides, let us consider again a uniaxial test with loading in the direction of the base vector $\boldsymbol{e}_1$. In this case, the stress, stress rate and stress deviator tensors have the matrix representations given in (6.171) and (6.172). Now note that the integration of the rate equation (6.212) with initial condition $\boldsymbol{\beta} = \mathbf{0}$ (i.e. $\boldsymbol{\eta} = \boldsymbol{s}$) and $\boldsymbol{s}$ as in (6.172) gives a back-stress tensor of the form

$$[\boldsymbol{\beta}] = \beta \begin{bmatrix} 1 & 0 & 0 \\ 0 & -\frac{1}{2} & 0 \\ 0 & 0 & -\frac{1}{2} \end{bmatrix}, \tag{6.213}$$

where β is the axial back-stress component. With the above, we obtain for the relative stress tensor

$$[\boldsymbol{\eta}] = \eta \begin{bmatrix} 1 & 0 & 0 \\ 0 & -\frac{1}{2} & 0 \\ 0 & 0 & -\frac{1}{2} \end{bmatrix}, \tag{6.214}$$

where

$$\eta = \tfrac{2}{3}\sigma - \beta \tag{6.215}$$

is the axial relative stress. From (6.212) and (6.214) we obtain

$$[\dot{\boldsymbol{\beta}}] = \tfrac{2}{3} H \dot{\varepsilon}^P \begin{bmatrix} 1 & 0 & 0 \\ 0 & -\frac{1}{2} & 0 \\ 0 & 0 & -\frac{1}{2} \end{bmatrix}, \tag{6.216}$$

where $\dot{\varepsilon}^P$ is the axial plastic strain rate given by

$$\dot{\varepsilon}^P = \dot{\gamma}\, \mathrm{sign}(\eta). \tag{6.217}$$

Now, by recalling (6.60) and specialising (6.61) for the present case we have that, under plastic yielding, the following consistency condition must be satisfied:

$$\dot{\Phi} = \frac{\partial \Phi}{\partial \boldsymbol{\sigma}} : \dot{\boldsymbol{\sigma}} + \frac{\partial \Phi}{\partial \boldsymbol{\beta}} : \dot{\boldsymbol{\beta}} = 0. \tag{6.218}$$

After some straightforward tensor algebra, taking into account $(6.171)_2$ and the above expressions for $\dot{\boldsymbol{\beta}}$, $\boldsymbol{\beta}$, the definition of $\boldsymbol{\eta}$, and the identity

$$\frac{\partial \Phi}{\partial \boldsymbol{\beta}} = -\frac{\partial \Phi}{\partial \boldsymbol{\sigma}} = -\sqrt{\frac{3}{2}} \frac{\boldsymbol{\eta}}{\|\boldsymbol{\eta}\|}, \tag{6.219}$$

equation (6.218) yields

$$\dot{\sigma} = H \dot{\varepsilon}^P. \tag{6.220}$$

Then, with the introduction of the elastoplastic split of the axial strain rate, together with the equation

$$\dot{\sigma} = E \dot{\varepsilon}^e, \tag{6.221}$$

of the linear elastic model under uniaxial stress conditions, into (6.220), we obtain

$$\dot{\sigma} = \frac{EH}{E+H}\,\dot{\varepsilon}, \tag{6.222}$$

which coincides with the stress rate equation (6.176) of the von Mises isotropic strain-hardening model with constant H. To complete the demonstration, let us assume that the uniaxial loading is monotonic, i.e. we have either $\dot{\varepsilon} > 0$ or $\dot{\varepsilon} < 0$ throughout the entire loading process. In this case, the integration of (6.222) having the initial yield stress (σ_{y0} for both models) as the initial condition produces the same stress–strain curve as the isotropic model.

Armstrong–Frederick hardening

A refinement upon the linear kinematic hardening law proposed by Armstrong and Frederick (1966) is obtained by introducing an extra term in the above expression (refer to Lemaitre and Chaboche (1990), Chapter 5, or Jirásek and Bažant (2002), Chapter 20, for details) with the evolution of $\boldsymbol{\beta}$ given by

$$\begin{aligned}\dot{\boldsymbol{\beta}} &= \frac{2}{3}\,H\,\dot{\boldsymbol{\varepsilon}}^p - \dot{\gamma}\,b\,\boldsymbol{\beta} \\ &= \dot{\gamma}\left(\frac{2}{3}H\,\frac{\partial\Phi}{\partial\boldsymbol{\sigma}} - b\,\boldsymbol{\beta}\right),\end{aligned} \tag{6.223}$$

where b is a material constant. The extra term $-\dot{\gamma}\,b\,\boldsymbol{\beta}$ introduces the effect of saturation in the kinematic hardening rule. In the case of the von Mises criterion, the saturation corresponds to a maximum limit value for the norm of $\boldsymbol{\beta}$, at which the material behaves as perfectly plastic.

Nonlinear extension to Prager's rule

Another possible improvement upon Prager's linear kinematic hardening rule is the introduction of nonlinearity by replacing the constant kinematic hardening modulus, H, of (6.212) with a generic function of the accumulated plastic strain, $\bar{\varepsilon}^p$,

$$\dot{\boldsymbol{\beta}} = \frac{2}{3}H(\bar{\varepsilon}^p)\,\dot{\boldsymbol{\varepsilon}}^p = \dot{\gamma}\,\frac{2}{3}H(\bar{\varepsilon}^p)\,\frac{\partial\Phi}{\partial\boldsymbol{\sigma}}. \tag{6.224}$$

In this case, a scalar function

$$\bar{\beta} \equiv \bar{\beta}(\bar{\varepsilon}^p), \tag{6.225}$$

such that

$$H(\bar{\varepsilon}^p) = \frac{\mathrm{d}\bar{\beta}}{\mathrm{d}\bar{\varepsilon}^p}, \tag{6.226}$$

defines the *kinematic hardening curve*. This curve can be obtained from simple uniaxial tests in a manner analogous to the determination of the hardening curve for the purely isotropic hardening model.

Thermodynamical aspects of kinematic hardening

From the thermodynamical viewpoint, the above kinematic hardening laws follow from the assumption that the plastic contribution, ψ^p, to the free energy is a function of a second-order tensor-valued internal variable, $\boldsymbol{X}$,

$$\psi^p = \psi^p(\boldsymbol{X}). \tag{6.227}$$

The variable $\boldsymbol{X}$ is related to self-equilibrated residual stresses that remain after elastic unloading. These stresses may increase or decrease resistance to plastic slip according to the direction considered. The kinematic hardening thermodynamical force – the back-stress tensor, $\boldsymbol{\beta}$ – is then defined as the derivative

$$\boldsymbol{\beta} \equiv \frac{\partial\psi^p}{\partial\boldsymbol{X}}. \tag{6.228}$$

For the Armstrong–Frederick kinematic hardening law (6.223), for instance, we have

$$\psi^p(\boldsymbol{X}) = \frac{a}{2}\,\boldsymbol{X} : \boldsymbol{X}, \tag{6.229}$$

where the material constant a has been defined as

$$a \equiv \tfrac{2}{3}\,H. \tag{6.230}$$

The back-stress tensor (6.228) is then a scalar multiple of $\boldsymbol{X}$, given by

$$\boldsymbol{\beta} = a\,\boldsymbol{X}. \tag{6.231}$$

The evolution law for the internal variable $\boldsymbol{X}$ is obtained by postulating a flow potential

$$\Psi \equiv \Phi + \frac{b}{2a}\boldsymbol{\beta} : \boldsymbol{\beta}, \tag{6.232}$$

and assuming normal dissipativity

$$\dot{\boldsymbol{X}} \equiv -\dot{\gamma}\,\frac{\partial\Psi}{\partial\boldsymbol{\beta}} = -\dot{\gamma}\left(\frac{\partial\Phi}{\partial\boldsymbol{\beta}} + \frac{b}{a}\,\boldsymbol{\beta}\right). \tag{6.233}$$

Obviously (since $\Psi \neq \Phi$), this evolution law is *non-associative*. The equivalence between the above equation and (6.223) can be established by taking into account (6.231) and the fact that, since Φ is obtained from a non-kinematic hardening yield function by replacing the argument $\boldsymbol{\sigma}$ with $\boldsymbol{\sigma} - \boldsymbol{\beta}$, we have

$$\frac{\partial\Phi}{\partial\boldsymbol{\beta}} = -\frac{\partial\Phi}{\partial\boldsymbol{\sigma}}. \tag{6.234}$$

6.6.5. MIXED ISOTROPIC/KINEMATIC HARDENING

Rather than purely isotropic or purely kinematic hardening, real-life materials show in general a combination of both; that is, under plastic straining, the yield surface expands/shrinks and translates simultaneously in stress space. Thus, more realistic plasticity models can be obtained by combining the above laws for isotropic and kinematic hardening.

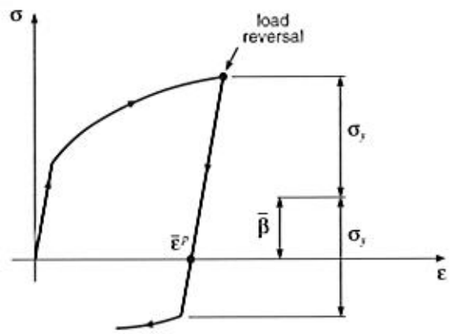

Figure 6.25. Mixed hardening. Uniaxial test with load reversal.

For example, a relatively simple von Mises-based model with mixed isotropic/kinematic hardening can be devised by adopting the yield function (6.208) and allowing σ_y to be a function of $\bar{\varepsilon}^p$. If the nonlinear rule defined by (6.224) and (6.225) is adopted, the hardening behaviour of the model is determined by the curves

$$\sigma_y = \sigma_y(\bar{\varepsilon}^p), \quad \bar{\beta} = \bar{\beta}(\bar{\varepsilon}^p), \tag{6.235}$$

which can be obtained from relatively simple uniaxial tests with load reversal (see schematic illustration of Figure 6.25). At each point $\bar{\varepsilon}^p$, the *kinematic hardening stress*, $\bar{\beta}$, is the kinematic contribution to overall hardening.

A more refined mixed hardening model can be devised by coupling the Armstrong–Frederick law (6.223) with the von Mises-type yield function (6.208) where σ_y, as in $(6.235)_1$, is a function of the accumulated plastic strain. A model including mixed hardening of this type is discussed in Section 12.3 (starting on page 478) in the context of damage mechanics.

7 FINITE ELEMENTS IN SMALL-STRAIN PLASTICITY PROBLEMS

IN the previous chapter, the mathematical theory of plasticity has been reviewed. A general small-strain elastoplastic constitutive model has been established within the formalism of thermodynamics with internal variables and the most popular theories, namely, the von Mises, Tresca, Mohr–Coulomb and Drucker–Prager models, have been described in detail.

Obviously, due to the mathematical complexity of such constitutive theories, an exact solution to boundary value problems of practical engineering interest can only be obtained under very simplified conditions. The existing analytical solutions are normally restricted to perfectly plastic models and are used for the determination of limit loads and steady plastic flow of bodies with simple geometries (Chakrabarty, 1987; Hill, 1950; Lubliner, 1990; Prager, 1959; Skrzypek, 1993). The analysis of the behaviour of elastoplastic structures and soils under more realistic conditions requires the adoption of an adequate numerical framework capable of producing approximate solutions within reasonable accuracy. As pointed out in Chapter 4, the approximate solution to such problems is addressed in this book within the context of the Finite Element Method. In fact, the Finite Element Method is by far the most commonly adopted procedure for the solution of elastoplastic problems. Since the first reported applications of finite elements in plasticity in the mid-1960s, a substantial development of the related numerical techniques has occurred. Today, the Finite Element Method is regarded as the most powerful and reliable tool for the analysis of solid mechanics problems involving elastoplastic materials and is adopted by the vast majority of commercial software packages for elastoplastic stress analysis.

This chapter describes in detail the numerical/computational procedures necessary for the implicit finite element solution of small strain plasticity problems within the framework of Chapter 4. For the sake of generality, the methodologies presented in this chapter are initially derived taking the general plasticity model introduced in Chapter 6 (summarised in Box 6.2, page 151) as the underlying constitutive model. Practical application of the theory and procedures introduced, including a complete description of the algorithms and corresponding FORTRAN subroutines of the HYPLAS program, is then made to the particular case of the von Mises model with nonlinear isotropic hardening. The choice of this model is motivated here by the simplicity of its computational implementation. A set of numerical examples is also presented. Further application of the theory is made at the end of the chapter to a mixed isotropic/kinematic hardening version of the von Mises model. This model is also included in the HYPLAS program. Application to the Tresca, Mohr–Coulomb and Drucker–Prager models is left for Chapter 8.

Computational Methods for Plasticity: Theory and Applications EA de Souza Neto, D Perić and DRJ Owen

11 VISCOPLASTICITY

THE elastoplastic constitutive theories presented so far in Part Two of this book are classed as *rate independent* or *time independent*; that is, the material response is regarded as independent of the rate of application of loads and/or the timescale of the problems considered. Time (or, more precisely, *pseudo-time*) is used merely to describe the sequence of events that defines the history of the loading process. For such theories, identical solutions are produced when a given load (or sequence of loads) is applied at different rates.

However, the observed behaviour of real materials is generally time dependent; that is, the stress response always depends on the rate of loading and/or the timescale considered. The extent of such dependence may or may not be significant according to the physical conditions of the problem. In situations where the rates of loading and/or the timescale of the analysis remain within a range where the time-dependent phenomena can be neglected, rate-independent elastoplasticity models can provide good descriptions of the material behaviour (Lemaitre and Chaboche, 1990; Lubliner, 1990; Skrzypek, 1993). If such conditions are not met, then accurate predictions can only be obtained if rate dependence is adequately accounted for by the constitutive model. Rate-dependence effects are described by means of so-called *viscoplasticity* (or *rate-dependent plasticity*) models, to which the present chapter is devoted.

This chapter is organised as follows. Section 11.1 presents a brief introduction to phenomenological aspects of viscoplasticity. It motivates the establishment of a one-dimensional mathematical model of viscoplasticity in Section 11.2. Here, some simple analytical solutions are presented to demonstrate the ability of the one-dimensional model in capturing the fundamental phenomenological features of viscoplastic behaviour. In Section 11.3 the one-dimensional viscoplastic theory is generalised to the multidimensional case within the context of von Mises plasticity. A more general multidimensional model is presented in Section 11.4. The general model can be rigorously described within the constitutive framework of internal variable theories initially referred to in Chapter 3 (Section 3.5.2, from page 71). Rate-independent plasticity is shown to be, under some circumstances, a limit case of the general viscoplasticity model. This establishes a formal link between rate-independent plasticity and the general constitutive framework of Chapter 3. Section 11.5 proceeds to introduce a numerical framework to treat the general viscoplasticity model within the finite element environment of Chapter 4. This includes the numerical integration algorithm for the general viscoplastic constitutive equations as well as a symbolic form of the associated consistent tangent modulus. Then, in Section 11.6, the general numerical framework is specialised to a von Mises-based model presented in Section 11.3. The integration algorithm and the associated consistent tangent operator are derived step by step. In addition, an error assessment of the numerical integration procedure is presented by means of iso-error maps.

Computational Methods for Plasticity: Theory and Applications EA de Souza Neto, D Perić and DRJ Owen

We remark that Section 11.6 is essential for the reader interested in the computational implementation of viscoplasticity. The chapter ends with finite element examples being shown in Section 11.7. In the reported examples, the procedures of Section 11.6 are used.

11.1. Viscoplasticity: phenomenological aspects

Many of the microscopic phenomena underlying the inelastic deformation of solids depend on time. Materials such as metals, rubbers, geomaterials in general, concrete and composites may all present substantially time-dependent mechanical behaviour under many practical circumstances. In metals, for instance, the phenomenological effects of time-dependent mechanisms become apparent typically at absolute temperatures higher than around one third of the melting point and can be clearly identified by a number of experimental procedures. To illustrate this fact, typical results of simple uniaxial tension tests with metallic bars at higher temperatures are schematically represented in Figure 11.1. Figure 11.1(a) shows stress–strain curves obtained in uniaxial tensile tests carried out under different prescribed strain rates. In general, the elasticity modulus is largely independent of the rate of loading but, clearly, the initial yield limit as well as the hardening curve depend strongly on the rate of straining. This rate-dependence is also observed at low temperatures, but usually becomes significant only at higher temperatures. Strain-rate dependence may be of crucial importance, for instance, in metal-forming operations such as hot forging and may have to be taken into consideration in the design of the process. It is also important to emphasise that, although not shown in Figure 11.1(a), the rupture limit, that is, the strain at which the specimen breaks, can also be strongly dependent on the rate of straining.

Another aspect of time dependence is the phenomenon of *creep*. This is illustrated in Figure 11.1(b). The curves of Figure 11.1(b) show the evolution of plastic strains over time in experiments where tensile specimens have been loaded to different stress levels and left at constant stress during long periods of time. The material experiences a continuous plastic flow that is accelerated for higher stress levels. The high strain rates shown towards the end of the schematic curves for high and moderate stresses is the phenomenon known as *tertiary creep*. Tertiary creep leads to the final rupture of the material and is associated with the evolution of internal damage. Internal damage will be discussed in Chapter 12. Prediction of creep behaviour is important, for instance, in situations where load-carrying metallic components are subjected to long duration loads at high temperatures. The need for consideration of creep response arises typically in the design and analysis of nuclear reactor and jet turbine engine components.

The third aspect of rate dependence, illustrated in Figure 11.1, is the phenomenon of stress *relaxation*. The graph of Figure 11.1(c) shows the typical evolution of stress in a relaxation test. The relaxation test consists of stretching the specimen (virtually instantaneously) to a prescribed axial strain and maintaining it strained (at constant strain) over a long period of time. The time-dependent response in this case is characterised by the continuous decay of stress in time. The prediction of stress relaxation can be vital, for instance, in the design of pre-stressed load-carrying components. We remark that the strain rate dependence of the stress response as well as the phenomena of creep and stress relaxation illustrated above for metals can also be observed for other materials by means of appropriate experiments.

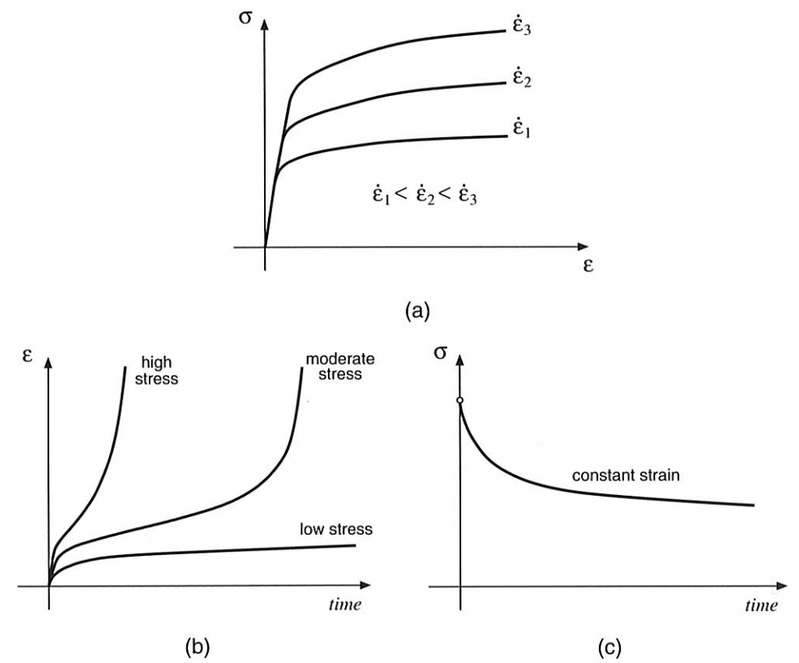

Figure 11.1. Viscoplasticity. Phenomenological aspects: uniaxial tensile tests at high temperature. (a) *Strain rate dependence*. Uniaxial tests at different strain rates. (b) *Creep*. Plastic flow at constant stress. (c) *Relaxation*. Stress decay at constant strain.

11.2. One-dimensional viscoplasticity model

Similarly to what has been done in Chapter 6 for rate-independent plasticity (refer to Section 6.2, from page 141), we find it convenient to introduce viscoplasticity by focusing first on a simple one-dimensional theory. Thus, we devote this section to the description of a simple uniaxial viscoplastic constitutive model. As we shall see, in spite of its simplicity, the uniaxial model possesses all the basic ingredients of the multidimensional models discussed in the remainder of this chapter. In particular, the model is able to capture many of the main features of the viscoplastic behaviour depicted in Figure 11.1.

11.2.1. ELASTOPLASTIC DECOMPOSITION OF THE AXIAL STRAIN

As for the rate-independent case, the decomposition of the total axial strain into a sum of an elastic (recoverable) and a plastic (permanent) component is introduced,

$$\varepsilon = \varepsilon^e + \varepsilon^p. \tag{11.1}$$

11.2.2. THE ELASTIC LAW

The axial stress is again assumed to be related to the elastic component of the axial strain by means of the standard linear elastic constitutive relation

$$\sigma = E\,\varepsilon^e. \tag{11.2}$$

11.2.3. THE YIELD FUNCTION AND THE ELASTIC DOMAIN

Here, the existence of an elastic domain for the stress within which the material behaviour is purely elastic is also experimentally observed in many cases.† Thus, analogously to the rate-independent model of Section 6.2, the elastic domain can be conveniently defined by means of a *yield function*

$$\Phi(\sigma, \sigma_y) = |\sigma| - \sigma_y, \tag{11.3}$$

where σ_y is the yield stress. The elastic domain is defined as the set

$$\mathscr{E} = \{\sigma \mid \Phi(\sigma, \sigma_y) < 0\}, \tag{11.4}$$

so that the behaviour is purely elastic whenever $|\sigma| < \sigma_y$.

11.2.4. VISCOPLASTIC FLOW RULE

The crucial difference between the uniaxial elastoplastic model of Section 6.2 and the viscoplasticity model introduced here lies in the definition of the flow rule, which describes the evolution of ε^p. The viscoplastic flow rule can be postulated with a format similar to that of the rate-independent case (see equation (6.10), page 144)

$$\dot{\varepsilon}^p = \dot{\gamma}(\sigma, \sigma_y)\,\mathrm{sign}(\sigma), \tag{11.5}$$

where sign is the *signum* function defined by (6.11).

In spite of its similarity to the rate-independent flow rule, the above constitutive equation for ε^p differs fundamentally from (6.10). Firstly, it needs to be emphasised that in the rate-independent model the plastic strain rate is in fact a *pseudo*-time rate; that is, $\dot{\varepsilon}^p$ in the rate-independent theory is the derivative of the plastic strain in respect to a *pseudo*-time parameter used solely to describe the sequence of events. In that case, the actual timescale is irrelevant. In contrast, the plastic strain rate in (11.5) is the actual time derivative of ε^p. In addition to this conceptual difference, $\dot{\gamma}$ – named the plastic multiplier and determined by the procedure of Section 6.2.7 (page 146) in the rate-independent theory – is here a *given* explicit function of σ and σ_y. Essentially, the explicit function for $\dot{\gamma}$ should model how the rate of plastic straining varies with the level of stress. Many forms are possible for $\dot{\gamma}$ and a discussion on this issue will be left for Section 11.3. Here, we will define the one-dimensional viscoplasticity model by adopting the following particular definition

$$\dot{\gamma}(\sigma, \sigma_y) = \begin{cases} \dfrac{1}{\mu}\left[\left(\dfrac{|\sigma|}{\sigma_y}\right)^{1/\epsilon} - 1\right] & \text{if } \Phi(\sigma, \sigma_y) \geq 0 \\ 0 & \text{if } \Phi(\sigma, \sigma_y) < 0, \end{cases} \tag{11.6}$$

†As we shall see later in this chapter, some models of viscoplasticity do not have an elastic domain. Such models do not require the definition of a yield function.

where the material constants are the *viscosity-related* parameter μ, whose dimension is time, and the non-dimensional *rate-sensitivity* parameter, ϵ. Both parameters are strictly positive. This particular form has been introduced by Perić (1993) similarly to the power law form of the viscoplastic potential proposed by Perzyna (1963). It is important to emphasise that the material parameters μ and ϵ are *temperature dependent*. As a general rule, as temperature increases (decreases) μ and ϵ increase (decrease). For many metals, $\mu, \epsilon \to 0$ for sufficiently low temperatures, when the material behaviour may be assumed rate-independent.

11.2.5. HARDENING LAW

In the rate-independent case, the phenomenon of hardening describes the changes in yield stress that result from plastic straining. In the viscoplastic model, hardening can be incorporated in the same manner as in the elastoplastic case by letting the yield stress, σ_y, be a given (experimentally determined) function

$$\sigma_y = \sigma_y(\bar{\varepsilon}^p) \tag{11.7}$$

of the accumulated plastic strain

$$\bar{\varepsilon}^p = \int_0^t |\dot{\varepsilon}^p|\,\mathrm{d}t. \tag{11.8}$$

Note that (11.6) implies that at a given constant applied stress σ, an increase (decrease) in σ_y will produce a decrease (increase) in the plastic strain rate $\dot{\varepsilon}^p$. As in the elastoplastic case, an increase of σ_y will be referred to as *hardening* whereas its reduction will be described as *softening*. If σ_y is a constant, the model is referred to as *perfectly* viscoplastic.

11.2.6. SUMMARY OF THE MODEL

The overall one-dimensional viscoplasticity model is defined by the constinutive equations (11.1)–(11.8). For convenience we summarise the model in Box 11.1.

11.2.7. SOME SIMPLE ANALYTICAL SOLUTIONS

Section 11.1 discussed some of the phenomenological aspects of viscoplastic behaviour. One important aspect to be emphasised here is that, in spite of its simplicity, the above-defined one-dimensional model can capture the key phenomenological features of rate-dependent plasticity shown in Figure 11.1. To illustrate this and give the reader a better insight into the theory, we derive in this section analytical solutions for three simple problems where the basic properties of *creep* at constant stress, *strain rate dependence* of the stress response and *stress relaxation* under constant strain are reproduced by the one-dimensional model.

Creeping at constant stress

Let us consider the case of a bar subjected to an axial load that produces a uniform stress $\sigma > \sigma_y$ over its cross-section. The load is applied instantaneously and, after being applied, remains constant in time.

With the instantaneous loading (at time $t = 0$), the bar will initially deform (also instantaneously) in a purely elastic manner. The fact that the model behaviour is elastic under

Box 11.1. One-dimensional viscoplastic constitutive model.

1. Elastoplastic split of the axial strain

$$\varepsilon = \varepsilon^e + \varepsilon^p$$

2. Uniaxial elastic law

$$\sigma = E\,\varepsilon^e$$

3. Yield function

$$\Phi(\sigma, \sigma_y) = |\sigma| - \sigma_y$$

4. Plastic flow rule

$$\dot{\varepsilon}^p = \dot{\gamma}\ \text{sign}(\sigma)$$

$$\dot{\gamma} = \begin{cases} \dfrac{1}{\mu}\left[\left(\dfrac{|\sigma|}{\sigma_y}\right)^{1/\epsilon} - 1\right] & \text{if } \Phi(\sigma, \sigma_y) \geq 0 \\ 0 & \text{if } \Phi(\sigma, \sigma_y) < 0 \end{cases}$$

5. Hardening law

$$\sigma_y = \sigma_y(\bar{\varepsilon}^p)$$

$$\dot{\bar{\varepsilon}}^p = \dot{\gamma}$$

instantaneous loading is formally demonstrated in the next example when the strain rate dependence of the stress response is discussed. However, even without a formal proof, it makes sense to accept that, as there is no time for plastic strains to develop over an (idealised) instantaneous loading event, the behaviour must be purely elastic under such a condition. Assuming zero initial plastic strain, it follows from the elastoplastic split of the total strain together with the elastic law that the total strain in the bar at $t = 0$, immediately after the instantaneous application of load, will be

$$\varepsilon_0 = \varepsilon_0^e = \frac{\sigma}{E}, \tag{11.9}$$

where the zero subscript denotes quantities at $t = 0$. From this moment on, the bar is kept under a constant stress above the yield limit. Under constant stress, the elastic law implies that the elastic strain will also remain constant. Thus, the straining of the bar after the instantaneous loading will be due purely to viscoplastic flow and will be modelled by constitutive equations (11.5), (11.6). Assuming that σ is positive (tensile), we then have

$$\dot{\varepsilon}^p = \frac{1}{\mu}\left[\left(\frac{\sigma}{\sigma_y}\right)^{1/\epsilon} - 1\right]. \tag{11.10}$$

For a perfectly viscoplastic material (constant σ_y), the integration of the above equation, in conjunction with the elastoplastic decomposition of the total strain and the initial condition (11.9), gives the following solution for the straining of the bar

$$\varepsilon(t) = \frac{\sigma}{E} + \frac{1}{\mu}\left[\left(\frac{\sigma}{\sigma_y}\right)^{1/\epsilon} - 1\right] t. \tag{11.11}$$

The creep rate in this case is constant and proportional to $(\sigma/\sigma_y)^{1/\epsilon} - 1$. The material constants (μ and ϵ) could be calibrated, for instance, so as to capture the initial branches of the creep curves of the material (refer to Figure 11.1(b)). The initial branches describe the phenomenon of *primary creep*. A hardening law could be incorporated to include the follow-up of the curves to their second straight branch that describes secondary creep.

Strain-rate dependence of the stress response

Here we analyse the monotonic stretching of an initially unstrained (and unstressed) bar at constant strain rates. These are the conditions typically encountered in conventional tensile tests. The objective here is to show that the one-dimensional model is capable of predicting the strain-rate dependence of the stress response as generally illustrated in Figure 11.1(a).

Before stating the associated initial value problem, let us first recall that the material response within the elastic domain ($\sigma < \sigma_y$) is purely elastic. Thus, at the initial stages of the monotonic stretching process, the stress response does not depend on the rate of stretching. The stress–strain response during this phase is expressed simply as

$$\sigma = E\,\varepsilon \quad \text{if} \quad \sigma < \sigma_y, \tag{11.12}$$

or, equivalently,

$$\sigma = E\,\varepsilon \quad \text{if} \quad \varepsilon < \varepsilon^*, \tag{11.13}$$

where ε^* is the strain at which the yield stress is reached

$$\varepsilon^* = \frac{\sigma_y}{E}. \tag{11.14}$$

Viscoplastic flow (and rate-dependent behaviour) may only take place when $\sigma \geq \sigma_y$ or, in terms of the applied strain, when $\varepsilon \geq \varepsilon^*$. Then, as our purpose is to illustrate the rate dependence predicted by the model, our initial value problem will be defined only over the portion of the loading process where $\sigma \geq \sigma_y$ (or $\varepsilon \geq \varepsilon^*$). To simplify the problem, we will assume that the material is perfectly viscoplastic (constant σ_y) and, in addition, the rate sensitivity parameter will be set to

$$\epsilon = 1,$$

so that an analytical solution to the initial value problem can be easily found.

The initial value problem.

The evolution of the plastic strain for the present model is defined by equation (11.10). Under the above assumptions, the associated initial value problem consists of finding a function $\varepsilon^p(t)$ such that

$$\dot{\varepsilon}^p(t) = \frac{1}{\mu}\left[\frac{\sigma(t)}{\sigma_y} - 1\right] = \frac{1}{\mu}\left\{\frac{E\,[\varepsilon(t) - \varepsilon^p(t)]}{\sigma_y} - 1\right\} = \frac{1}{\mu}\left[\frac{\varepsilon(t) - \varepsilon^p(t)}{\varepsilon^*} - 1\right], \tag{11.15}$$

where the total strain is the prescribed function

$$\varepsilon(t) = \alpha\, t + \varepsilon^* = \alpha\, t + \frac{\sigma_y}{E}, \tag{11.16}$$

corresponding to monotonic stretching with arbitrary (constant) strain rate $\alpha \geq 0$. Note that $t = 0$ corresponds to the onset of viscoplastic flow ($\sigma = \sigma_y \Leftrightarrow \varepsilon = \varepsilon^*$). The initial condition for ε^p (the plastic strain at the onset of viscoplastic flow) is obviously

$$\varepsilon^p(0) = 0. \tag{11.17}$$

The analytical solution.

By substituting (11.16) into the differential equation (11.15), the initial value problem can be written as

$$\dot{\varepsilon}^p(t) = \frac{1}{\mu\,\varepsilon^*}[\alpha\, t - \varepsilon^p(t)]; \quad \varepsilon^p(0) = 0. \tag{11.18}$$

The analytical solution can then be promptly obtained by standard methods for first-order ordinary linear differential equations as

$$\varepsilon^p(t) = \alpha\big[t - \mu\,\varepsilon^*\big(1 - \mathrm{e}^{\frac{-t}{\mu\,\varepsilon^*}}\big)\big]. \tag{11.19}$$

By placing the above solution together with (11.16) into the elastic law, $\sigma = E(\varepsilon - \varepsilon^p)$, we obtain, after a straightforward manipulation, the following solution for the stress as a function of time

$$\sigma(t) = \sigma_y\big[1 + \alpha\,\mu\big(1 - \mathrm{e}^{\frac{-t}{\mu\,\varepsilon^*}}\big)\big]. \tag{11.20}$$

The stress–strain response.

The strain rate dependence of the stress response can be more clearly illustrated by expressing the stress as a function of strain for an arbitrary (but constant in time) strain rate, so that curves such as those depicted in Figure 11.1(a) can be produced. In the present case, such a function can be obtained by means of a simple variable transformation in (11.20). Indeed, note that by inverting the function defined by (11.16), we have

$$t = t(\varepsilon) = \frac{\varepsilon - \varepsilon^*}{\alpha}. \tag{11.21}$$

With the introduction of this relation into (11.20), we obtain

$$\tilde{\sigma}(\varepsilon) = \sigma(t(\varepsilon)) = \sigma_y\big\{1 + \alpha\,\mu\big[1 - \mathrm{e}^{\frac{1}{\mu\,\alpha}(1 - \frac{\varepsilon}{\varepsilon^*})}\big]\big\}, \tag{11.22}$$

which gives the stress–strain curve for an arbitrary strain rate α. Insight into the problem can be gained by looking into the limit stress–strain curves, i.e. the curves obtained at infinitely slow rates ($\alpha \to 0$) and infinitely fast processes ($\alpha \to \infty$). In order to obtain the limit for infinitely slow rates, we first observe that, in the present monotonic loading process, the term

$$1 - \varepsilon/\varepsilon^*$$

in (11.22) is always negative. In addition, μ and α are positive so that the last term on the right-hand side of (11.22) is the exponential of a negative number. The limit is then easily obtained as

$$\lim_{\alpha \to 0} \tilde{\sigma}(\varepsilon) = \sigma_y; \tag{11.23}$$

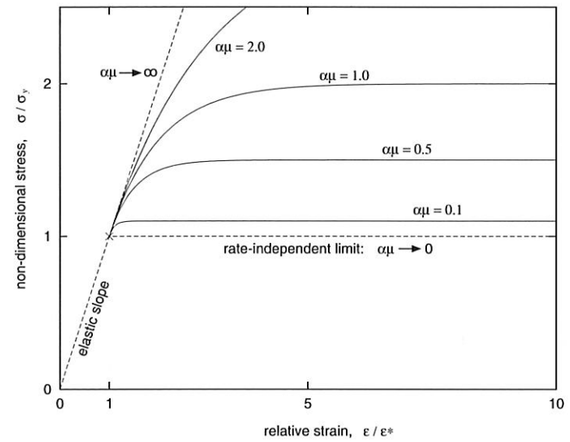

Figure 11.2. One-dimensional viscoplasticity model. Analytical solution showing the dependence of the stress response on the applied strain rate/viscosity parameter.

that is, at infinitely slow rates the perfectly viscoplastic model rigorously recovers the behaviour of the rate-independent plasticity model with yield stress σ_y. The rate-independent model was described in Section 6.2 (page 141). It is also very important to note that the same limit is obtained for the vanishing viscosity parameter, i.e. when $\mu \to 0$. At infinitely fast rates, the limit is derived by a standard limiting procedure which gives

$$\lim_{\alpha \to \infty} \tilde{\sigma}(\varepsilon) = E\,\varepsilon, \tag{11.24}$$

i.e. the process is purely elastic and the stress–strain curve after the yield limit is the continuation (with the same slope, E) of the elastic curve. Also note that the identical limit is found for $\mu \to \infty$ (infinitely viscous material). For any other rate (or viscosity parameter), the corresponding stress–strain curve will lie between these two limits with higher stress obtained at higher strain rates (or higher viscosity). To illustrate better the behaviour of the model under the present conditions, the analytical solution (11.22) is shown in the graph of Figure 11.2, where the non-dimensional stress, σ/σ_y, is plotted against the relative strain, $\varepsilon/\varepsilon^*$, for various normalised strain rates $\mu\alpha$. The limits $\mu\alpha \to 0$ (infinitely slow rates or non-viscous material) and $\mu\alpha \to \infty$ (infinitely fast rates or infinitely viscous material) are also included. Clearly, the model is able to capture the experimentally observed rate-dependence phenomenon illustrated in Figure 11.1(a).

Remark 11.1. In fact, even though it is not formally shown here, the above limits remain valid for any hardening curve and any rate sensitivity parameter ϵ; that is, at infinitely slow strain rates, the model recovers the rate-independent behaviour of the plasticity model of Section 6.2 (this limit is also obtained for $\mu \to 0$) and, at infinitely fast rates (or when $\mu \to \infty$), the model behaves in a purely elastic manner, regardless of the given hardening curve and rate-sensitivity parameter. In addition (again not formally shown in this section), the

rate-independent behaviour is also recovered with vanishing rate-sensitivity, i.e. when $\epsilon \to 0$. This last property will be demonstrated in Section 11.4.3 in the context of the general multidimensional theory.

Stress relaxation at constant strain

In this final example, we consider the case of a bar which is instantaneously stretched (stretched at an infinitely fast strain rate) to a total strain ε and then kept stretched indefinitely at that constant strain. The instantaneous stretching to ε is assumed to produce a stress above the yield limit of the material. Here the model should be able to capture the phenomenon of stress relaxation alluded to in Figure 11.1(c).

Over the instantaneous stretching (at time $t = 0$), the bar will deform purely elastically (refer to the limit expression (11.24) and the text surrounding it). Thus, assuming that the plastic strain is zero at $t = 0$ (immediately after the instantaneous stretching), we have

$$\varepsilon_0^e = \varepsilon, \tag{11.25}$$

and, in view of the elastic law, the corresponding stress is given by

$$\sigma_0 = E\,\varepsilon_0^e = E\,\varepsilon. \tag{11.26}$$

From this point on, the stress in the bar will be governed by the law

$$\sigma = E(\varepsilon - \varepsilon^p) = \sigma_0 - E\,\varepsilon^p, \tag{11.27}$$

where ε^p evolves in time according to the differential equation (11.10) which, in view of the above expression can be equivalently written as

$$\dot{\varepsilon}^p = \frac{1}{\mu}\left[\left(\frac{\sigma_0 - E\,\varepsilon^p}{\sigma_y}\right)^{1/\epsilon} - 1\right]. \tag{11.28}$$

To simplify the problem, we will assume, as in the previous example, that the material is perfectly viscoplastic (constant σ_y) and $\epsilon = 1$. In this case, the initial value problem is to find a function $\varepsilon^p(t)$ such that

$$\dot{\varepsilon}^p(t) = c_1 - c_2\,\varepsilon^p(t), \tag{11.29}$$

with initial condition

$$\varepsilon^p(0) = 0, \tag{11.30}$$

where the constants c_1 and c_2 are defined as

$$c_1 = \frac{1}{\mu}\left(\frac{\sigma_0}{\sigma_y} - 1\right), \quad c_2 = \frac{E}{\mu\,\sigma_y}. \tag{11.31}$$

The analytical solution to (11.29–11.30) can be trivially obtained as

$$\varepsilon^p(t) = \frac{c_1}{c_2}(1 - \mathrm{e}^{-c_2\,t}). \tag{11.32}$$

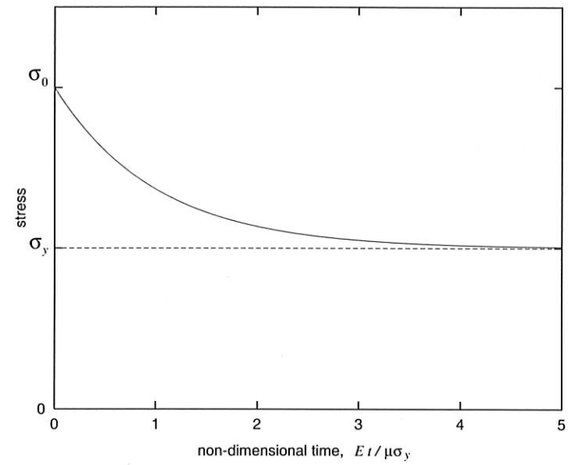

Figure 11.3. One-dimensional viscoplasticity model. Analytical solution to the stress relaxation problem.

Finally, by placing the above solution into (11.27), and taking into account the definition of c_1 and c_2, we obtain the stress as a function of time

$$\sigma(t) = \sigma_0 - (\sigma_0 - \sigma_y)(1 - \mathrm{e}^{-\frac{E}{\mu\,\sigma_y}t}). \tag{11.33}$$

Clearly, the above function describes the stress relaxation process of the bar, with the stress taking the value $\sigma = \sigma_0 > \sigma_y$ at $t = 0$ and subsequently relaxing asymptotically to σ_y as $t \to \infty$. This is illustrated in Figure 11.3 where a graph of the analytical function $\sigma(t)$ (with $\sigma_0 = 2\,\sigma_y$) is plotted. The analytical solution with the present one-dimensional model clearly captures the experimentally observed behaviour referred to in Figure 11.1(c).

11.3. A von Mises-based multidimensional model

This section introduces a multidimensional extension of the one-dimensional model discussed above (and summarised in Box 11.1). Rather than define a generic extension at the outset (as in Section 6.3 (page 148) where a general multidimensional extension of the one-dimensional rate-independent plasticity model of Section 6.2 (page 141) was presented), we chose here to focus first on a von Mises-based generalisation of the uniaxial theory. A discussion of a more generic model, including its potential structure and its relation to time-independent plasticity as a limit case, will be left for Section 11.4.

11.3.1. A VON MISES-TYPE VISCOPLASTIC MODEL WITH ISOTROPIC STRAIN HARDENING

The multidimensional generalisation of the uniaxial viscoplastic model follows the same basic steps as the generalisation presented in Section 6.3 for the rate-independent theory;

Box 11.2. A von Mises-type viscoplastic constitutive model.

1. Elastoplastic split of the strain tensor

$$\boldsymbol{\varepsilon} = \boldsymbol{\varepsilon}^e + \boldsymbol{\varepsilon}^p$$

2. Linear elastic law

$$\boldsymbol{\sigma} = \mathbf{D}^e : \boldsymbol{\varepsilon}^e$$

3. Yield function

$$\Phi(\boldsymbol{\sigma}, \sigma_y) = q(\boldsymbol{s}(\boldsymbol{\sigma})) - \sigma_y; \quad q = \sqrt{\tfrac{3}{2}\, \boldsymbol{s} : \boldsymbol{s}}$$

and elastic domain

$$\mathscr{E} = \{\boldsymbol{\sigma} \mid \Phi(\boldsymbol{\sigma}, \sigma_y) < 0\}$$

4. Plastic flow rule

$$\dot{\boldsymbol{\varepsilon}}^p = \dot{\gamma}\, \frac{\partial \Phi}{\partial \boldsymbol{\sigma}} = \dot{\gamma} \sqrt{\frac{3}{2}}\, \frac{\boldsymbol{s}}{\|\boldsymbol{s}\|}$$

$$\dot{\gamma} = \begin{cases} \dfrac{1}{\mu}\left[\left(\dfrac{q}{\sigma_y}\right)^{1/\epsilon} - 1\right] & \text{if } \Phi(\boldsymbol{\sigma}, \sigma_y) \geq 0 \\ 0 & \text{if } \Phi(\boldsymbol{\sigma}, \sigma_y) < 0 \end{cases}$$

5. Isotropic strain hardening law

$$\sigma_y = \sigma_y(\bar{\varepsilon}^p); \quad \bar{\varepsilon}^p = \int_0^t \|\dot{\boldsymbol{\varepsilon}}^p\|\, \mathrm{d}t$$

6. Evolution of accumulated plastic strain

$$\dot{\bar{\varepsilon}}^p = \dot{\gamma}$$

that is, the elastoplastic split of the total strain, the linear elasticity law, the flow rule and yield function are recast in terms of the corresponding *tensor* quantities (total, elastic and plastic strain tensors, stress tensor and flow vector). The yield function is also redefined as a function of variables of appropriate tensorial order. The usual concept of an elastic domain bounded by a yield surface in the rate-independent theory will remain valid in the viscoplastic case. Here, as our multidimensional extension is von Mises-based, the yield function and the plastic flow rule (including the hardening internal variable) will have the same format as that of the standard rate-independent von Mises model with (associative) Prandtl–Reuss flow vector. The resulting model is a viscoplastic version of the rate-independent isotropically hardening von Mises model summarised in Section 7.3.1 (from page 216). The constitutive equations of the von Mises-based extension are listed in Box 11.2.

Remark 11.2. Analogously to its rate-independent counterpart, under uniaxial stress conditions, the model of Box 11.2 reduces exactly to the one-dimensional theory of Box 11.1. It is also important to emphasise that the basic properties of creep, stress relaxation and strain-rate dependence of the stress response (including the behaviour at limits) as demonstrated for the

uniaxial model in Section 11.2.7 are reproduced by the multidimensional theory under any state of stress.

11.3.2. ALTERNATIVE PLASTIC STRAIN RATE DEFINITIONS

So far, the explicit function for $\dot{\gamma}$ that takes part in the definition of the plastic flow equation (see expression (11.6) and item 4 of Boxes 11.1 and 11.2) has been assumed to be of the form proposed by Perić (1993). As mentioned in Section 11.2.4, many forms for $\dot{\gamma}$ have been proposed and, in practice, a particular choice should be dictated by its ability to model the dependence of the plastic strain rate on the state of stress for the material under consideration. In this section, we list some of the most widely used forms. Clearly, each form of $\dot{\gamma}$ defines a different model of viscoplasticity. However, within the framework of von Mises viscoplasticity, the format of the flow rule

$$\dot{\boldsymbol{\varepsilon}}^p = \dot{\gamma}\, \boldsymbol{N}, \tag{11.34}$$

with associative flow vector $\boldsymbol{N}$ defined by

$$\boldsymbol{N} = \frac{\partial \Phi}{\partial \boldsymbol{\sigma}} = \sqrt{\frac{3}{2}}\, \frac{\boldsymbol{s}}{\|\boldsymbol{s}\|}, \tag{11.35}$$

and yield function

$$\Phi(\boldsymbol{\sigma}, \sigma_y) = q(\boldsymbol{s}(\boldsymbol{\sigma})) - \sigma_y, \tag{11.36}$$

will remain unchanged for any definition of $\dot{\gamma}$.

Bingham model

The Bingham model is the simplest model of viscoplasticity. The multiplier $\dot{\gamma}$ in this case is defined as

$$\dot{\gamma}(\boldsymbol{\sigma}, \sigma_y) = \begin{cases} \dfrac{1}{\eta}\, \Phi(\boldsymbol{\sigma}, \sigma_y) = \dfrac{q(\boldsymbol{\sigma}) - \sigma_y}{\eta} & \text{if } \Phi(\boldsymbol{\sigma}, \sigma_y) \geq 0 \\ 0 & \text{if } \Phi(\boldsymbol{\sigma}, \sigma_y) < 0. \end{cases} \tag{11.37}$$

The only material constant in this case is the (temperature-dependent) viscosity parameter η and the strain rate is modelled as a *linear* function of the von Mises effective stress. Note that this law is obtained from Perić's model given in item 4 of Box 11.2 (and also from the Perzyna model described below) by setting

$$\epsilon = 1; \quad \mu = \frac{\eta}{\sigma_y}. \tag{11.38}$$

In the uniaxial case, the plastic strain rate for the Bingham model is a linear function of the axial stress:

$$\dot{\varepsilon}^p = \frac{1}{\eta}\, (|\sigma| - \sigma_y)\, \mathrm{sign}(\sigma). \tag{11.39}$$

This may severely limit the ability of the model to fit experimental data as, in many cases, the observed strain rate may be a markedly nonlinear function of the stress. However, over a relatively narrow range of stresses, the linear approximation may give good results. Other models, with more material constants, have, in general, better flexibility to allow a wider range of experimental data to be fitted.

Perzyna model

This model was introduced by Perzyna (1966, 1971) and is widely used in computational applications of viscoplasticity. It is defined by

$$\dot{\gamma}(\boldsymbol{\sigma}, \sigma_y) = \begin{cases} \dfrac{1}{\mu}\left[\dfrac{q(\boldsymbol{\sigma})}{\sigma_y} - 1\right]^{1/\epsilon} & \text{if } \Phi(\boldsymbol{\sigma}, \sigma_y) \geq 0 \\ 0 & \text{if } \Phi(\boldsymbol{\sigma}, \sigma_y) < 0. \end{cases} \tag{11.40}$$

As in Perić's model, the material constants are the viscosity-related parameter, μ, and the rate sensitivity, ϵ. We remark here that, in spite of its similarity to Perić's definition, as the rate-independent limit is approached with vanishing rate-sensitivity $\epsilon \to 0$ (refer to Remark 11.1 on page 443), the Perzyna model does not reproduce the uniaxial stress–strain curve of the corresponding rate-independent model with yield stress σ_y. As shown by Perić (1993), in this limit, the Perzyna model produces a curve with $\sigma = 2\,\sigma_y$ instead. However, for vanishing viscosity ($\mu \to 0$) or vanishing strain rates, the response of both Perzyna and Perić models coincide with the standard rate-independent model with yield stress σ_y.

11.3.3. OTHER ISOTROPIC AND KINEMATIC HARDENING LAWS

In the viscoplasticity model of Box 11.2, only isotropic strain hardening has been taken into account. Other hardening laws, such as isotropic work hardening (where the plastic work is taken as the internal variable) as well as kinematic hardening and more general mixed isotropic/kinematic hardening rules can be considered in a manner completely analogous to that of the rate-independent theory as described in Section 6.6 (page 177); that is, isotropic work hardening is obtained by having σ_y as a given function of the plastic work, w^p, defined by expression (6.177)

$$\sigma_y = \sigma_y(w^p). \tag{11.41}$$

Kinematic hardening is introduced by simply replacing the von Mises effective stress, q, with the *relative* effective stress

$$\bar{q} = \sqrt{\tfrac{3}{2}\,\boldsymbol{\eta} : \boldsymbol{\eta}}, \tag{11.42}$$

where $\boldsymbol{\eta}$ is the relative stress

$$\boldsymbol{\eta} = \boldsymbol{s} - \boldsymbol{\beta}, \tag{11.43}$$

and $\boldsymbol{\beta}$ is the backstress tensor. Evolution laws for $\boldsymbol{\beta}$, such as Prager's rule and the Armstrong–Frederick kinematic hardening law, can be defined as in Section 6.6.

11.3.4. VISCOPLASTIC MODELS WITHOUT A YIELD SURFACE

The assumption of the existence of an elastic domain bounded by a yield surface is essential in the formulation of rate-independent plasticity models. For viscoplasticity models, however, such an assumption is by no means required. In fact, particularly at higher temperatures, many materials can be modelled as flowing whenever under stress; that is, the yield stress is effectively zero. For example, many metals at high temperatures will flow at virtually any stress state with a non-zero deviatoric component. In such cases, a yield surface and a corresponding elastic domain do not need to be introduced in the formulation of the

theory. Viscoplasticity models without a yield surface have been used widely, especially in the analysis of creep and hot metal forming operations. Within the present framework, such models can be defined simply by postulating the explicit function for $\dot{\gamma}$ accordingly.

Norton's creep law

The classical Norton creep law has been employed extensively in the analysis of creep of metals. It is used mainly in the description of secondary creep. In its original (uniaxial) version, the flow rule is given by

$$\dot{\varepsilon}^p = \left(\frac{|\sigma|}{\lambda}\right)^N \operatorname{sign}(\sigma), \tag{11.44}$$

where N and λ are temperature-dependent material constants. Clearly, plastic flow is assumed to occur whenever $\sigma \neq 0$. Its multidimensional generalisation, sometimes referred to as Odqvist's law, is obtained by simply replacing the definition of the function for $\dot{\gamma}$ in item 4 of Box 11.2 with the following

$$\dot{\gamma}(\boldsymbol{\sigma}) = \left[\frac{q(\boldsymbol{\sigma})}{\lambda}\right]^N. \tag{11.45}$$

Here, plastic flow takes place for any stress with non-zero deviator. Note that, by setting $\sigma_y = 0$ in (11.37) the Bingham model recovers the Norton law with $N = 1$ and $\lambda = \eta$.

Lemaitre–Chaboche law

A modification of Norton's law in order to improve its ability to model secondary creep over a wider range of stresses and strain rates is provided by the Lemaitre–Chaboche law (Lemaitre and Chaboche, 1990). The function $\dot{\gamma}$ in this case reads

$$\dot{\gamma}(\boldsymbol{\sigma}) = \left[\frac{q(\boldsymbol{\sigma})}{\lambda}\right]^N \exp[\alpha\, q(\boldsymbol{\sigma})^{N+1}]. \tag{11.46}$$

In addition to the material parameters N and λ required by Norton's law, the present model has a third (also temperature-dependent) parameter α.

Other creep laws

A rather general class of viscoplastic laws can be obtained by assuming that $\dot{\gamma}$ is a function of the stress, time and temperature, with the following multiplicative format

$$\dot{\gamma} = \dot{\gamma}(\boldsymbol{\sigma}, t, T) = f_\sigma(\boldsymbol{\sigma})\, f_t(t)\, f_T(T), \tag{11.47}$$

where t and T denote, respectively, the time and absolute temperature and f_σ, f_t and f_T are experimentally defined functions. A comprehensive list of proposed empirical functions is given by Skrzypek (1993), to which the interested reader is referred. For instance, f_σ could be Norton's law or the Lemaitre–Chaboche relation above. The temperature function f_T is

normally defined by the Arrhenius law

$$f_T(T) = C \exp\left[\frac{-Q}{RT}\right] \tag{11.48}$$

where C is a constant, Q is the *activation energy* usually independent of the temperature, R is the gas constant 8.31 J mol^{-1} K^{-1}. A typical example of an empirical relation of the above format is given by the law (Boyle and Spence, 1983)

$$\dot{\gamma} = C \exp\left[\frac{-Q}{RT}\right] t^M \, q^N, \tag{11.49}$$

with M and N being material parameters.

Another interesting viscoplastic model used primarily in the description of the behaviour of metallic alloys at high temperatures is the *Bodner–Partom* model (Bodner and Partom, 1975). An implicit computational implementation of the Bodner–Partom model has been recently described by Anderson (2003).

11.4. General viscoplastic constitutive model

Having described in the previous section some of the most commonly used viscoplasticity models, we proceed here to formulate a more general constitutive theory of viscoplasticity. The theory presented here is a viscoplastic version of the general rate-independent model described in Section 6.3 (from page 148) and summarised in Box 6.2 (page 151). At this point, note that we will use here the notation of Section 6.3. The reader who is not familiar with that notation, or concepts used in that section, is advised to review them before proceeding further. The formulation of the viscoplastic model is analogous to that of its rate-independent counterpart. It follows the same considerations as Sections 6.3.1 to 6.3.4, except that the flow rule and hardening law are defined as

$$\begin{aligned} \dot{\boldsymbol{\varepsilon}}^p &= \boldsymbol{G}(\boldsymbol{\sigma}, \boldsymbol{A}) \\ \dot{\boldsymbol{\alpha}} &= \boldsymbol{J}(\boldsymbol{\sigma}, \boldsymbol{A}); \end{aligned} \tag{11.50}$$

that is, the plastic strain rate and the evolution law for the set $\boldsymbol{\alpha}$ of hardening internal variables are defined by means of the *explicit* constitutive functions $\boldsymbol{G}$ and $\boldsymbol{J}$ of $\boldsymbol{\sigma}$ and the set $\boldsymbol{A}$ of hardening thermodynamic forces. In addition, as we have seen above, an elastic domain may not exist. Thus, a yield function is not necessarily present in the viscoplastic formulation. The constitutive equations of the general viscoplasticity model are listed in Box 11.3.

Note that the von Mises-based model of Box 11.2 (which incorporates an elastic domain) is trivially recovered by defining the functions $\boldsymbol{G}$ and $\boldsymbol{J}$ as well as the free-energy potential ψ and the internal variable set $\boldsymbol{\alpha}$ accordingly. The same applies to all other models (with or without an elastic domain) described in Section 11.3.

11.4.1. RELATION TO THE GENERAL CONTINUUM CONSTITUTIVE THEORY

The above viscoplasticity model fits within the generic internal variable-based constitutive framework discussed in Section 3.5.2 (from page 71). Indeed, it can be trivially established

Box 11.3. A general viscoplastic constitutive model.

1. Additive decomposition of the strain tensor
$$\boldsymbol{\varepsilon} = \boldsymbol{\varepsilon}^e + \boldsymbol{\varepsilon}^p$$
2. Free-energy function
$$\psi = \psi(\boldsymbol{\varepsilon}^e, \boldsymbol{\alpha})$$
where $\boldsymbol{\alpha}$ is a set of hardening internal variables
3. Constitutive equation for $\boldsymbol{\sigma}$ and hardening thermodynamic forces $\boldsymbol{A}$
$$\boldsymbol{\sigma} = \bar{\rho}\,\frac{\partial \psi}{\partial \boldsymbol{\varepsilon}^e} \quad \boldsymbol{A} = \bar{\rho}\,\frac{\partial \psi}{\partial \boldsymbol{\alpha}}$$
4. Plastic flow rule and hardening law
$$\dot{\boldsymbol{\varepsilon}}^p = \boldsymbol{G}(\boldsymbol{\sigma}, \boldsymbol{A})$$
$$\dot{\boldsymbol{\alpha}} = \boldsymbol{J}(\boldsymbol{\sigma}, \boldsymbol{A})$$

that the model of Box 11.3 is a particular case of the general purely mechanical infinitesimal constitutive law defined by (3.165) on page 76. The general viscoplasticity model is obtained by simply defining the set $\boldsymbol{\alpha}$ of (3.165) as composed of the plastic strain tensor and the set of hardening internal variables (as described in Section 6.3.2) and then introducing the explicit constitutive functions for the rates of plastic strain and hardening variables listed in item 4 of Box 11.3.

11.4.2. POTENTIAL STRUCTURE AND DISSIPATION INEQUALITY

A specialisation of the general theory of Box 11.3 can be obtained by endowing the model with a potential structure (refer to the discussion surrounding expression (3.162) on page 74). In this case, we define a *dissipation potential*

$$\Xi = \Xi(\boldsymbol{\sigma}, \boldsymbol{A}), \tag{11.51}$$

from which, through the hypothesis of *normal dissipativity*, the evolution of the internal variables of the problem are derived as

$$\begin{aligned} \dot{\boldsymbol{\varepsilon}}^p &= \frac{\partial \Xi}{\partial \boldsymbol{\sigma}} \\ \dot{\boldsymbol{\alpha}} &= -\frac{\partial \Xi}{\partial \boldsymbol{A}}. \end{aligned} \tag{11.52}$$

At this point, it is important to recall that the *plastic dissipation* in the present case is given by (again, refer to Section 6.3.2)

$$\boldsymbol{\sigma} : \dot{\boldsymbol{\varepsilon}}^p - \boldsymbol{A} * \dot{\boldsymbol{\alpha}},$$

so that the dissipation inequality reads

$$\Upsilon^p(\boldsymbol{\sigma}, \boldsymbol{A}; \dot{\boldsymbol{\varepsilon}}^p, \dot{\boldsymbol{\alpha}}) \geq 0, \tag{11.53}$$

where

$$\Upsilon^p(\boldsymbol{\sigma}, \boldsymbol{A}; \dot{\boldsymbol{\varepsilon}}^p, \dot{\boldsymbol{\alpha}}) \equiv \boldsymbol{\sigma} : \dot{\boldsymbol{\varepsilon}}^p - \boldsymbol{A} * \dot{\boldsymbol{\alpha}} \tag{11.54}$$

is the *dissipation function*.

By defining Ξ such that it is convex with respect to both variables, non-negative and zero-valued at $\{\boldsymbol{\sigma}, \boldsymbol{A}\} = \{\mathbf{0}, \mathbf{0}\}$ it is ensured that the dissipation inequality is satisfied *a priori* by the model.

11.4.3. RATE-INDEPENDENT PLASTICITY AS A LIMIT CASE

In this section we show that rate-independent plasticity can be recovered as a limit case of the above general viscoplastic theory with a potential structure. As emphasised above, the general viscoplastic model is a particular instance of the internal variable-based constitutive framework of Section 3.5.2. Thus, the demonstration that follows here shows effectively that, as anticipated in Section 6.3.7, the elastoplastic model of Box 6.3 (page 151) can be rigorously described, under some circumstances, as a particular case of the general continuum constitutive theory of Section 3.5.2.

The indicator function of a convex set

The demonstration presented here is based on arguments of convex analysis.[‡] Crucial to the proof to be shown is the concept of *indicator function* of a convex set. In this context, let us consider the closure, $\mathscr{A}$, of the elastic domain defined by means of a yield function Φ:

$$\mathscr{A} = \{(\boldsymbol{\sigma}, \boldsymbol{A}) \mid \Phi(\boldsymbol{\sigma}, \boldsymbol{A}) \leq 0\}. \tag{11.55}$$

In rate-independent plasticity, $\mathscr{A}$ is the set of all *admissible* states $(\boldsymbol{\sigma}, \boldsymbol{A})$ of stress and hardening thermodynamical forces. The set $\mathscr{A}$ is *convex*, i.e. it defines a convex region in the space of stresses and hardening forces. Following the above considerations, we now introduce the *indicator function*, $\Psi_{\mathscr{A}}$, of the convex set $\mathscr{A}$ as the scalar-valued function defined by

$$\Psi_{\mathscr{A}}(\boldsymbol{\sigma}, \boldsymbol{A}) = \begin{cases} 0 & \text{if } (\boldsymbol{\sigma}, \boldsymbol{A}) \in \mathscr{A} \\ \\ \infty & \text{if } (\boldsymbol{\sigma}, \boldsymbol{A}) \notin \mathscr{A}. \end{cases} \tag{11.56}$$

The indicator function is clearly *non-differentiable*.

The rate-independent limit

In what follows, we shall see that an associative rate-independent plasticity model is obtained by adopting $\Psi_{\mathscr{A}}$ as the dissipation potential in the general viscoplastic theory; that is, we choose

$$\Xi(\boldsymbol{\sigma}, \boldsymbol{A}) \equiv \Psi_{\mathscr{A}}(\boldsymbol{\sigma}, \boldsymbol{A}). \tag{11.57}$$

[‡]Readers not familiar with convex analysis are referred to Rockafellar (1970).

At this point we need to make use of the concept of *subdifferential*.[§] In view of the non-differentiability of the indicator function, the constitutive equations (11.52), which follow from normal dissipativity, are replaced with the *subdifferential* relations

$$\begin{aligned} \dot{\boldsymbol{\varepsilon}}^p &\in \partial_{\boldsymbol{\sigma}} \Psi_{\mathscr{A}} \\ \dot{\boldsymbol{\alpha}} &\in -\partial_{\boldsymbol{A}} \Psi_{\mathscr{A}}, \end{aligned} \tag{11.58}$$

where $\partial_{\boldsymbol{\sigma}} \Psi_{\mathscr{A}}$ and $\partial_{\boldsymbol{A}} \Psi_{\mathscr{A}}$ are the subdifferentials of $\Psi_{\mathscr{A}}$ with respect to $\boldsymbol{\sigma}$ and $\boldsymbol{A}$, respectively. From the subdifferential definition (6.69) together with (11.56) it can easily be established that (11.58) is equivalent to the inequality

$$\dot{\boldsymbol{\varepsilon}}^p : (\boldsymbol{\sigma} - \boldsymbol{\sigma}^*) + \dot{\boldsymbol{\alpha}} * (\boldsymbol{A} - \boldsymbol{A}^*) \geq 0, \quad \forall\, (\boldsymbol{\sigma}^*, \boldsymbol{A}^*) \in \Psi_{\mathscr{A}}, \tag{11.59}$$

or, equivalently, in terms of the dissipation function (11.54)

$$\Upsilon^p(\boldsymbol{\sigma}, \boldsymbol{A}; \dot{\boldsymbol{\varepsilon}}^p, \dot{\boldsymbol{\alpha}}) \geq \Upsilon^p(\boldsymbol{\sigma}^*, \boldsymbol{A}^*; \dot{\boldsymbol{\varepsilon}}^p, \dot{\boldsymbol{\alpha}}), \quad \forall\, (\boldsymbol{\sigma}^*, \boldsymbol{A}^*) \in \mathscr{A}. \tag{11.60}$$

This last inequality states that, among all states $(\boldsymbol{\sigma}^*, \boldsymbol{A}^*) \in \mathscr{A}$, the actual stress and hardening force $(\boldsymbol{\sigma}, \boldsymbol{A})$ maximise the dissipation function. This is known as the *principle of maximum plastic dissipation*, discussed in Section 6.5.2 (page 170) to which the reader is referred for details. The solution to the maximisation problem associated with the principle of maximum plastic dissipation is the classical associative laws

$$\begin{aligned} \dot{\boldsymbol{\varepsilon}}^p &= \dot{\gamma}\, \frac{\partial \Phi}{\partial \boldsymbol{\sigma}} \\ \dot{\boldsymbol{\alpha}} &= -\dot{\gamma}\, \frac{\partial \Phi}{\partial \boldsymbol{A}}, \end{aligned} \tag{11.61}$$

together with the loading/unloading conditions of rate-independent plasticity

$$\Phi(\boldsymbol{\sigma}, \boldsymbol{A}) \leq 0, \quad \dot{\gamma} \geq 0, \quad \Phi(\boldsymbol{\sigma}, \boldsymbol{A})\dot{\gamma} = 0. \tag{11.62}$$

In summary, it has been shown above that the classical rate-independent associative plasticity equations are rigorously recovered from the general viscoplasticity model when the indicator function of the set $\mathscr{A}$ is taken as the dissipation potential.

Example: von Mises-based model

Let us now consider the von Mises-based model of Box 11.2 and, for simplicity, assume that the model is perfectly viscoplastic (constant σ_y). Our purpose here is to illustrate the above ideas by demonstrating that the viscoplastic model can be defined in terms of a dissipation potential whose limit when $\epsilon \to 0$ or $\mu \to 0$ is the indicator function of the set of admissible stresses of the perfectly plastic von Mises model. Thus, in such limits, the perfectly viscoplastic model rigorously recovers the classical perfectly elastoplastic von Mises model.

[§]Refer to Section 6.3.9 (from page 153) for the definition of subdifferential.

We start by defining the dissipation potential as

$$\Xi(\boldsymbol{\sigma}) = \begin{cases} \dfrac{\sigma_y}{\mu}\left\{\dfrac{1}{1+\epsilon} + \dfrac{\epsilon}{1+\epsilon}\left[\dfrac{q(\boldsymbol{\sigma})}{\sigma_y}\right]^{\frac{1+\epsilon}{\epsilon}} - \dfrac{q(\boldsymbol{\sigma})}{\sigma_y}\right\} & \text{if } q/\sigma_y \geq 1 \\ 0 & \text{if } q/\sigma_y < 1, \end{cases} \tag{11.63}$$

where $\boldsymbol{\sigma}$ is the only variable. With the above definition, the flow rule

$$\dot{\boldsymbol{\varepsilon}}^p = \frac{\partial \Xi}{\partial \boldsymbol{\sigma}}, \tag{11.64}$$

is found through a straightforward differentiation to be that of item 4 of Box 11.2; that is, the above potential indeed defines the von Mises-based viscoplasticity model of Box 11.2 when hardening is not considered.

Finally, by simple inspection, we can easily see that, when $\epsilon \to 0$ or $\mu \to 0$, the limit of the potential Ξ of (11.63) is the indicator function of the set of admissible stresses defined by the von Mises yield function:

$$\lim_{\epsilon \to 0} \Xi(\boldsymbol{\sigma}) = \lim_{\mu \to 0} \Xi(\boldsymbol{\sigma}) = \Psi_{\mathscr{A}}(\boldsymbol{\sigma}), \tag{11.65}$$

where

$$\mathscr{A} = \{\boldsymbol{\sigma} \mid q(\boldsymbol{\sigma}) - \sigma_y \leq 0\}. \tag{11.66}$$

This completes the demonstration. The schematic illustration of Figure 11.4 shows the potential Ξ for various choices of the rate-sensitivity parameter ϵ. Clearly, as $\epsilon \to 0$, Ξ tends to the indicator function of $\mathscr{A}$.

11.5. General numerical framework

This section describes the basic ingredients needed to incorporate the general viscoplasticity model of Box 11.3 into the finite element framework of Chapter 4. The basic requirements are:

(i) an algorithm for numerical integration of the viscoplastic constitutive equations, to be used to update stresses and other state variables of the model;

(ii) the associated consistent tangent modulus, to be used in the assemblage of the finite element stiffness matrix.

For further discussions and analysis of various aspects of the numerical treatment of viscoplasticity, we refer to Simo and Govindjee (1991), Perić (1993), Chaboche and Cailletaud (1996), Simo and Hughes (1998), Simo (1998), Runesson and Mahler (1999), and Alfano and Rosati (2001).

11.5.1. A GENERAL IMPLICIT INTEGRATION ALGORITHM

Before proceeding to the derivation of an integration algorithm for the general viscoplastic model, it seems convenient, for the sake of clarity, to start by stating the underlying initial value problem we wish to solve. The problem here is analogous to its rate-independent counterpart, Problem 7.1, stated on page 193.

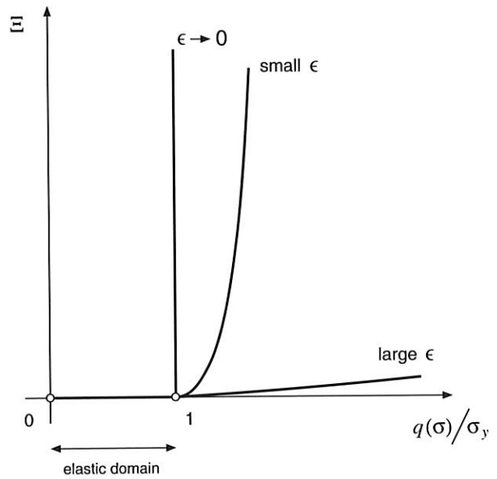

Figure 11.4. Viscoplastic potential Ξ for various rate-sensitivity parameters ϵ.

Problem 11.1 (The viscoplastic constitutive initial value problem). *Given the initial values $\boldsymbol{\varepsilon}^e(t_0)$ and $\boldsymbol{\alpha}(t_0)$ and given the history of the strain tensor, $\boldsymbol{\varepsilon}(t)$, $t \in [t_0, T]$, find the functions $\boldsymbol{\varepsilon}^e(t)$ and $\boldsymbol{\alpha}(t)$, for the elastic strain tensor and hardening internal variable set that satisfy the reduced general viscoplastic constitutive equations*

$$\dot{\boldsymbol{\varepsilon}}^e(t) = \dot{\boldsymbol{\varepsilon}}(t) - \boldsymbol{G}(\boldsymbol{\sigma}(t), \boldsymbol{A}(t)), \quad \dot{\boldsymbol{\alpha}}(t) = \boldsymbol{J}(\boldsymbol{\sigma}(t), \boldsymbol{A}(t)) \tag{11.67}$$

for each instant $t \in [t_0, T]$, with

$$\boldsymbol{\sigma}(t) = \bar{\rho}\left.\frac{\partial \psi}{\partial \boldsymbol{\varepsilon}^e}\right|_t, \quad \boldsymbol{A}(t) = \bar{\rho}\left.\frac{\partial \psi}{\partial \boldsymbol{\alpha}}\right|_t. \tag{11.68}$$

As in the definition of the rate-independent problem, the reduced system (11.67) of ordinary differential equations has been obtained by incorporating the viscoplastic flow equation $(11.50)_1$ into the elastoplastic split of the total strain rate so that the plastic strain does not appear explicitly in the initial value problem. Clearly, once the history of elastic strain is determined in the solution to the above problem, the history of the plastic strain is promptly obtained as

$$\boldsymbol{\varepsilon}^p(t) = \boldsymbol{\varepsilon}(t) - \boldsymbol{\varepsilon}^e(t). \tag{11.69}$$

The fully implicit algorithm for the numerical solution of the above problem is derived by simply applying a standard backward Euler time discretisation of the rate equations. The resulting incremental problem is presented in Box 11.4, where a typical step over the time interval $[t_n, t_{n+1}]$ is considered. The time and strain increments are defined in the usual way as

$$\Delta t = t_{n+1} - t_n, \quad \Delta \boldsymbol{\varepsilon} = \boldsymbol{\varepsilon}_{n+1} - \boldsymbol{\varepsilon}_n. \tag{11.70}$$

Box 11.4. Fully implicit algorithm for numerical integration of general viscoplastic constitutive equations.

Given the strain and time increment, $\Delta\boldsymbol{\varepsilon}$ and Δt, over $[t_n, t_{n+1}]$ and the state variables at t_n, compute the updated state by solving the nonlinear system of equations

$$\left\{\begin{array}{c} \boldsymbol{\varepsilon}^e_{n+1} - \boldsymbol{\varepsilon}^e_n - \Delta\boldsymbol{\varepsilon} + \Delta t\, \boldsymbol{G}(\boldsymbol{\sigma}_{n+1}, \boldsymbol{A}_{n+1}) \\ \boldsymbol{\alpha}_{n+1} - \boldsymbol{\alpha}_n - \Delta t\, \boldsymbol{J}(\boldsymbol{\sigma}_{n+1}, \boldsymbol{A}_{n+1}) \end{array}\right\} = \left\{\begin{array}{c} \mathbf{0} \\ \mathbf{0} \end{array}\right\}$$

for $\boldsymbol{\varepsilon}^e_{n+1}$ and $\boldsymbol{\alpha}_{n+1}$, with

$$\boldsymbol{\sigma}_{n+1} = \bar{\rho}\, \frac{\partial \psi}{\partial \boldsymbol{\varepsilon}^e}\bigg|_{n+1}, \quad \boldsymbol{A}_{n+1} = \bar{\rho}\, \frac{\partial \psi}{\partial \boldsymbol{\alpha}}\bigg|_{n+1}$$

Models with a yield surface

Note that in the algorithm of Box 11.4 no assumption is made on the existence of an elastic domain. The algorithm is valid for models with or without a yield surface. If a yield surface is present, however, the specialisation of the algorithm of Box 11.4 takes a two-stage format completely analogous to the elastic predictor/return-mapping procedure of the rate-independent case. To see this, let us first consider that for a general model with a yield surface, the constitutive functions $\boldsymbol{G}$ and $\boldsymbol{J}$ can be defined with the following form

$$\begin{aligned} \boldsymbol{G}(\boldsymbol{\sigma}, \boldsymbol{A}) &= \dot{\gamma}(\boldsymbol{\sigma}, \boldsymbol{A})\, \boldsymbol{N}(\boldsymbol{\sigma}, \boldsymbol{A}) \\ \boldsymbol{J}(\boldsymbol{\sigma}, \boldsymbol{A}) &= \dot{\gamma}(\boldsymbol{\sigma}, \boldsymbol{A})\, \boldsymbol{H}(\boldsymbol{\sigma}, \boldsymbol{A}), \end{aligned} \tag{11.71}$$

where, following the terminology of the rate-independent theory, $\boldsymbol{N}$ is the flow vector and $\boldsymbol{H}$ is the generalised hardening modulus. The scalar $\dot{\gamma}$ is zero within the elastic domain or on the yield surface and may only be non-zero outside the elastic domain. Clearly, evolution of $\boldsymbol{\varepsilon}^p$ and $\boldsymbol{\alpha}$ may only occur here at states with $\Phi(\boldsymbol{\sigma}, \boldsymbol{A}) > 0$, i.e. states lying neither in the elastic domain nor on the yield surface. Then, as in the rate-independent case, it makes sense to first compute an *elastic trial state* by assuming that the material behaviour is purely elastic within the interval $[t_n, t_{n+1}]$. If the trial state is within the elastic domain or on the yield surface, then no viscoplastic flow takes place within the considered time step and the trial state is the actual state at the end of the step. Otherwise, the evolution of $\boldsymbol{\varepsilon}^p$ and $\boldsymbol{\alpha}$ is computed by means of the standard backward Euler method. The resulting algorithm, which we shall refer to as the *elastic predictor/viscoplastic corrector* or *elastic predictor/viscoplastic return mapping* algorithm, is listed in Box 11.5.

Remark 11.3. The viscoplastic return mapping differs from its elastoplastic (rate-independent) counterpart (refer to Box 7.1, page 199) in that, here, the updated stress state at t_{n+1} generally lies on the outside of the yield surface, i.e.

$$\Phi(\boldsymbol{\sigma}_{n+1}, \boldsymbol{A}_{n+1}) > 0.$$

This is in contrast with the rate-independent case in which the consistency equation, $\Phi_{n+1} = 0$, forces the updated state to be on the yield surface when there is plastic flow over

Box 11.5. Fully implicit elastic predictor/viscoplastic return-mapping algorithm for numerical integration of general viscoplastic constitutive equations with a yield surface over a generic time interval $[t_n, t_{n+1}]$ with $\Delta t = t_{n+1} - t_n$.

(i) Elastic predictor. Given $\Delta\boldsymbol{\varepsilon}$ and the state variables at t_n, evaluate the *elastic trial state*

$$\boldsymbol{\varepsilon}^{e\,\mathrm{trial}}_{n+1} = \boldsymbol{\varepsilon}^e_n + \Delta\boldsymbol{\varepsilon}$$
$$\boldsymbol{\alpha}^{\mathrm{trial}}_{n+1} = \boldsymbol{\alpha}_n$$
$$\boldsymbol{\sigma}^{\mathrm{trial}}_{n+1} = \bar{\rho}\, \frac{\partial \psi}{\partial \boldsymbol{\varepsilon}^e}\bigg|^{\mathrm{trial}}_{n+1}, \quad \boldsymbol{A}^{\mathrm{trial}}_{n+1} = \bar{\rho}\, \frac{\partial \psi}{\partial \boldsymbol{\alpha}}\bigg|^{\mathrm{trial}}_{n+1}$$

(ii) Check for viscoplastic flow

IF $\Phi(\boldsymbol{\sigma}^{\mathrm{trial}}_{n+1}, \boldsymbol{A}^{\mathrm{trial}}_{n+1}) \leq 0$

THEN set $(\cdot)_{n+1} = (\cdot)^{\mathrm{trial}}_{n+1}$ and EXIT

(iii) Viscoplastic return mapping. Solve the system

$$\left\{\begin{array}{c} \boldsymbol{\varepsilon}^e_{n+1} - \boldsymbol{\varepsilon}^{e\,\mathrm{trial}}_{n+1} + \Delta\gamma\, \boldsymbol{N}(\boldsymbol{\sigma}_{n+1}, \boldsymbol{A}_{n+1}) \\ \boldsymbol{\alpha}_{n+1} - \boldsymbol{\alpha}^{\mathrm{trial}}_{n+1} - \Delta\gamma\, \boldsymbol{H}(\boldsymbol{\sigma}_{n+1}, \boldsymbol{A}_{n+1}) \end{array}\right\} = \left\{\begin{array}{c} \mathbf{0} \\ \mathbf{0} \end{array}\right\}$$

for $\boldsymbol{\varepsilon}^e_{n+1}$, and $\boldsymbol{\alpha}_{n+1}$ with

$$\Delta\gamma = \Delta\gamma(\boldsymbol{\sigma}_{n+1}, \boldsymbol{A}_{n+1}) = \Delta t\, \dot{\gamma}(\boldsymbol{\sigma}_{n+1}, \boldsymbol{A}_{n+1})$$

and

$$\boldsymbol{\sigma}_{n+1} = \bar{\rho}\, \frac{\partial \psi}{\partial \boldsymbol{\varepsilon}^e}\bigg|_{n+1}, \quad \boldsymbol{A}_{n+1} = \bar{\rho}\, \frac{\partial \psi}{\partial \boldsymbol{\alpha}}\bigg|_{n+1}$$

(iv) EXIT

the considered interval. Nevertheless, the terminology viscoplastic *return mapping* remains justifiable in the present case since, upon application of the procedure, the updated stress is obtained by moving (or *returning*) the trial stress towards the yield surface.

11.5.2. ALTERNATIVE EULER-BASED ALGORITHMS

Similarly to the rate-independent case (refer to Section 7.2.7, page 201), different numerical integration algorithms can be employed in the stress updating procedure. In what follows we list the basic equations of the generalised trapezoidal and midpoint algorithms. For further details on alternative integration algorithms we refer to Cormeau (1975), Zienkiewicz and Cormeau (1974), Hughes and Taylor (1978), Marques and Owen (1983), Peirce *et al.* (1984) and Kojić and Bathe (1987).

The generalised trapezoidal algorithm

Here, the backward Euler discrete equations of Box 11.4 are replaced with the following system

$$\begin{aligned} \varepsilon^e_{n+1} &= \varepsilon^e_n + \Delta\varepsilon - \Delta t\,[(1-\theta)\,\boldsymbol{G}_n + \theta\,\boldsymbol{G}_{n+1}] \\ \boldsymbol{\alpha}_{n+1} &= \boldsymbol{\alpha}_n + \Delta t\,[(1-\theta)\,\boldsymbol{J}_n + \theta\,\boldsymbol{J}_{n+1}], \end{aligned} \tag{11.72}$$

where θ is a prescribed parameter

$$0 \le \theta \le 1. \tag{11.73}$$

For the choice $\theta = 1$, the implicit algorithm of Box 11.4 is recovered and $\theta = 0$ corresponds to the explicit algorithm.

The generalised midpoint algorithm

For the generalised midpoint rule, the discrete system of equations reads

$$\begin{aligned} \varepsilon^e_{n+1} &= \varepsilon^e_n + \Delta\varepsilon - \Delta t\,\boldsymbol{G}_{n+\theta} \\ \boldsymbol{\alpha}_{n+1} &= \boldsymbol{\alpha}_n + \Delta t\,\boldsymbol{J}_{n+\theta}, \end{aligned} \tag{11.74}$$

where the prescribed parameter, θ, also lies within the interval $[0, 1]$ and

$$\begin{aligned} \boldsymbol{G}_{n+\theta} &= \boldsymbol{G}((1-\theta)\boldsymbol{\sigma}_{n+1} + \theta\,\boldsymbol{\sigma}_n, (1-\theta)\boldsymbol{A}_n + \theta\,\boldsymbol{A}_{n+1}) \\ \boldsymbol{J}_{n+\theta} &= \boldsymbol{J}((1-\theta)\boldsymbol{\sigma}_{n+1} + \theta\,\boldsymbol{\sigma}_n, (1-\theta)\boldsymbol{A}_n + \theta\,\boldsymbol{A}_{n+1}). \end{aligned} \tag{11.75}$$

Again, for $\theta = 1$, the implicit algorithm of Box 11.4 is recovered and $\theta = 0$ defines the explicit algorithm.

11.5.3. GENERAL CONSISTENT TANGENT OPERATOR

To complete the requirements for the implementation of the model within an implicit finite element environment, the tangent modulus consistent with the general algorithm is needed. Let us then consider the algorithm of Box 11.4. Given all variables of the problem at t_n and a prescribed time increment Δt, the task here is to find the exact tangent operator

$$\mathsf{D} \equiv \frac{\mathrm{d}\boldsymbol{\sigma}_{n+1}}{\mathrm{d}\boldsymbol{\varepsilon}_{n+1}} = \frac{\mathrm{d}\boldsymbol{\sigma}_{n+1}}{\mathrm{d}\Delta\boldsymbol{\varepsilon}}, \tag{11.76}$$

consistent with the stress updating procedure defined by the backward Euler algorithm of Box 11.4.

Analogously to the general procedure for the rate-independent case (refer to Section 7.4.4, from page 238), we start by linearising the system of time-discrete equations of Box 11.4. The linearised system reads

$$\begin{Bmatrix} \mathrm{d}\varepsilon^e + \Delta t\,\dfrac{\partial \boldsymbol{G}}{\partial \boldsymbol{\sigma}} : \mathrm{d}\boldsymbol{\sigma} + \Delta t\,\dfrac{\partial \boldsymbol{G}}{\partial \boldsymbol{A}} * \mathrm{d}\boldsymbol{A} \\ \mathrm{d}\boldsymbol{\alpha} - \Delta t\,\dfrac{\partial \boldsymbol{J}}{\partial \boldsymbol{\sigma}} * \mathrm{d}\boldsymbol{\sigma} - \Delta t\,\dfrac{\partial \boldsymbol{J}}{\partial \boldsymbol{A}} * \mathrm{d}\boldsymbol{A} \end{Bmatrix} = \begin{Bmatrix} \mathrm{d}\Delta\varepsilon \\ \mathbf{0} \end{Bmatrix}, \tag{11.77}$$

where the symbol * denotes the product of the appropriate type and the subscripts $n+1$ have been omitted for notational convenience. With the introduction of the differential relations (7.129) (page 239), the linearised system is equivalently written as

$$\begin{bmatrix} \mathsf{C} + \Delta t\,\dfrac{\partial \boldsymbol{G}}{\partial \boldsymbol{\sigma}} & \mathsf{B} + \Delta t\,\dfrac{\partial \boldsymbol{G}}{\partial \boldsymbol{A}} \\ \mathsf{A} - \Delta t\,\dfrac{\partial \boldsymbol{J}}{\partial \boldsymbol{\sigma}} & \mathsf{J} - \Delta t\,\dfrac{\partial \boldsymbol{J}}{\partial \boldsymbol{A}} \end{bmatrix} \begin{bmatrix} \mathrm{d}\boldsymbol{\sigma} \\ \mathrm{d}\boldsymbol{A} \end{bmatrix} = \begin{bmatrix} \mathrm{d}\Delta\boldsymbol{\varepsilon} \\ \mathbf{0} \end{bmatrix}. \tag{11.78}$$

By inverting the linearised system above, we finally obtain a tangent relation which can be written symbolically as

$$\begin{bmatrix} \mathrm{d}\boldsymbol{\sigma} \\ \mathrm{d}\boldsymbol{A} \end{bmatrix} = \begin{bmatrix} \mathsf{D}_{11} & \mathsf{D}_{12} \\ \mathsf{D}_{21} & \mathsf{D}_{22} \end{bmatrix} \begin{bmatrix} \mathrm{d}\Delta\boldsymbol{\varepsilon} \\ \mathbf{0} \end{bmatrix}, \tag{11.79}$$

where D_{ij} are tensors of appropriate order resulting from the inversion of (11.78). The consistent tangent operator we are looking for is the fourth-order tensor

$$\mathsf{D} \equiv \frac{\mathrm{d}\boldsymbol{\sigma}_{n+1}}{\mathrm{d}\Delta\boldsymbol{\varepsilon}} = \mathsf{D}_{11}. \tag{11.80}$$

Models with a yield surface

For models with a yield surface, the tangent modulus is elastic if the state is within the elastic domain; that is, as in rate-independent plasticity, when $\Phi(\boldsymbol{\sigma}_{n+1}, \boldsymbol{A}_{n+1}) \le 0$, we have

$$\mathsf{D} = \mathsf{D}^e = \bar{\rho}\frac{\partial^2 \psi}{\partial \varepsilon^{e2}}. \tag{11.81}$$

Under viscoplastic flow, i.e. when $\Phi(\boldsymbol{\sigma}_{n+1}, \boldsymbol{A}_{n+1}) > 0$, the stress is the result from the solution of the equation system of item (iii) of Box 11.5. In this case, the tangent operator is a specialisation of the general tangent modulus (11.80) where the functions $\boldsymbol{G}$ and $\boldsymbol{J}$ taking part in the symbolic matrix (11.78) are defined by (11.71). The derivatives of $\boldsymbol{G}$ then specialise as

$$\begin{aligned} \frac{\partial \boldsymbol{G}}{\partial \boldsymbol{\sigma}} &= \dot{\gamma}\,\frac{\partial \boldsymbol{N}}{\partial \boldsymbol{\sigma}} + \boldsymbol{N} \otimes \frac{\partial \dot{\gamma}}{\partial \boldsymbol{\sigma}} \\ \frac{\partial \boldsymbol{G}}{\partial \boldsymbol{A}} &= \dot{\gamma}\,\frac{\partial \boldsymbol{N}}{\partial \boldsymbol{A}} + \boldsymbol{N} * \frac{\partial \dot{\gamma}}{\partial \boldsymbol{A}}. \end{aligned} \tag{11.82}$$

Similarly, the derivatives of $\boldsymbol{J}$ specialise as

$$\begin{aligned} \frac{\partial \boldsymbol{J}}{\partial \boldsymbol{\sigma}} &= \dot{\gamma}\,\frac{\partial \boldsymbol{H}}{\partial \boldsymbol{\sigma}} + \boldsymbol{H} * \frac{\partial \dot{\gamma}}{\partial \boldsymbol{\sigma}} \\ \frac{\partial \boldsymbol{J}}{\partial \boldsymbol{A}} &= \dot{\gamma}\,\frac{\partial \boldsymbol{H}}{\partial \boldsymbol{A}} + \boldsymbol{H} * \frac{\partial \dot{\gamma}}{\partial \boldsymbol{A}}. \end{aligned} \tag{11.83}$$

11.6. Application: computational implementation of a von Mises-based model

To illustrate the application of the above numerical framework, this section describes in detail the basic ingredients of the computational implementation of the von Mises-based model with isotropic strain hardening given in Box 11.2. In addition to the detailed description of the associated integration algorithm and consistent tangent operator, we present an accuracy analysis of the algorithm based on iso-error maps. We remark that the procedures presented here are *not* incorporated in the standard version of program HYPLAS that accompanies this book.

11.6.1. INTEGRATION ALGORITHM

The integration algorithm described here is a specialisation of the generic algorithm described in Section 11.5 to the model whose constitutive equations are summarised in Box 11.2. The algorithm comprises the standard *elastic predictor* and the *viscoplastic return mapping* which, for the present model, has the following format.

1. *Elastic predictor*. The material is assumed to behave purely elastically within the time interval $[t_n, t_{n+1}]$. The *elastic trial* state is then computed as

$$\begin{aligned} \boldsymbol{\varepsilon}^{e\,\mathrm{trial}} &= \boldsymbol{\varepsilon}^e_n + \Delta\boldsymbol{\varepsilon} \\ \boldsymbol{\varepsilon}^{p\,\mathrm{trial}} &= \boldsymbol{\varepsilon}^p_n \\ \bar{\varepsilon}^{p\,\mathrm{trial}} &= \bar{\varepsilon}^p_n \\ \boldsymbol{\sigma}^{\mathrm{trial}} &= \mathbf{D}^e : \boldsymbol{\varepsilon}^{e\,\mathrm{trial}}. \end{aligned} \tag{11.84}$$

If $\Phi(\boldsymbol{\sigma}^{\mathrm{trial}}, \sigma_y(\bar{\varepsilon}^{p\,\mathrm{trial}})) \leq 0$, then the process is indeed elastic within the interval and the variables at t_{n+1} are assigned the values of the trial variables. Otherwise, we apply the viscoplastic return-mapping algorithm described in the following.

2. *Viscoplastic return mapping*. At this stage, we solve the system of discretised equations of item (iii) of Box 11.5 which, for the present model, by taking the linear elastic law into consideration, are specialised as

$$\begin{aligned} \boldsymbol{\sigma}_{n+1} &= \boldsymbol{\sigma}^{\mathrm{trial}} - \Delta\gamma\, \mathbf{D}^e : \left.\frac{\partial \Phi}{\partial \boldsymbol{\sigma}}\right|_{n+1} \\ \bar{\varepsilon}^p_{n+1} &= \bar{\varepsilon}^p_n + \Delta\gamma, \end{aligned} \tag{11.85}$$

where the *incremental multiplier*, $\Delta\gamma$, is given by

$$\Delta\gamma = \frac{\Delta t}{\mu}\left[\left(\frac{q(\boldsymbol{\sigma}_{n+1})}{\sigma_y(\bar{\varepsilon}^p_{n+1})}\right)^{1/\epsilon} - 1\right], \tag{11.86}$$

with Δt denoting the time increment within the considered interval. After solving (11.85), we can update

$$\boldsymbol{\varepsilon}^p_{n+1} = \boldsymbol{\varepsilon}^p_n + \Delta\gamma \left.\frac{\partial \Phi}{\partial \boldsymbol{\sigma}}\right|_{n+1}, \quad \boldsymbol{\varepsilon}^e_{n+1} = \boldsymbol{\varepsilon}^{e\,\mathrm{trial}} - \Delta\gamma \left.\frac{\partial \Phi}{\partial \boldsymbol{\sigma}}\right|_{n+1}. \tag{11.87}$$

Single-equation corrector

The viscoplastic corrector can be more efficiently implemented by reducing (11.85) to a single scalar equation. The situation here is completely analogous to that of the implementation of the elastoplastic (rate-independent) von Mises model described in Section 7.3.2 (page 217). For convenience, the steps leading to the system reduction are repeated here. Firstly, we observe that the plastic flow vector

$$\frac{\partial \Phi}{\partial \boldsymbol{\sigma}} = \sqrt{\frac{3}{2}}\,\frac{\boldsymbol{s}}{\|\boldsymbol{s}\|} \tag{11.88}$$

is deviatoric so that the hydrostatic stress is independent of the viscoplastic flow. The stress update equation $(11.85)_1$ can then be split as

$$\begin{aligned} \boldsymbol{s}_{n+1} &= \boldsymbol{s}^{\mathrm{trial}} - \Delta\gamma\, 2G \sqrt{\frac{3}{2}}\,\frac{\boldsymbol{s}_{n+1}}{\|\boldsymbol{s}_{n+1}\|} \\ p_{n+1} &= p^{\mathrm{trial}}. \end{aligned} \tag{11.89}$$

Further, simple inspection of $(11.89)_1$ shows that $\boldsymbol{s}_{n+1}$ is a scalar multiple of $\boldsymbol{s}^{\mathrm{trial}}$ so that, trivially, we have the identity

$$\frac{\boldsymbol{s}_{n+1}}{\|\boldsymbol{s}_{n+1}\|} = \frac{\boldsymbol{s}^{\mathrm{trial}}}{\|\boldsymbol{s}^{\mathrm{trial}}\|}, \tag{11.90}$$

which allows us to rewrite $(11.89)_1$ as

$$\boldsymbol{s}_{n+1} = \left(1 - \sqrt{\frac{3}{2}}\,\frac{\Delta\gamma\, 2G}{\|\boldsymbol{s}^{\mathrm{trial}}\|}\right)\boldsymbol{s}^{\mathrm{trial}} = \left(1 - \frac{\Delta\gamma\, 3G}{q^{\mathrm{trial}}}\right)\boldsymbol{s}^{\mathrm{trial}} \tag{11.91}$$

where q^{trial} is the elastic trial von Mises equivalent stress. Application of the definition of the von Mises equivalent stress to the above equation gives the update formula

$$q_{n+1} = q^{\mathrm{trial}} - 3G\,\Delta\gamma. \tag{11.92}$$

Finally, with the substitution of the above formula together with $(11.85)_2$ into (11.86) we obtain the following scalar algebraic equation for the multiplier $\Delta\gamma$

$$\Delta\gamma - \frac{\Delta t}{\mu}\left[\left(\frac{q^{\mathrm{trial}} - 3G\,\Delta\gamma}{\sigma_y(\bar{\varepsilon}^p_n + \Delta\gamma)}\right)^{1/\epsilon} - 1\right] = 0, \tag{11.93}$$

or, equivalently, after a straightforward rearrangement,

$$(q^{\mathrm{trial}} - 3G\,\Delta\gamma)\left(\frac{\Delta t}{\mu\,\Delta\gamma + \Delta t}\right)^{\epsilon} - \sigma_y(\bar{\varepsilon}^p_n + \Delta\gamma) = 0. \tag{11.94}$$

The single-equation viscoplastic corrector comprises the solution of (11.93) or (11.94) for the unknown $\Delta\gamma$ followed by the straightforward update of $\boldsymbol{\sigma}$, $\bar{\varepsilon}^p$, $\boldsymbol{\varepsilon}^p$, $\boldsymbol{\varepsilon}^e$ according to the relevant formulae. The solution of the equation for $\Delta\gamma$ is, as usual, undertaken by the Newton–Raphson iterative scheme. The overall algorithm is summarised in Box 11.6 in pseudo-code format.

Box 11.6. Integration algorithm for von Mises-type viscoplastic model (over a generic time interval $[t_n, t_{n+1}]$ with $\Delta t = t_{n+1} - t_n$).

(i) Elastic predictor. Given $\Delta\boldsymbol{\varepsilon}$, and the state variables at t_n, evaluate the *elastic trial state*

$$\boldsymbol{\varepsilon}^{e\,\mathrm{trial}} := \boldsymbol{\varepsilon}^e_n + \Delta\boldsymbol{\varepsilon}$$
$$\bar{\varepsilon}^{p\,\mathrm{trial}}_{n+1} := \bar{\varepsilon}^p_n$$
$$p^{\mathrm{trial}}_{n+1} := K\,\varepsilon^{e\,\mathrm{trial}}_{\mathrm{v}\,n+1}; \quad \boldsymbol{s}^{\mathrm{trial}} := 2G\,\boldsymbol{\varepsilon}^{e\,\mathrm{trial}}_{\mathrm{d}\,n+1}$$
$$q^{\mathrm{trial}}_{n+1} := \sqrt{\tfrac{3}{2}}\,\|\boldsymbol{s}^{\mathrm{trial}}_{n+1}\|$$

(ii) Check for viscoplastic flow

IF $\quad q^{\mathrm{trial}}_{n+1} - \sigma_y(\bar{\varepsilon}^{p\,\mathrm{trial}}_{n+1}) \le 0 \quad$ (elastic step)

THEN set $\quad (\cdot)_{n+1} := (\cdot)^{\mathrm{trial}}_{n+1} \quad$ and EXIT

(iii) Viscoplastic flow. Solve the return-mapping equation

$$R(\Delta\gamma) \equiv (q^{\mathrm{trial}}_{n+1} - 3G\,\Delta\gamma)\left(\frac{\Delta t}{\mu\,\Delta\gamma + \Delta t}\right)^{\epsilon} - \sigma_y(\bar{\varepsilon}^p_n + \Delta\gamma) = 0$$

for $\Delta\gamma$ using the Newton–Raphson scheme. Then update

$$p_{n+1} := p^{\mathrm{trial}}_{n+1}; \quad \boldsymbol{s}_{n+1} := \left(1 - \frac{\Delta\gamma\,3G}{q^{\mathrm{trial}}_{n+1}}\right)\boldsymbol{s}^{\mathrm{trial}}_{n+1}$$
$$\boldsymbol{\sigma}_{n+1} := \boldsymbol{s}_{n+1} + p_{n+1}\,\boldsymbol{I}$$
$$\boldsymbol{\varepsilon}^e_{n+1} := \frac{1}{2G}\,\boldsymbol{s}_{n+1} + \frac{1}{3}\,\varepsilon^{e\,\mathrm{trial}}_{\mathrm{v}\,n+1}\,\boldsymbol{I}$$
$$\bar{\varepsilon}^p_{n+1} := \bar{\varepsilon}^p_n + \Delta\gamma$$

(iv) EXIT

Remark 11.4 (Rate-independent limit). Note that, as expected, equation (11.94) rigorously recovers its elastoplastic (rate-independent) counterpart (7.91) (refer to page 219) when $\mu \to 0$ (no viscosity), $\epsilon \to 0$ (no rate-sensitivity) or $\Delta t \to \infty$ (infinitely slow straining). Clearly, in such cases, the algorithm of Box 11.6 reproduces the rate-independent elastoplastic numerical solution.

Remark 11.5 (Computational implementation aspects). In the computer implementation of the model (as shown in Box 11.6), it is more convenient to solve (11.94) rather than (11.93) in the viscoplastic corrector stage of the algorithm. The reason for this lies in the fact that, for low rate-sensitivity, i.e. small values of ϵ, the Newton–Raphson scheme for solution of (11.93) becomes unstable as its convergence bowl is sharply reduced with decreasing ϵ. The reduction of the convergence bowl stems from the fact that large exponents $1/\epsilon$ can easily produce numbers which are computationally intractable. This fact has been recognised by Perić (1993) in the context of a more general viscoplastic algorithm. In equation (11.94), on the other hand,

the term to the power ϵ on the left-hand side can only assume values within the interval $[0, 1]$ and causes no numerical problems within practical ranges of material constants.

Remark 11.6 (Solution existence and uniqueness). Within a viscoplastic step, we have

$$q^{\mathrm{trial}} > \sigma_y(\bar{\varepsilon}^{p\,\mathrm{trial}}) = \sigma_y(\bar{\varepsilon}^p_n).$$

Let $R(\Delta\gamma)$ be the function defined by the right-hand side of (11.94). The above inequality clearly implies that $R(0) > 0$. In addition, taking into account the strict positiveness of the hardening function σ_y, we can easily verify that $R(q^{\mathrm{trial}}/3G) < 0$. The continuity of R then implies that (11.94) has a root within the interval $(0, q^{\mathrm{trial}}/3G)$. Let us now consider the derivative of R,

$$R'(\Delta\gamma) = -\left(3G + \epsilon\mu\,\frac{q^{\mathrm{trial}} - 3G\Delta\gamma}{\mu\,\Delta\gamma + \Delta t}\right)\left(\frac{\Delta t}{\mu\,\Delta\gamma + \Delta t}\right)^{\epsilon} - H(\bar{\varepsilon}^p_n + \Delta\gamma),$$

where H is the derivative of the isotropic hardening function σ_y. Upon simple inspection, we can easily establish that the derivative R' is strictly negative for $\Delta\gamma \in (0, q^{\mathrm{trial}}/3G)$ if the viscoplastic model is *non-softening*, i.e. if H is non-negative for any value of accumulated plastic strain. The strict negativeness of R' in conjunction with the existence of a root for R established in the above implies that the root of R (the solution of the viscoplastic corrector equation) within the interval $(0, q^{\mathrm{trial}}/3G)$ is unique for non-softening materials.

11.6.2. ISO-ERROR MAPS

To illustrate the accuracy of the above integration algorithm in practical situations, this section presents some iso-error maps, produced with material constants covering a range of high rate-sensitivity to rate-independence. The material is assumed perfectly viscoplastic (no hardening). The maps have been generated in the standard fashion as described in Section 7.2.10 (refer to Figure 7.7, page 215). Using the three-dimensional implementation of the model, we start from a stress point at time t_n, with $\boldsymbol{\sigma}_n$ lying on the yield surface, and apply a sequence of strain increments (at *constant strain rate* within the interval $[t_n, t_{n+1}]$), corresponding to linear combinations of trial stress increments in the direction normal and tangential (directions of the unit tensors $\boldsymbol{N}$ and $\boldsymbol{T}$ of Figure 7.7, respectively) to the von Mises circle in the deviatoric plane. Figures 11.5 and 11.6 show iso-error maps obtained at low and high strain rates with the non-dimensional rate

$$\mu\,\|\dot{\boldsymbol{\varepsilon}}\|$$

set respectively to 1 and 1000. For each non-dimensional rate, three values of rate-sensitivity parameter, ϵ, have been used: 10^0, 10^{-1} and 0. Recall that for $\epsilon = 0$ the algorithm reproduces the rate-independent solution. The resulting map in this case is obviously identical to the rate-independent map of Figure 7.7(b) and is shown here only to emphasise the effect of rate-dependence on the integration error. The main conclusion drawn from the iso-error maps is that, in general, increasing (decreasing) rate-sensitivity and/or increasing (decreasing) strain rates tend to produce decreasing (increasing) integration errors. The largest errors are expected in the rate-independent limit.

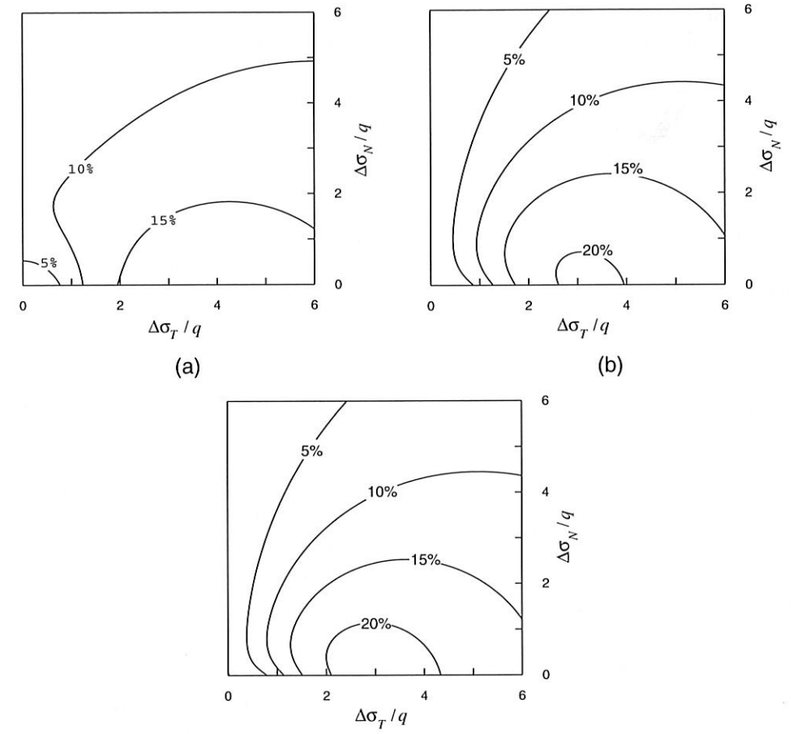

Figure 11.5. Iso-error maps with $\mu \, \|\dot{\varepsilon}\| = 1$; (a) $\epsilon = 10^0$; (b) $\epsilon = 10^{-1}$; (c) $\epsilon = 0$ (rate-independent).

11.6.3. CONSISTENT TANGENT OPERATOR

The consistent tangent operator here is a particular case of the general tangent operator derived in Section 11.5.3. Clearly, when the stress state lies within the elastic domain and no viscoplastic flow is possible, the tangent operator is the elastic tangent, D^e. Under viscoplastic flow, the tangent operator which (as in the rate-independent case) will be denoted D^{ep}, is derived by consistently linearising the viscoplastic return-mapping algorithm referred to in item (iii) of Box 11.6. Its closed-form expression can be obtained by following the same steps of the derivation of the elastoplastic (rate-independent) tangent presented in Section 7.4.2 (from page 232). The incremental constitutive function for the stress tensor in the present case has identical format to that of the rate-independent implementation given by (7.93) – which reduces to (7.113) under plastic flow – but the incremental plastic multiplier $\Delta\gamma$ here is the solution of viscoplastic return-mapping equation (11.94). Thus, to obtain the viscoplastic consistent tangent, we simply replace the derivative of the incremental plastic

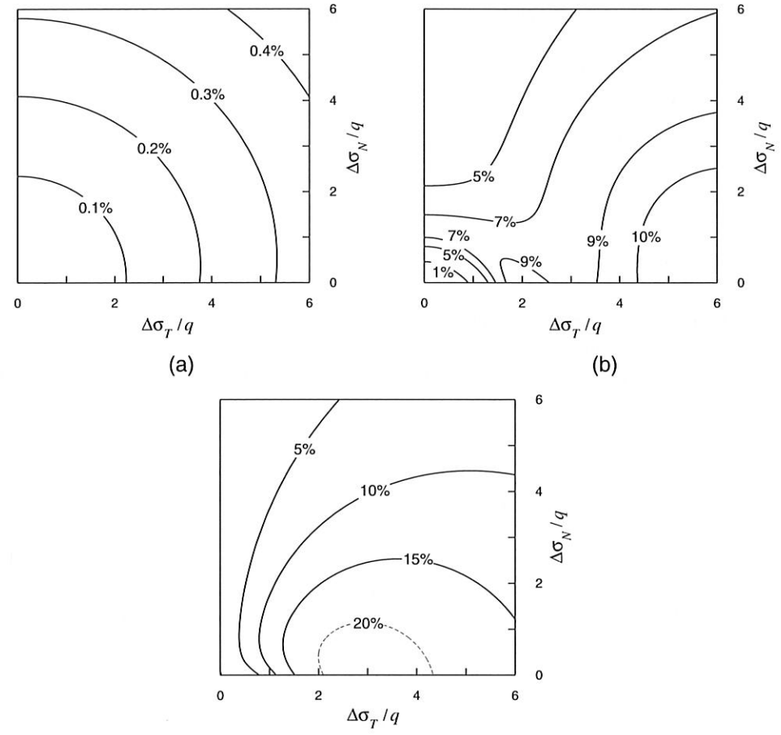

Figure 11.6. Iso-error maps with $\mu \, \|\dot{\varepsilon}\| = 10^3$; (a) $\epsilon = 10^0$; (b) $\epsilon = 10^{-1}$; (c) $\epsilon = 0$ (rate-independent).

multiplier (7.118) with the expression

$$\frac{\partial \Delta\gamma}{\partial \varepsilon^{e\,\mathrm{trial}}_{n+1}} = \frac{2G\sqrt{\frac{3}{2}}}{3G + \left(\frac{\Delta t}{\mu\,\Delta\gamma + \Delta t}\right)^{-\epsilon} H + \frac{\epsilon\mu\, q_{n+1}}{\mu\,\Delta\gamma + \Delta t}} \bar{\boldsymbol{N}}_{n+1}, \tag{11.95}$$

which is consistent with (11.94). Analogously to the elastoplastic case, this expression is obtained by taking the differential of the viscoplastic corrector equation (11.94), having $\Delta\gamma$ and q^{trial}_{n+1} as variables, and equating it to zero. With the above differential relation, the final

elasto-viscoplastic consistent tangent operator is obtained in closed form as

$$\mathsf{D}^{ep} = 2G\left(1 - \frac{\Delta\gamma\, 3G}{q^{\text{trial}}_{n+1}}\right)\mathsf{I}_{\text{d}} + 6G^2\left[\frac{\Delta\gamma}{q^{\text{trial}}_{n+1}} - \frac{1}{3G + \left(\frac{\Delta t}{\mu\,\Delta\gamma+\Delta t}\right)^{-\epsilon} H + \frac{\epsilon\mu\, q_{n+1}}{\mu\,\Delta\gamma+\Delta t}}\right]\bar{\boldsymbol{N}}_{n+1}\otimes\bar{\boldsymbol{N}}_{n+1} + K\,\boldsymbol{I}\otimes\boldsymbol{I}. \tag{11.96}$$

Note that the tangent operator is symmetric.

Remark 11.7 (Rate-independent limit). By simple inspection we find that in the limits $\epsilon \to 0$ (vanishing rate-sensitivity parameter), $\mu \to 0$ (vanishing viscosity) or $\Delta t \to \infty$ (infinitely slow straining), expression (11.96) rigorously recovers the elastoplastic consistent tangent operator of the isotropically hardening rate-independent von Mises model with implicit return mapping given by expression (7.120).

11.6.4. PERZYNA-TYPE MODEL IMPLEMENTATION

The implementation of the von Mises-based model with Perzyna's viscoplastic law (11.40) follows exactly the same procedure as described in the above except that, consistently with the backward Euler time discretization of (11.40), the return-mapping equation (11.94) (or item (iii) of Box 11.6) is replaced with

$$q^{\text{trial}} - 3G\,\Delta\gamma - \left[1 + \left(\frac{\mu\,\Delta\gamma}{\Delta t}\right)^{\epsilon}\right]\sigma_y(\bar{\varepsilon}^p_n + \Delta\gamma) = 0. \tag{11.97}$$

Here, we have assumed isotropic strain hardening. Note that, as $\mu \to \infty$ (vanishing viscosity) or $\Delta t \to \infty$ (infinitely slow process) equation (11.97) reduces to that of the elastoplastic rate-independent von Mises model with yield stress σ_y. For vanishing rate sensitivity parameter, $\epsilon \to 0$, (11.97) reduces to a von Mises elastoplastic return-mapping equation with yield stress $2\sigma_y$. This is, as one should expect, in agreement with the theoretical limits of the Perzyna model discussed in the text immediately following equation (11.40).

Elasto-viscoplastic consistent tangent operator

The differential relation between the incremental plastic multiplier and $\boldsymbol{\varepsilon}^{e\,\text{trial}}_{n+1}$ consistent with the return-mapping equation (11.97) reads

$$\frac{\partial\Delta\gamma}{\partial\boldsymbol{\varepsilon}^{e\,\text{trial}}_{n+1}} = \frac{2G\sqrt{\frac{3}{2}}}{3G + \left[1 + \left(\frac{\mu\,\Delta\gamma}{\Delta t}\right)^{\epsilon}\right]H + \frac{\epsilon\mu}{\Delta t}\left(\frac{\mu\,\Delta\gamma}{\Delta t}\right)^{\epsilon-1}\sigma_y}\,\bar{\boldsymbol{N}}_{n+1}, \tag{11.98}$$

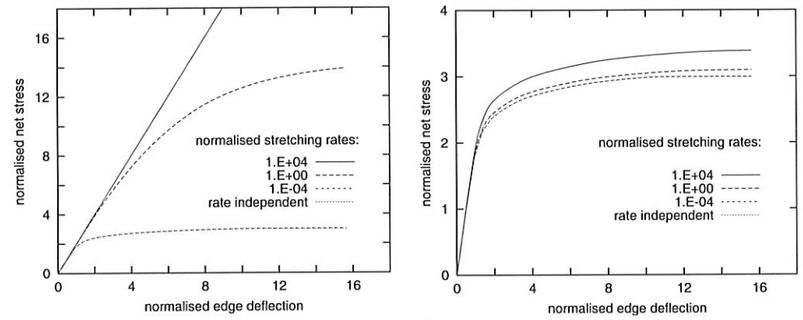

Figure 11.7. Double-notched specimen. Reaction–deflection diagrams: (a) $\epsilon = 10^0$; (b) $\epsilon = 10^{-2}$.

where σ_y is evaluated at $\bar{\varepsilon}^p_{n+1} = \bar{\varepsilon}^p_n + \Delta\gamma$. This expression is the counterpart of (11.95) for the present implementation of Perzyna's viscoplasticity law. The corresponding elasto-viscoplastic consistent tangent operator is obtained following the usual procedure as

$$\mathsf{D}^{ep} = 2G\left(1 - \frac{\Delta\gamma\, 3G}{q^{\text{trial}}_{n+1}}\right)\mathsf{I}_{\text{d}} + 6G^2\left[\frac{\Delta\gamma}{q^{\text{trial}}_{n+1}} - \frac{1}{3G + \left[1 + \left(\frac{\mu\,\Delta\gamma}{\Delta t}\right)^{\epsilon}\right]H + \frac{\epsilon\mu}{\Delta t}\left(\frac{\mu\,\Delta\gamma}{\Delta t}\right)^{\epsilon-1}\sigma_y}\right]\bar{\boldsymbol{N}}_{n+1}\otimes\bar{\boldsymbol{N}}_{n+1} + K\,\boldsymbol{I}\otimes\boldsymbol{I}. \tag{11.99}$$

Its format is completely analogous to that of (11.96).

11.7. Examples

The finite element examples presented in this section illustrate applications of the computational treatment of viscoplasticity described above. The underlying viscoplastic material model is the one shown in Box 11.2, which includes isotropic strain hardening.

11.7.1. DOUBLE-NOTCHED TENSILE SPECIMEN

The rate-independent version of this problem has been studied in Section 7.5.5 (from page 255). The problem consists of the plane strain analysis of a deep double-notched tensile specimen. The geometry of the specimen and the finite element mesh used are shown in Figure 7.29 (page 256). Analogously to the prescription of edge displacement u (refer to Figure 7.29), the simulation consists of stretching the specimen by prescribing a constant (in time) vertical velocity v on the top nodes of the mesh. For convenience, we define the normalised stretching rate

$$v^* = \frac{\mu\, v}{l/2}$$

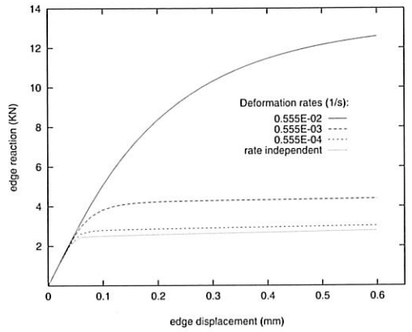

(a)

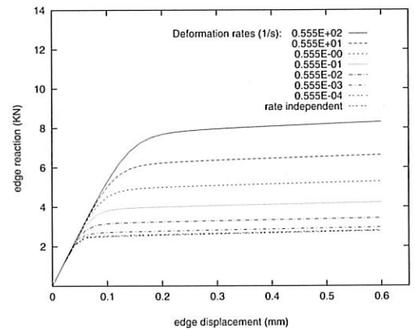

(b)

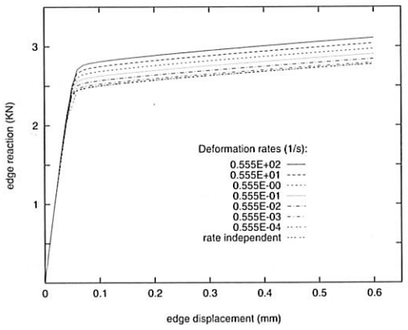

(c)

Figure 11.8. Stretching of a perforated plate. Displacement-reaction diagrams. (a) $\epsilon = 10^0$; (b) $\epsilon = 10^{-1}$; (c) $\epsilon = 10^{-2}$.

and the simulation is carried out for three different values of v^*

$$v^* = 10^{-4},\ 10^0,\ 10^4.$$

This choice covers very slow to very fast strain rates and is meant to demonstrate the robustness of the integration algorithm over a wide range of strain rates. The following material parameters are adopted

$$E = 206.9\,\text{GPa}; \quad \nu = 0.29; \quad \sigma_y = 0.45\,\text{GPa (constant)}.$$

The linearly hardening case listed in Figure 7.29 is not considered here. In order to show the effect of the rate-sensitivity parameter on the behaviour of the model, two values of ϵ are considered

$$\epsilon = 10^0 \quad \text{and} \quad 10^{-2}.$$

The results of the finite element simulations are presented in Figure 11.7 whose diagrams show the evolution of the reaction forces on the constrained edge against the corresponding edge deflection. As in the rate-independent case, the results are plotted in terms of the *normalised net stress* and the *normalised edge deflection* defined in Section 7.5.5. The results for $\epsilon = 10^0$ and 10^{-2} are shown, respectively, in Figures 11.7(a) and (b). They illustrate the expected higher reactions and limit loads for higher rates of stretching. For the lowest non-dimensional rate of 10^{-4}, the rate-independent solution is recovered for any rate-sensitivity parameter. We remark that the rate-independent solution shown in the graphs for comparison can be obtained with the present model/algorithm simply by setting $\epsilon = 0$ or $\mu = 0$.

11.7.2. PLANE STRESS: STRETCHING OF A PERFORATED PLATE

This section describes the viscoplastic version of the plane stress problem of Section 9.5.3 (from page 390). This example has been analysed by Perić (1993). Here, a plane stress version of the numerical integration algorithm discussed in Section 11.6.1 is employed. The plane stress implementation adopted follows the nested iteration approach described in Section 9.2.2 (page 362) in the context of rate-independent plasticity. The problem consists of the axial stretching at constant rate of a perforated rectangular plate whose geometry is shown in Figure 9.7 (page 392). The mesh, boundary conditions and the material parameters that are common to both plastic and viscoplastic models are also shown in Figure 9.7. Note that linear strain hardening is assumed. The viscosity parameter adopted (required for the viscoplastic model) is

$$\mu = 500\,\text{s}.$$

Similarly to the previous example, in order to illustrate the response predicted by the viscoplastic model over a wide range of conditions, several simulations are carried out with various stretching rates, with three values of rate sensitivity coefficients ($\epsilon = 1, 10^{-1}, 10^{-2}$) being considered. The results obtained in the simulations are shown in Figure 11.8 where the reaction on the constrained edge of the plate is plotted against the prescribed edge displacement for the various conditions considered. The stretching rate in the present case is defined as

$$2v/l,$$

where v is the stretching velocity imposed on the nodes of the upper edge. The three graphs of Figure 11.8 show the effect of stretching rates on the response of the plate, with higher reactions obtained at high rates and the rate-independent solution being approached as the stretching rate vanishes. The effects of the rate sensitivity parameter are also clearly illustrated. At higher (lower) values of ϵ, a greater (smaller) variation of reaction as a function of the stretching rate is produced.

12 DAMAGE MECHANICS

INTERNAL damage can be defined as the presence and evolution of cracks and cavities at the microscopic level which may, eventually, lead to failure – a complete loss of load-carrying capability of the material. In many engineering applications, particularly those where mechanical/structural components are subjected to severe service conditions, the useful life of components is a crucial item of information which has to be carefully considered during the design process. In such cases, the ability of the designer to predict mechanical failure becomes an important factor. In some applications, such as in certain types of industrial machinery, non-scheduled stops for maintenance owing to unpredicted failure may incur serious economic consequences. In the design of manufacturing processes, such as metal-forming operations, prediction of failure is also a crucial issue. In safety-critical applications, frequently encountered in the aeronautical and nuclear industries, unpredicted failure may have catastrophic effects with consequences far beyond purely economical issues.

Traditionally, the prediction of useful life/failure of materials is based on mostly empirical experience accumulated over long periods of time. In some cases, failure prediction is achieved by the systematic (and expensive) testing of real models under laboratory-reproduced service conditions. However, with the growing knowledge of the mechanisms of progressive internal damage that cause failure in a wide range of materials, it is becoming possible to formulate continuum constitutive models capable of accounting for the evolution of internal deterioration. This relatively new branch of continuum solid mechanics is known as *Continuum Damage Mechanics* (*CDM*). This fact, allied to the fast development of computational mechanics techniques, has made the use of computational tools to carry out life/failure prediction a realistic alternative that can be successfully adopted in many design and damage assessment situations.

The present chapter is devoted to computational continuum damage mechanics. Our intention here is to provide the reader with an introduction to this new and promising ramification of computational solid mechanics that has been gaining widespread acceptance over the last two decades. The material presented in this chapter is summarised as follows. After providing a brief review of some basic mechanisms that characterise the presence and evolution of damage in Section 12.1, we give in Section 12.2 a brief historical account of CDM together with a discussion on the continuum modelling of damage phenomena. Sections 12.3, 12.4 and 12.5, describe, respectively, Lemaitre's ductile damage model (Lemaitre, 1985b), a simplified version of Lemaitre's model where kinematic hardening is not considered and Gurson's void growth model (Gurson, 1977). In each of these sections, the computational implementation of the corresponding constitutive models within an implicit finite element environment is described in detail. Note that the simplified version of Lemaitre's model discussed in Section 12.4 is fully incorporated into program `HYPLAS`. Further issues, including crack closure effects and damage anisotropy are addressed in Section 12.6.

Computational Methods for Plasticity: Theory and Applications EA de Souza Neto, D Perić and DRJ Owen

and

$$\mathbf{a} = \begin{bmatrix} a_{1111} & a_{1121} & a_{1112} & a_{1122} & a_{1133} \\ a_{2111} & a_{2121} & a_{2112} & a_{2122} & a_{2133} \\ a_{1211} & a_{1221} & a_{1212} & a_{1222} & a_{1233} \\ a_{2211} & a_{2221} & a_{2212} & a_{2222} & a_{2233} \\ a_{3311} & a_{3321} & a_{3312} & a_{3322} & a_{3333} \end{bmatrix}. \tag{D.26}$$

An analogous conversion rule can be defined for three-dimensional problems.

REFERENCES

Alfano, G., de Angelis F. and Rosati, L. 2001. General Solution Procedures in Elasto/Viscoplasticity. *Comp. Meth. Appl. Mech. Engng*, **190**, 5123–5147.

Anderson, H. 2003. An Implicit Formulation of the Bodner–Partom Constitutive Equations. *Comp. Struct*, **81**, 1405–1414.

ANSI. 1978. *American National Standard Programming Language FORTRAN*. New York.

Aravas, N. 1987. On the Numerical Integration of a Class of Pressure-Dependent Plasticity Models. *Int. J. Num. Meth. Engng*, **24**, 1395–1416.

Argyris, J.H. and Kleiber, M. 1977. Incremental Formulation in Nonlinear Mechanics and Large Strain Elasto-plasticity – Natural Approach. Part I. *Comp. Meth. Appl. Mech. Engng*, **11**, 215–247.

Argyris, J.H. and Symeonidis, Sp. 1981. Nonlinear Finite Element Analysis of Elastic Systems Under Nonconservative Loading – Natural Formulation. Part I. Quasistatic Problems. *Comp. Meth. Appl. Mech. Engng*, **26**, 75–123.

Argyris, J.H., Doltsinis, J.St. and Kleiber, M. 1978. Incremental Formulation in Nonlinear Mechanics and Large Strain Elasto-plasticity – Natural Approach. Part II. *Comp. Meth. Appl. Mech. Engng*, **14**, 259–294.

Armero, F. and Oller, S. 2000. A General Framework for Continuum Damage Models. I. Infinitesimal Plastic Damage Models in Stress Space. *Int. J. Solids Structs*, **37**, 7409–7436.

Armero, F. and Pérez-Foguet, A. 2002. On the Formulation of Closest-Point Projection Algorithms in Elastoplasticity – Part I: The Variational Structure. *Int. J. Numer. Meth. Engng*, **53**, 297–329.

Armstrong, P.J. and Frederick, C.O. 1966. *A Mathematical Representation of the Multiaxial Bauschinger Effect*. CEGB: Report RD/B/N 731.

Arridge, R.G.C. 1985. *An Introduction to Polymer Mechanics*. London: Taylor and Francis.

Asaro, R.J. 1983. Micromechanics of Crystals and Polycrystals. *Adv. Appl. Mech.*, **23**, 1–115.

Asaro, R.J. and Needleman, A. 1985. Texture Development and Strain Hardening in Rate Dependent Polycrystals. *Acta Metall.*, **33**(6), 923–953.

Ascher, U.M. and Petzold, L.R. 1998. *Computer Methods for Ordinary Differential Equations and Differential-Algebraic Equations*. Philadelphia: SIAM.

Atluri, S.N. 1984. On Constitutive Relations at Finite Strains: Hypo-Elasticity and Elasto-Plasticity with Isotropic or Kinematic Hardening. *Comp. Meth. Appl. Mech. Engng*, **43**, 137–171.

Auricchio, F., Beirão da Veiga, L., Lovadina, C. and Reali, A. 2005. A Stability Study of Some Mixed Finite Elements for Large Deformation Elasticity Problems. *Comp. Meth. Appl. Mech. Engng*, **194**, 1075–1092.

Barlat, F. and Lian, J. 1989. Plastic Behavior and Stretchability of Sheet Metals. Part I: A Yield Function for Orthotropic Sheets Under Plane Stress Condition. *Int. J. Plast.*, **5**, 51–66.

Computational Methods for Plasticity: Theory and Applications EA de Souza Neto, D Perić and DRJ Owen

Basista, M., Krajčinović, D. and Šumarac, D. 1992. Micromechanics, Phenomenology and Statistics of Brittle Deformation. *Pages 1479–1490 of:* Owen, D.R.J., Oñate, E. and Hinton, E. (eds), *Computational Plasticity: Fundamentals and Applications – Proceedings of the Third International Conference held in Barcelona, 6–10 April 1992*. Swansea: Pineridge Press.

Bataille, J. and Kestin, J. 1979. Irreversible Processes and Physical Interpretation of Rational Thermodynamics. *J. Non-Equilib. Thermodyn.*, **4**, 229–258.

Bathe, K.-J. 1996. *Finite Element Procedures*. Englewood Cliffs, New Jersey: Prentice-Hall.

Bazaraa, M. and Shetty, C. 1979. *Non-linear Programming: Theory and Applications*. New York: Wiley.

Beatty, M.F. 1987. Topics in Finite Elasticity: Hyperelasticity of Rubber, Elastomers, and Biological Tissues – with Examples. *Appl. Mech. Rev.*, **40**, 1699–1734.

Belytschko, T. and Bindeman, L.P. 1991. Assumed Strain Stabilization of the 4-Node Quadrilateral with 1-Point Quadrature for Nonlinear Problems. *Comp. Meth. Appl. Mech. Engng*, **88**, 311–340.

Belytschko, T. and Bindeman, L.P. 1993. Assumed Strain Stabilization of the Eight Node Hexahedral Element. *Comp. Meth. Appl. Mech. Engng*, **105**, 225–260.

Belytschko, T., Liu, W.-K. and Moran, B. 2000. *Nonlinear Finite Elements for Continua and Structures*. Chichester: Wiley.

Belytschko, T., Ong, J.S.-J., Liu, W.K. and Kennedy, J.M. 1984. Hourglass Control in Linear and Nonlinear Problems. *Comp. Meth. Appl. Mech. Engng*, **43**, 251–276.

Benallal, A., Billardon, R. and Doghri, I. 1988. An Integration Algorithm and the Corresponding Consistent Tangent Operator for Fully Coupled Elastoplastic and Damage Equations. *Comm. Appl. Num. Meth.*, **4**, 731–740.

Benallal, A., Billardon, R. and Lemaitre, J. 1991. Continuum Damage Mechanics and Local Approach to Fracture: Numerical Procedures. *Comp. Meth. Appl. Mech. Engng*, **92**, 141–155.

Benallal, A., Billardon, R., Doghri, I. and Moret-Bailly, L. 1987. Crack Initiation and Propagation Analyses Taking into Account Initial Strain Hardening and Damage Fields. *Pages 337–351 of:* Luxmore, A.L., Owen, D.R.J., Rajapakse, Y.P.S. and Kanninen, M.F. (eds), *Numerical Methods in Fracture Mechanics: Proceedings of the Fourth International Conference held in San Antonio, Texas, 23–27 March 1987*. Pineridge Press.

Billington, E.W. and Tate, A. 1981. *The Physics of Deformation and Flow*. New York: McGraw-Hill.

Blatz, P.J. and Ko, W.L. 1962. Application of Finite Elasticity to the Deformation of Rubbery Materials. *Trans. Soc. Rheol.*, **6**, 223–251.

Bodner, S.R. and Partom, Y. 1975. Constitutive Equations for Elastic Viscoplastic Strain Hardening. *J. Appl. Mech.*, **42**, 385–389.

Boisse, Ph., Bussy, P. and Ladevèze, P. 1990. A New Approach in Non-linear Mechanics: The Large Time Increment Method. *Int. J. Num. Meth. Engng*, **29**, 647–663.

Boisse, Ph., Ladevèze, P. and Rougee, P. 1989. A Large Time Increment Method for Elastoplastic Problems. *Eur. J. Mech. A/Solids*, **8**(4), 257–275.

Bonet, J. and Wood, R.D. 1997. *Nonlinear Continuum Mechanics*. Cambridge: Cambridge University Press.

Borja, R. and Wren, J.R. 1993. Discrete Micromechanics of Elastoplastic Crystals. *Int. J. Num. Meth. Engng*, **36**, 3815–3840.

Boucard, P.-A., Ladevèze, P., Poss, M. and Rougée, P. 1997. A Nonincremental Approach for Large Displacement Problems. *Comput. Struct.*, **64**(1–4), 499–508.

Boyle, J.T. and Spence, J. 1983. *Stress Analysis for Creep*. London: Butterworths.

Brezzi, F. and Fortin, M. 1991. *Mixed and Hybrid Finite Element Methods*. New York: Springer-Verlag.

Bueche, F. 1960. Molecular Basis for the Mullins Effect. *J. Appl. Poly. Sci.*, **4**(10), 107–114.

Caddemi, S. and Martin, J.B. 1991. Convergence of the Newton–Raphson Algorithm in Elastic-plastic Incremental Analysis. *Int. J. Num. Meth. Engng*, **31**, 177–191.

Carlson, D.E. and Hoger, A. 1986. The Derivative of a Tensor-valued Function of a Tensor. *Quart. Appl. Math.*, **44**(3), 409–423.

Cescotto, S. and Zhu, Y.Y. 1995. Modelling of Ductile Fracture Initiation During Bulk Forming. *Pages 987–998 of:* Owen, D.R.J., Oñate, E. and Hinton, E. (eds), *Computational Plasticity: Fundamentals and Applications – Proceedings of the Fourth International Conference held in Barcelona, 3–6 April 1995*. Swansea: Pineridge Press.

Chaboche, J.L. 1978. *Description thermodynamique et phénoménologique de la viscoplasticité cyclique avec endommagement*. Technical Report 1978–3. Office National d'Etudes et de Recherches Aérospatiales.

Chaboche, J.L. 1981. Continuous Damage Mechanics – A Tool to Describe Phenomena Before Crack Initiation. *Nucl. Engng. Des.*, **64**, 233–247.

Chaboche, J.L. 1984. Anisotropic Creep Damage in the Framework of Continuum Damage Mechanics. *Nucl. Engng. Des.*, **79**, 309–319.

Chaboche, J.L. 1988. Continuum Damage Mechanics: Part I – General Concepts and Part II – Damage Growth, Crack Initiation and Crack Growth. *J. Appl. Mech.*, **55**, 59–72.

Chaboche, J.L. and Cailletaud, G. 1996. Integration Methods for Complex Plastic Constitutive Equations. *Comp. Meth. Appl. Mech. Engng*, **133**, 125–155.

Chadwick, P. and Ogden, R.W. 1971. A Theorem in Tensor Calculus and its Application to Isotropic Elasticity. *Arch. Rat. Mech. Anal.*, **44**, 54–68.

Chakrabarty, J. 1987. *Theory of Plasticity*. London: McGraw-Hill.

Chen, W-F. 1975. *Limit Analysis and Soil Plasticity*. New York: Elsevier.

Chen, W-F. 1982. *Plasticity in Reinforced Concrete*. McGraw-Hill.

Chen, W-F. and Mizuno, E. 1990. *Nonlinear Analysis in Soil Mechanics. Theory and Implementation*. New York: Elsevier.

Chorin, A.J., Hughes, T.J.R., McCracken, M.F. and Marsden, J.E. 1978. Product Formulas and Numerical Algorithms. *Comm. Pure and Appl. Math.*, **31**, 205–256.

Ciarlet, P.G. 1988. *Mathematical Elasticity. Volume I: Three-dimensional Elasticity*. Amsterdam: North-Holland.

Cognard, J.Y. and Ladèveze, P. 1993. A Large Time Increment Approach for Cyclic Viscoplasticity. *Int. J. Plast.*, **9**(2), 141–157.

Cognard, J.Y., Ladèveze, P. and Talbot, P. 1999. A Large Time Increment Approach for Thermo-Mechanical Problems. *Adv. Engng. Software*, **30**(9–11), 583–593.

Coleman, B.D. and Gurtin, M.E. 1967. Thermodynamics with Internal State Variables. *J. Chem. Phys.*, **47**(2), 597–613.

Comi, C., Corigliano, A. and Maier, G. 1991. Extremum Properties of Finite-step Solutions in Elastoplasticity with Nonlinear Mixed Hardening. *Int. J. Solids Struct.*, **27**(8), 965–981.

Cordebois, J.P. and Sidoroff, F. 1979. Damage Induced Elastic Anisotropy. *Pages 761–774 of: Euromech 115 – Villard de Lans – Juin 1979*.

Cordebois, J.P. and Sidoroff, F. 1982. Endomagement Anisotrope en Élasticité et Plasticité. *Journal de Mécanique Théorique et Appliquée*, 45–60. Numéro spécial.

Cormeau, I.C. 1975. Numerical Stability in Quasi-Static Elasto/Visco-Plasticity. *Int. J. Num. Meth. Engng*, **9**, 109–127.

Cosserrat, E. and Cosserrat, F. 1909. *Théorie des corps déformables*. Paris: Hermann.

Cox, A.D., Eason, G. and Hopkins, H.G. 1961. Axially Symmetric Plastic Deformation in Soils. *Trans. R. Soc. Lond. A*, **254**, 1–45.

Crisfield, M.A. 1981. A Fast Incremental/Iterative Solution Procedure that Handles 'Snap-Through'. *Comp. Structs*, **13**, 55–62.

Crisfield, M.A. 1983. An Arc-Length Method Including Line Searches and Accelerations. *Int. J. Num. Meth. Engng*, **19**, 1269–1289.

Crisfield, M.A. 1987. Plasticity Computations Using the Mohr–Coulomb Yield Criterion. *Engng. Comp.*, **4**, 300–308.

Crisfield, M.A. 1991. *Non-linear Finite Element Analysis of Solids and Structures. Volume 1: Essentials*. Chichester: John Wiley & Sons.

Crisfield, M.A. 1997. *Non-linear Finite Element Analysis of Solids and Structures. Volume 2: Advanced Topics*. Chichester: John Wiley & Sons.

Crisfield, M.A. and Moita, G.F. 1996. A Co-rotational Formulation for 2-D Continua Including Incompatible Modes. *Int. J. Numer. Meth. Engng*, **39**, 2619–2633.

Crisfield, M.A., Moita, G.F., Jelenić, G. and Lyons, L.P.R. 1995. Enhanced Lower-Order Element Formulations for Large Strains. *Pages 293–320 of:* Owen, D.R.J., Oñate, E. and Hinton, E. (eds), *Computational Plasticity: Fundamentals and Applications – Proceedings of the Fourth International Conference held in Barcelona, 3–6 April 1995*. Swansea: Pineridge Press.

Cuitiño, A. and Ortiz, M. 1992a. A Material-independent Method for Extending Stress Update Algorithms from Small-strain Plasticity to Finite Plasticity with Multiplicative Kinematics. *Engng. Comp.*, **9**, 437–451.

Cuitiño, A.M. and Ortiz, M. 1992b. Computational Modelling of Single Crystals. *Modelling Simul. Mater. Sci. Engng*, **1**, 225–263.

Dafalias, Y.F. 1984. The Plastic Spin Concept and a Simple Illustration of its Role in Finite Plastic Transformations. *Mech. Mater.*, **3**, 223–233.

Dafalias, Y.F. 1985. The Plastic Spin. *J. Appl. Mech.*, **52**, 865–871.

Dashner, P.A. 1986. Invariance Considerations in Large Strain Elasto-Plasticity. *J. Appl. Mech.*, **53**, 55–60.

de Borst, R. 1987. Integration of Plasticity Equations for Singular Yield Functions. *Comp. Structs*, **26**, 823–829.

de Borst, R. 1991. The Zero-normal-stress Condition in Plane-stress and Shell Elastoplasticity. *Comm. Appl. Numer. Meth.*, **7**, 29–33.

de Borst, R. and Feenstra, P.H. 1990. Studies in Anisotropic Plasticity with Reference to the Hill Criterion. *Int. J. Numer. Meth. Engng*, **29**, 315–336.

de Souza Neto, E.A., Andrade Pires, F.M. and Owen, D.R.J. 2005. F-bar-based Linear Triangles and Tetrahedra for Finite Strain Analysis of Nearly Incompressible Solids. Part I: Formulation and Benchmarking. *Int. J. Numer. Meth. Engng*, **62**(3), 353–383.

de Souza Neto, E.A. and Feng, Y.T. 1999. On the Determination of the Path Direction for Arc-length Methods in the Presence of Bifurcations and 'Snap-Backs'. *Comp. Meth. Appl. Mech. Engng*, **179**, 81–89.

de Souza Neto, E.A. and Perić, D. 1996. A Computational Framework for a Class of Models for Fully Coupled Elastoplastic Damage at Finite Strains with Reference to the Linearization Aspects. *Comp. Meth. Appl. Mech. Engng*, **130**, 179–193.

de Souza Neto, E.A., Perić, D. and Owen, D.R.J. 1992. A Computational Model for Ductile Damage at Finite Strains. *Pages 1425–1441 of:* Owen, D.R.J., Oñate, E. and Hinton, E. (eds), *Computational Plasticity: Fundamentals and Applications – Proceedings of the Third International Conference held in Barcelona, 6–10 April 1992*. Swansea: Pineridge Press.

de Souza Neto, E.A., Perić, D. and Owen, D.R.J. 1993. Some Aspects of Formulation and Implementation of Ductile Damage at Finite Strains. *In: Proceedings of the ACME 93 Conference: Computational Mechanics in the UK*.

de Souza Neto, E.A., Perić, D. and Owen, D.R.J. 1994a. A Model for Elasto-plastic Damage at Finite Strains: Computational Issues and Applications. *Engng. Comp.*, **11**(3), 257–281.

de Souza Neto, E.A., Perić, D. and Owen, D.R.J. 1994b. A Phenomenological Three-dimensional Rate-independent Continuum Damage Model for Highly Filled Polymers: Formulation and Computational Aspects. *J. Mech. Phys. Solids*, **42**(10), 1533–1550.

de Souza Neto, E.A., Perić, D. and Owen, D.R.J. 1998. Continuum Modelling and Numerical Simulation of Material Damage at Finite Strains. *Arch. Comput. Meth. Engng*, **5**, 311–384.

de Souza Neto, E.A., Perić, D., Dutko, M. and Owen, D.R.J. 1996. Design of Simple Low Order Finite Elements for Large Strain Analysis of Nearly Incompressible Solids. *Int. J. Solids Structs*, **33**, 3277–3296.

Desmorat, R. 2000. Dissymétrie de comportement élastique anisotrope couplé ou non à l'endomagement. *C. R. Acad. Sci. Paris, Série II b*, **328**, 445–450.

Dettmer, W. and Reese, S. 2004. On the Theoretical and Numerical Modelling of Armstrong–Frederick Kinematic Hardening in the Finite Strain Regime. *Comp. Meth. Appl. Mech. Engng*, **192**, 87–116.

Dienes, J.K. 1979. On the Analysis of Rotation and Stress Rates in Deforming Bodies. *Acta Mech.*, **32**, 217–232.

Dieter, G. 1986. *Mechanical Metallurgy*. McGraw-Hill.

Dodds, Jr., R.H. 1987. Numerical Techniques for Plasticity Computations in Finite Element Analysis. *Comput. Structs*, **26**(5), 767–779.

Doghri, I. 1995. Numerical Implementation and Analysis of a Class of Metal Plasticity Models Coupled with Ductile Damage. *Int. J. Numer. Meth. Engng*, **38**, 3403–3431.

Doll, S., Hauptmann, R., Schweizerhof, K. and Freischlager, C. 2000. On Volumetric Locking of Low-order Solid and Solid-shell Elements for Finite Elastoviscoplastic Deformations and Selective Reduced Integration. *Engng. Comp.*, **17**, 874–902.

Drucker, D.C. and Prager, W. 1952. Soil Mechanics and Plasticity Analysis of Limit Design. *Quart. J. Appl. Math.*, **10**, 157–162.

Dureisseix, D., Ladevèze, P. and Schrefler, B.A. 2003. A LATIN Computational Strategy for Multi-physics Problems: Application to Poroelasticity. *Int. J. Numer. Meth. Engng*, **56**(10), 1489–1510.

Dutko, M., Perić, D. and Owen, D.R.J. 1993. Universal Anisotropic Yield Criterion Based on Superquadric Functional Representation. Part I: Algorithmic Issues and Accuracy Analysis. *Comp. Meth. Appl. Mech. Engng*, **109**, 73–93.

Duvaut, G. and Lions, J.L. 1976. *Inequalities in Mechanics and Physics*. Springer-Verlag: Berlin.

Engel, L. and Klingele, H. 1981. *An Atlas of Metal Damage*. Wolfe Science Books.

Eterovic, A.L. and Bathe, K.-J. 1990. A Hyperelastic Based Large Strain Elasto-plastic Constitutive Formulation with Combined Isotropic-kinematic Hardening Using the Logarithmic Stress and Strain Measures. *Int. J. Numer. Meth. Engng*, **30**, 1099–1114.

Eve, R.A., Reddy, B.D. and Rockafellar, R.T. 1990. An Internal Variable Theory of Elastoplasticity based on the Maximum Plastic Work Inequality. *Quart. Appl. Math.*, **48**, 59–83.

Feijóo, R.A. and Zouain, N. 1988. Formulations in Rates and Increments for Elastic-plastic Analysis. *Int. J. Numer. Meth. Engng*, **26**, 2031–2048.

Feng, Y.T., Owen, D.R.J. and Perić, D. 1997. On the Sign of the Determinant of the Structural Stiffness Matrix for Determination of Loading Increment in Arc-length Methods. *Comm. Numer. Meth. Engng*, **13**, 47–49.

Feng, Y.T., Perić, D. and Owen, D.R.J. 1995. Determination of Travel Directions in Path-following Methods. *Math. and Comput. Modelling*, **21**, 43–59.

Feng, Y.T., Perić, D. and Owen, D.R.J. 1996. A New Criterion for Determination of Initial Loading Parameter in Arc-length Methods. *Comput. Structs*, **58**, 479–485.

Flanagan, D.P. and Taylor, L.M. 1987. An Accurate Numerical Algorithm for Stress Integration with Finite Rotations. *Comp. Meth. Appl. Mech. Engng*, **62**, 305–320.

Fletcher, R. 1980. *Practical Methods of Optimization. Volume 1: Unconstrained Problems, and Volume 2: Constrained Problems*. New York: Wiley.

Fonseka, G.U. and Krajčinović, D. 1981. The Continuous Damage Theory of Brittle Materials – Part 2: Uniaxial and Plane Response Modes. *J. Appl. Mech.*, **48**, 816–824.

Fuschi, P., Perić, D. and Owen, D.R.J. 1992. Studies on Generalized Midpoint Integration in Rate-Independent Plasticity with Reference to Plane Stress J_2-Flow Theory. *Comput. Structs*, **43**, 1117–1133.

Gear, C.W. 1971. *Numerical Initial Value Problems in Ordinary Differential Equations*. Englewood Cliffs, New Jersey: Prentice-Hall.

Gelin, J.C. and Mrichcha, A. 1992. Computational Procedures for Finite Strain Elasto Plasticity with Isotropic Damage. *Pages 1401–1412 of:* Owen, D.R.J., Oñate, E. and Hinton, E. (eds), *Computational Plasticity: Fundamentals and Applications – Proceedings of the Third International Conference held in Barcelona, 6–10 April 1992*. Swansea: Pineridge Press.

Gethin, D.T., Lewis, R.W. and Ransing, R.S. 1998. Compaction of Powder via a Deformable Discrete Element Approach. *Pages 45–50 of: Proceedings of the 1998 Powder Metallurgy World Congress and Exhibition*. Shrewsbury, UK: European Powder Metallurgy Association.

Glaser, S. and Armero, F. 1997. On the Formulation of Enhanced Strain Finite Element Methods in Finite Deformations. *Engng. Comp.*, **14**(7), 759–791.

Govindjee, S. and Simo, J. 1991. A Micro-mechanically Based Continuum Damage Model for Carbon Black-filled Rubbers Incorporating Mullins' Effect. *J. Mech. Phys. Solids*, **39**(1), 87–112.

Govindjee, S. and Simo, J.C. 1992. Mullins' Effect and the Strain Amplitude Dependence of the Storage Modulus. *Int. J. Solids Structs*, **20**, 1737–1751.

Green, A.E. and Naghdi, P.M. 1965. A General Theory of an Elasto-plastic Continuum. *Arch. Rat. Mech. Anal.*, **18**, 251–281.

Green, A.E. and Zerna, W. 1954. *Theoretical Elasticity*. Oxford University Press.

Green, A.P. 1953. The Plastic Yielding of Notched Bars Due to Bending. *Quart. J. Mech. Appl. Math.*, **6**, 223–239.

Green, A.P. 1954. A Theory of the Plastic Yielding Due to Bending of Cantilevers and Fixed-ended Beams. Part I. *J. Mech. Phys. Solids*, **3**, 1–15.

Gurson, A.L. 1977. Continuum Theory of Ductile Rupture by Void Nucleation and Growth – Part I: Yield Criteria and Flow Rule for Porous Media. *J. Engng. Mater. Tech.*, **99**, 2–15.

Gurtin, M.E. 1972. The Linear Theory of Elasticity. *Pages 1–295 of:* Flügge, S. and Truesdell, C. (eds), *Handbuch der Physik*, vol. VIa/2. Springer-Verlag.

Gurtin, M.E. 1981. *An Introduction to Continuum Mechanics*. New York: Academic Press.

Gurtin, M.E. and Francis, E.C. 1981. Simple Rate-Independent Model for Damage. *J. Spacecraft*, **18**(3), 285–286.

Gurtin, M.E. and Martins, L.C. 1976. Cauchy's Theorem in Classical Physics. *Arch. Rat. Mech. Anal.*, **60**(4), 305–324.

Haftka, R.T., Gürdal, Z. and Kamat, M.P. 1990. *Elements of Structural Optimization*. 2nd edn. Kluwer Academic Publishers.

Halphen, B. and Nguyen, Q.S. 1975. Sue les matériaux Standards généralisés. *J. de Mécanique*, **14**, 39–63.

Han, W. and Reddy, B.D. 1999. *Plasticity: Mathematical Theory and Numerical Analysis*. Berlin: Springer-Verlag.

Hancock, J.W. and Mackenzie, A.C. 1976. On the Mechanism of Ductile Fracture in High-strength Steels Subjected to Multi-axial Stress-states. *J. Mech. Phys. Solids*, **24**, 147–169.

Havner, K.S. 1992. *Finite Plastic Deformation of Crystalline Solids*. Cambridge: Cambridge University Press.

Hencky, H. 1933. The Elastic Behavior of Vulcanized Rubber. *J. Appl. Mech.*, **1**, 45–53.

Hibbitt, H.D., Marcal, P.V. and Rice, J.R. 1970. A Finite Element Formulation for Problems of Large Strain and Large Displacement. *Int. J. Solids Structs*, **6**, 1069–1086.

Hill, R. 1948. A Theory of the Yielding and Plastic Flow in Anisotropic Metals. *Proc. Roy. Soc. A*, **193**, 281–297.

Hill, R. 1950. *The Mathematical Theory of Plasticity*. London: Oxford University Press.

Hill, R. 1958. A General Theory of Uniqueness and Stability in Elastic-plastic Solids. *J. Mech. Phys. Solids*, **6**, 236–249.

Hill, R. 1978. Aspects of Invariance in Solid Mechanics. *Adv. Appl. Mech.*, **18**, 1–75.

Hinton, E. and Owen, D.R.J. 1977. *Finite Element Programming*. New York: Academic Press.

Hirsch, M.W. and Smale, S. 1974. *Differential Equations, Dynamical Systems, and Linear Algebra*. New York: Academic Press.

Hoffman, O. 1967. The Brittle Strength of Orthotropic Materials. *J. Composite Mater.*, **1**, 200–206.

Holzapfel, G.A. 2000. *Nonlinear Solid Mechanics. A Continuum Approach for Engineering*. London: John Wiley & Sons.

Horii, H. and Nemat-Nasser, S. 1983. Overall Moduli of Solids with Microcracks: Load Induced Anisotropy. *J. Mech. Phys. Solids*, **31**(2), 155–171.

Huerta, A., Pérez-Foguet, A. and Rodrigues-Ferran, A. 1999. Consistent Tangent Matrices for Complex Problems: Substepping Schemes and Numerical Differentiation. *In:* Wunderlich, W. (ed), *Proceedings of the ECCM'99 – European Conference on Computational Mechanics, Munich 1999*.

Hughes, T.J., Taylor, R.L. and Sackman, J.L. 1975. *Finite Element Formulation and Solution of Contact-impact Problems in Continuum Mechanics – III*. Technical Report UC SESM 75-7. Department of Civil Engineering, University of California, Berkeley.

Hughes, T.J.R. 1980. Generalization of Selective Integration Procedures to Anisotropic and Nonlinear Media. *Int. J. Num. Meth. Engng*, **15**, 1413–1418.

Hughes, T.J.R. 1984. Numerical Implementation of Constitutive Models: Rate-independent Deviatoric Plasticity. *Pages 29–63 of:* Nemat-Nasser *et al.* (Ed.), *Theoretical Foundations for Large-scale Computations for Nonlinear Material Behavior*. Dordrecht, The Netherlands: Martinus Nijhoff.

Hughes, T.J.R. 1987. *The Finite Element Method. Linear Static and Dynamic Finite Element Analysis*. Englewood Cliffs, New Jersey: Prentice-Hall.

Hughes, T.J.R. and Pister, K. 1978. Consistent Linearization in Mechanics of Solids and Structures. *Comp. Structs*, **8**, 391–397.

Hughes, T.J.R. and Taylor, R.L. 1978. Unconditionally Stable Algorithms for Quasi-static Elasto/Viscoplastic Finite Element Analysis. *Comput. Structs*, **8**, 169–173.

Hughes, T.J.R. and Winget, J. 1980. Finite Rotation Effects in Numerical Integration of Rate Constitutive Equations Arising in Large-deformation Analysis. *Int. J. Numer. Meth. Engng*, **15**, 1862–1867.

Ibrahimbegović, A. 1994. Finite Elastoplastic Deformations of Space-Curved Membranes. *Comp. Meth. Appl. Mech. Engng*, **119**, 371–394.

Irons, B.M. 1970. A Frontal Solution Program for Finite Element Analysis. *Int. J. Numer. Meth. Engng*, **2**, 5–32.

Janson, J. 1978. A Continuous Damage Approach to the Fatigue Process. *Engng. Fract. Mech.*, **10**, 651–657.

Jetteur, Ph. 1986. Implicit Integration Algorithm for Elastoplasticity in Plane Stress Analysis. *Engng. Comp.*, **3**, 251–253.

Jirásek, M. and Bažant, Z.P. 2002. *Inelastic Analysis of Structures*. Chichester: Wiley.

Johnson, G. and Bammann, D.J. 1984. A Discussion of Stress Rates in Finite Deformation Problems. *Int. J. Solids Structs*, **20**, 725–737.

Kachanov, L.M. 1958. Time of the Rupture Process under Creep Condition. *Izv. Akad. Nauk. SSSR, Otd. Tekhn. Nauk.*, **8**, 26–31.

Kachanov, L.M. 1977. Creep and Rupture under Complex Loading. *Problemi Prochnosti*, **6**.

Kestin, J. and Bataille, J. 1977. Irreversible Thermodynamics of Continua and Internal Variables. *Pages 39–67 of: Proceedings of the International Symposium on Continuum Models of Discrete Systems*. University of Waterloo Press.

Kocks, U.F. 1970. The Relation Between Polycrystal Deformation and Single-crystal Deformation. *Metall. Trans.*, **1**, 1121–1143.

Koh, C.G., Owen, D.R.J. and Perić, D. 1995. Explicit Dynamic Analysis of Elasto-plastic Laminated Composite Shells: Implementation of Non-iterative Stress Update Schemes for the Hoffman Yield Criterion. *Comput. Mech.*, **16**, 307–314.

Koiter, W.T. 1953. Stress-strain Relations, Uniqueness and Variational Theorems for Elasto-plastic Materials with Singular Yield Surface. *Quart. Appl. Math.*, **11**, 350–354.

Kojić, M. and Bathe, K.-J. 1987. Studies of Finite Element Procedures – Stress Solution of a Closed Elastic Strain Path with Stretching and Shearing Using the Updated Lagrangian Jaumann Formulation. *Comp. Structs*, **26**, 175–179.

Kojić, M. and Bathe, K.J. 1987. The 'Effective-stress-function' for Thermo-elasto-plasticity and Creep. *Int. J. Numer. Meth. Engng*, **24**, 1509–1532.

Korelc, J. and Wriggers, P. 1996. Consistent Gradient Formulation for a Stable Enhanced Strain Method for Large Deformations. *Engng. Comp.*, **13**(1), 103–123.

Krajčinović, D. 1996. *Damage Mechanics*. Amsterdam: North-Holland.

Krajčinović, D. 1983. Constitutive Equations for Damaging Materials. *J. Appl. Mech.*, **50**, 355–360.

Krajčinović, D. 1985. Continuous Damage Mechanics Revisited: Basic Concepts and Definitions. *J. Appl. Mech.*, **52**, 829–834.

Krajčinović, D. and Fonseka, G.U. 1981. The Continuous Damage Theory of Brittle Materials – Part 1: General Theory. *J. Appl. Mech.*, **48**, 809–815.

Krieg, R.D. and Krieg, D.B. 1977. Accuracies of Numerical Solution Methods for the Elastic-perfectly Plastic Model. *J. Pressure Vessel Tech.*, **99**, 510–515.

Ladèveze, P. 1983. On an Anisotropic Damage Theory. *Pages 355–363 of:* Boehler, J.P. (ed), *Proc. CNRS Int. Coll. 351 – Failure Criteria of Structured Media*. Villars-de-Lans.

Ladevèze, P. 1984. Sur une famille d'algorithmes en méchanique des structures. *Comptes-Rendus de l'Academie des Sciences (Paris), Sér. II*, **300**(2), 41–44.

Ladevèze, P. 1989. La méthode à grand incrément de temps pour l'analyse de structures à comportement nonlinéaire décrit par variable internes. *Comptes Rendus de l'Academie des Sciences (Paris), Sér. II*, **309**(11), 1095–1099.

Ladevèze, P. 1999. *Nonlinear Computational Structural Mechanics – New Approaches and Non-Incremental Methods of Calculation*. Springer.

Ladevèze, P. and Lemaitre, J. 1984. Damage Effective Stress in Quasi Unilateral Conditions. *In: 16th Int. Congress Theor. Appl. Mech.*

Ladevèze, P. and Perego, U. 2000. Duality Preserving Discetization of the Large Time Increment Method. *Comp. Meth. Appl. Mech. Engng*, **189**(1), 205–232.

Leckie, F.A. and Hayhurst, D.R. 1974. Creep Rupture of Structures. *Proc. Roy. Soc. Lond. A*, **340**, 323–347.

Leckie, F.A. and Onat, E.T. 1981. Tensorial Nature of Damage Measuring Internal Variables. *Pages 140–155 of: Proceedings of the IUTAM Symposium on Physical Nonlinearities in Structures*. Springer.

Lee, E.H. 1969. Elastic-plastic Deformation at Finite Strains. *J. Appl. Mech.*, **36**, 1–6.

Lee, E.H. and Liu, D.T. 1967. Finite Strain Elastic-plastic Theory with Application to Plane-wave Analysis. *J. Appl. Phys.*, **38**, 19–27.

Lege, D.J., Barlat, F. and Brem, J.C. 1989. Characterization and Modeling of the Mechanical Behaviour and Formability of a 2008-T4 Sheet Sample. *Int. J. Mech. Sci.*, **31**(7), 549–563.

Lemaitre, J. 1983. A Three-dimensional Ductile Damage Model Applied to Deep-drawing Forming Limits. *Pages 1047–1053 of: ICM 4 Stockholm*, vol. 2.

Lemaitre, J. 1985a. A Continuous Damage Mechanics Model for Ductile Fracture. *J. Engng. Mat. Tech.*, **107**, 83–89.

Lemaitre, J. 1985b. Coupled Elasto-plasticity and Damage Constitutive Equations. *Comp. Meth. Appl. Mech. Engng*, **51**, 31–49.

Lemaitre, J. 1987. Formulation and Identification of Damage Kinetic Constitutive Equations. *Pages 37–89 of:* Krajčinović, D. and Lemaitre, J. (eds), *Continuum Damage Mechanics: Theory and Applications*. Springer-Verlag.

Lemaitre, J. 1996. *A Course on Damage Mechanics*. 2nd edn. Springer.

Lemaitre, J. and Chaboche, J.L. 1990. *Mechanics of Solid Materials*. Cambridge University Press.

Lemaitre, J. and Dufailly, J. 1987. Damage Measurements. *Engng. Fract. Mech.*, **28**(8), 643–661.

Lemaitre, J., Desmorat, R. and Sauzay, M. 2000. Anisotropic Damage Law of Evolution. *Eur. J. Mech. A/Solids*, **19**, 187–208.

Li, X. 1995. Large Strain Constitutive Modelling and Computation for Isotropic, Creep Elastoplastic Damage Solids. *Int. J. Numer. Meth. Engng*, **38**, 841–860.

Lion, A. 2000. Constitutive Modelling in Finite Thermoviscoplasticity: A Physical Approach Based on Nonlinear Rheological Models. *Int. J. Plast.*, **16**, 469–494.

Lubarda, V.A. and Lee, E.H. 1981. A Correct Definition of Elastic and Plastic Deformation and its Computational Significance. *J. Appl. Mech.*, **48**, 35–40.

Lubliner, J. 1990. *Plasticity Theory*. New York: Macmillan.

Luenberger, D.G. 1973. *Introduction to Linear and Nonlinear Programming*. Reading, Massachusetts: Addison-Wesley.

Maier, G. 1970. A Matrix Structural Theory of Piece-wise Linear Plasticity with Interacting Yield Planes. *Meccanica*, **6**, 55–66.

Mandel, J. 1973. Equations constitutives et directeurs dans les milieux plastiques et viscoplastiques. *Int. J. Solids Structs*, **9**, 725–740.

Marques, J.M.M.C. 1984. Stress Computation is Elastoplasticity. *Engng. Comp.*, **1**, 42–51.

Marques, J.M.M.C. and Owen, D.R.J. 1983. Strain Hardening Representation for Implicit Quasistatic Elasto-viscoplastic Algorithms. *Comput. Structs*, **17**, 301–304.

Marquis, D. and Lemaitre, J. 1988. Constitutive Equations for the Coupling Between Elasto-plasticity Damage and Ageing. *Rev. Phys. Applic*, **23**, 615–624.

Marsden, J.E. and Hughes, T.J.R. 1983. *Mathematical Foundations of Elasticity*. Englewood Cliffs, New Jersey: Prentice-Hall.

Martin, J.B. 1975. *Plasticity: Fundamentals and General Results*. Cambridge: MIT Press.

Martin, J.B., Reddy, B.D. and Griffin, T.B. 1987. Applications of Mathematical Programming Concepts to Incremental Elastic-plastic Analysis. *Engng. Structs*, **9**, 171–176.

Matthies, H. 1979. Existence Theorems in Thermo-plasticity. *J. Mécanique*, **18**(4), 695–712.

Matthies, H. and Strang, G. 1979. The Solution of Nonlinear Finite Element Equations. *Int. J. Numer. Meth. Engng*, **14**, 1613–1626.

McMeeking, R.M. and Rice, J.R. 1975. Finite-element Formulations for Problems of Large Elastic-plastic Deformation. *Int. J. Solids Structs*, **11**, 601–616.

Meschke, G. and Liu, W.N. 1999. A Re-formulation of the Exponential Algorithm for Finite Strain Plasticity in Terms of Cauchy Stresses. *Comp. Meth. Appl. Mech. Engng*, **173**, 167–187.

Miehe, C. 1993. Computation of Isotropic Tensor Functions. *Comm. Numer. Meth. Engng*, **9**, 889–896.

Miehe, C. 1995. Discontinuous and Continuous Damage Evolution in Ogden-type large-strain elastic materials. *Eur. J. Mech. A/Solids*, **14**(5), 697–720.

Miehe, C. 1996a. Exponential Map Algorithm for Stress Updates in Anisotropic Multiplicative Elastoplasticity for Single Crystals. *Int. J. Numer. Meth. Engng*, **39**, 3367–3390.

Miehe, C. 1996b. Multisurface Thermoplasticity for Single Crystals at Large Strains in Terms of Eulerian Vector Updates. *Int. J. Solids Structs*, **33**, 3103–3130.

Miehe, C. 1998a. Comparison of Two Algorithms for the Computation of Fourth-order Isotropic Tensor Functions. *Comp. Structs*, **66**, 37–43.

Miehe, C. 1998b. A Theoretical and Computational Model for Isotropic Elastoplastic Stress Analysis in Shells at Large Strains. *Comp. Meth. Appl. Mech. Engng*, **155**, 193–233.

Miehe, C. and Keck, J. 2000. Superimposed Finite Elastic-viscoelastic-plastoelastic Stress Response with Damage in Filled Rubbery Polymers. Experiments, Modelling and Algorithmic Implementation. *J. Mech. Phys. Solids*, **48**, 323–365.

Miehe, C., Apel, N. and Lambrecht, M. 2002a. Anisotropic Additive Plasticity in the Logarithmic Strain Space: Modular Kinematic Formulation and Implementation based on Incremental Minimization Principles for Standard Materials. *Comp. Meth. Appl. Mech. Engng*, **191**, 5383–5425.

Miehe, C., Shotte, J. and Lambrecht, M. 2002b. Homogenization of Inelastic Solid Materials at Finite Strains Based on Incremental Minimization Principles. Application to the Texture Analysis of Polycrystals. *J. Mech. Phys. Solids*, **50**(10), 2123–2167.

Millard, A. 1995. Numerical Algorithms for Plane Stress Elastoplasticity: Review and Recommendation. *Pages 237–247 of:* Owen, D.R.J., Oñate, E. and Hinton, E. (eds), *Computational Plasticity: Fundamentals and Applications – Proceedings of the Fourth International Conference held in Barcelona, 3–6 April 1995*. Swansea: Pineridge Press.

Mitchell, G.P. 1990. *Topics in the Numerical Analysis of Inelastic Solids*. PhD thesis, Department of Civil Engineering, University College of Swansea.

Moran, B., Ortiz, M. and Shih, F. 1990. Formulation of Implicit Finite Element Methods for Multiplicative Finite Deformation Plasticity. *Int. J. Numer. Meth. Engng*, **29**, 483–514.

Moss, W.C. 1984. On Instabilities in Large Deformation Simple Shear Loading. *Comp. Meth. Appl. Mech. Engng*, **46**, 329–338.

Mróz, Z. 1967. On the Description of Anisotropic Work Hardening. *J. Mech. Phys. Solids*, **15**, 163–175.

Muir Wood, D. 1990. *Soil Behaviour and Critical State Soil Mechanics*. Cambridge: Cambridge University Press.

Mullins, L. 1969. Softening of Rubber by Deformation. *Rubber Chemistry and Technology*, **42**, 339–351.

Murakami, S. 1988. Mechanical Modeling of Material Damage. *J. Appl. Mech.*, **55**, 280–286.

Murakami, S. and Ohno, N. 1981. A Continuum Theory of Creep and Creep Damage. *Pages 422–443 of:* Ponter, A.R.S. (ed), *Proceedings of the IUTAM Symposium on Creep in Structures, Leicester, 1980*. Berlin: Springer.

Nagtegaal, J.C. 1982. On the Implementation of Inelastic Constitutive Equations with Special Reference to Large Deformation Problems. *Comp. Meth. Appl. Mech. Engng*, **33**, 469–484.

Nagtegaal, J.C. and de Jong, J.E. 1981. Some Computational Aspects of Elastic-plastic Large Strain Analysis. *Int. J. Numer. Meth. Engng*, **17**, 15–41.

Nagtegaal, J.C. and de Jong, J.E. 1982. Some Aspects of Non-isotropic Work-hardening in Finite Strain Plasticity. *Pages 65–102 of:* Lee, E.H. and Mallet, R.L. (eds), *Plasticity of Metals at Finite Strain: Theory, Experiment and Computation*. Division of Applied Mechanics, Stanford University and Department of Engineering & Mechanics, Rensselaer Polytechnic Institute.

Nagtegaal, J.C., Parks, D.M. and Rice, J.M. 1974. On Numerically Accurate Finite Element Solutions in the Fully Plastic Range. *Comp. Meth. Appl. Mech. Engng*, **4**, 153–177.

Nayak, G.C. and Zienkiewicz, O.C. 1972. Elastoplastic Stress Analysis: A Generalisation for Various Constitutive Laws including Strain Softening. *Int. J. Numer. Meth. Engng*, **5**, 113–135.

Naylor, D.J., Pande, G.N., Simpson, B. and Tabb, R. 1981. *Finite Elements in Geotechnical Engineering*. Swansea: Pineridge Press.

Needleman, A. 1977. Inflation of Spherical Rubber Balloons. *Int. J. Solids Structs*, **13**, 409–421.

Needleman, A., Asaro, R.J., Lemonds, J. and Peirce, D. 1985. Finite Element Analysis of Crystalline Solids. *Comp. Meth. Appl. Mech. Engng*, **52**, 689–708.

Nemat-Nasser, S. 1979. Decomposition of Strain Measures and their Rates in Finite Deformation Elastoplasticity. *Int. J. Solids Structs*, **15**, 155–166.

Nemat-Nasser, S. 1982. On Finite Deformation Elasto-plasticity. *Int. J. Solids Structs*, **18**(10), 857–872.

Nemat-Nasser, S. 1999. Averaging Theorems in Finite Deformation Plasticity. *Mech. Mater.*, **31**, 493–523.

Oñate, E., Rojek, J. and García Garino, C. 1995. NUMISTAMP: A Research Project for Assessment of Finite-element Models for Stamping Processes. *J. Mater. Proc. Technol.*, **50**, 17–38.

Oden, J.T. 1972. *Finite Elements of Nonlinear Continua*. London: McGraw-Hill.

Oden, J.T. 1979. *Applied Functional Analysis*. Englewood Cliffs, New Jersey: Prentice-Hall.

Ogden, R.W. 1972. Large Deformation Isotropic Elasticity – On the Correlation of Theory and Experiment for Incompressible Rubberlike Solids. *Proc. R. Soc. Lond. A*, **326**, 565–584.

Ogden, R.W. 1984. *Non-Linear Elastic Deformations*. Chichester: Ellis Horwood.

Onat, E.T. 1986. Representation of Mechanical Behaviour in the Presence of Internal Damage. *Engng. Fract. Mech.*, **25**, 605–614.

Onat, E.T. and Leckie, F.A. 1988. Representation of Mechanical Behavior in the Presence of Changing Internal Structure. *J. Appl. Mech.*, **55**, 1–10.

Ortiz, M. and Martin, J.B. 1989. Symmetry-preserving Return Mapping Algorithms and Incrementally Extremal Paths: A Unification of Concepts. *Int. J. Numer. Meth. Engng*, **28**, 1839–1853.

Ortiz, M. and Popov, E.P. 1985. Accuracy and Stability of Integration Algorithms for Elastoplastic Constitutive Relations. *Int. J. Numer. Meth. Engng*, **21**, 1561–1576.

Ortiz, M. and Simo, J.C. 1986. An Analysis of a New Class of Integration Algorithms for Elastoplastic Constitutive Relations. *Int. J. Numer. Meth. Engng*, **23**, 353–366.

Owen, D.R.J. and Hinton, E. 1980. *Finite Elements in Plasticity: Theory and Practice*. Swansea: Pineridge Press.

Owen, D.R.J., Souza Neto, E.A. de, Zhao, S.Y., Perić, D., and Loughran, J.G. 1998. Finite Element Simulation of the Rolling and Extrusion of Multi-phase Materials: Application to the Rolling of Prepared Sugar Cane. *Comp. Meth. Appl. Mech. Engng*, **151**, 479–495.

Pankaj, and Bićanić, N. 1989. On Multivector Stress Returns in Mohr–Coulomb Plasticity. *Pages 421–436 of:* Owen, D.R.J., Hinton, E. and Oñate, E. (eds), *Proceedings of the Second International Conference on Computational Plasticity: Models, Software and Applications*. Swansea: Pineridge Press.

Papadopoulos, P. and Taylor, R.L. 1994. On the Application of Multi-step Integration Methods to Infinitesimal Elastoplasticity. *Int. J. Numer. Meth. Engng*, **37**, 3169–3184.

Parisch, H. 1986. Efficient Non-linear Finite Element Shell Formulation Involving Large Strains. *Engng. Comp.*, **3**, 121–128.

Peirce, D. 1983. Shear Band Bifurcation in Ductile Single Crystals. *J. Mech. Phys. Solids*, **31**, 133–153.

Peirce, D., Asaro, R.J. and Needleman, A. 1982. An Analysis of Nonuniform and Localized Deformation in Ductile Single Crystals. *Acta Metall.*, **30**, 1087–1119.

Peirce, D., Asaro, R.J. and Needleman, A. 1983. Material Rate Dependence and Localized Deformation in Crystalline Solids. *Acta Metall.*, **31**, 1951–1976.

Peirce, D., Shih, C.F. and Needleman, A. 1984. A Tangent Modulus Method for Rate Dependent Solids. *Comput. Sructs*, **18**, 875–887.

Pérez-Foguet, A. and Armero, F. 2002. On the Formulation of Closest-point Projection Algorithms in Elastoplasticity – Part II: Globally Convergent Schemes. *Int. J. Numer. Meth. Engng*, **53**, 331–374.

Perić, D. 1992. On Consistent Stress Rates in Solid Mechanics: Computational Implications. *Int. J. Numer. Meth. Engng*, **33**, 799–817.

Perić, D. 1993. On a Class of Constitutive Equations in Viscoplasticity: Formulation and Computational Issues. *Int. J. Numer. Meth. Engng*, **36**, 1365–1393.

Perić, D. and de Souza Neto, E.A. 1999. A New Computational Model for Tresca Plasticity at Finite Strains with an Optimal Parametrization in the Principal Space. *Comp. Meth. Appl. Mech. Engng*, **171**, 463–489.

Perić, D. and Dettmer, W. 2003. A Computational Model for Generalized Inelastic Materials at Finite Strains Combining Elastic, Viscoelastic and Plastic Material Behaviour. *Engng. Comput.*, **20**, 768–787.

Perić, D. and Owen, D.R.J. 1991. A Model for Large Deformation of Elasto-viscoplastic Solids at Finite Strains: Computational Issues. *Pages 299–312 of:* Besdo, D. and Stein, E. (eds), *Proceedings of the IUTAM Symposium on Finite Inelastic Deformations – Theory and Applications*. Berlin: Springer.

Perić, D. and Owen, D.R.J. 1992. Computational Model for 3-D Contact Problems with Friction Based on the Penalty Method. *Int. J. Numer. Meth. Engng*, **35**, 1289–1309.

Perić, D., Owen, D.R.J. and Honnor, M.E. 1992. A Model for Finite Strain Elasto-plasticity Based on Logarithmic Strains: Computational Issues. *Comp. Meth. Appl. Mech Engng*, **94**, 35–61.

Perić, D., Yu, J. and Owen, D.R.J. 1994. On Error Estimates and Adaptivity in Elastoplastic Solids: Application to the Numerical Simulation of Strain Localization in Classical and Cosserat Continua. *Int. J. Numer. Meth. Engng*, **37**, 1351–1379.

Perzyna, P. 1963. The Constitutive Equations for Rate Sensitive Plastic Materials. *Quart. Appl. Math.*, **20**, 321–332.

Perzyna, P. 1966. *Fundamental Problems in Viscoplasticity*. Advances in Applied Mechanics, vol. 9. New York: Academic Press. Pages 243–377.

Perzyna, P. 1971. *Thermodynamic Theory of Viscoplasticity*. Advances in Applied Mechanics, vol. 11. New York: Academic Press. Pages 313–354.

Pinsky, P.M., Ortiz, M. and Pister, K.S. 1983. Numerical Integration of Rate Constitutive Equations in Finite Deformation Analysis. *Comp. Meth. Appl. Mech. Engng*, **40**, 137–158.

Pires, F.M.A., de Souza Neto, E.A. and Owen, D.R.J. 2004. On the Finite Element Prediction of Damage Growth and Fracture Initiation in Finitely Deforming Ductile Materials. *Comp. Meth. Appl. Mech. Engng*, **193**, 5223–5256.

Prager, W. 1959. *An Introduction to Plasticity*. London: Addison-Wesley.

Pramono, E. and Willam, K. 1989. Implicit Integration of Composite Yield Surfaces with Corners. *Engng. Comp.*, **6**, 186–197.

Rabotnov, Y.N. 1963. On the Equations of State for Creep. *Page 307 of: Progress in Applied Mechanics, Prager Anniversary Volume*. New York: Macmillan.

Ramm, E. 1981. Strategies for Tracing the Nonlinear Response Near Limit Point. *Pages 63–89 of:* Wunderlich, W. Stein, E. and Bathe, K.-J. (eds), *Nonlinear Finite Element Analysis in Structural Mechanics*. Berlin: Springer-Verlag.

Ramm, E. and Matzenmiller, A. 1987. Computational Aspects of Elasto-plasticity in Shell Analysis. *Pages 711–734 of:* Owen, D.R.J., Hinton, E. and Oñate, E. (eds), *Computational Plasticity: Models, Software and Applications – Proceedings of the International Conference held in Barcelona, 6–10 April 1987*. Swansea: Pineridge Press.

Ransing, R.S., Lewis, R.W., Gethin, D.T., Crook, A.J.L. and Dutko, M. 1998. Compaction of Granular Materials using Deformable Discrete Elements. *Pages 143–147 of:* Huétink, J. and Baaijens, F.P.T. (eds), *Proceedings of the Sixth International Conference on Numerical Methods in Industrial Forming*

Processes – NUMIFORM 98 – Enschede, Netherlands, 22–25 June 1998 – Simulation of Materials Processing: Theory, Methods and Applications. Rotterdam: Balkema.

Rashid, M.M. and Nemat-Nasser, S. 1995. A Constitutive Algorithm for Rate-dependent Crystal Plasticity. *Comp. Meth. Appl. Mech. Engng*, **94**, 201–228.

Reddy, B.D. 1998. *Introductory Functional Analysis*. Springer.

Reddy, B.D. and Martin, J.B. 1991. Algorithms for the Solution of Internal Variable Problems in Plasticity. *Comp. Meth. Appl. Mech. Engng*, **93**, 253–273.

Reddy, B.D. and Simo, J.C. 1995. Stability and Convergence of a Class of Enhanced Strain Methods. *SIAM J. Num. Anal.*, **32**(6), 1705–1728.

Reese, S. and Govindjee, S. 1998. A Theory of Finite Viscoelasticity and Numerical Aspects. *Int. J. Solid Structs*, **35**, 3455–3482.

Reese, S. and Wriggers, P. 2000. A Stabilization Technique to Avoid Hourglassing in Finite Elasticity. *Int. J. Numer. Meth. Engng*, **48**, 79–109.

Rice, J.R. 1968. A Path Independent Integral and the Approximate Analysis of Strain Concentration by Notches and Cracks. *J. Appl. Mech.*, **35**, 379–386.

Rice, J.R. 1971. Inelastic Constitutive Relations for Solids: An Internal-Variable Theory and its Application to Metal Plasticity. *J. Mech. Phys. Solids*, **19**, 433–455.

Rice, J.R. 1976. The Localization of Plastic Deformation. *Pages 207–220 of:* Koiter, W.T. (ed), *Theoretical and Applied Mechanics*, vol. 1. Amsterdam: North-Holland.

Riks, E. 1972. The Application of Newton's Method to the Problem of Elastic Stability. *J. Appl. Mech.*, **39**, 1060–1066.

Riks, E. 1979. An Incremental Approach to the Solution of Snapping and Buckling Problems. *Int. J. Solids Structs*, **15**, 529–551.

Rockafellar, R.T. 1970. *Convex Analysis*. Princeton University Press.

Rockafellar, R.T. and Wets, R.J.-B. 1998. *Variational Analysis*. A Series of Comprehensive Studies in Mathematics, vol. 317. Berlin: Springer.

Romano, G., Rosati, L. and Marotti de Sciarra, M. 1993. Variational Principles for a Class of Finite Step Elastoplastic Problems with Non-linear Mixed Hardening. *Comp. Meth. Appl. Mech. Engng*, **109**, 293–314.

Rosati, L. and Valoroso, N. 2004. A Return Map Algorithm for General Isotropic Elasto/Visco-plastic Materials in Principal Space. *Int. J. Numer. Meth. Engng*, **60**(2), 461–498.

Roscoe, K.H. and Burland, J.B. 1968. On the Generalised Stress-strain Behaviour of 'Wet' Clay. *Pages 535–609 of:* Heyman, J. and Leckie, F.A. (eds), *Engineering Plasticity*. Cambridge: Cambridge University Press.

Rubinstein, R. and Atluri, S.N. 1983. Objectivity of Incremental Constitutive Relations Over Finite Time Steps in Computational Finite Deformation Analysis. *Comp. Meth. Appl. Mech. Engng*, **36**, 277–290.

Runesson, K., Ristinmaa, M. and Mahler, L. 1999. A Comparison of Viscoplasticity Formats and Algorithms. *Mech. Cohesive-Frict. Mater.*, **4**, 75–98.

Saanouni, K., Chaboche, J.L. and Lesne, P.M. 1989. Creep Crack-growth Prediction by a Non-local Damage Formulation. *Pages 404–414 of:* Mazars, J. and Bazant, Z.P. (eds), *Cracking and Damage, Strain Localization and Size Effect*. Amsterdam: Elsevier.

Schellekens, J.C.J. and de Borst, R. 1990. The Use of the Hoffman Yield Criterion in Finite-element Analysis of Anisotropic Composites. *Comput. Structs*, **37**, 1087–1096.

Schönauer, M., de Souza Neto, E.A. and Owen, D.R.J. 1995. Hencky Tensor Based Enhanced Large Strain Element for Elasto-plastic Analysis. *Pages 333–348 of:* Owen, D.R.J., Oñate, E. and Hinton, E. (eds), *Computational Plasticity: Fundamentals and Applications – Proceedings of the Fourth International Conference held in Barcelona, 3–6 April 1995*. Swansea: Pineridge Press.

Schröder, J., Gruttmann, F. and Löblein, J. 2002. A Simple Orthotropic Finite Elasto-plasticity Model based on Generalized Stress–strain Measures. *Comp. Mech.*, **30**, 48–64.

Schweizerhof, K. and Ramm, E. 1984. Displacement Dependent Pressure Loads in Nonlinear Finite Element Analyses. *Comput. Structs*, **18**, 1099–1114.

Seth, B.R. 1964. Generalized Strain Measure with Applications to Physical Problems. *Pages 162–172 of:* Reiner, M. and Abir, D. (eds), *Second-order Effects in Elasticity, Plasticity and Fluid Dynamics*. Oxford: Pergamon Press.

Simo, J.C. 1985. On the Computational Significance of the Intermediate Configuration and Hyperelastic Stress Relations in Finite Deformation Elastoplasticity. *Mech. Mater.*, **4**, 439–451.

Simo, J.C. 1987. On a Fully Three-dimensional Finite-strain Viscoelastic Damage Model: Formulation and Computational Aspects. *Comp. Meth. Appl. Mech. Engng*, **60**, 153–173.

Simo, J.C. 1992. Algorithms for Static and Dynamic Multiplicative Plasticity that Preserve the Classical Return Mapping Schemes of the Infinitesimal Theory. *Comp. Meth. Appl. Mech. Engng*, **99**, 61–112.

Simo, J.C. 1998. Numerical Analysis and Simulation of Plasticity. *Pages 183–499 of:* Ciarlet, P.G. and Lions, J.L. (eds), *Handbook of Numerical Analysis, Volume VI*. Amsterdam: Elsevier.

Simo, J.C. and Armero, F. 1992. Geometrically Non-linear Enhanced Strain Mixed Methods and the Method of Incompatible Modes. *Int. J. Numer. Meth. Engng*, **33**, 1413–1449.

Simo, J.C., Armero, F. and Taylor, R.L. 1993. Improved Versions of Assumed Enhanced Strain Tri-linear Elements for 3D Finite Deformation Problems. *Comp. Meth. Appl. Mech. Engng*, **110**, 359–386.

Simo, J.C. and Govindjee, S. 1991. Non-linear B-stability and Symmetry Preserving Return Mapping Algorithms for Plasticity and Viscoplasticity. *Int. J. Numer. Meth. Engng*, **31**, 151–176.

Simo, J.C. and Hughes, T.J.R. 1986. On the Variational Foundations of Assumed Strain Methods. *J. Appl. Mech.*, **53**, 1685–1695.

Simo, J.C. and Hughes, T.R.J. 1987. General Return Mapping Algorithms for Rate-independent Plasticity. *Pages 221–231 of:* Desai, C.S. *et al.* (Ed.), *Constitutive Laws for Engineering Materials: Theory and Applications*. Elsevier.

Simo, J.C. and Hughes, T.J.R. 1998. *Computational Inelasticity*. New York: Springer-Verlag.

Simo, J.C. and Ju, J.W. 1987. Strain- and Stress-based Continuum Damage Models – I. Formulation and II. Computational Aspects. *Int. J. Solids Structs*, **23**, 821–869.

Simo, J.C., Ju, J.-W., Pister, K.S. and Taylor, R.L. 1988a. Assessment of Cap Model: Consistent Return Algorithms and Rate-dependent Extension. *ASCE J. Engng. Mech.*, **114**(2), 191–218.

Simo, J.C., Kennedy, J.G. and Govindjee, S. 1988b. Non-smooth Multisurface Plasticity and Viscoplasticity. Loading/Unloading Conditions and Numerical Algorithms. *Int. J. Numer. Meth. Engng*, **26**, 2161–2185.

Simo, J.C. and Meschke, G. 1993. A New Class of Algorithms for Classical Plasticity Extended to Finite Strains. Application to Geomaterials. *Comp. Mech.*, **11**, 253–278.

Simo, J.C. and Miehe, C. 1992. Associative Coupled Thermoplasticity at Finite Strains: Formulation, Numerical Analysis and Implementation. *Comp. Meth. Appl. Mech. Engng*, **98**, 41–104.

Simo, J.C. and Ortiz, M. 1985. A Unified Approach to Finite Deformation Plasticity Based on the Use of Hyperelastic Constitutive Equations. *Comp. Meth. Appl. Mech. Engng*, **49**, 221–245.

Simo, J.C. and Pister, K.S. 1984. Remarks on the Rate Constitutive Equations for Finite Deformation Problems: Computational Implications. *Comp. Meth. Appl. Mech. Engng*, **46**, 201–215.

Simo, J.C. and Rifai, S. 1990. A Class of Mixed Assumed Strain Methods and the Method of Incompatible Modes. *Int. J. Numer. Meth. Engng*, **29**, 1595–1638.

Simo, J.C. and Taylor, R.L. 1985. Consistent Tangent Operators for Rate-Independent Elastoplasticity. *Comp. Meth. Appl. Mech. Engng*, **48**, 101–118.

Simo, J.C. and Taylor, R.L. 1986. A Return Mapping Algorithm for Plane Stress Elastoplasticity. *Int. J. Numer. Meth. Engng*, **22**, 649–670.

Simo, J.C. and Taylor, R.L. 1991. Quasi-incompressible Finite Elasticity in Principal Stretches. Continuum Basis and Numerical Algorithms. *Comp. Meth. Appl. Mech. Engng*, **85**, 273–310.

Simo, J.C., Taylor, R.L. and Pister, K.S. 1985. Variational and Projection Methods for the Volume Constraint in Finite Deformation Elasto-plasticity. *Comp. Meth. Appl. Mech. Engng*, **51**, 177–208.

Skrzypek, J.J. 1993. *Plasticity and Creep. Theory, Examples and Problems*. London: CRC Press.

Sloan, S.W. and Booker, J.R. 1992. Integration of Tresca and Mohr–Coulomb Constitutive Relations in Plane Strain Elastoplasticity. *Int. J. Numer. Meth. Engng*, **33**, 163–196.

Sowerby, R. and Chu, E. 1984. Rotations, Stress Rates and Strain Measures in Homogenous Deformation Processes. *Int. J. Solids Structs*, **20**, 1037–1048.

Spencer, A.J.M. 1980. *Continuum Mechanics*. London: Longman.

Steinmann, P. and Stein, E. 1996. On the Numerical Treatment and Analysis of Finite Deformation Ductile Single Crystal Plasticity. *Comp. Meth. Appl. Mech. Engng*, **129**, 235–254.

Steinmann, P., Miehe, C. and Stein, E. 1994. Comparison of Different Finite Deformation Inelastic Damage Models within Multiplicative Elastoplasticity for Ductile Metals. *Compat. Mech.*, **13**, 458–474.

Stern, H.J. 1967. *Rubber: Natural and Synthetic*. London: McLaren and Sons.

Suquet, P. 1981. Sur les équations de la plasticité: existence et régularité des solutions. *J. Mécanique*, **20**, 3–40.

Sussman, T. and Bathe, K.-J. 1987. A Finite Element Formulation for Nonlinear Incompressible Elastic and Inelastic Analysis. *Comp. Structs*, **26**, 357–409.

Taylor, R.L., Beresford, P.J. and Wilson, E.L. 1976. A Non-conforming Element for Stress Analysis. *Int. J. Numer. Meth. Engng*, **10**, 1211–1219.

Toupin, R.A. 1962. Elastic Materials with Couple-Stresses. *Arch. Rat. Mech. Anal.*, **11**, 385–414.

Treloar, L.R.G. 1944. Stress–strain Data for Vulcanized Rubber under Various Types of Deformation. *Trans. Faraday Soc.*, **40**, 59–70.

Tresca, H. 1868. Mémoire sur l'écoulement des corps solides. *Mém. pres. par div. sav.*, **18**, 733–799.

Truesdell, C. 1969. *Rational Thermodynamics*. New York: McGraw-Hill.

Truesdell, C. and Noll, W. 1965. The Non-linear Field Theories of Mechanics. *In:* Flügge, S. (ed), *Handbuch der Physik*, vol. III/3. Springer-Verlag.

Tsakmakis, C. 1996a. Kinematic Hardening Rules for Finite Plasticity. Part I: A Constitutive Approach. *Cont. Mech. Thermodyn.*, **8**, 215–231.

Tsakmakis, C. 1996b. Kinematic Hardening Rules for Finite Plasticity. Part II: Some Examples. *Cont. Mech. Thermodyn.*, **8**, 233–246.

Tvergaard, V. 1981. Influence of Voids on Shear Band Instabilities under Plane Strain Conditions. *Int. J. Fract.*, **17**, 389–407.

Tvergaard, V. 1982a. Material Failure by Void Coalescence in Localized Shear Bands. *Int. J. Solids Structs*, **18**, 659–672.

Tvergaard, V. 1982b. On Localization in Ductile Materials Containing Spherical Voids. *Int. J. Fract.*, **18**, 237–252.

Tvergaard, V. and Needleman, A. 1984. Analysis of the Cup-cone Fracture in a Round Tensile Bar. *Acta Metall.*, **32**, 157–169.

Vaz Jr., M. 1998. *Computational Approaches to Simulation of Metal Cutting Processes*. PhD thesis, Department of Civil Engineering, University of Wales Swansea.

Vaz Jr., M. and Owen, D.R.J. 2001. Aspects of Ductile Fracture and Adaptive mesh Refinement in Damaged Elasto-plastic Materials. *Int. J. Numer. Meth. Engng*, **50**, 29–54.

von Mises, R. 1913. Mechanik der Festen Körper im Plastische-deformablen Zustand. *Nachr. d. Gesellsch d. Wissensch. zu Göttingen, Math.-phys. Klasse*.

Wall, W.A., Bischoff, M. and Ramm, E. 2000. A Deformation Dependent Stabilization Technique Exemplified by EAS Elements at Large Strains. *Comp. Meth. Appl. Mech. Engng*, **188**, 859–871.

Wang, C.C. and Truesdell, C. 1973. *Introduction to Rational Elasticity*. Leyden: Noordhoff.

Washizu, K. 1968. *Variational Methods in Elasticity and Plasticity*. London: Pergamon Press.

Weber, G. and Anand, L. 1990. Finite Deformation Constitutive Equations and a Time Integration Procedure for Isotropic, Hyperelastic-Viscoplastic Solids. *Comp. Meth. Appl. Mech. Engng*, **79**, 173–202.

Wempner, G.A. 1971. Discrete Approximations Related to the Nonlinear Theory of Solids. *Int. J. Solids Structs*, **7**, 1581–1599.

Wilkins, M.L. 1964. Calculation of Elasto-plastic Flow. *In:* Alder, B. *et al.* (Ed.), *Methods of Computational Physics, Vol. 3*. New York: Academic Press.

Wolfram, S. 1991. *Mathematica: A System for Doing Mathematics by Computer*. New York: Addison-Wesley.

Wriggers, P. 2001. *Nichtlineare Finite-Element-Methoden*. Berlin: Springer-Verlag.

Wriggers, P. and Reese, S. 1996. A Note on Enhanced Strain Methods for Large Deformations. *Comp. Meth. Appl. Mech. Engng*, **135**, 201–209.

Wriggers, P. and Taylor, R.L. 1990. A Fully Non-linear Axisymmetrical Membrane Element for Rubber-like Materials. *Engng. Comp.*, **7**, 303–310.

Zienkiewicz, O.C. and Cormeau, I.C. 1974. Visco-plasticity – Plasticity and Creep in Elastic Solids - A Unified Numerical Solution Approach. *Int. J. Numer. Meth. Engng*, **8**, 821–845.

Zienkiewicz, O.C. and Taylor, R.L. 2000. *The Finite Element Method. Volume II: Solid Mechanics*. 5th edn. Butterworth–Heinemann.

Zienkiewicz, O.C., Norris, V.A., Winnicki, L.A., Naylor, D.J. and Lewis, R.W. 1978. A Unified Approach to the Soil Mechanics Problems of Offshore Foundations. *In:* Zienkiewicz, O.C., Lewis, R.W. and Stagg, K.G. (eds), *Numerical Methods in Offshore Engineering*. John Wiley and Sons.

Zouain, N., Borges, L.A. and Hecke, M.B. 1988. A Force Method for Elastic-plastic Analysis of Frames by Quadratic Optimization. *Int. J. Solids Structs*, **24**, 211–221.

Zouain, N., Hecke, M.B. and Feijóo, R.A. 1992. Elastic-plastic Analysis with Potential Functionals Using Internal Variables. *Pages 163–174 of:* Owen, D.R.J., Oñate, E. and Hinton, E. (eds), *Computational Plasticity: Fundamentals and Applications – Proceedings of the Third International Conference held in Barcelona, 6–10 April 1992*. Swansea: Pineridge Press.

INDEX

Accumulated plastic slip, 698
Accumulated plastic strain, 145, 179, 183, 184
Accuracy order, 211
Almansi strain tensor, 54
Alternating tensor, 24
Angle of internal friction, *see* Frictional angle
Angular velocity, 44
Arc-length method, 107
    computer implementation of, 120
Armstrong–Frederick kinematic hardening law, 188, 190, 448, 480
    at finite strains, 635, 644
Array notation, *see* Matrix notation in finite elements
Array of engineering strains, 93, 760
Array of stress components, 88, 759
Arrhenius law, 450
Assembly operator, *see* Finite element assembly operator
Associative hardening, 183, 184, 243, 267, 296
    for multisurface models, 183
Axial vector of a tensor, 25

B-matrix, *see* Discrete gradient operator, symmetric
Back-stress tensor, 185, 257, 480
    Green–Naghdi rate of, 634
    Oldroyd rate of, 645
    spatial, 634
Bauschinger effect, 185, 257, 420
bcc crystal, 692
Bending locking, 669
BFGS scheme, *see* Quasi-Newton methods, BFGS scheme
Bingham viscoplastic model, 447
Biot strain tensor, 54
Blatz–Ko material, 530
Bodner–Partom viscoplastic model, 450
Body force, 61
    reference, 68
Boundary traction, 68
    reference, 68
Brittle damage, 472
Bulk modulus, 93

Calorodynamic process, 69
Cartesian components
    of a tensor, 21
    of a vector, 18
Cartesian coordinate frame, 18
Cartesian coordinates of a point, 18
Cauchy elastic material, 520
Cauchy stress tensor, 62
Cauchy stress vector, 61
Cauchy's axiom, 61
Cauchy's equation of motion, 68
Cauchy's theorem, 62, 67
Cauchy–Green strain tensors, 50, 53
Chain rule, 36
Characteristic equation, 27
Characteristic space, 25
Clausius–Duhem inequality, 69, 149
Closest point projection algorithm, 200
Cohesion, 164
Compaction pressure, 405
Complementarity condition, 144, 147
    discrete, 195
Configuration-dependent load, 106
Conservation of mass, 67, 499
Consistency condition, 147, 152
Consistent tangent matrix, 98
Consistent tangent modulus, *see* Consistent tangent operator
Consistent tangent operator, 192, 199
    for a hyperelastic-damage model, 567
    for a single crystal model implementation, 713
    for elastoplasticity, 229
    for finite strain multiplicative plasticity, 597, 601
        with kinematic hardening, 642
    for implicit return mappings, 238
        capped Drucker–Prager model, 413
        Drucker–Prager model, 337
        Gurson model, 502

Computational Methods for Plasticity: Theory and Applications EA de Souza Neto, D Perić and DRJ Owen

Hoffman model, 433
Lemaitre damage model, 485
modified Cam-Clay model, 408
Mohr–Coulomb model, 316
simplified Lemaitre damage model, 490
Tresca model, 286
von Mises model, 232, 242, 262, 382, 383
for the damaged elasticity model, 510
for viscoplasticity, 458
at finite strains, 606
Perzyna type model, 466
single crystal model implementation, 725
von Mises-based model implementation, 464
in plane stress, 366, 382
infinitesimal, 98, 754
material, 755
non-symmetry of, 409, 426
spatial, 104, 105, 756
symmetry property of, 243
Timoshenko elastoplastic beam, 401
Constitutive function, incremental, *see* Incremental constitutive function
Constitutive functional, 70, 71
Constitutive initial value problem, 76
elastoplastic, 193
at finite strains, 590
plane stress, 359
incremental, *see* Incremental constitutive problem
infinitesimal, 76
viscoplastic, 455
Continuum Damage Mechanics, 471, 473
Continuum elastoplastic tangent operator, 153, 235, 242, 243
for the Green–Naghdi rate-based model, 624
for the Jaumann rate-based model, 623
for the von Mises model, 234
symmetry of, 153, 244
Convected rate of stress, 621
Convergence criterion, finite element equilibrium solution, 98
Crack closure effects, 504, 510
Creep, 436, 439
tertiary, 436, 474
Creep-damage, 474
Critical state line, 404
Cross product, *see* Vector product
Crystallographic slip, 579, 692, 695
Cutting plane method, 205, 208, 213
Damage, 436, 472
Damage effective stress, 474, 478
Damage energy release rate, 479
Damage mechanics problems, *see* Numerical examples, damage mechanics
Damage models
anisotropic, 512
damaged elasticity law, 507
Gurson, 496
Gurtin–Francis, 560
hyperelasticity with damage, 557
Lemaitre, 478
simplified, 486
with crack closure, 511
Damage surface, 564
Damage tensor, 512
Damage threshold, 481, 490
Damage variable, 474–476
Deformation, 41
Deformation gradient, 46
determinant of, 48
elastoplastic multiplicative decomposition of, 578
incremental, 127, 592
isochoric/volumetric split of, 49
polar decomposition of, 49
Determinant of a tensor, 23
Deviatoric plane (or π-plane), 160
Deviatoric projection tensor, 59
Deviatoric strain, *see* Strain deviator
Deviatoric stress, *see* Stress deviator
Differential-algebraic equations, 209
Differentiation, 32
Dilatancy, 175, 176
Dilatancy angle, 175–177, 185
Directional derivative, 32
Discrete gradient operator
spatial, 104
symmetric, 87
spatial, 103
Discretised virtual work equation, 88
linearised, 96
Dissipation function, 149, 452, 453
Dissipation potential, 74, 451, 453
Distortional elastic strain energy, 162
Divergence, 37
material, 46
spatial, 46
Divergence theorem, 37
Ductile damage, 472

Effective plastic strain, *see* Accumulated plastic strain
Eigenprojection, 26
Eigenvalue, 25

Eigenvector, 25
Elastic deformation gradient, 578
Elastic domain, 140, 143, 150
for multisurface models, 156
Elastic predictor/return mapping algorithm, 196, 199
for a Timoshenko beam model, 400
for finite strain Green–Naghdi rate-based models, 632
for finite strain Jaumann rate-based models, 631
for finite strain multiplicative plasticity, 590
in plane stress, 602
with kinematic hardening, 637
for finite strain single crystal plasticity, 699
planar double-slip model, 707
for the Barlat–Lian model, 431
for the capped Drucker–Prager model, 412
for the Drucker–Prager model, 324
plane stress, 363
for the Gurson model, 501
for the Hoffman model, 424
for the Lemaitre damage model, 482
for the modified Cam-Clay model, 406
for the Mohr–Coulomb model, 297
for the simplified Lemaitre damage model, 486
for the Tresca model, 268
for the von Mises model, 215, 221
in plane stress, 364, 373
with mixed hardening, 258
for viscoplasticity, 456
at finite strains, 606
Perzyna-type model, 466
von Mises-based model, 460
Elastic rotation, 579
Elastic strain, 142, 148
logarithmic, 582
Elastic stretch, 579
Elastic trial hardening force, 196
Elastic trial state, 196, 424, 593
Elastic trial stress, 196
Elastic velocity gradient, 580
Elasticity
linear, *see* Linear elasticity
orthotropic, 423
plane stress, 358
Elasticity matrix, 93
Elasticity tensor
first, 755
infinitesimal, 93
spatial, 534, 756
Blatz–Ko model, 537
Hencky model, 537
Ogden model, 535
Elastoplastic tangent modulus, 147
Engineering strains, *see* Array of engineering strains
Enhanced assumed strain finite elements, 669
Equilibrium path, 107
Equivalent plastic strain, *see* Accumulated plastic strain
Error map, *see* Iso-error map
Essential boundary condition, 79
Euler method
backward, 194, 213, 455, 591
forward, 207
Eulerian strain, 54
Eulerian triad, 52
Exponential map integrator, 591, 700, 724, 751
Exponential of a tensor, *see* Tensor exponential function
External force vector, 88

Fatigue damage, 472
F-bar finite elements, 648
F-bar-Patch finite elements, 665
fcc crystal, 692
Filled rubbers, 473, 557
Finite element assembly operator, 89
Finite element equilibrium equation, *see* Discretised virtual work equation
Finite element mesh, 85
Finite step accuracy, 212, 213
First Piola–Kirchhoff stress, 65
First principle of thermodynamics, 68
Flow potential, 151
non-smooth, 155
Flow rule, 150
associative, 152
associative Barlat–Lian, 430
associative Hill, 420
associative Hoffman, 422
associative Tresca, 171, 267
based on Drucker–Prager function, 175
based on modified Cam-Clay function, 405
based on Mohr–Coulomb function, 173
derived from a flow potential, 151
finite strain multiplicative plasticity, 584
for associative multisurface models, 157
for single crystals, 695
for the capped Drucker–Prager model, 410
for the Gurson model, 498
Prandtl–Reuss, 171

uniaxial, 144
viscoplastic, 450
one-dimensional, 438
Flow vector, 150
derived from a flow potential, 151
derived from a non-smooth flow potential, 155
Fourth-order tensor, 29
Frame invariance, *see* Material objectivity
Free-energy, 69
for an elastoplastic material, 148
for finite strain hyperelasticity, 520
for the Lemaitre damage model, 478
isotropic, 521
Frictional angle, 164, 175, 185

G-matrix, *see* Discrete gradient operator, spatial
Gaussian quadrature, 89
Geometric stiffness, *see* Stiffness matrix, geometric
Gradient of a field, 32
Green–Lagrange strain tensor, 53
Green–Naghdi rate of stress, 621
Gurson porous plasticity model, *see* Damage models, Gurson
Gurtin–Francis damage model, *see* Damage models, Gurtin–Francis

Hardening, 140
Hardening curve, 145, 179, 181
Hardening modulus, 147
generalised, 150
linear isotropic, 182
linear kinematic, 186
Hardening slope, *see* hardening modulus
Hardening, derived from a flow potential, 151
Hardening, derived from a non-smooth flow potential, 155
Hardening, general model, 150
Hardening, uniaxial model, 145
Heaviside step function, 221
Helmholtz free-energy, *see* Free-energy
Hencky material, 528
in plane stress, 532
Hencky strain tensor, *see* Logarithmic strain tensor
Homogeneous deformation, 47
hpc crystal, 692
Hu–Washizu variational principle, 669
Hughes–Winget algorithm, 631
Hydrostatic stress, 64
Hyperelasticity, 520
compressible regularisation, 525
in plane stress, *see* Plane stress hyperelasticity
incompressible, 524
isotropic, 521
Hyperelasticity problems, *see* Numerical examples, finite hyperelasticity
Hyperelasticity with damage, *see* Damage models, hyperelasticity with damage
HYPLAS program
data input and initialisation, 117
elements, implementation and management, 128–131
global database, 117
increment cutting, 123
load incrementation, 120
main program, 117
material models, implementation and management, 131–135
HYPLAS subprograms:
ARCLEN, 109, 120, 122–124
CONVER, 100, 109
CSTEP2, 601
CSTOGD, 542, 545, 546
CSTPDS, 713
CTDAMA, 486, 491
CTDMEL, 510
CTDP, 324, 337, 340, 342, 343
CTDPPN, 366
CTMC, 295, 315, 318, 319, 324, 342
CTOGD, 134, 538
CTTR, 266, 283, 291, 294, 295, 324, 599
CTVM, 134, 235, 364–366, 383, 569, 599
CTVMMX, 257, 263
CTVMPS, 383, 384
DEXPMP, 702
DGISO2, 287, 289, 291, 295, 317, 731, 737, 738
DISO2, 537, 599, 731
DPLFUN, 228, 238
ELEIIF, 125, 126, 128, 129, 131
ELEIST, 100, 109, 129, 131
ERRPRT, 119, 227
FRONT, 100, 109, 120, 123, 124, 129
IFFB2, 538
IFFBA2, 129, 656
IFSTD2, 100, 128, 129, 538, 656
INCREM, 120
INDATA, 118, 119, 129
ININCR, 118
INITIA, 119, 120
INLOAD, 118, 119, 129
INTFOR, 100, 109, 124, 126
ISO2, 731
LENGTH, 121

MATICT, 134, 135, 235, 237, 569, 601
MATIOR, 135
MATIRD, 132, 135
MATISU, 100, 128, 133, 135, 224, 227, 596
MATISW, 120, 134, 135
ORDAMA, 486
ORVM, 135
OUTPUT, 125
PLFUN, 228
RDDAMA, 486
RDDP, 337
RDMC, 315
RDOGD, 541
RDTR, 283
RDVM, 227
RSQ4, 129
RST3, 129
RSTART, 118, 125
SFQ4, 130
SFT3, 130
SHPFUN, 130
SPDEC2, 731, 735
STFBA2, 129, 656
STSTD2, 100, 128, 129, 656
SUDAMA, 486, 490
SUDMEL, 509
SUDP, 324, 329–334, 337, 340, 342
SUDPPN, 363
SUFAIL, 227
SUMC, 295, 303–310, 315, 316, 318, 319, 324, 334, 337
SUOGD, 528, 531, 536, 538, 541, 542, 567
SUPDSC, 708
SUPGD, 538
SUTR, 128, 273, 274, 276–279, 282, 283, 291, 294, 310, 315
SUVM, 133, 224, 235, 261, 310, 364, 567, 569, 596
SUVMMX, 257, 261
SUVMPS, 133, 376, 378, 379
SWDAMA, 486
SWITCH, 124, 125
SWOGD, 134
SWVM, 134
UPCONF, 100, 109

Identity tensor
of fourth-order, 31
symmetric, 31
of second order, 19
Incremental boundary value problem
at finite strains, 103
infinitesimal, 95
Incremental constitutive function, 95, 102, 127, 133, 192, 229, 598
for elastoplasticity, 230
for the viscoplastic von Mises-based model, 464
for the von Mises model, 220, 223, 233, 260
Incremental constitutive problem
of finite strain multiplicative plasticity, 592
of infinitesimal elastoplasticity, 194
Incremental displacement vector, 98
Incremental finite element equilibrium equations
at finite strains, 103
infinitesimal, 96
Incremental objectivity, 625
Incremental plastic multiplier, 195
Incremental potential, 243
Indicator function, 452
Infinitesimal deformation, 57
Infinitesimal strain tensor, 57
Initial boundary value problem, 79
infinitesimal, 81
material, 80
spatial, 79
Initial stiffness method, 99
Initial yield stress, 182
Inner product of tensors, 22
Inner product of vectors, 17
Intermediate configuration, *see* Plastic intermediate configuration
Internal force vector, 88, 192
Internal variables, 72
Interpolation function, *see* Shape function
Interpolation matrix, 87
Invertible tensor, 23
Iso-error map, 214, 215
implicit Drucker–Prager model implementation, 337
implicit Lemaitre model implementation, 483
implicit Mohr–Coulomb model implementation, 315
implicit Tresca model implementation, 283
viscoplastic von Mises-based model implementation, 463
Isochoric deformation, 48
Isoparametric finite element, 90
Isotropic hardening, 178, 448
Isotropic scalar function, 731
Isotropic solid, 71
Isotropic tensor, 30
Isotropic tensor function, 287, 316, 733

J-integral, 479
J_2,J_3-invariants, *see* Stress deviator, invariants of
Jaumann rate of stress, 619

Kinematic hardening, 185, 257, 448
  at finite strains, 633
Kinematically admissible displacements set, 79
  discretised, 86
Kirchhoff stress, 67
Kuhn–Tucker optimality conditions, 170

Lagrangian strain, 53
Lagrangian triad, 52
LATIN Method, 101
LBB condition, 687
Left Cauchy–Green strain tensor, *see* Cauchy–Green strain tensors
Left stretch tensor, *see* Stretch tensors
Lemaitre–Chaboche viscoplasticity model, 449
Lie derivative, 585
Limit load, *see* Plastic collapse problems
Line-search, 200, 431, 433, 489, 490, 501, 720
Linear elasticity, 93
Linear hardening, 182, 223, 244, 261
Linearisation, 38
  in infinite-dimensional functional spaces, 39
Linearised finite element equilibrium equation, *see* Discretised virtual work equation, linearised
Load factor, 96
Load-stiffness matrix, *see* Stiffness matrix, load stiffness
Loading/unloading conditions, 145, 150
  for multisurface models, 157
Lode angle, 161
Logarithmic strain tensor, 54, 528, 582

Macauley bracket, 505
Master damage curve, 560, 564
Material description, 44
Material field, 44
Material gradient, 46
Material objectivity, 70, 520, 619
Material stiffness, *see* Stiffness matrix, material
Material symmetry, 71, 521
Material tangent modulus, *see* Consistent tangent operator, material
Material time derivative, 46
Mathematical programming, 210
Matrix notation in finite elements, 87, 759
Matrix representation of a tensor, 21
Maximum plastic dissipation, principle of, 170, 453
  at large strains, 589
Midpoint method, 203, 213, 458, 752
Mixed hardening, 189, 257
Modified Newton methods, 99
Mohr circle, 164
Momentum balance, 67
Mooney–Rivlin material, 525
Motion, 42
Mullins effect, 557
Multiplicative decomposition of the deformation gradient, 578
Multivector return mapping, *see* Return mapping, multivector

Natural boundary condition, 79
neo-Hookean material, 525
Newton–Raphson Method, 96, 97, 198
  with combined line-search, *see* Line-search
  with improved initial guess, 200, 484
Nodal displacements vector, 87
Nominal stress, *see* Stress, first Piola–Kirchhoff
Nonlinear hardening, 182
Norm of a tensor, 22
Norm of a vector, 17
Normal dissipativity, 74, 451
Norton creep law, 449, 474, 723
Numerical examples
  damage mechanics
    damageable rubber balloon, 569
    fracturing of a cylindrical notched specimen, 493
  finite strain hyperelasticity
    annular plate, 547
    Cook's membrane, 656
    elastomeric bead compression, 556
    flat membranes inflation, 552
    perforated rubber sheet, 547
    rubber cylinder compression, 555
    rugby ball, 551
    spherical rubber balloon, 550
  finite strain plasticity
    bending of a V-notched Tresca bar, 606
    double-notched specimen, 658
    necking of a cylindrical bar, 607
    perforated plate, 613
    plane strain localisation, 611
    thin sheet forming, 614
    unconstrained single element, 660
    upsetting of a cylindrical billet, 661

  finite strain single crystal plasticity
    crystal shearing, 710
    symmetric rectangular strip, 717
    unsymmetric rectangular strip, 720
  infinitesimal plasticity
    circular plate, 250
    circular-footing, 350
    concrete shear wall, 391
    double-notched specimen, 255
    end-loaded cantilever, 387
    perforated plate, 390, 469
    plate with circular hole, 387
    pressurised cylinder, 244
    pressurised spherical shell, 247
    slope stability, 351
    strip footing, 252, 346
    tapered cantilever, 344
    V-notched bar, 343
  viscoplasticity
    creep of a single crystal, 726
    notched specimen, 467
    perforated plate, 469

Objective rate, 74
Objective stress rates, 619
Observer change, 70
Ogden material, 527
  in plane stress, 531
Oldroyd rate of stress, 620
Operator split method, 201
Orthogonal tensor, 23
Orthonormal basis, 18
Out-of-balance force vector, *see* Residual vector

Perfect plasticity, *see* Plasticity models, perfectly plastic
Perić viscoplastic model, 438, 724
Permanent strain, *see* Plastic strain
Perzyna viscoplastic model, 448, 724
Piola–Kirchhoff stress, *see* First Piola–Kirchhoff stress
Plane stress assumption, 357
Plane stress elasticity, *see* Elasticity, plane stress
Plane stress enforcement
  in finite hyperelasticity, 530
  in finite strain plasticity, 604
  in linear elasticity, 359
  in plasticity, 360, 361, 367
Plane stress hyperelasticity, 530
Plastic anisotropy, 414
Plastic collapse problems, 244, 247, 250, 252, 255, 343, 344, 346, 350, 351, 387, 390, 391
Plastic deformation gradient, 578
Plastic dilatancy, *see* Dilatancy
Plastic dissipation, 149, 451
Plastic flow, 140
Plastic flow rule, *see* Flow rule
Plastic intermediate configuration, 575
Plastic multiplier, 144
  determination of, 146, 152, 577
Plastic rotation, 579
Plastic spin, 581
Plastic strain, 143, 148
  volumetric, 175, 176, 405, 412, 422, 588
Plastic stretch, 575, 579
Plastic stretching, 581
  spatial, 582
Plastic velocity gradient, 580
Plastic work, 181
Plastic yielding, *see* Plastic flow
Plastically admissible stresses, 143
  set of, 150, 583
Plasticity models (general):
  associative, 152
  finite strains
    general hyperelastic-based multiplicative, 578
    hypoelastic-based, 615
    in plane stress, 601
    Jaumann rate-based, 622
    one-dimensional, 575
    single crystal, 694
  multisurface, 156
  one-dimensional, 141–147
  perfectly plastic, 177
  plane stress-projected, 360, 370, 601
  three-dimensional, 148–157
  Timoshenko beam, 399
Polar decomposition, 28
Polycrystalline metal, 414, 472
Position vector, 18
Positive definite tensor, 23
Prager kinematic hardening law, 186, 448
  at finite strains, 635, 645
Prandtl–Reuss flow rule, *see* Flow rule, Prandtl–Reuss
Principal axis, 26
Principal direction, *see* Principal axis
Principal invariants, 27
Principal stresses, 63, 67
Principal stretches, 52
Principal value, *see* Eigenvalue
Product rule, 37
Proper orthogonal tensor, 23
Proportional loading, 96

Quasi-Newton methods, 101
BFGS scheme, 101

Rate of deformation tensor, *see* Stretching tensor
Rate-dependence, 435, 436, 441
Reference map, 43
Relative effective stress, 448
Relative strain, 560, 563
Relative stress tensor, 185, 257
Relative yield stress, 415, 421
Relaxation, *see* Stress relaxation
Relaxation test, 436
Residual vector, 97
Resultant forces, 397
Return mapping, 196
closed form, 223, 261, 300, 327
in principal stress space, 269, 298, 599
multivector, 270, 298, 700, 707
viscoplastic, 456
Right Cauchy–Green strain tensor, *see* Cauchy–Green strain tensors
Right stretch tensor, *see* Stretch tensors
Rigid deformation, 42
infinitesimal, 58
Rigid motion, 44
Rigid velocity, 44
Rotated plastic stretching, *see* Plastic stretching, spatial
Rotation tensor, 23

Schmid resolved shear stress, 693
Second Piola–Kirchhoff stress, 66
Second principle of thermodynamics, 68
Second-order tensor, 19
Shape function, 85
global, 85
Shear modulus, 93
Shear yield stress, 157
Skew symmetric tensor, 19
Slip system, 692
Slope stability, *see* Numerical examples, infinitesimal plasticity, slope stability
Snap-back, 107
Snap-through, 107
Spatial description, 44
Spatial elasticity tensor, *see* Elasticity tensor, spatial
Spatial field, 44
Spatial gradient, 46
Spatial tangent modulus, *see* Consistent tangent operator, spatial
Spatial time derivative, 46
Spectral decomposition, 25
Spectral theorem, 26
Spin tensor, 55
Stability, 212
State update interface, 127
State update procedure, 123–126, 128, 132, 133, 135, 192
State variables, 72
Static condensation, 676, 687
Stiffness matrix, 97, 192
for finite strains, 104
for infinitesimal strains, 98
for linear elasticity, 94
geometric, 106
load-stiffness, 106
material, 106
Strain deviator, 58, 529, 582
Strain equivalence, hypothesis of, 475, 478, 479
Strain hardening, 178
Strain-displacement matrix, *see* Discrete gradient operator, symmetric
Strain-rate dependence, *see* Rate-dependence
Stress deviator, 64
invariants of, 160–161
Stress equivalence, hypothesis of, 476
Stress power, 68
Stress relaxation, 436, 444
Stretch tensors, 49
Stretching tensor, 55
Subdifferential, 154, 453
Subgradient, 154
Symmetric gradient, 57
Symmetric tensor, 19
Symmetry group, 71

Tangent modulus, *see* Consistent tangent operator
Tangent stiffness, *see* Stiffness matrix
Tangential solution, 110
Taylor hardening law, 698
Tensile/compressive split of the stress, 505
Tensor exponential function, 747
derivative of, 750
Tensor inverse, 23
Tensor product, 20, 28, 29
Tensor square root, 28
Tensors of higher order, 28
Tertiary creep, *see* Creep, tertiary
Texturing, 414
Thermodynamic determinism, 70
Thermodynamical force, 73, 149
Thermodynamics with internal variables, 71
Thermokinetic process, 69
Timoshenko beam, 396
Trace of a tensor, 22

Transpose, 19
Trapezoidal method, 202, 458
Triaxial shear test, 141
Truesdell rate of stress, 620

Uniaxial tension test, 140, 436
Uniaxial yield stress, 140, 143
Unit vector, 17
Unstable equilibrium, 107
u/p finite elements, 683

Vector product, 24
Velocity, 43
Velocity gradient, 55
Virtual displacements space, 77, 78, 80, 81
discretised, 86
Virtual work linearisation
under finite deformations, 755
under infinitesimal deformations, 753
Virtual work principle, 77
discretised, *see* Discretised virtual work equation
infinitesimal, 78
material, 78
spatial, 77
Viscoplastic flow rule, *see* Flow rule, viscoplastic
Viscoplastic integration algorithm
general implicit, 454
midpoint, 458
models with a yield surface, *see* Elastic predictor/return mapping algorithm, for viscoplasticity
trapezoidal, 458
Viscoplastic return mapping, *see* Return mapping, viscoplastic
Viscoplasticity models (general):
at finite strains, 605
multidimensional general, 450
multidimensional von Mises-based, 445
one-dimensional, 437
single crystal, 721
without a yield surface, 448
Viscoplasticity problems, *see* Numerical examples, viscoplasticity
Void volume fraction, 496
Volume change ratio, 48
Volumetric deformation, 49
Volumetric elastic strain energy, 162
Volumetric locking, 647
Volumetric plastic strain, *see* Plastic strain, volumetric
Volumetric strain, 59, 529, 582
von Mises effective (or equivalent) stress, 163

Work hardening, 180

Yield criterion, 143
Drucker–Prager, 166
isotropic, 158
Mohr–Coulomb, 164
multisurface representation, 165
pressure-insensitive, 158
Tresca, 157
multisurface representation, 160
under finite strains, 583
von Mises, 162
Yield function, 143
Barlat–Lian, 427, 428
capped Drucker–Prager model, 410
Drucker–Prager, 167, 324
Gurson, 498
Hill orthotropic, 414
Hoffman orthotropic, 420
isotropic, 158
Lemaitre damage model, 480
modified Cam-Clay, 404
Mohr–Coulomb, 164
invariant representation, 166
Tresca, 158
invariant representation, 160
von Mises, 163
Yield pressure, *see* Compaction pressure
Yield surface, 150
graphical representation of, 159, 416, 697

Zero tensor, 19
Zero vector, 17